

Anthropogenic effects on the hydro-morphological development of turbid estuaries

Zhu, C.

DOI

[10.4233/uuid:8c504232-4c79-4534-ae75-d9842aa802a1](https://doi.org/10.4233/uuid:8c504232-4c79-4534-ae75-d9842aa802a1)

Publication date

2021

Document Version

Final published version

Citation (APA)

Zhu, C. (2021). *Anthropogenic effects on the hydro-morphological development of turbid estuaries*. [Dissertation (TU Delft), Delft University of Technology]. <https://doi.org/10.4233/uuid:8c504232-4c79-4534-ae75-d9842aa802a1>

Important note

To cite this publication, please use the final published version (if applicable). Please check the document version above.

Copyright

Other than for strictly personal use, it is not permitted to download, forward or distribute the text or part of it, without the consent of the author(s) and/or copyright holder(s), unless the work is under an open content license such as Creative Commons.

Takedown policy

Please contact us and provide details if you believe this document breaches copyrights. We will remove access to the work immediately and investigate your claim.

CHUNYAN ZHU

Anthropogenic effects on the hydro-morphological development of turbid estuaries



**ANTHROPOGENIC EFFECTS ON THE
HYDRO-MORPHOLOGICAL DEVELOPMENT OF
TURBID ESTUARIES**

高浊度河口动力地貌演变及人类驱动响应

ANTHROPOGENIC EFFECTS ON THE HYDRO-MORPHOLOGICAL DEVELOPMENT OF TURBID ESTUARIES

Proefschrift

ter verkrijging van de graad van doctor
aan de Technische Universiteit Delft,
op gezag van de Rector Magnificus prof. dr. ir. T.H.J.J. van der Hagen,
voorzitter van het College voor Promoties,
in het openbaar te verdedigen op donderdag 2 december om 10:00 uur

by

Chunyan ZHU

Bachelor of Harbor, Waterway and Coastal Engineering,
Wuhan University, Wuhan, China,
geboren te Changzhou, China.

Dit proefschrift is goedgekeurd door de promotoren.

Samenstelling promotiecommissie:

Rector Magnificus,	voorzitter
Prof. dr. ir. Z.B. Wang,	Technische Universiteit Delft, promotor
Prof. dr. Q. He,	East China Normal University, promotor
Prof. dr. D.S. van Maren,	East China Normal University, promotor

Onafhankelijke leden:

Prof. dr. P.X. Ding	East China Normal University
Prof. dr. ir. A.J.F. Hoitink	Wageningen University & Research
Prof. dr. ir. J.C. Winterwerp	Technische Universiteit Delft
Prof. dr. ir. S.G.J. Aarninkhof	Technische Universiteit Delft
Prof. dr. ir. H.J. de Vriend	Technische Universiteit Delft, reservelid

Dr. Leicheng Guo of East China Normal University contributed significantly to the completion of the dissertation.

The doctoral research has been carried out in the context of an agreement on joint doctoral supervision between East China Normal University, China and Delft University of Technology, the Netherlands.



This study is a product of the project "Coping with deltas in transition" within the Programme of Strategic Scientific Alliances between China and the Netherlands (PSA), financed by the Chinese Ministry of Science and Technology (MOST) and Royal Netherlands Academy of Arts and Sciences (KNAW). It was also financially supported by Natural Science Foundation of China (NSFC) and Shanghai Committee of Science and Technology. The author is partially supported by the China Scholarship Council and the Stichting Het Lamminga Fonds, Delft, the Netherlands.

Keywords: Hydrodynamics; Sediment dynamics; Morphology; Estuaries; Human interventions; Turbidity maximum; Numerical modelling

Printed by: ProefschriftMaken || www.proefschriftmaken.nl

Front & Back: Simone Golob

Copyright © 2021 by C. Zhu

ISBN 978-94-6423-551-7

An electronic version of this dissertation is available at
<http://repository.tudelft.nl/>.

*In memory of
my uncle and grandfather*

CONTENTS

Summary	xi
Samenvatting	xv
1 Introduction	1
1.1 Estuarine sediment dynamics	2
1.1.1 General description of estuary, ETM and mouth bar	2
1.1.2 Characteristics of suspended sediment	3
1.1.3 Hydro-morphodynamic interactions.	4
1.1.4 Sediment trapping	4
1.2 Estuarine response: challenges	6
1.2.1 Human interventions	6
1.2.2 Is there a regime shift in the Yangtze Estuary?	7
1.3 Objectives and research questions	11
1.4 Outline of this thesis	12
2 Decadal morphological evolution of the mouth zone of the Yangtze Estuary in response to human interventions	15
2.1 Introduction	17
2.2 Data and methods	18
2.2.1 Study area	18
2.2.2 Data and methods	22
2.3 Results	23
2.3.1 Phenomenological description.	23
2.3.2 Quantitative bathymetric change	24
2.3.3 Hypsometry changes.	26
2.3.4 Salt marsh changes	28
2.4 Discussion	29
2.4.1 Differences between Hengsha flat and Jiudian shoal	29
2.4.2 Effect of human interventions	31
2.4.3 Synthesis.	34
2.5 Conclusions.	36
2.A Appendix: Supplementary tables and figures	38
3 Exploration of decadal tidal evolution in response to morphological and sedimentary changes in the Yangtze Estuary	41
3.1 Introduction	43
3.2 Study area.	45
3.3 Material and methods.	46
3.3.1 Data	46

3.3.2	Data analysis	47
3.3.3	Numerical modelling	48
3.4	Results	50
3.4.1	Observed decadal tidal evolution	50
3.4.2	Computed tidal evolution	52
3.5	Discussion	54
3.5.1	Model limitations: effect of river discharge.	54
3.5.2	Effect of morphological changes	55
3.5.3	Mechanisms responsible for changes in bed roughness	57
3.5.4	Implications for other estuaries	60
3.6	Conclusions.	61
3.A	Appendix: Supplementary tables and figures	63
4	Effects of sediment-induced density gradients on the estuarine turbidity maximum in the Yangtze Estuary	67
4.1	Introduction	69
4.2	Methodology	71
4.2.1	Study area	71
4.2.2	Model setup	72
4.2.3	Density parameters	75
4.3	Results	77
4.3.1	Tidal dynamics.	77
4.3.2	ETM location and extension	78
4.3.3	Density gradients	79
4.3.4	Seasonal and spring-neap variations.	83
4.4	Discussion	84
4.4.1	Model limitations	84
4.4.2	ETM development by SedDG	86
4.4.3	Implications for other estuaries	89
4.5	Conclusions.	91
4.A	Appendix: Parameters in the sediment transport model	93
4.B	Appendix: Model calibration for hydrodynamics and sediment transport.	93
4.C	Appendix: Sensitivity studies on ETM formation	94
5	Feedback effects of sediment suspension on transport mechanisms in estuarine turbidity maximum	105
5.1	Introduction	107
5.2	Methods	109
5.2.1	Basic model setup	109
5.2.2	Effects of sediments	111
5.2.3	Net sediment flux	112
5.3	Results	113
5.3.1	Impact of sediment properties	113
5.3.2	Longitudinal SSC distribution	113
5.3.3	ETM location	114

5.4	Discussion	115
5.4.1	Effect of tidal asymmetry.	115
5.4.2	Effect of sediment: sediment-induced density effects	117
5.4.3	Effect of sediment: water-bed exchange	119
5.4.4	A synthesis.	121
5.5	Conclusions.	124
6	Future changes in saltwater intrusion in the Yangtze Estuary: the importance of sediment dynamics	125
6.1	Introduction	127
6.2	Study area.	128
6.3	Methods	130
6.4	Results	132
6.4.1	Responses of SSC and salinity	132
6.4.2	Effect of sediments.	134
6.4.3	Effect on freshwater supply	136
6.5	Discussion	139
6.6	Conclusions.	142
7	Conclusions and Recommendations	145
7.1	Answers to the research questions	146
7.2	General conclusions	148
7.3	Recommendations for future research	150
	References	153
	Acknowledgements	179
	Curriculum Vitae	183
	List of Publications	185

SUMMARY

ESTUARINE sediment dynamics involves estuarine hydrodynamics, sediment transport, and morphology, and strongly influence ecosystem dynamics and sustainability. In the current geological epoch, referred to as the Anthropocene, human activities are exerting increasing impacts on the environment on all scales, changing hydrodynamics, sediment transport, and morphology in many ways outcompeting natural processes. For sustainable use of these impacted estuaries, human activities must be part of, or compensated by, estuarine sediment management strategies. Such management strategies must be based on detailed physical knowledge of natural sediment dynamics, and the effect of human activities thereon. The Yangtze Estuary is a system where estuarine sediment dynamics is influenced by intensive human interventions in the upstream river basin and within the estuary. This study aims to explore the changes in morphological development and tidal evolution in the Yangtze Estuary on a decadal scale. More specifically, this dissertation differentiates the effects of local engineering works and of the decline of fluvial sediment supply due to human interventions in the upstream river basin, and understand the role of sediments on hydro- and sediment dynamics in highly turbid estuaries.

Using a series of bathymetric maps from 1953 to 2016, we investigate the morphological changes in the mouth zone of the Yangtze Estuary. Both shoals in the mouth zone, i.e., the Hengsha flat and Jiudian shoal, exhibited accretion at different rates until ~2010, followed by a period of erosion since then. The Hengsha flat accreted slower than the Jiudian shoal. Moreover, the accretion in the Hengsha flat is mainly ascribed to land reclamation whereas salt marsh introduction strongly contributes to the accretion in the Jiudian shoal. Erosion in the two shoals after 2010 may be caused by the reduction in silt supply due to dam constructions in the river basin. Erosion of the entire mouth zone that occurred between 1997 and 2010 is mainly the result of local engineering works whose impact masks the impacts of the fluvial sediment decline. Our results further indicate that dredging volumes should be included in the analysis of bed level changes accounting for its large contribution (~50%) on the erosion after 2010. A response time lag of ~30 years is suggested to occur in the mouth zone to the riverine sediment decline.

The changes in tides are evaluated with the water levels observed at Xuliujing and Yanglin in 1990-1991, 2009-2010 and 2019-2020 and the yearly-averaged high and low water levels between 1996 and 2011 in seven downstream stations. Data reveal a strong reduction in tidal damping from 1990 to 2010, followed by a slightly enhanced tidal damping from 2010 to 2020 in the South Branch. The reduced tidal damping in the South Branch from 1990 to 2010 is controlled by sediment decline which induces an increase in water depth (erosion). In the mouth zone, tidal damping is enhanced from 1997 to 2010 and weakened after 2010. The change in tidal damping in the mouth zone is not as pronounced as that in the South Branch, and the effect of morphological changes is limited. We applied a two-dimensional (2D) barotropic numerical model to explore the effect of

bed friction. The model suggests a 60% increase in the effective bottom roughness from 1990 to 2010 in the South Branch, which is probably caused by the observed 80% decrease in suspended sediment concentration (SSC). This effect enhances tidal damping, which counteracts the contribution of water depth increase on amplifying tides between 1990 and 2010 and may dominate the stronger tidal damping from 2010 to 2020. In the mouth zone, the effective bottom roughness mainly becomes larger due to engineering works but may be counterbalanced by the opposite role of fluid mud formation. The influence of fluid mud may become progressively larger, leading to a decrease in friction after 2010. Overall, we have identified that the strong effects of SSC influence tidal dynamics through its impact on bed level and effective bottom roughness. The changes in tides in the South Branch are controlled by the sediment decline whereas the changes in tides in the mouth zone are still dominated by the local engineering works.

To obtain insight into the density-induced effects of SSC on hydro- and sediment dynamics in highly turbid estuaries, we set up and calibrated a three-dimensional (3D) baroclinic sediment transport model for the Yangtze Estuary. In this model, sediment transport is supply-limited implying that sediment is prescribed at the model boundaries and not as an initial condition. The computed estuarine turbidity maximum (ETM) therefore results from converging sediment transport pathways and not from local bed erosion, representing equilibrium conditions. Model results suggest that the horizontal and vertical sediment-induced density gradients have an opposite effect: the horizontal sediment-induced density gradients lead to the dispersion of the ETM and the vertical sediment-induced density gradients promote sediment trapping. Vertical sediment-induced density gradients influence trapping directly by reducing vertical mixing but also by indirectly through its effect on water levels, velocities and salinities. Furthermore, comparisons between the dry and wet seasons indicate that horizontal and vertical SSC density gradients are relatively more important under weaker and stronger salinity stratification conditions, respectively.

The effect of sediment-induced density gradients is also influenced by tidal asymmetries. To evaluate this effect, we set up a schematized model and carried out simulations with a symmetric tide and asymmetric tide prescribed at the open sea boundary. Depending on the type of tidal asymmetry (represented by the relative phase lag between semi-diurnal and quarter-diurnal tides), sediment-induced density effects strengthen or weaken the ETM due to enhanced or weakened landward tidal pumping, respectively. Higher near-bed sediment concentrations as a result of water-bed exchange processes strengthen the effect of estuarine circulation and therefore promote ETM formation, but simultaneously strengthen the divergence of sediment by tidal pumping.

We finally explore the importance of sediment-induced density effects on saltwater intrusion in the Yangtze Estuary for conditions representing climate change and human interventions (changes in river discharge, sediment supply and sea-level rise (SLR)). Changes in river discharge and SLR affect sediment trapping efficiency and ETM location, thereby influencing saltwater intrusion. Therefore the impact of future changes is influenced by the turbidity of the estuary. For realistic future scenarios, the period in which sufficient freshwater is available at a major freshwater intake (Qingcaosha reservoir), decreases by several days for sediment concentrations below $\sim 2 \text{ kg/m}^3$ but may exceed a month for sediment concentrations exceeding $10\text{--}30 \text{ kg/m}^3$. A 70% decline in the

Yangtze sediment load leads to reduced sediment concentrations in the estuary, which leads to a seaward migration of the salt wedge of ~3 km and an extension of freshwater supply period for over 2 months. A reduction in the sediment load of the Yangtze therefore mitigates saltwater intrusion and water shortage issues.

Concluding, the morphology and tides have been regulated by various human interventions in the Yangtze Estuary. The Yangtze Estuary response to human interventions varies spatially: the changes in tides, SSC, and morphology in the South Branch and mouth zone are controlled by the riverine sediment decline and local engineering works, respectively. Temporally, the short-term effects of local engineering works mask the long-term effects of riverine sediment decline (time lag effects). The response of turbid estuaries to interventions is influenced by sediment-induced density effects, introducing feedback mechanisms coupling changes in the hydrodynamics (saltwater intrusion) and sediment dynamics (ETM formation). A better understanding of the estuarine sediment dynamics in response to riverine sediment decline requires detailed monitoring and integrated studies relating the observed changes to sediment-induced feedback mechanisms controlling hydrodynamics and sediment transport.

SAMENVATTING

ESTUARIENE sediment dynamica wordt gestuurd door de waterbeweging, het sedimenttransport en de morfologie, en hebben een grote invloed op estuariene ecosystemen en duurzaamheid. In het huidige geologische tijdperk, het Anthropoceen, oefent menselijk handelen op meerdere schaalniveaus een steeds grotere invloed uit op haar omgeving en heeft een grote invloed op de waterbeweging, het sedimenttransport, en de morfologie in vergelijking met natuurlijke processen. Duurzaam gebruik van deze beïnvloede estuaria vereist dat menselijk handelen een onderdeel is van, of wordt gecompenseerd door, estuarien sedimentbeheer. Sedimentbeheer moet gebaseerd zijn op gedetailleerde kennis van de natuurlijke sedimenttransport processen, en de invloed van menselijk handelen daarop. Het Yangtze estuarium is een systeem wat sterk beïnvloed wordt door menselijke ingrepen in zowel het bovenstroomse stroomgebied als in het estuarium. De huidige studie heeft als doel om de veranderingen in morfologie en waterbeweging in het Yangtze estuarium in de afgelopen decaden te onderzoeken. Hierbij wordt specifiek ingegaan op de rol van de waterbouwkundige constructies in de vaarweg van het estuarium, van de afnemende sedimenttoevoer uit het stroomgebied als gevolg van menselijke ingrepen, en de invloed van sediment op de waterbeweging en sedimentdynamica in troebele estuaria.

Gebruik makend van historische kaarten over de periode tussen 1953 en 2016, worden de morfologische veranderingen in het mondingsgebied van het Yangtze estuarium onderzocht. De twee platen in dit mondingsgebied (Hengsha en Jiuduansha) groeien aan tot aan ~2010, waarna erosie optreedt. Hengsha plaat groeide langzamer aan dan Jiuduansha plaat. De aangroei van Hengsha plaat is sterk beïnvloed door landaanwinningen terwijl Jiuduansha plaat aangroeide door de introductie van kweldervegetatie. De erosie na 2010 wordt toegeschreven aan de afname in sedimenttransport ten gevolge van de constructie van reservoirs in het bovenstroomse stroomgebied. Het mondingsgebied erodeert vanaf 2007. Deze erosiefase wordt initieel toegeschreven aan lokale ingrepen, gevolgd door een fase waarin de afname in het bovenstroomse sedimentaanbod tot erosie leidt. Onze studie laat ook zien dat 50% van de erosie in het mondingsgebied in de periode na 2010 bestaat uit gebaggerd sediment, waardoor het betrekken van gebaggerde sedimentvolumes cruciaal is voor de analyse van bodemveranderingen. De volumeanalyse suggereert ook dat het mondingsgebied een vertragingstijd heeft van ongeveer 30 jaar om te reageren op de afname van de sedimenttoevoer vanuit de rivier.

De veranderingen in het getij worden onderzocht met waterstandsmetingen nabij Xuliujing en Yanglin in 1990-1991, 2009-2010 en 2019-2020, en met jaarlijks gemiddelde hoog- en laagwaters in 7 benedenstroomse stations over de periode 1996 – 2011. Deze data laten een sterke afname in getijdemping in de South Branch zien tussen 1990 en 2010, gevolgd door een beperkte toename in getijdemping tussen 2010 en 2020. De afname in de periode 1990 – 2010 is het gevolg van een afname in de sedimenttoevoer, wat tot erosie en daardoor een grotere waterdiepte leidt. In het mondingsgebied wordt getij-

demping versterkt in de periode 1997 – 2010, maar neemt weer af na 2010. Getijdemping veranderd veel minder in het mondingsgebied dan in de South Branch, en morfologische veranderingen hier zijn beperkt. We gebruiken een barotroop twee-dimensionaal (2D) waterbewegingsmodel om het effect van bodemwrijving te onderzoeken. Dit model suggereert dat de bodemwrijving 60% is toegenomen in de South Branch in de periode 1990 – 2010, wat waarschijnlijk wordt veroorzaakt door de waargenomen afname van 80% in de sedimentconcentratie. Deze toename in bodemwrijving versterkt getijdemping, en is daarmee tegengesteld aan het effect van verdieping door erosie op getijdemping. Tussen 1990 en 2010 is het effect van verdieping dominant, maar na 2010 lijkt de afnemende sedimentconcentratie te domineren en wordt het getij gedempt. In het mondingsgebied wordt de bodemruwheid vooral groter door lokale waterbouwkundige constructies, maar deze toename wordt tegengewerkt door de vorming van fluid mud. De steeds sterkere bijdrage van fluid mud heeft waarschijnlijk geleid tot een afname in de schijnbare bodemruwheid na 2010. In het hele estuarium zien we een aanzienlijk effect van sediment op getij via de invloed op de bodemruwheid en de bodemligging. In de South Branch domineert de afname van de sedimentconcentratie, terwijl het mondingsgebied nog steeds wordt gedomineerd door lokale waterbouwkundige constructies.

Om meer inzicht te krijgen in de dichtheidseffecten van de sedimentconcentratie op de waterbeweging en het sedimenttransport, is een drie-dimensionaal (3D) baroclien sedimenttransport model voor het Yangtze estuarium opgezet en gekalibreerd. In dit model komt sediment binnen door opgelegde sedimentconcentratie aan de randen, en niet via een initiële sedimentverdeling op de bodem. Het berekende estuariene troebelheidsmaximum (ETM) wordt daarom bepaald door convergentie van sedimenttransport en niet door lokale erosie, waardoor dit model representatief is voor evenwichtscondities. Modelresultaten suggereren dat horizontale en verticale dichtheidsgradiënten tegengestelde effecten hebben: horizontale dichtheidsgradiënten leiden tot dispersie van het ETM terwijl verticale dichtheidseffecten juist tot versterking van het ETM leiden. Verticale dichtheidseffecten beïnvloeden invang van sediment rechtstreeks door een afname van verticale menging, maar ook indirect door effecten op waterstanden, stroomsnelheden en zoutverdeling. Een vergelijking tussen het natte seizoen en het droge seizoen laten zien dat horizontale en verticale dichtheidseffecten belangrijker zijn voor respectievelijk zwakkere en sterkere zout-gelaagde toestanden.

Sediment-gedreven dichtheidseffecten worden beïnvloed door asymmetriën in het getij. Om dit effect te onderzoeken is een geschematiseerd model opgezet, waarbij zowel een symmetrisch als een asymmetrisch getij op de rand wordt voorgeschreven. Afhankelijk van het type asymmetrie (gerepresenteerd door het faseverschil tussen het M_2 getij en het M_4 getij) versterken of verzwakken sediment-gedreven dichtheidseffecten het ETM door respectievelijk versterking of verzwakking van het getij-gedreven transport. Hogere sediment concentraties aan de bodem ten gevolge van water-bodem uitwisselingsprocessen versterken het effect van estuariene circulatie en daarmee ETM vorming, maar leiden tegelijkertijd door meer divergentie door getij-gedreven sedimenttransport.

Tenslotte wordt het belang van sediment-gedreven dichtheidseffecten op zoutin-dringing onderzocht voor omstandigheden representatief voor klimaatverandering en menselijke ingrepen (veranderingen in de rivierafvoer en sedimenttoevoer, en zeespiegelstijging (ZSS)). Veranderingen in rivierafvoer en ZSS beïnvloeden sediment conver-

gentie en ETM locatie, en daardoor zoutindringing. Hierdoor wordt het effect van toekomstige veranderingen beïnvloed door de troebelheid van het estuarium. Voor realistische toekomstige scenario's neemt de periode met voldoende drinkwaterbeschikbaarheid in een belangrijk innamepunt (Qingcaosha reservoir) af met enkele dagen bij sedimentconcentraties lager dan $\sim 2 \text{ kg/m}^3$, maar dit verschil kan oplopen tot meer dan een maand voor sedimentconcentraties hoger dan $10\text{-}30 \text{ kg/m}^3$. Een afname van de sedimenttoevoer van de Yangtze rivier van 70% leidt tot een afname van de sedimentconcentratie in het estuarium, wat vervolgens leidt tot een zeewaartse verplaatsing van de zouttong met 3 km en een verlenging van de periode met voldoende drinkwaterbeschikbaarheid met 2 maanden. Een afname in de sedimenttoevoer van de Yangtze mitigeert daarom zoutindringing en drinkwatertekorten.

Samenvattend kan gesteld worden dat de morfologie en het getij van het Yangtze estuarium beïnvloed zijn door diverse menselijke ingrepen. Het effect van deze ingrepen verschilt ruimtelijk: veranderingen in de sedimentconcentratie, het getij en de morfologie in de South Branch en de mondingszone worden gestuurd door, respectievelijk, een afname in de sedimenttoevoer en lokale waterbouwkundige constructies. Het effect van deze constructies maskeert tijdelijk het lange-termijn effect van een afname in de sedimenttoevoer. De reactie van troebele estuaria op menselijke ingrepen worden beïnvloed door sediment-gedreven dichtheidseffecten, welke een terugkoppelingsmechanisme introduceren waardoor de waterbeweging (zoutindringing) gekoppeld is aan het sedimenttransport (ETM vorming). Meer inzicht in het effect van een afname van de sedimenttoevoer vanuit de rivier op estuariene sedimentdynamica vereist nauwkeurige monitoring, en geïntegreerde studies waarin deze gemeten veranderingen gerelateerd worden aan sediment-gedreven terugkoppelingsmechanismen welke de waterbeweging en sedimenttransport aansturen.

This samenvatting is translated by D.S. van Maren.

摘要

河口是陆海相互作用和人类生产生活高度密集的关键带，在全球变化环境下，其水沙动力及地貌演变过程受到人类活动的强势影响，包括流域水库群等引起的持续减沙、河口港口航道开发、围垦和生态治理等工程影响，导致河口动力-泥沙-地貌耦合系统的多重调整和适应过程，由此影响河口保护和开发利用，亟需研究河口动力地貌调整过程及作用机制。

本研究聚焦长江河口这一大型高浊度河口系统，回答河口最大浑浊带的水沙动力地貌过程对人类驱动响应机制问题，由此丰富动力-泥沙-地貌耦合系统的理论，为河口未来的可持续发展提供科技支撑。拟解决的关键科学问题是人类活动影响下河口水沙动力地貌响应特征及相互作用机制。主要研究内容包括：1) 人类驱动的长江河口水沙动力及地貌响应和转型特征；2) 认识泥沙对水动力和最大浑浊带发育的反馈机制及人类活动的重要作用。

1. 人类驱动的长江河口水沙动力及地貌响应和转型特征

河口地貌响应对减沙具有缓冲能力，拦门沙淤蚀转变滞后于流域减沙约30年。河流减沙影响的河口地貌响应变化是研究热点，但对其中地貌响应的非线性、非瞬时特征认识还很欠缺。基于长江口1953-2016年实测地形资料及近30年遥感影像，对比分析了横沙东滩和九段沙两个大型沙体年代际演变过程。发现两个沙体均维持淤涨态势至2010年，九段沙的淤涨速率高于横沙两倍以上，且九段沙呈现“长高不长大”，横沙呈现“长大不长高”的淤涨特征，两个沙体不同的淤涨速率和发育特征一方面受径流、潮流、风浪等动力差异和泥沙特性条件影响，另一方面植被引种工程和围垦工程分别对九段沙和横沙的淤涨起到了重要作用。2010-2016期间两个沙体出现冲刷态势，低潮滩的侵蚀与航道疏浚工程密切相关，高潮滩的侵蚀部分反映了对流域来沙级配的调整。长江口拦门沙对流域减沙的地貌响应存在明显时间滞后效应，且局部人类活动是引起侵蚀的重要原因。以横沙东滩、九段沙和北槽为整体，分析最大浑浊带冲淤变化，研究表明其在1997和2007年前后经历了从淤积向侵蚀的迅速转变，该转变主要由航道疏浚工程导致。2010年以后持续侵蚀，该侵蚀由流域减沙和航道工程共同导致。其中，航道疏浚的泥沙量对最大浑浊带2010年以后的侵蚀贡献了约50%。

河口潮汐存在对地形、工程和悬沙浓度等变化的复杂响应关系，体现河口动力与地貌之间的耦合调整过程。潮汐是河口的主要驱动力之一，潮汐变化可以反映河口动力地貌的调整特征。基于长江口南支及以下河段1990年以来的潮汐数据认

识到, 1990-2010年徐六泾-杨林河段潮汐衰减减弱, 水头差减小, 2010-2020年期间潮汐衰减略有增强, 水头差略有增大; 1996-2011年间, 南港(石洞口-横沙)的潮汐衰减先减弱后增强, 北槽口外(牛皮礁-绿华)的潮汐衰减经历了增强-减弱-增强的变化, 而最大浑浊带(横沙-牛皮礁)2010年以前潮汐衰减增强, 之后有减弱的趋势。结合潮动力数值模型, 发现流域减沙对南支潮汐演变控制作用, 主要包括南支侵蚀使得水深增大, 主导了1990-2010年间的潮汐衰减减弱; 南支含沙量减小幅度高达70%, 其引起的床面阻力增大约60%, 在1990-2010年间削弱了约75%由水深增大引起的潮汐衰减减弱, 且对2010-2020年潮汐衰减增强起主导作用。阻力变化控制了最大浑浊带潮汐演变, 主要包括1997-2010年间, 航道工程建设期间导堤丁坝引起的形态阻力增大阻力约40%, 导致期间潮汐衰减增强; 2010年以后阻力有减小的趋势, 这主要与浮泥形成引起的减阻效应有关, 使得潮汐衰减减弱。但近两年(2019-2020)实测最大浑浊带含沙量有明显减小的趋势, 这导致床面阻力增大, 该作用与浮泥发育减阻作用相反, 将共同影响近期潮汐演变。

2. 泥沙对水动力和最大浑浊带发育的反馈机制及人类活动的影响

揭示了高含沙水体密度效应与最大浑浊带之间的互馈作用。河口高含沙水体中的泥沙会改变水体密度及其空间梯度, 叠加盐度引起的密度梯度, 导致更复杂的水动力结构特征, 但以往对泥沙的密度梯度效应认识不足。为此基于三维水沙动力模型, 研究表明含沙量密度梯度或盐度密度梯度均能抑制紊动、减小阻力, 增大潮差, 但单一含沙量密度梯度引起的斜压力较小, 难以形成最大浑浊带。单一盐度密度梯度能产生较大的斜压力, 形成表层向海、底层向陆的垂向环流, 促进口内泥沙净输运, 利于最大浑浊带的形成。含沙量和盐度密度梯度之间的相互作用下, 产生较强的纵向及垂向含沙量密度梯度。纵向含沙量密度梯度使最大浑浊带近陆区域的斜压力增大, 促进泥沙净输运向陆, 使最大浑浊带近海区域的斜压力减小, 促进泥沙净输运向海, 抑制最大浑浊带的发育。垂向含沙量密度梯度一方面由于泥沙沉降增大底部含沙量, 增大垂线含沙量密度梯度, 另一方面促进垂向环流和盐度层化, 增大潮差和盐度, 促进盐水入侵, 并增大盐度密度梯度的作用, 进一步促进泥沙捕集, 与水动力形成正反馈作用, 促进最大浑浊带的发育。

阐明了泥沙特性、潮汐不对称和床面泥沙交换对含沙量密度作用的影响。通过三维水沙动力概化模型, 采用悬沙机制分解法, 解析了口内泥沙净输运的主要控制机制。阐明泥沙粒径通过影响沉降速度影响最大浑浊带的位置, 床面临界切应力主要影响最大浑浊带含沙量的量级。发现含沙量密度梯度通过改变河口环流和潮泵效应的相对大小, 影响最大浑浊带。主要表现为含沙量密度梯度增强河口环流对口内泥沙净输运的贡献, 促进最大浑浊带核心区向口内移动, 当泥沙为细颗粒时, 该作用涨憩时间占优较涨潮流速占优更为显著; 其对潮泵效应的改变受潮汐不对称影响, 并控制最大浑浊带的发育; 当潮泵效应被削弱时, 核心区含沙量量级减小, 抑制最大浑浊带的发育, 反之则促进最大浑浊带发育。床面交换引起的底部含沙量浓

度升高,进一步增强含沙量密度梯度作用,使得河口环流强于潮泵效应,主导口内泥沙净输运。

分析了人类活动和气候变化影响下,含沙水体密度效应对盐水入侵的重要作用。人类活动和气候变化改变流域水沙和海域潮汐特征,影响盐水入侵,其中泥沙起到了重要的桥梁作用。上述结果表明,含沙量密度梯度作用促进盐水入侵,本文进而考虑径潮流相互作用对含沙量密度梯度的影响,模型结果表明,洪季,垂向含沙量密度梯度起主导作用,其控制最大浑浊带含沙量量级;枯季,纵向含沙量密度梯度起主导作用,其控制最大浑浊带范围。针对最大浑浊带含沙量量级与盐水入侵的关系问题,发现泥沙密度效应影响加剧盐水入侵的强度:最大浑浊带底部含沙量约 2 kg/m^3 时,盐水入侵基本不受泥沙密度影响,底部含沙量增大至高于 $20\text{-}30\text{ kg/m}^3$ 后,盐水入侵加剧明显,年取水天数可缩短数月。因此,人类活动和气候变化通过改变来水来沙条件调节最大浑浊带的发育,不同程度地影响盐水入侵;流域减沙70%使河口含沙量降低的同时,有缓解盐水入侵的作用。

综上所述,人类驱动的长江河口潮汐、含沙量和地貌,对流域减沙具有空间分段响应的特征,且最大浑浊带含沙量和地貌响应表现出明显的时间滞后。通过数学模型深入研究了动力-泥沙-地貌的耦合作用机制,包括含沙量对水动力和最大浑浊带发育的反馈机制和影响条件,分析了不同人类活动,特别是流域减沙影响下最大浑浊带的发育对盐水入侵的作用,加深了对人类驱动的河口水沙动力及地貌演变规律和控制机制的认识,对河口可持续发展具有重要意义。本文模型研究简化了床沙供给、泥沙组分、风浪和沿岸流等因素,未来还需关注这些因素以及河口不同区域和整体的演变特征及差异性;加强观测,确定河口演变的短期波动和长期趋势。

关键词: 动力地貌,水沙相互作用,潮汐演变,最大浑浊带,长江口,流域减沙,数学模型

1

INTRODUCTION

*A journey of thousands of miles may not be achieved
through accumulation of each single step,
just as the enormous ocean may not be formed
gathering every brook or stream.*

不积跬步，无以至千里
不积小流，无以成江海

Xun Zi (Confucian, 313 B.C.-238 B.C.)



1987: Yangtze Estuary, China

1.1. ESTUARINE SEDIMENT DYNAMICS

1.1.1. GENERAL DESCRIPTION OF ESTUARY, ETM AND MOUTH BAR

ESTUARIES are dynamic and vulnerable regions where rivers meet the sea and where freshwater and saltwater interact. The definition of an estuary, probably the most widely recognized, is 'a semi-enclosed coastal body of water, which has a free connection with the open sea, and within which sea water is measurably diluted with freshwater derived from land drainage' (Pritchard, 1967). Typically, the term defined by Pritchard (1967) is called a tidal estuary excluding the tidal river which is tidally influenced but the water is entirely fresh (Fairbridge, 1980). This thesis works with the upstream limit of tidal penetration, not salt penetration and adopts the following definition (Wolanski and McLusky, 2011):

an estuary is an inlet of the sea reaching into a river valley as far as the upper limit of tidal rise, usually being divisible into three sectors: (1) a marine or lower estuary, in free connection with the open sea; (2) a middle estuary subject to strong salt and freshwater mixing; and (3) an upper or fluvial estuary, characterized by freshwater but subject to strong tidal action. The limits between these sectors are variable and subject to constant changes in the river discharges.

Estuaries can be classified as: 1) micro-tidal (0-2 m), meso-tidal (2-4 m) and macro-tidal (>4 m) based on the tidal range (Davis, 1964; Hayes, 1975); 2) river-dominated, tide-dominated and wave-dominated in terms of dominant hydrodynamic process (Galloway, 1975) and 3) stratified, partially mixed, and well-mixed regarding the vertical structure concerning the mixing between the saltwater and the freshwater (Prichard, 1955; Dyer, 1997). This thesis focuses on meso-tidal, combined river and tide-dominated, and partially-mixed estuaries characterized by strong river and tidal forcing.

Sediment in the estuary originates either from the river or the sea, transported into the estuary by the unidirectional or bidirectional current. The sediment comes into estuaries in varying grain size from gravel (>2 mm) and coarse sand to clay (<2 μm) and is filtered into the estuary (Schubel and Carter, 1984). Sediment transport can be distinguished as bedload transport and suspended load transport (Dyer, 1986; Van Rijn, 1993). In the first case, the particle stays in contact with the bed at most of the time and its motion is conducted by rolling, sliding and saltating over the bed within a thin boundary layer. In the second case, a sediment particle is maintained in suspension by turbulence in the flowing water for a considerable period of time without contacting the bed. Sediment starts moving when the bed shear stress exceeds a critical threshold (erosion) and settles down to the bottom under the influence of the gravitational force (deposition). Due to advective and diffusive processes, the initial location and the deposition location of an individual sediment particle are usually different, resulting in net sediment transport in estuaries. Various mechanisms are responsible for the landward sediment transport (elaborated below) balancing the seaward river flow, leading to sediment accumulated in specific regions, called estuarine turbidity maximum (ETM) (Figure 1.1). An ETM is defined as a region along an estuary with a localized maximum in tidally and cross-sectionally averaged SSC (Burchard et al., 2018). The elevated suspended sediment in the ETM deposits on the bed of the estuary, resulting in high accumulation rates and therefore siltation and formation of mouth bars (Figure 1.1).

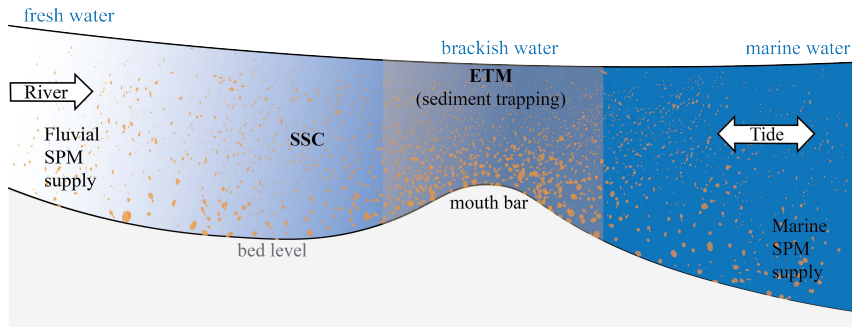


Figure 1.1: Sketch of the estuary, estuarine turbidity maximum (ETM) and mouth bar. SSC: suspended sediment concentration.

Understanding estuarine sediment dynamics is extremely important because of the impact on light penetration and thereby primary production, pathways for adsorbed contaminants, and rates of accretion and erosion and associated bathymetric evolution. More importantly, natural and human-driven forcing have been changing throughout the world, which may inevitably influence the estuarine sediment dynamics, leading to possible regime shift. Therefore, understanding estuarine sediment dynamics is of critical importance on its social, economic and ecological values and implications.

1.1.2. CHARACTERISTICS OF SUSPENDED SEDIMENT

Suspended sediment concentration (SSC) varies from several mg/l to over 100 g/l. The large range of SSC exerts different behavior of the sediment-fluid mixture (Figure 1.2). For low sediment concentrations (<1 g/l), fine sediments can form flocs under simultaneous aggregation and breakup processes known as *flocculation*. Flocs tend to have larger settling velocities, influencing the vertical distribution of SSC. For very high sediment concentrations (>100 g/l), sediments form a space-filling network, called *gelling*. A typical value of the gelling concentration for clay-dominated suspensions is 100 kg/m³. At or above the gelling concentration, the suspension starts to behave more like a solid.

For sediment concentrations of the order of 100 mg/l-100 g/l, sediments significantly affect the density of the suspension. *High concentration mud suspensions* (HCMS) is a suspension of cohesive sediment at a concentration of a few 100 to a few 1,000 mg/l (Winterwerp, 1999; Winterwerp and Van Kesteren, 2004). The suspension behaves Newtonian and, most importantly, the suspension interacts with turbulent flow, i.e. the vertical concentration gradients affect the flow motion through the suppression of turbulence, leading to less friction experienced by the flow and less mixing of the water column. Another important feature of HCMS is *hindered settling*, leading to a reduction of effective settling velocity (Richardson and Zaki, 1954). Hindered settling is caused by the influence of neighboring particles on the settling velocity of an individual particle within suspension under high concentrations. *Fluid mud* (in the order of several 10 to 100 g/l) is a term that is not unambiguous, but differently from HCMS, as it exhibits non-Newtonian behavior and is either stationary or moving. This thesis focuses on HCMS (although including low concentrations as well).

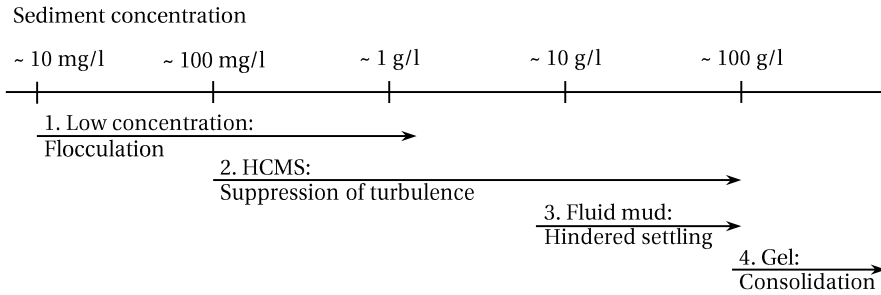


Figure 1.2: Range of sediment concentration with names and characterizing physical processes of four intervals, from [Dijkstra \(2019\)](#). HCMS: high concentration mud suspensions.

1.1.3. HYDRO-MORPHODYNAMIC INTERACTIONS

Estuarine sediment dynamics involves a series of hydro-morphodynamic interactions between river and tidal currents, SSC, salinity and morphology (Figure 1.3). Currents suspend sediments (①), influencing the morphology through deposition (②). The morphology in turn influences the flow velocity (③). These three processes (①②③) form a morphodynamic feedback loop. In estuarine systems, the current modifies salinity (④) whereas salinity in turn influences currents through damping of turbulence (⑤). In this thesis, we explore additional interactions. Sediments influence the current through damping of turbulence – although building on previous work, this thesis provides various novel contributions to this topic (⑥). We also explore large-scale impacts of water-bed exchange processes on ETM dynamics, particularly focusing on sediment deposition (②) which is a topic that has received very little scientific attention. And finally, this thesis explores the impact of sediments on saltwater intrusion (⑦), which has not yet been described in literature. More subtle interactions not addressed in this thesis are the effect of salinity on SSC through flocculation (⑧) and on morphology through biochemical processes related to biota (⑨).

1.1.4. SEDIMENT TRAPPING

Sediment trapping is often associated with the formation of an ETM characterized by elevated near-bed SSC. An ETM results from sediment convergence, with especially the up-estuary transport component resulting from a range of mechanisms (see recent overviews by e.g. [Winterwerp, 2011](#); [Burchard et al., 2018](#); [Dijkstra, 2019](#)). The main up-estuary transport mechanisms are elaborated in more detail below:

ESTUARINE CIRCULATION

Classically, estuarine circulation has been attributed to gravitational circulation ([Festa and Hansen, 1978](#)). However, they are not identical ([Burchard and Hetland, 2010](#); [Cheng et al., 2011](#); [Burchard et al., 2011](#); [Geyer and MacCready, 2014](#)). Gravitational circulation (or exchange flow) is related to the along-channel salinity gradients generating a landward residual current near the bottom and a seaward current near the surface. This two-layer circulation is also known as baroclinic circulation and results in upstream sed-

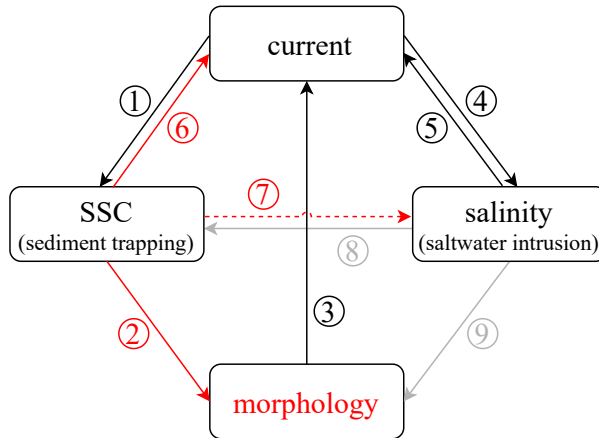


Figure 1.3: Sketch of physical processes describing the interactions between current, suspended sediment concentration (SSC), salinity and morphology. The interactions in black indicate processes which are used but not improved, the grey interactions are ignored, whereas this thesis advances our knowledge on the red interactions. The dashed line indicates the impact of SSC on salinity through current.

iment transport as the sediment concentration is usually larger near the bed. Other processes which cause net landward transport and are strongly related to salinity (regarded as classical processes in [Dijkstra, 2019](#)) are classified as estuarine circulation in this thesis: 1) the effect of turbulence damping by salinity gradients further concentrates sediments near the bed, leading to stronger transport by gravitational circulation and a more intense ETM [Geyer \(1993\)](#); 2) tidal variations in salinity stratification and therefore variations in turbulence, known as strain-induced periodic stratification (SIPS) or tidal straining ([Simpson et al., 1990](#)), amplify the gravitational circulation ([Jay and Musiak, 1994](#)); 3) the strong vertical mixing asymmetry between ebb and flood resulting from tidal straining also strengthens gravitational circulation ([Jay and Musiak, 1994, 1996](#)).

Note that the estuarine circulation can be also caused by other processes (e.g. wind-induced tidal straining); however, they are not necessary to cause net landward sediment transport and thus are excluded or classified as other processes. In addition, lateral estuarine circulation associated with lateral depth variations, curvature, density gradients, winds, Coriolis may be also important but its magnitude is often smaller than that in the longitudinal direction.

TIDAL PUMPING

Tidal pumping is an ambiguous term that has been used to describe a variety of tide-influenced residual transport processes. The description and classification proposed by [Dijkstra \(2019\)](#) are adopted here: tidal pumping is the tidal covariance of the flow velocity and sediment concentration which can be subdivided into two main contributions:

- Temporal asymmetries (i.e., differences during ebb and flood)
 - Temporal asymmetries in flow velocity and water level: tidal asymmetry (see

Friedrichs, 2011).

- Tidal asymmetries in sediment concentration: tidal variation in the settling velocity; sediment mixing asymmetry due to tidal straining (Burchard and Baumert, 1998; Scully and Friedrichs, 2003); tidally variations in sediment stratification or *mud-induced periodic stratification* (MIPS, Becker et al., 2018); asymmetry in the availability of erodible sediment, known as scour lag (Dyer, 1997).
 - Effect of inertia on the SSC: temporal settling lag (Groen, 1967).
- Spatial gradients in flow velocity, water level, SSC and sediment availability: spatial settling lag (Postma, 1954; Van Straaten and Kuenen, 1957).

OTHER PROCESSES

A variety of additional processes have been identified which may also contribute to net landward sediment transport, such as wind-induced tidal straining (Scully et al., 2005; Burchard and Hetland, 2010), along-channel non-linear advective processes (Li and O’Donnell, 2005), flow generated by channel curvature (Chant, 2002), flow generated by Earth’s rotation (Huijts et al., 2006), sediment-induced density effect (Winterwerp, 1999; Talke et al., 2009b), eddy viscosity-shear covariance (ESCO) circulation (Burchard et al., 2013; Dijkstra et al., 2017) and along-channel differences in sediment properties (e.g. settling velocity) (Donker and de Swart, 2013).

1.2. ESTUARINE RESPONSE: CHALLENGES

1.2.1. HUMAN INTERVENTIONS

ESTUARIES are some of the most dynamic sedimentary environments. They are of special concern because the associated deltas support large populations with large growing cities. However, estuarines are vulnerable to human interventions and global changes, e.g. sediment decline, deepening and sea level rise, which may potentially influence estuarine sediment dynamics in recent and future development (Renaud et al., 2013; Wang et al., 2015).

Sediments in an estuary largely depend on a permanent supply of sediments in order to maintain ETM, delta shoreline position and to balance subsidence. However, over 70% of the world’s deltas had experienced a reduction in fluvial sediment discharge (Figure 1.4). More recently, sediment supply in some estuaries has further shifted from a surplus to a shortage, e.g., the Parana, Limpopo, Vistula and Fly Estuary, or the sediment decline has accelerated, e.g., the Yangtze Estuary (Yang et al., 2020). Although the present-day sediment discharge has increased in several estuaries, sediment decline is still a worldwide issue (see reviews on changes in fluvial sediment supply by e.g. Syvitski et al., 2009; Dunn et al., 2019; Besset et al., 2019; Li et al., 2020a; Yang et al., 2020).

Deepening projects and associated dredging and dumping activities also take place in many estuaries in the past decades to centuries to accommodate larger ships, which may subsequently influence estuarine sediment dynamics. A positive feedback between deepening and higher SSC has been hypothesised (Figure 1.4, Winterwerp and Wang,

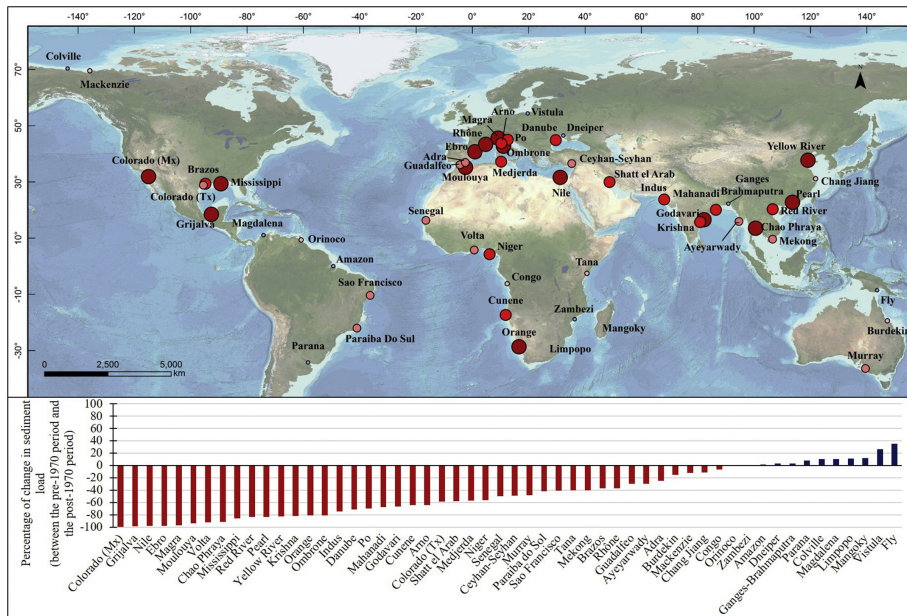


Figure 1.4: Map and graph showing the percentages of loss of fluvial sediment load between the pre-1970 period and the period 1970-2014 in 54 deltas, from [Besset et al. \(2019\)](#).

2013). According to the hypothesis, deepening leads to tidal amplification, which benefits sediment trapping, causing higher SSC. The higher SSC induces a reduction of hydraulic drag, further resulting in tidal amplification. Therefore, a positive feedback occurs and may lead to a regime shift into hyperturbid conditions. It is noted that this feedback can work as a snowball effect and may occur already at SSC of several 100 mg/l ([Winterwerp et al., 2009](#)).

1.2.2. IS THERE A REGIME SHIFT IN THE YANGTZE ESTUARY?

Regime shift is a term that has not yet reached a common definition but has been described in lots of research. For instance, a ‘regime’ implies a characteristic behavior of a natural phenomenon (sea level pressure, recruitment, etc.) over time; a ‘shift’ suggests an abrupt change, in relation to the duration of a regime, from one characteristic behavior to another ([Hare and Mantua, 2000](#)). It can be described as a smooth, abrupt and discontinuous function of changing external conditions and can indicate changes abruptly from one stable state to another that might be difficult to reverse ([Scheffer et al., 2001](#); [Scheffer and Carpenter, 2003](#); [Scheffer et al., 2009](#)). [Lees et al. \(2006\)](#) highlighted that a ‘standard’ definition of a regime shift should include sudden, high-amplitude, infrequent events, which are detectable in multiple aspects of the physical and biological components and on large spatial scales. Regime shifts are abrupt, substantial and persistent changes in the state of natural systems ([Reid et al., 2016](#)).

It should be noted that regime shifts have been mainly identified in climate change and ecology and less documented in estuarine sediment dynamics (Table 1.1). This the-

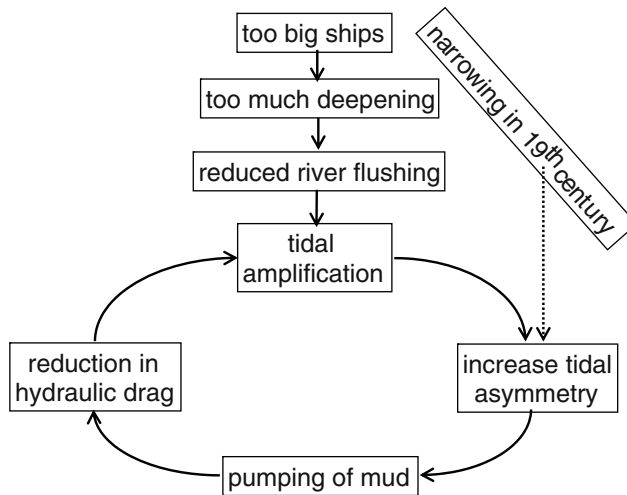


Figure 1.5: Conceptual positive feedback loop in the case of channel deepening, from [Winterwerp and Wang \(2013\)](#).

sis focuses on estuarine sediment dynamics, therefore regime shifts are described as ‘a shift from one dynamic regime (morphodynamic equilibrium state) to another, which is influenced by global environmental changes and human interferences’ and ‘is characterized by a *tipping point* in the forcing factors beyond which the estuary loses its natural characteristics, thereby endangering the environmental sustainability. In some cases, such a change becomes irreversible if a tipping point is exceeded’ ([Wang et al., 2015](#)). Morphodynamic equilibrium is a common concept in the field of morphodynamics describing specific conditions of the system mass balance that lead to no net sedimentation or erosion. Various types of morphodynamic equilibrium exist, as recently reviewed by [Zhou et al. \(2017\)](#): 1) static equilibrium (no sediment is transported); 2) dynamic equilibrium of type I (sediment is transported but the bed level locally does not change) and 3) dynamic equilibrium of type II (whilst the bed may adjust locally to accommodate the changing conditions, there is no net change when considered in the relevant frame of reference and integrated over a suitable timescale). A tipping point is defined as a breakpoint between two regimes or states which is reached when major and controlling variables of a system no longer support the prevailing system and the entire system shifts to a different state which is distinct from the previous state and recognizable with specific characteristics ([Renaud et al., 2013](#)).

The Yangtze Estuary is a typical large-scale estuary characterized by a high sediment concentration in the ETM with extensive deepening within the estuary. These human interventions may trigger a regime shift (in sediment concentration) to a high turbidity with strong tidal amplification; however, the reduced sediment supply may also induce a shift to a low turbid and weakly amplifying tidal system opposite to the former case. Moreover, the reduced sediment supply has resulted in erosion in the inner estuary (e.g. [Luan et al., 2016](#)) and the subaqueous delta (e.g. [Yang et al., 2011](#)) but not in the mouth

zone. Whether the regime shift (in morphology) towards to a new morphodynamic equilibrium occurs in the mouth zone is also unknown. As a consequence, the estuarine sediment dynamics in the Yangtze Estuary in general, but especially the impact of human interventions therein needs to be better understood.

Table 1.1: Identified regime shift: examples and evidences.

Regime shift	Examples	Evidence	References
Climate change	San Francisco Bay, USA	Changes in atmosphere pressure and wind patterns, ocean temperature, and biological productivity Shifts in the timing of phytoplankton phenology Toward increasingly high precipitation associated with tropical cyclones over the last 120 year	Lehman, 2000
	Gyeonggi Bay, Korea North Carolina, USA		Cloern and Jassby, 2012 Jahan and Choi, 2014 Paerl et al., 2019
Ecology (more examples can be referred to Folke et al., 2004 and https://www.resalliance.org/tdb-database)	Gulf of Alaska, USA North Sea	Reorganization of community structure From individual species to key ecosystem parameters (diversity)	Anderson and Piatt, 1999 Beaugrand, 2004
	Brackish Lagoons, Denmark	From clear to turbid at high nutrient concentrations	Jeppesen et al., 2007
	Ringkøbing Fjord, Denmark	From a bottom-up controlled turbid state to a top-down controlled clear-water state	Petersen et al., 2008
	Gironde estuary, France	Changes in both the physical and chemical environments and pelagic communities (plankton and fish)	Chaalali et al., 2013
	Chesapeake Bay, USA Australia	higher susceptibility to hypoxia Temperate reef communities lost their defining kelp forests and became dominated by persistent seaweed turfs	Chevillot et al., 2016 Liu and Scavia, 2010 Wernberg et al., 2016
Sediment concentration	Ems estuary, Netherlands-Germany; Loire estuary, France	From low-turbidity conditions with weak tidal amplification to high-turbidity conditions with strong tidal amplification	Winterwerp, 2011 Winterwerp and Wang, 2013
			Winterwerp et al., 2013 de Jonge et al., 2014 van Maren et al., 2015b Dijkstra et al., 2019a,b
Morphology	Western Scheldt, Netherlands	New morphological equilibrium with larger depth Transition from developing to declining phase of a bifurcation	De Vriend et al., 2011
	Yangtze Estuary, China		Wang et al., 2015 Wang et al., 2015

1.3. OBJECTIVES AND RESEARCH QUESTIONS

FOLLOWING from section 1.1 and section 1.2, two important challenges in the Yangtze estuary are related to the complex role of sediments on hydrodynamics (and resulting on salinity and morphology), and the role of human interventions on sediment dynamics (and to what extent this may lead to a regime shift). These challenges are addressed in this thesis through two main aims:

- **To identify if human interventions have triggered regime shifts in the Yangtze Estuary**
- **To understand the effect of SSC on hydrodynamics (including saltwater intrusion) under current and future conditions**

To achieve these aims, a number of research questions are formulated:

- (1) *What are the decadal morphological changes in the mouth zone of the Yangtze Estuary in response to a reduced sediment supply?*

Understanding the morphological time scales of the response of the mouth zone to reduced sediment supply is of critical importance. However, this assessment is complex because estuarine morphological development is simultaneously impacted by local engineering works including dredging and dumping activities, land reclamation and salt marsh introduction. Based on measured data, we aim to examine and understand morphological changes of the mouth zone in response to these various mechanisms and identify time scales of the response to these interventions.

- (2) *What is the tidal evolution in response to morphological and sedimentary changes in the Yangtze Estuary?*

Tidal evolution is influenced by both bathymetric and sedimentary changes and human interventions simultaneously alter tide, sediments and morphology. In addition, they interact with each other from the interplay identified earlier (Figure 1.3). Using a numerical model, we investigate the effect of morphological changes as well as sediment-related changes in hydraulic friction to understand how changes in sediment loads and human interventions have influenced tidal dynamics in the Yangtze Estuary.

- (3) *How does the high suspended sediment concentration interact with hydrodynamics and in turn influence the estuarine turbidity maximum?*

High SSC influences tidal amplification through reduced hydraulic drag and thereby influences the formation of an ETM. However, how the small-scale interaction processes between sediment and hydrodynamics influence large-scale ETM behavior still remains insufficiently understood. Particularly, high SSC may induce strong density gradients (comparable to the salinity-induced density gradients), generating mechanisms that profoundly influence large-scale ETM dynamics.

- (4) *What are the roles of tidal asymmetry and sediment-induced density effects on the formation of the estuarine turbidity maximum?*

Though the effects of tidal asymmetry on the formation of an ETM are well-known, sediment-induced effects are rarely explored. For instance, sediment properties and sediment-induced density effects, and water-bed exchange processes may play different roles in the formation of ETM. It is therefore important to systematically explore the sediment-induced effects combined with tidal asymmetries to understand their relative contribution.

- (5) *How do sediment-induced density effects influence the predicted impact of global change?*

Sediments influence ETM dynamics. Climate change may drive a change in river discharge, sediment load as well as sea-level rise, which also impacts sediment dynamics. Properly addressing the effect of climate change on the Yangtze Estuary requires a methodology accounting for these sediment effects. We therefore use a three-dimensional (3D) model accounting for these sediment effects to explore scenarios with varying river and sediment discharges and sea-level rise on estuarine sediment dynamics and salt intrusion.

1.4. OUTLINE OF THIS THESIS

The thesis has seven chapters (Figure 1.6). Chapter 1 and Chapter 7 are introduction and conclusions, respectively. Chapter 1 presents an overview of estuarine sediment dynamics, the challenges of understanding estuarine response due to human-driven forcing and research questions. Chapter 7 provides conclusions and suggestions for future research. The main body includes two parts:

- (1) Observations in the Yangtze Estuary (Chapters 2 & 3)

This part aims **to identify if human interventions have triggered regime shifts in the Yangtze Estuary** based on observed morphological changes, SSC, and tidal water levels. Decadal morphological changes, interpreted from bathymetry maps which are easier accessible than SSC, affect the decadal changes in tidal water levels (③), see Figure 1.3 and thereby the SSC (①). Therefore, we firstly examine the decadal morphological changes in the mouth zone in response to reduced sediment supply and local engineering works in Chapter 2 (research question 1). Then, Chapter 3 deals with the decadal tidal changes using tidal water levels. The mechanisms responsible for the decadal tidal changes are explored in terms of the effects of morphological changes (③) and sedimentary changes (⑥) with a two-dimensional (2D) model (research question 2). The 2D model accounts for the sedimentary changes including the density effects and bed characteristics etc. via the effective bottom roughness. The sediment-induced density effects on hydrodynamics (⑥) are further explored using 3D models in the second part.

- (2) Estuarine sediment dynamics (Chapters 4, 5 and 6)

The second part aims **to understand the effect of SSC on hydrodynamics (including saltwater intrusion) under current and future conditions**. Chapter 4 & 5 look into the effect of sediment-induced density gradients on hydrodynamics including velocity, water level and salinity (⑥④) and the processes concerning the relative

contribution of estuarine circulation and tidal pumping, respectively. In Chapter 4, we evaluate the effects of the longitudinal and vertical density gradients on ETM formation using a 3D model of the Yangtze Estuary (research question 3). Chapter 5 is about different roles of tidal asymmetry (①) and sediment-induced effects, i.e., sediment-induced density effect (⑥) and water-bed exchange processes (②), on the formation of ETM based on a schematized 3D model (research question 4). Chapter 6 evaluates future conditions for the effects of the changes in river discharge, sediment supply and sea-level rise on saltwater intrusion (⑦), particularly focusing on the importance of sediment dynamics (research question 5).

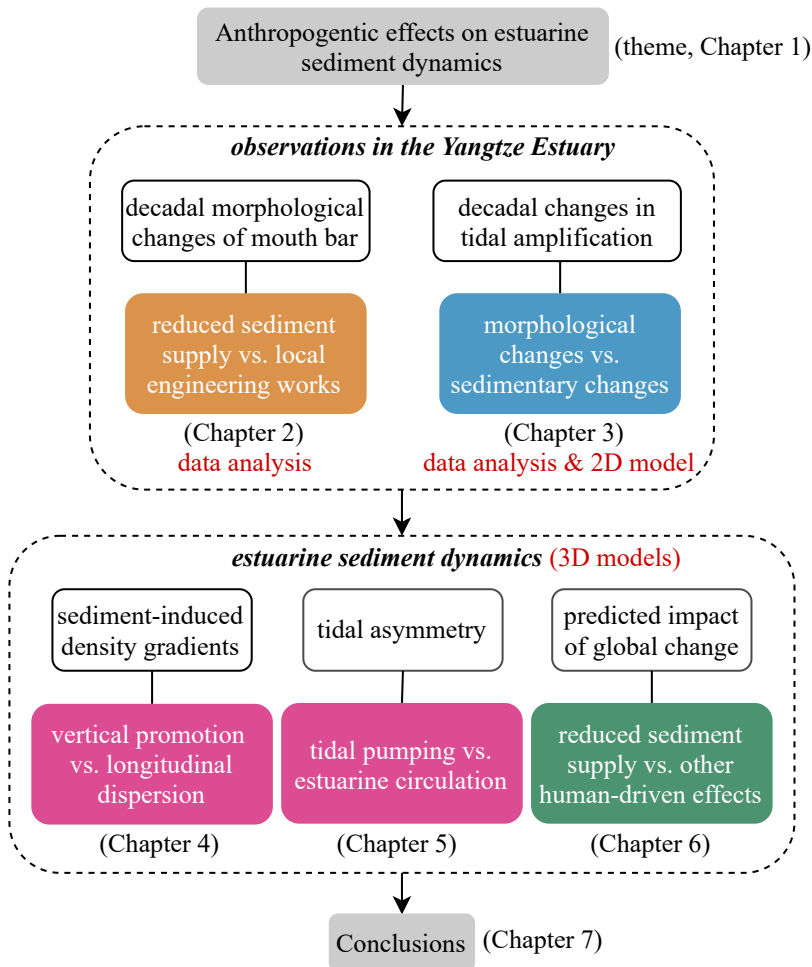
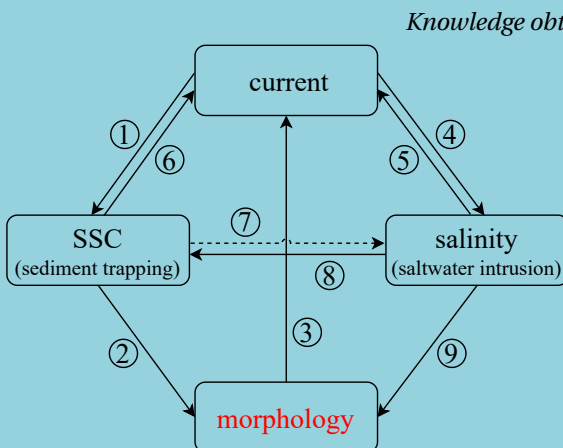


Figure 1.6: An overview of the content and structure of this thesis.

2

DECADAL MORPHOLOGICAL EVOLUTION OF THE MOUTH ZONE OF THE YANGTZE ESTUARY IN RESPONSE TO HUMAN INTERVENTIONS



*Knowledge obtained on the papers always feel shallow,
must know this thing to practice.*

纸上得来终觉浅
绝知此事要躬行

Lu You (Poet, 1125-1210)

This chapter focuses on the content in red and is largely based on the publication:

Zhu, C., Guo, L., van Maren, D.S., Tian, B., Wang, X., He, Q. and Wang, Z.B., 2019. Decadal morphological evolution of the mouth zone of the Yangtze Estuary in response to human interventions. *Earth Surface Processes and Landforms*. 44(12), pp.2319-2332.

The morphology of the Yangtze Estuary has changed substantially at decadal time scales in response to natural processes, local human interference and reduced sediment supply. Due to its high sediment load, the morphodynamic response time of the estuary is short, providing a valuable semi-natural system to evaluate large-scale estuarine morphodynamic responses to interference. Previous studies primarily addressed local morphologic changes within the estuary, but since an overall sediment balance is missing, it remains unclear whether the estuary as a whole has shifted from sedimentation to erosion in response to reduced riverine sediment supply (resulting from, e.g., construction of the Three Gorges Dam). In this work, we examine the morphological changes of two large shoals in the mouth zone (i.e., the Hengsha flat and the Jiudian shoal) using bathymetric data collected between 1953 and 2016 and a series of satellite images. We observe that the two shoals accreted at different rates before 2010 but reverted to erosion thereafter. Human activities such as dredging and dumping contribute to erosion, masking the impacts of sediment source reduction. The morphodynamic response time of the mouth zone to riverine sediment decrease is further suggested to be ~30 years (starting from the mid-1980s). Accounting for the different adaptation time scales of various human activities is essential when interpreting morphodynamic changes in large-scale estuaries and deltas.



2.1. INTRODUCTION

MANY river deltas are densely populated and connected to the sea by tidal channels, which are progressively deepened to provide access to increasingly larger vessels. Sustainable management of such systems (maintaining ecological and recreational functions while allowing economic development) requires in-depth understanding of estuarine and deltaic morphological changes, especially in view of projected sea level rise. Riverine sediment supply plays an important role in controlling the morphological evolution of many estuaries. The suspended sediment load of rivers has globally declined due to dam construction and soil conservation (Vörösmarty et al., 2003; Syvitski and Saito, 2007; Walling, 2009). Simultaneously, local engineering works (e.g., construction of training walls and jetties; dredging and dumping activities) influence channel and shoal morphology (Sherwood et al., 1990; Thomas et al., 2002; Lane, 2004; Blott et al., 2006; De Vriend et al., 2011; Wang et al., 2015). Since many of these human activities take place concurrently, isolating the morphodynamic impacts of individual human interventions (including sediment supply reduction) from natural morphological evolution is challenging.

The Yangtze Estuary (YE) in China is a large-scale alluvial system whose morphology is influenced by a significant reduction in sediment supply and extensive local human activities. River-borne sediment discharges initially decreased gradually since the mid-1980s but accelerated to the present-day amount of ~70% due to the Three Gorges Dam (constructed in 2003; Yang et al., 2015; Luan et al., 2016; Zhao et al., 2018). Fine sands and silts are mainly trapped in the upstream reservoirs, whereas clay particles are flushed downstream (van Maren et al., 2013). Such a reduced sediment supply is expected to decrease deposition rates and possibly even lead to erosion along the sand-dominated riverbed and in the silt-dominated estuary. Previous work (Table S2.1 and Figure S2.1) suggests that the inner estuary has indeed eroded in the past decade. The inner estuary includes the South Branch, South Channel and North Channel (Figure 2.1), which is mainly controlled by upstream river and sediment discharge (e.g. Luan et al., 2016; Zhao et al., 2018). Erosion has also been observed in the subaqueous delta (e.g. Yang et al., 2003, 2011, 2018). In contrast, investigating a larger part of the subaqueous delta, Dai et al. (2014) concluded that the delta was still depositional (at least until 2009). This discrepancy probably results from the definition of the study area: Yang et al. (2011) investigated the delta front (depths from 5-10 m to 15-30 m) and prodelta (depths > 15-30 m), whereas Dai et al. (2014) also included the delta plain (depths < 5-10 m), which lies in the mouth zone. The mouth zone is a region under combined river and tidal forcing, where accretion continued for a long time (Wang et al., 2013; Luan et al., 2016; Zhao et al., 2018). Interestingly, erosion of the mouth zone has been detected very recently (Zhao et al., 2018), suggesting that the subaqueous delta as a whole may indeed revert to erosion. These studies highlight the need for further study of the mouth zone, where the morphological response time may be much longer than those in the inner estuary and subaqueous delta.

At a smaller spatial scale, the shoals and tidal flats in the mouth zone are accreting, including the eastern Chongming flat (Yang et al., 2008), Nanhui shoal (Wei et al., 2017; Fan et al., 2017), Jiudian shoal (Gao et al., 2010; Wei et al., 2015; Li et al., 2016a) and Hengsha flat (Wei et al., 2015). Although the accretion rates of some shoals and tidal flats

typically decrease (Yang et al., 2008; Wei et al., 2015), erosion has not yet been observed. As a result, it remains unclear whether the mouth zone is presently eroding or deposition still prevails.

Additionally, the mechanisms controlling bathymetric evolution remain unclear. Erosion in the subaqueous delta has been attributed to a reduction in riverine sediment supply (Yang et al., 2003, 2011). In addition, the subaqueous delta of the YE has a transition from the gentle delta plain to the steep delta front at depths of 12–15 m, which is called a rollover point (Hori et al., 2002; Eidam et al., 2017). Such a rollover depth along with waves may also contribute to subaqueous erosion, resulting in coarsening of sediment in the subaqueous delta (Luo et al., 2017; Yang et al., 2018).

Local human activities additionally drive morphological changes in the YE (see e.g. Wang et al., 2015). A major intervention was engineering work in the North Passage (NP), involving the construction of a nearly 50 km-long double training wall with groins (see Figure 2.1). The jetties and groins in the NP are so large that they may induce severe erosion in the mouth of the NP and in the region to the east of Hengsha flat (Zhu et al., 2016). The jetties partially block regional horizontal circulation (Zhu et al., 2016), possibly leading to sediment deposition and accretion over the surrounding flats. In addition, intense dredging and dumping activities take place in the NP. Despite the large dredging effort (~70 million m³/year; Wang et al., 2015), this sediment mass is not accounted for in previous estimates of the estuarine sediment balance.

Overall, it therefore remains unclear (1) whether the mouth zone of the YE is still accreting or has become erosive and (2) what the impacts of local human interventions and reduced sediment supply are and at what time scales they operate. We perform an in-depth analysis of bathymetric changes in the mouth zone using all high-quality bed level data available (covering a period of ~60 years until 2016) and relate these observations to changes in sediment supply, regional engineering works and salt marsh growth. The eastern Chongming flat, which lacks data in its northern part (see Figure S2.2) and has a long history of reclamation (since the early 1960s), is omitted from this study. Our study area includes the Hengsha flat, the Jiudian shoal and the NP landward of the 10 m isobaths in 1997, constituting a total area of approximately 1,740 km² (Figure 2.1). The data, including bathymetric maps (1953–2016), are used to provide an overview of the erosion and deposition patterns as well as the long-term hypsometry changes. Satellite images (1985–2016) are employed to study the evolution of the tidal flats and the interactions between morphology and vegetation.

2.2. DATA AND METHODS

2.2.1. STUDY AREA

THE Yangtze River is one of the largest rivers in the world in terms of its length (~6,300 km) and catchment area (~1.9 million km²). The Datong station, ~640 km landward of the river mouth, is the tidal wave limit in the dry seasons. Here, the mean river discharge is 28,200 m³/s, and the annual suspended sediment load is 364 million tons per year from 1951 to 2016. The river-supplied sediment has stimulated rapid infilling of the pre-incised river valley and build-up of the delta since the mid-Holocene (since ~7,500 years ago). In the past 60 years, the river discharge at Datong has remained sta-

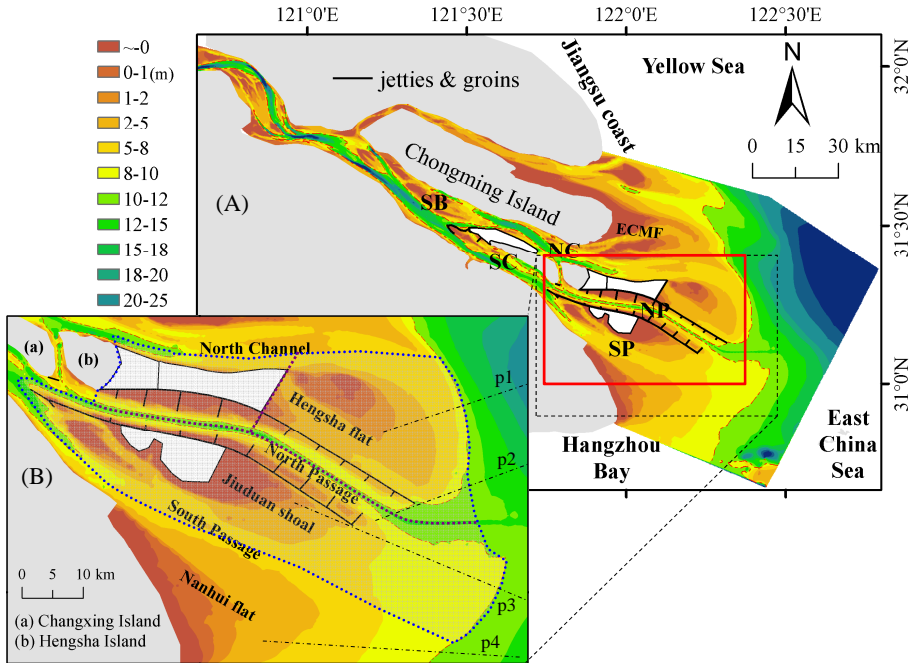


Figure 2.1: (A) Map of the Yangtze Estuary (YE) with the bathymetry in 2013 referencing the TLWL and (B) details of the area of interest, including the Hengsha flat and Jiuduan shoal. The white areas are the reclaimed regions in the landward part of the Hengsha flat and the vegetated super-tidal flats of the Jiuduan shoal. NB, SB, NC, SC, NP, and SP indicate the North Branch, South Branch, North Channel, South Channel, North Passage, and South Passage, respectively. ECMF indicates the eastern Chongming flat, which is located to the east of Chongming Island. The red box in (A) indicates the area used to estimate sand volumes and hypsometry. TLWL: theoretical lowest water level.

ble, whereas the suspended sediment load has gradually decreased since the mid-1980s (Guo et al., 2018a) (Figure 2.2). The decrease in suspended sediment loads is mainly due to soil conservation strategies and dam construction (e.g. Yang et al., 2015). Suspended sediment load reduction is more dramatic (~70%) since 2003, when the Three Gorges Dam (TGD) began operation (Figure 2.2). Since then, erosion has been detected in the 1200-km river reach between Yichang (approximately 40 km downstream of TGD) and Datong (resulting in a downstream increase in suspended sediment load; see Figure 2.2). On decadal time scales, the sedimentation rate (1-3 cm/year; Jia et al., 2018) in the study area is an order of magnitude larger than the rate of sea level rise in the recent century (3 mm/year from 1980 to 2015; SOA, 2015).

At its seaward side, the YE is forced by tides with a mean range of 2.7 m and a maximum spring tidal range of 5.5 m (Yun, 2004). Wave energy is moderate at the mouth with a mean wave height of 0.9 m, although wave heights can reach 6.2 m during storm conditions (Yang et al., 2001). Under combined river and tidal forcing, the mouth zone of the YE is a partially mixed environment with strong density currents and lateral circulations due to water exchange between different branches (Wu et al., 2010; Zhu et al.,

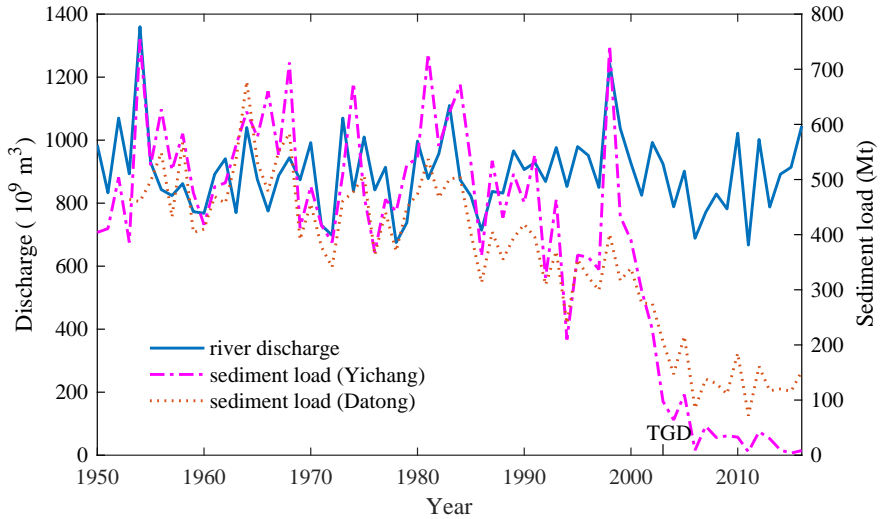


Figure 2.2: Annual river discharge and suspended sediment load measured at Datong (the most downstream gauging station) and suspended sediment load measured at Yichang (the gauging station immediately downstream of the Three Gorges Dam) between 1950 and 2016.

2017). These lateral circulations, however, are presently decreasing because of elevated tidal flats and the blocking effects of the jetties discussed in the next paragraphs (Zhu et al., 2017).

Morphologically, the YE maintains a configuration with four outlets, i.e., the North Branch, the North Channel, the NP and the South Passage, discharging south-eastward into the sea (Figure 2.1). This bifurcating and branching pattern develops at centennial to millennial time scales, as suggested by a bar migration model (Chen et al., 1985). The mouth zone (coinciding with the maximum turbidity zone) is a morphologically active region where horizontal and vertical circulations play substantial roles in water and sediment transport (Shen et al., 1988; Wu et al., 2010). Tidal currents during flood or ebb peaks are up to 3 m/s, and strong resuspension causes near-bed suspended sediment concentrations as high as 10 kg/m³ (Li and Zhang, 1998; Chen et al., 2006; Liu et al., 2010).

The largest local human intervention in the mouth zone is the Deep Channel Navigation Project (DCNP) constructed in the North Passage (Figure 2.3a). The elevation of the jetties is approximately 2.0 m above the theoretical lowest water level (TLWL), and the elevation of the groins decreases from 2.0 m at the attachment point to 0 m at the groin head. This elevation suggests that water and sediment are exchanged between the NP and its surrounding shoals only during spring tide high water. The DCNP was constructed between 1998 and 2008, during which the channel depth was increased from 6–9 m to 12.5 m. On average, 72 million m³ of sediment was dredged annually from the NP between 2007 and 2016 (Figure 2.3). The dredging material was disposed of partly in the shallow areas between the groins and partly offshore (Figure 2.3a). Some of the sediment

disposed between the groins was later transported to the landward part of the Hengsha flat to reclaim land (Figure 2.3b). Submerged dykes have been built on the landward part of the Hengsha flat, forming an area of ~115 km², which has trapped sediment since 2003 (Figure 2.3a). Moreover, *Spartina alterniflora* and *Phragmites* were artificially introduced to the Jiudian shoal in 1997 to create a reserve for endangered birds and other species. These measures have significantly influenced the morphological evolution of the mouth zone and are analysed in more detail hereafter.

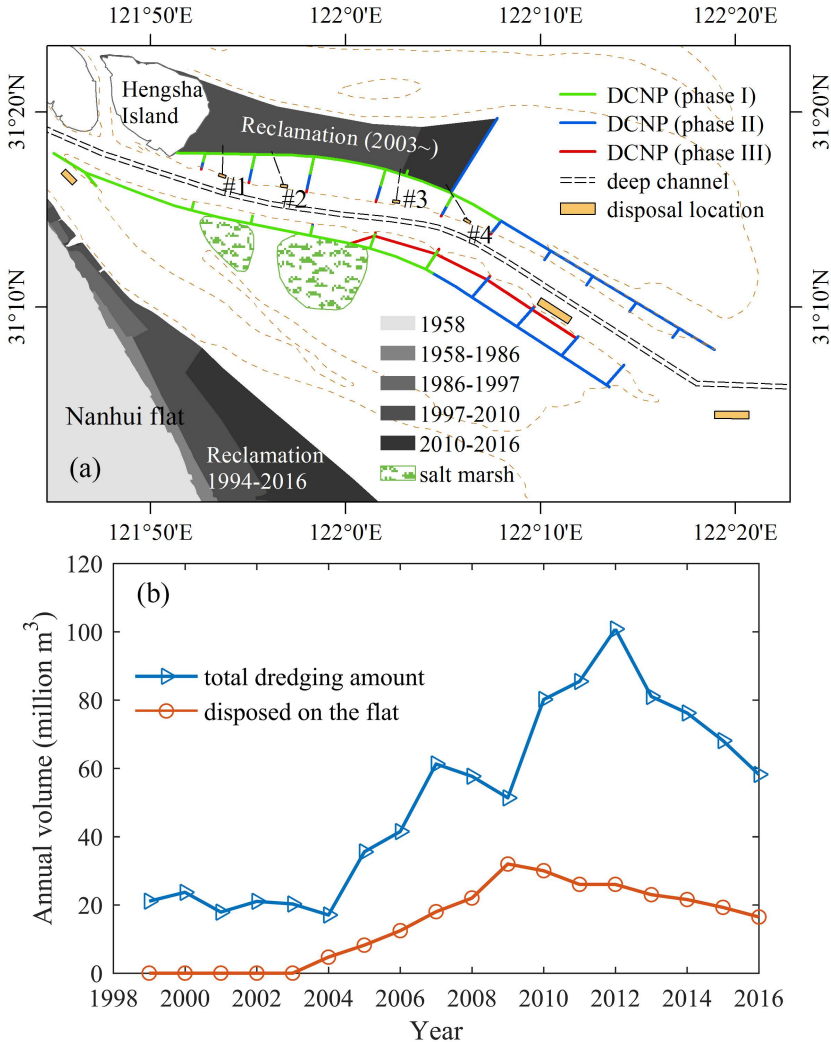


Figure 2.3: (a) Main human activities in the study area: land reclamation, salt marsh introduction and the Deep Channel Navigation Project (DCNP); #1, #2, #3 and #4 are disposal stations where sediment is pumped to the flat. (b) Annual dredging volume and the volume of sediment disposed on the flats in the North Passage.

2.2.2. DATA AND METHODS

RIVER discharge and suspended sediment load data were obtained at Datong and Yichang stations from 1950 to 2016 (Changjiang Water Resources Commission, the Ministry of Water Resources of China). Bathymetric data from 1953 to 1997 were digitized from marine charts, which record historical measurements with an accuracy of ±0.2 m (Table 2.1). The data after 1997 are measured with echo sounders with a vertical accuracy of ±0.1 m. The data accuracy is acceptable for calculation of accretion and erosion volumes on decadal time scales (especially given the relatively large volume changes).

The marine charts were digitized into depth points using the ArcGIS and Surfer software packages. The depth points were interpolated to a digital elevation model (DEM) with a uniform 200 × 200 m grid resolution using kriging techniques. All bathymetric data derived from marine charts and sounding measurements were converted to TLWL (other than for 1953). The difference between the TLWL and the mean water level decreases in the landward direction due to landward decreasing tidal range. All depths used in this study (if not otherwise specified) are positive downward and relative to TLWL.

Table 2.1: Information about the bathymetric data used in this study.

No.	Year	Datum	Sources	Scale	Survey month
1	1953	Approximate lowest low water	Shanghai	1:100,000	-
2	1958		Dredging	1:25,000	8-10
3	1965		Corporation,	1:100,000	4-11
4	1973		Ministry of		3~11
5	1978		Transport of	1:50,000	3~7
6	1986		China		5~9
7	1997	Lowest normal low water	The Navigation		12
8	2002		Guarantee		10~11
9	2007		Department	1:25,000	8
10	2010		of the		8
11	2013		Chinese Navy		8
12	2016		Headquarters		8

Bed level data became unavailable at the Jiudian shoal (because of vegetation development at bed levels exceeding TLWL) and the landward part of the Hengsha flat (because of land reclamations). To compute volume changes for the complete study area and period, we assumed that (1) the volumes of the Jiudian shoal above TLWL and (2) the reclaimed region in the landward part of the Hengsha flat did not change after 1997.

We also collected Landsat satellite images of the mouth zone (<http://glovis.usgs.gov/>) to examine changes in the salt marsh between 1985 and 2016. Salt marshes are mainly present in the supratidal flats and the upper parts of the intertidal flats, whereas the lower parts and the subtidal flats are bare. The interface between bare flats and salt

Table 2.2: A summary of the satellite images used in this study. The tidal height references the Wusong datum, which is nearly at the lowest tidal water level. The tidal gauge station Beicaozhong is located in the middle section of the North Passage.

No.	Sensor	Acquisition date	Mapping time (GMT)	Tidal height at Beicaozhong (m)
1	Landsat 5 TM	1989-08-11	01:51:48.2890000Z	2.50
2	Landsat 5 TM	1995-08-12	01:28:34.6590130Z	3.96
3	Landsat 7 ETM +	2000-08-01	02:16:10.7049124Z	3.35
4	Landsat 7 ETM +	2005-08-15	02:14:20.1657199Z	1.91
5	Landsat 5 TM	2009-07-17	02:13:52.5920500Z	2.34
6	Landsat 8 OLI	2013-08-29	02:27:03.2951292Z	2.75
7	Landsat 8 OLI	2016-07-21	02:24:59.1270480Z	3.38

marshes is identified using the normalized difference vegetation index (NDVI) method used in [Gao and Zhang \(2006\)](#) and [Li et al. \(2016a\)](#). The satellite images are georeferenced and corrected for tidal variations (Table 2.2). Since the salt marsh-bare flat interface is clear and above the water level in all images, the interface is independent of tidal elevations. To sustain data consistency and accuracy, only the images obtained in summer seasons (when vegetation is most evident) are selected. Positive NDVIs indicate intertidal wetlands and marshes occupied by vegetation. To differentiate between vegetation and non-vegetation, a threshold of 0.1 ($NDVI > 0.1$) is chosen to calculate the vegetated area.

2.3. RESULTS

2.3.1. PHENOMENOLOGICAL DESCRIPTION

IN 1953, disconnected flood and ebb channels with slightly different channel alignments developed over a large shoal (Tongsha shoal) in the mouth zone (Figure 2.4a). The flood and ebb channels were connected in 1958, initiating a new bifurcation and formation of the NP that split Tongsha shoal into the Hengsha flat (the northern part) and the Jiudian shoal (the southern part) (Figure 2.4b). The changes between 1953 and 1958 are largely the result of a major river flood occurring in 1954 (with a peak discharge of $92,000 \text{ m}^3/\text{s}$ at Datong), which connected the existing ebb and flood channels ([Yun, 2004](#)). Morphologically, the main channels in the mouth zone are very wide and shallow, having width-to-depth ratios >1000 . The sand bars, e.g., the Jiudian shoal, present large spatial scales with a typical width of $\sim 10 \text{ km}$ and length of $\sim 50 \text{ km}$. The wide and shallow features of the YE mouth zone are different from other tide-dominated estuaries (e.g., the Fly Estuary), and the mechanisms responsible for these large dimensions remain poorly known. The morphological evolution of the Hengsha flat and Jiudian shoal since 1958 is characterized by fast accretion following their separation. In the period between 1973 and 1986, the northern part of the Hengsha flat grew rapidly (Figure 2.4d and e). The Jiudian shoal also grew rapidly after merging with a sand bar from the landward side in 1997 (Figure 2.4e and f).

The DCNP in the NP significantly disturbed the morphological evolution processes in the mouth zone. The NP narrowed greatly, and its axial alignment was fixed due to the jetties and groins. Lateral water and sediment exchange with adjacent channels were partially blocked, resulting in fast accretion between the groins and over the surrounding flats. Later, the landward part of the Hengsha flat was reclaimed, and the higher part of the Jiudian shoal (the white area in Figure 2.4h) became a supra-tidal flat with limited tidal inundation. Overall, the recent development of the Hengsha flat and the Jiudian shoal has been strongly influenced by extensive human interference.

2.3.2. QUANTITATIVE BATHYMETRIC CHANGE

THE erosion and deposition patterns exhibit strong spatial variations (Figure 2.5). Erosion and deposition are greatest in the channel-shoal system, reflecting lateral migration of the channels and sand bars. Most net accretion occurs on the Hengsha flat and Jiudian shoal. The mouth zone displays erosion and deposition alternating in time. As an example, deposition prevailed east of the Hengsha flat in the periods from 1958-1973, 1973-1978, and 1986-1997, whereas erosion dominated in the intervals from 1978-1986, 1997-2007, 2007-2010 and 2010-2016 (Figure 2.5a-g). In the four decades between 1958 and 1997, the Jiudian shoal accreted continuously. Heavy deposition also occurred in the region to the east of the Hengsha flat and Jiudian shoal (approximately along the 10-20 m isobaths) (Figure 2.5h). In contrast, severe erosion was observed there from 1997 to 2016 (Figure 2.5i). The sheltered regions between the groins within the NP were rapidly filled from 1997 to 2016 (Figure 2.5e-g). Deepening along the main waterway was the result of scouring and dredging; their relative importance is evaluated hereafter.

When considering the water volume of the whole study area (Figure 2.6a), we observe that the water volume below TLWL showed a slight increase between 1997 and 2002 but was followed by an overall decrease from 2002 to 2007. Since 2007, however, the water volume below TLWL has increased, indicating recent erosion of the study area as a whole. The long-term accretion rates on the Jiudian shoal are faster than those on the Hengsha flat from 1958 to 2007-2010, followed by erosion until the most recent survey in 2016 (Figure 2.6b). Specifically, the sediment volume of the Jiudian shoal (defined as the sand body with a surface depth <6 m, which approximately corresponds to the mean depth of the main channels in the mouth zone), increased continuously by 1269.8 million m^3 between 1958 and 2007 (26 million m^3/year) and decreased by 132 million m^3 until 2016. The sediment volume of the Hengsha flat did not continuously increase. It decreased slightly between 1958 and 1986, except for a temporary increase between 1973 and 1978. The increase was attributed to deposition of sediment flushed through the North Channel (Yun, 2004). The sediment volume increased slightly (a net volume increase of 109 million m^3) between 1986 and 1997. The sediment volume of the seaward part of the Hengsha flat increased continuously (by 489 million m^3 between 1958 and 2010 except for a decrease from 1997 to 2002) but then decreased by 37 million m^3 between 2010 and 2016. In summary, the volume changes of the channel and the Hengsha flat and Jiudian shoal indicate a shift from deposition to erosion in approximately 2010.

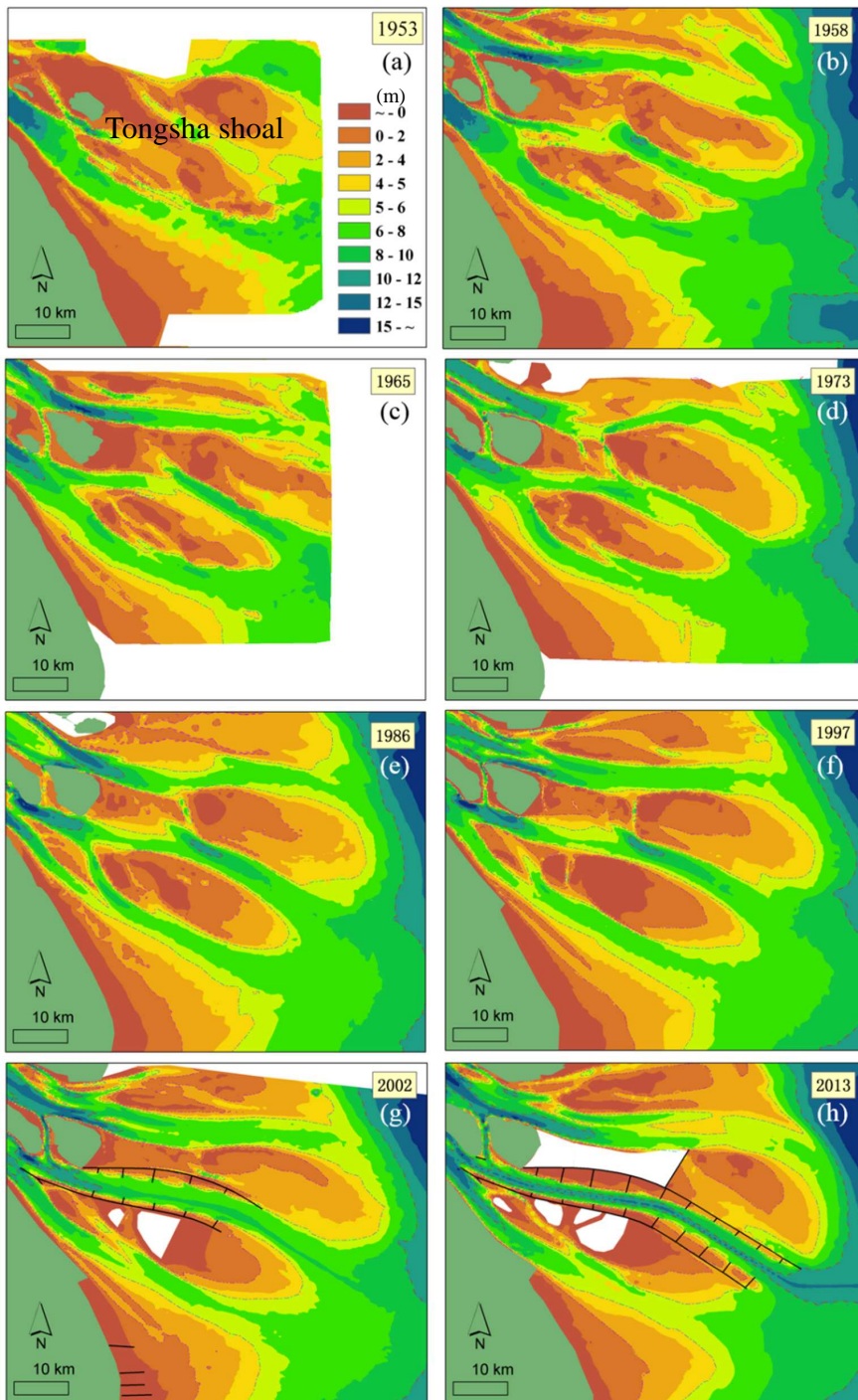


Figure 2.4: Bathymetric changes of the Jiudian shoal and the Hengsha flat between 1953 and 2013.

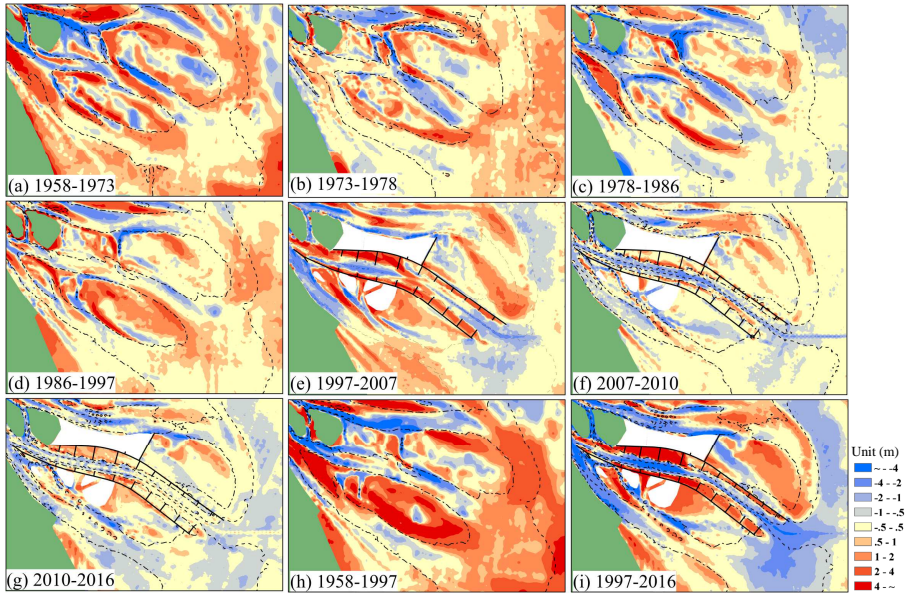


Figure 2.5: Erosion and deposition patterns (negative bed level changes (in m) indicate erosion and positive values, deposition) in the study area between 1958 and 2016. The 5 (dot-dashed) and 10 (dashed) m contour lines based on the bathymetry at the end of each period are included for position reference.

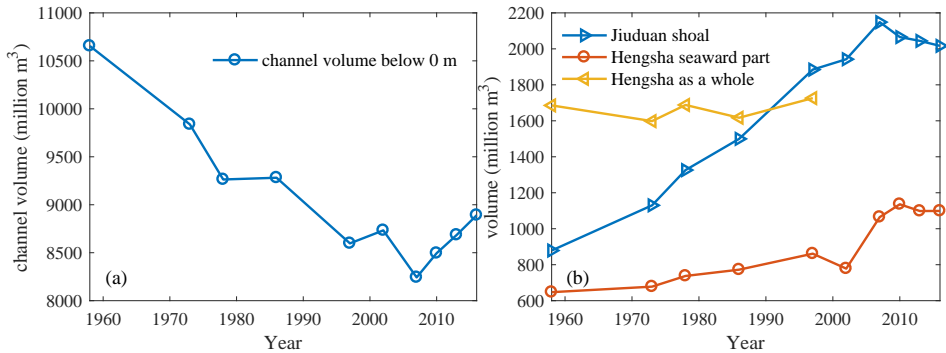


Figure 2.6: Volume changes of (a) channels below TLWL (in the study area defined in Figure 1) and (b) the Jiudian shoal and the Hengsha flat (the sediment volume of the area with elevation higher than 6 m below TLWL) between 1958 and 2016. TLWL: theoretical lowest water level.

2.3.3. HYPSONETRY CHANGES

THE morphodynamic evolution of the shoals is analysed in more detail with hypsometric curves, providing areal changes over a continuum of depth classes (Figure 2.7). The Jiudian shoal grew fastest at depths below 2 m between 1958 and 1986, followed by rapid accretion at greater depths (>6 m; see Figure 2.7a). Since 1997, erosion has occurred at depths below 6 m, which is mainly ascribed to deepening of the NP. As

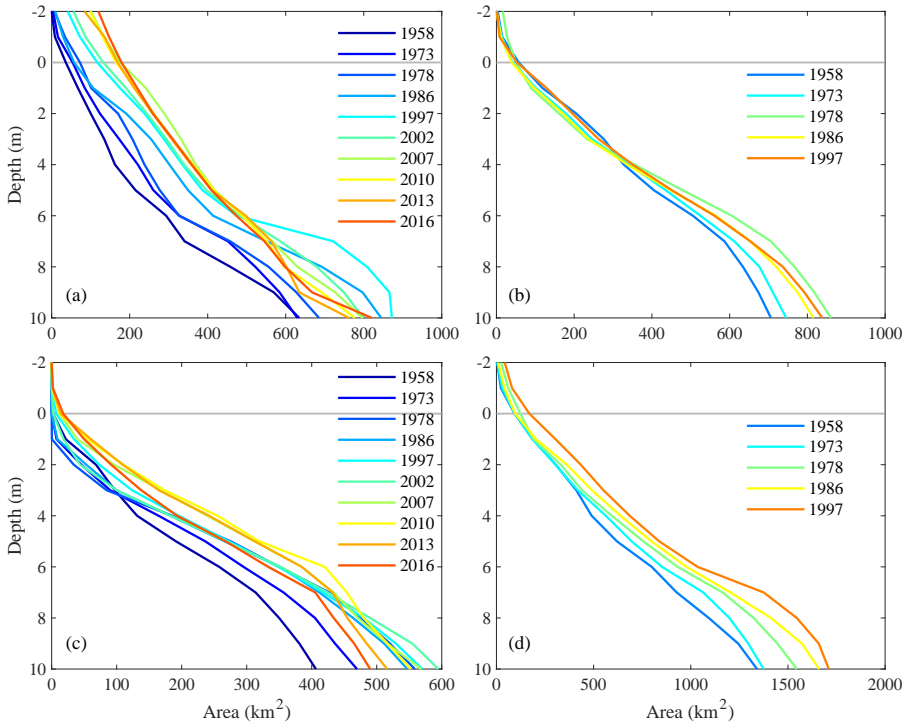


Figure 2.7: Hypsometry of (a) the Jiudian shoal, (b) the entire Hengsha flat, (c) the seaward part of the Hengsha flat, and (d) the Jiudian shoal and Hengsha flat.

a result, the subtidal slope of the Jiudian shoal became steeper. From 1958 to 1997, the area enclosed by the 6 m isobath increased by 61.5% (from 293.6 km² to 474.3 km²). A major increase occurred in the period between 1978 and 1986 due to merging with a sand bar (Figure 2.8b). Since 1997, the areal growth rate of the flat with a depth smaller than 6 m has decreased, whereas the growth rate of the region with a depth smaller than 0 m continued until 2007 (Figure 2.8). Therefore, up to 1997, the Jiudian shoal sustained its profile shape, but after 1997, the profile steepened due to deposition in the upper part and erosion in the lower part.

Because of the partial reclamation of the Hengsha flat, hypsometric curves are provided for the whole flat and for the seaward part only. The hypsometric curves indicate that the shallow parts of the entire Hengsha flat eroded slightly, whereas fast accretion occurred in the deep region between 1958 and 1978. In contrast, the shallow region accreted, whereas the deep region eroded between 1978 and 1997 (Figure 2.7b). The seaward part of the Hengsha flat developed similarly to the entire Hengsha flat before 1997 and to the Jiudian shoal after 1997. Specifically, erosion occurred in the regions with depths <3 m (accretion in the deeper zone) during 1958 and 1978, whereas erosion occurred in the regions with depths >8 m (accretion in the shallower zone) between 1997 and 2010 (Figure 2.7c). The depth at which deposition switches to erosion (or vice

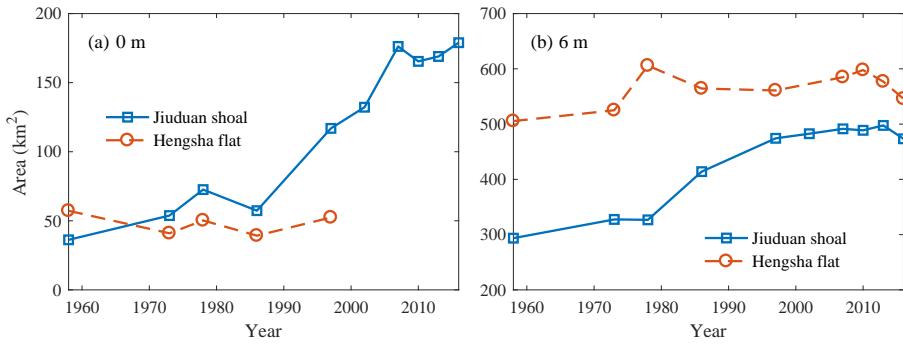


Figure 2.8: Evolution of the flat area encircled by the (a) 0 m and (b) 6 m isobaths for the Jiudian shoal and the Hengsha flat between 1958 and 2016.

versa) was approximately 3–5 m for the Hengsha flat before 1997. For both the Hengsha flat and Jiudian shoal, this transitional depth was approximately 8 m from 1997 to 2010. The larger depth threshold is partially explained by the dredging activities in the NP influencing both the Hengsha flat and Jiudian shoal. In recent years (2010–2016), the seaward part of the Hengsha flat has been characterized by erosion in the subtidal region at depths >2 m (Figure 2.7c). The flat area at the 0 m isobath was stable at approximately 50 km² before 1997 (Figure 2.8a). However, the flat area at 6 m increased until 2010, although at a lower rate than the Jiudian shoal (Figure 2.8b).

2.3.4. SALT MARSH CHANGES

SALT marshes were first observed on the Jiudian shoal in the late 1980s (Yun, 2004; Shen et al., 2006). *Scirpus mariqueter* was a native pioneer species growing in the lower parts of intertidal zones, while a *Phragmites Australis* community dominated the higher parts of the intertidal zone (Li et al., 2016a). Plant growth rates rapidly increased after *Spartina alterniflora*, an invasive species, was artificially introduced on the Jiudian shoal. The salt marsh area increased by 3.0 and 3.9 km²/year in the periods from 1995–2000 and 2000–2016, respectively (Figure 2.9). Most growth (~91%) occurred between 2000 and 2005 (Figure 2.10). Currently, *Phragmites australis*, *Scirpus mariqueter*, and *Spartina alterniflora* are distributed over the Jiudian shoal, and *Spartina alterniflora* has developed as the dominant species.

The Hengsha flat was sparsely vegetated before 2009 (Figure 2.9 and Figure 2.10) because of its low elevation. In 2016, the salt marsh area was 71.62 km² and was mainly found on the landward part of the Hengsha flat. This growth was the result of the dumping of dredged sediment in the embanked area, sufficiently increasing tidal flat elevation to allow salt marsh growth (Figure 2.9d). Salt marsh is absent to date in the seaward part of the Hengsha flat because of insufficient elevation. Overall, the different salt marsh growth patterns and temporal behaviours between the Hengsha flat and Jiudian shoal are in line with their morphological evolution patterns (Figure 2.10). The expansion of salt marshes on the Jiudian shoal has been continuous since the mid-1990s, whereas salt marshes expanded rapidly on the landward Hengsha flat after 2007.

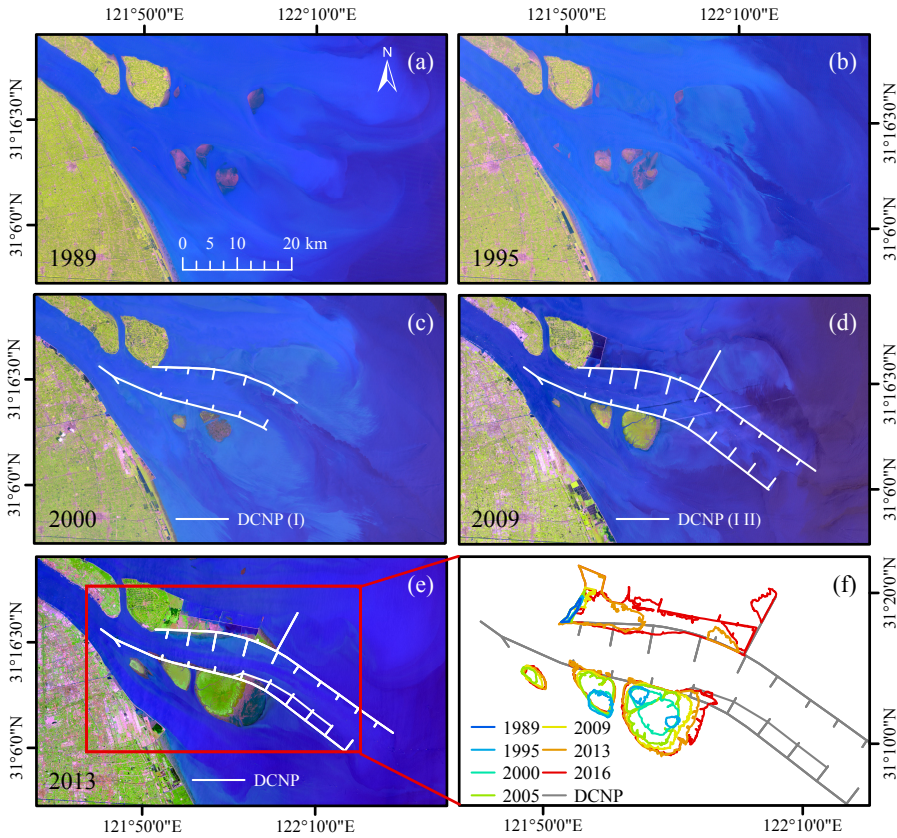


Figure 2.9: Morphological evolution of the Jiudian shoal and the Hengsha flat in (a) 1989, (b) 1995, (c) 2000, (d) 2009 and (e) 2013, as recorded by satellite images. (f) Detailed salt marsh boundaries for all years. DCNP: Deep Channel Navigation Project.

2.4. DISCUSSION

2.4.1. DIFFERENCES BETWEEN HENGSHA FLAT AND JIUDUAN SHOAL

THE morphodynamic evolutions of the Hengsha flat and Jiudian shoal are notably different even though they are geographically close. The Jiudian shoal accreted at an overall much higher rate than the seaward part of the Hengsha flat in the period from 1958 to 2007-2010. The hypsometric curves of the Jiudian shoal are more linear, while those of the Hengsha flat are generally S-shaped (see Figure 2.7). The flat area of the Hengsha flat at the 6 m depth contour increased more than that at 0 m, whereas the flat area of the Jiudian shoal increased more at the 0 m than at the 6 m isobath (see Figure 2.8). In other words, the morphodynamic evolution of the Hengsha flat is more prominent in area (horizontal expansion) but less by volume (vertical accretion) (see Figure 2.7 and Figure 2.8). Similar results were found by Liu et al. (2010) and Jiang et al. (2012). On its eastern side, the Hengsha flat has a steeper bed slope (i.e., $\sim 1/1200$) than

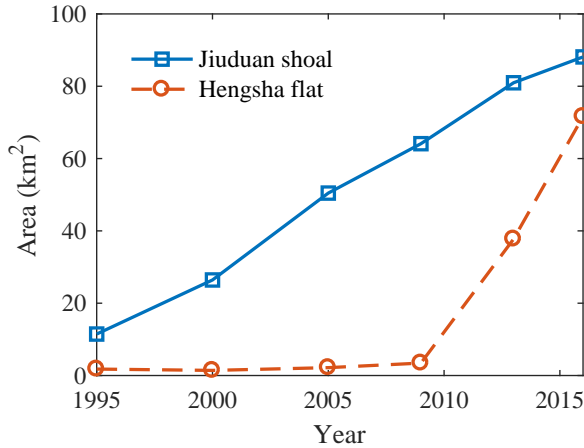


Figure 2.10: The salt marsh wetland areas of the Jiudian shoal and Hengsha flat between 1995 and 2016.

the Jiudian shoal (i.e., $<1/4000$) (Figure 2.11). The differences between the two shoals regarding vegetation and the DCNP are discussed later (see section 2.4.2).

We ascribe the differences in the morphodynamic development of the Hengsha flat and Jiudian shoal to multiple mechanisms. The shape of the tidal flat is strongly influenced by local hydrodynamics (Kirby, 2000; Le Hir et al., 2000; Roberts et al., 2000). Wave-induced resuspension leads to a landward increase in the sediment concentration. The cross-sectional diffusion of this horizontal concentration gradient by oscillating tidal currents leads to an offshore-directed sediment flux. In the absence of waves, the tidal current favours net sediment transport by settling and scour lags (Van Straaten and Kuenen, 1957; Postma, 1961). As a result, a dominance of wave-induced resuspension produces a concave-up profile, whereas a convex-up tidal flat shape is favoured by the dominance of tidal currents (Friedrichs and Aubrey, 1996; Kirby, 2000; Le Hir et al., 2000; Roberts et al., 2000). The Hengsha flat is exposed to stronger north-westerly winds in winter, while the Jiudian shoal is exposed to weaker south-easterly winds prevailing in summer. As a result, the Hengsha flat should have a more concave-up shape than the Jiudian shoal (Figure 2.11). The cross-shore profile shape further depends on the sediment grain size, with muddier sediment tending to generate a more convex profile (Kirby, 2000; Friedrichs, 2011; Zhou et al., 2015). The Jiudian shoal is muddier than the Hengsha flat (Figure S2.3), which would further suggest a more convex-up profile. However, the Jiudian shoal is not convex-upwards, particularly in 1958 (Figure 2.11c). In 1958, the Jiudian shoal had not yet been merged, so the convex shapes located at 0 m and 10 m represent two sand bars (see Figure 2.4). Since 1997, after the merging of these sand bars, the convex shape of the intertidal zone corresponds to the hydrodynamics and sediment type. The alternating convex and concave shape of the subtidal zone suggests that the profile shape may be influenced by additional factors, likely related to human interventions. The branching system distributing water and sediment to the various outlets is another factor contributing to the differences. The ebb tidal parti-

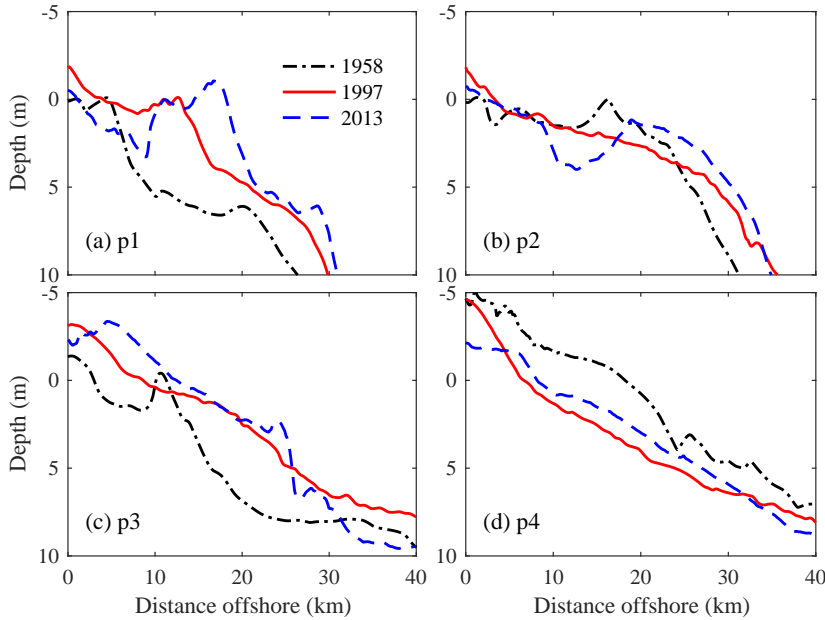


Figure 2.11: Evolution of the cross-shore profiles to the east of the Hengsha flat and Jiudian shoal: (a) p1, (b) p2, (c) p3, and (d) p4. The positions of the four profiles are indicated in Figure 2.1.

tion ratio of the North Channel is much larger than those of the South or North Passages (Chen et al., 1988). In the past, deposition prevailed in the channel and surrounding flats of a branch that received the largest proportion (>50%) of water and sediment (Yun, 2004). In contrast, erosion occurred in the branch that received less sediment (Dai et al., 2014). The branching dynamics are evidenced by the evolution of the Hengsha flat and Jiudian shoal during the late 1970s (see Figure 2.8). Specifically, the fast accretion of the Hengsha flat in the late 1970s is attributed to deposition of a larger amount of sediment flushed through the North Channel than through the South Channel, while in the meantime, the Jiudian shoal eroded slightly (Yun, 2004). As deposition occurred in the North Channel, the cross-sectional area decreased, leading to a decreasing water volume and sediment supply. This situation provides a negative morphodynamic feedback mechanism, eventually stabilizing the system. Seaward sediment flushing and associated sand bar movements have been observed since 1997 in the North Channel and South Passage but at much smaller rates, as the channel-shoal pattern has developed towards an equilibrium state (Wang et al., 2013). Similar phenomena are also observed in other tidal estuaries or river deltas with branching channel networks (Sassi et al., 2011; Buschman et al., 2013).

2.4.2. EFFECT OF HUMAN INTERVENTIONS

RIVERINE sediment supply has been decreasing since the mid-1980s, especially in response to the Three Gorges Dam operation since 2003. The Hengsha flat and the Jiudian shoal sustained accretion until 2007-2010 (Figure 2.12). A major question there-

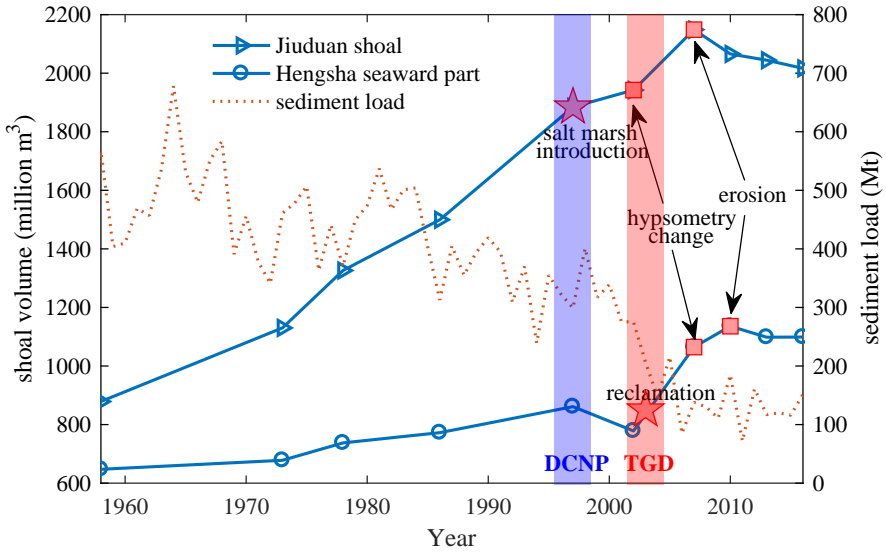


Figure 2.12: Overview of the evolution of the Hengsha flat and Jiudian shoal and changes in suspended sediment load at Datong, with time markers of major human interventions and important morphological changes. The shoal volume refers to the sediment volume of the area with elevation higher than 6 m below TLWL. TLWL: theoretical lowest water level; DCNP: Deep Channel Navigation Project; TGD: Three Gorges Dam.

fore is to what extent flat erosion is the result of sediment decline (with a certain time lag) or of local engineering works and/or vegetation changes. Therefore, the various impacts and system responses are summarized in Figure 2.12.

EFFECT OF SEDIMENT DECLINE

Silt and sand are deposited in the Three Gorges Dam reservoir, while most of the clay is flushed seaward. The seaward sediment flux from the Yangtze partly recovers because of along-river erosion between Yichang and Datong (Figure 2.2, Yang et al., 2011) and downstream of Datong, e.g., the 600 km river reach between Datong and the mouth zone (Wang et al., 2009; Zhao et al., 2018). Since the riverbed downstream of Yichang is dominantly sandy, the sand fraction achieves a new equilibrium concentration from bed exchange, whereas the silt fraction does not. The clay fraction is relatively little impacted because it is partly flushed through the reservoirs. Therefore, a reduction in the supply of clay is small; the reduction in silt is large and occurs within a relatively short time period (10-20 years with an assumption of 10% silt content in the riverbed; van Maren et al., 2013, whereas the sand supply has a much longer response time (decades to possibly even centuries, although this estimate is highly speculative at this point).

Erosion has been observed in the subaqueous delta of the YE (e.g. Yang et al., 2011), even though the sediment being deposited there is fine (and therefore not trapped by reservoirs). Even more, the depocenter of the Yangtze subaqueous delta, a mud belt with high sediment exchange, maintains a high deposition rate (Dai et al., 2014). This result suggests that sufficient fine sediment is still supplied from the estuary to maintain

the subaqueous delta.

The Hengsha flat and Jiuduan shoal are composed of sand and silt (Figure S2.3) and therefore respond to suspended sediment load reduction within one to several decades. At present, the sediment concentration appears to have changed little in the study area (Dai et al., 2013b; Zhu et al., 2015). However, if the study area reacts to a reduction in the suspended sediment load, such a response would be gradual, leading to a gradual decrease in deposition (possibly followed by a gradual increase in erosion rates). This situation is not observed in the bed level changes, as discussed hereafter. We further investigate the impacts of human interventions: salt marsh introduction and the DCNP.

POTENTIAL IMPACTS OF SALT MARSHES

Salt marshes influence morphodynamics by attenuating incoming short waves, trapping fine sediment, and stabilizing the bed. All these impacts promote sediment deposition and flat accretion, which is important for coastal restoration and protection. Accretion is further enhanced by the accumulation of biomass in salt marshes (Morris et al., 2002). The introduction of *S. alterniflora* in 1997 most likely facilitated salt marsh growth on the Jiuduan shoal since *S. alterniflora* expands more rapidly than native species (Huang and Zhang, 2007). The seaward Hengsha flat has only limited vegetation (Figure 2.9), and as a result, the Jiuduan shoal accretes faster than the seaward Hengsha flat.

THE IMPACT OF THE DEEP CHANNEL NAVIGATION PROJECT

After the construction of the DCNP started in 1997, severe sedimentation occurred during 2002-2007 following a rapid decrease in accretion. The DCNP can promote accretion by sheltering and sediment trapping effects induced by deepening. The two jetties along the NP largely reduce horizontal water and sediment circulations among the North Channel, the NP and the South Passage in the mouth zone, thereby enhancing accretion of the surrounding flats (Jiang et al., 2012; Li et al., 2016a). The embankment of the landward Hengsha flat and the associated dumping there resulted in a rapid increase in the flat elevation. On the other hand, deepening may increase the tidal range (Kerner, 2007; van Maren et al., 2015b), salt intrusion (Zhu et al., 2006; Hu and Ding, 2009), and estuarine circulation (Ge et al., 2010; van Maren et al., 2015a) and alter regional hydrodynamics (Jiang et al., 2012) and therefore residual sediment transport. All of these changes are likely to increase sediment concentrations, which is found in many estuaries, e.g., the Ems (Winterwerp et al., 2013; de Jonge et al., 2014), the Elbe (Kerner, 2007; Winterwerp et al., 2013), the Weser (Schrottke et al., 2006), and the Loire (Winterwerp et al., 2013). Additionally, a positive feedback effect between high sediment concentration and tidal amplification further enhances near-bottom sediment trapping (Winterwerp et al., 2009, 2013; van Maren et al., 2015b).

On the other hand, the DCNP can affect morphological changes by regulating the diversion ratio of water and sediment discharge through the NP and South Passage (SP) (Jiang et al., 2012). Before the construction of the DCNP, the NP discharged more water (~60%) than the SP, but at present, the SP discharges ~60% of the water volume (Kuang et al., 2014; Wang et al., 2015). Moreover, the sediment discharged through the NP decreased from ~45% to ~30%, whereas sediment discharging through the SP increased by

15% from 1998-2009 (Kuang et al., 2014). Jiang et al. (2012) reported downstream sedimentation in the SP, but erosion can also be expected due to southward dispersion by northerly winds and waves in winter and the longshore current. As a result, the changing water and sediment diversion ratio between the NP and SP influence erosion and sedimentation in the study area.

DREDGING

Dredging volumes along the main waterway in the NP are so large (Figure 2.3) that they also influence estuarine morphodynamics. Approximately 30% of the dredged sediment has been brought to land since 2003, and this part of the sediment volume needs to be accounted for when interpreting volume changes (Table 2.3 and Figure 2.13). Allowing for some errors, we calculated dredging volumes corresponding to the periods for which chart data are available. When interpreting the bathymetric changes, we define a 'dredging-induced' volume (the volume actually taken out) and a 'natural' volume (the observed changes compensated by dredging volumes). Approximately 35%, 63%, and 47% of the erosion volumes in the periods 2007-2010, 2010-2013 and 2013-2016 (respectively, on average ~50% during 2007-2016) are the result of sediment extraction for land reclamations (dredging-induced). This result highlights the importance of including dredging volumes in the analysis of bed level changes. Particularly after 2010, the natural development and bathymetric observations (dashed lines in Figure 2.13) were erosional, suggesting the time lag effects of sediment decline that are discussed later.

It is noted that the dredged and disposed sediment volumes provided here refer to the undisturbed sediment with a dry density estimated as $\sim 1200 \text{ kg/m}^3$ and not to hopper densities that are more commonly available (see e.g. van Maren et al., 2016). This approach allows a direct comparison of volumes without conversion to sediment mass.

2.4.3. SYNTHESIS

THE response of the Yangtze Estuary to human interventions is complicated by time lag effects; the system is so large that time is required for a reduction in sediment supply to take effect. Local engineering works and (human-induced) salt marsh development take place concurrently, probably with much smaller (or even no) time lag effects.

A crucial difference between the impacts of sediment supply and local interventions is the type of system response. A gradual decrease in sediment supply leads to a gradual change in accretion (potentially leading to erosion). A local intervention typically has immediate effects, with a response that rapidly changes with time. Figure 2.13 reveals a very rapid change from erosion to deposition in approximately 2002 and from deposition to erosion in approximately 2007. The accretion is mainly caused by the deposition due to sheltering effects in jetties and groins whereas the erosion occurred in the deep channel below 6-7 m (see Figure 2.7) corresponds to the dredging activities. This observation strongly supports the interpretation that local interventions were responsible for the major changes that took place in the mouth zone in the period 1997-2010.

The observation that volume changes were approximately 50 million m^3 /year from 1958 to 1997 (Figure 2.13) suggests that net volume changes (without local interventions) are fairly constant and not much affected by a reduction in sediment supply (which

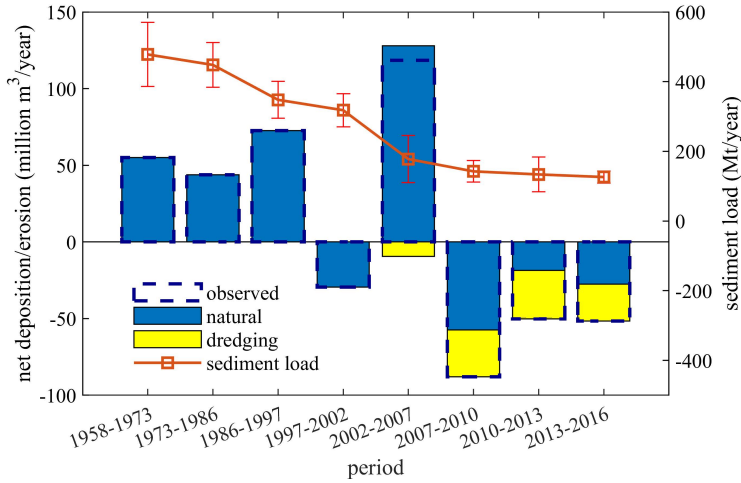


Figure 2.13: Annual net deposition/erosion of natural development, human-induced development due to dredging and yearly average suspended sediment load changes during different periods. The bars with dashed lines are the volumes quantified by bathymetric data.

started around 1985). It is unlikely that the rapid changes in the period 1997-2007 can be attributed to these gradual changes. However, it may be that the rapid changes by local human interventions masked the effect of the sediment decline. After 2010, the mouth zone became erosional with a sediment loss of approximately -25 and -50 million m^3/year (respectively). This strongly suggests that sediment decline becomes effective after 2010. However, the continuous erosion may also be attributed to the hydrodynamic conditions in the mouth zone resulting from the local human interventions.

In general, the effects of local human interventions on an estuary are rapid and temporary, leading to local redistribution of sediments. Because sediment decline is more permanent in nature, erosion of the estuary mouth lasts much longer (until a new equilibrium between marine erosion and fluvial supply is achieved). Based on our analysis in Figure 2.13, it is more likely that the erosion during 1997-2010 was temporary and therefore mainly caused by local human interventions whereas the longer-term erosion afterwards was attributed to sediment decline. Therefore, we suggest that the morphological adaptation time scale of the mouth zone in response to riverine sediment decline is ~ 30 years (starting from the mid-1980s).

2.5. CONCLUSIONS

BEHAVING as a sink of river-supplied sediment, the mouth zone of the YE and its morphological variability are strongly influenced by sediment supply and local human activities. In this study, we use a long time series of bathymetric data and a series of satellite images to examine the 63-year (1953-2016) morphological changes of two large shoals in the YE, the Hengsha flat and the Jiudian shoal. We conclude that the two shoals sustained accretion until ~2010, followed by erosion. Local human activities are important for morphodynamic changes on the two shoals. The morphodynamic evolution in the pre-1997 period is largely naturally controlled, while the post-1997 evolution is dominantly anthropogenically driven. In particular, in the period 2002-2010, salt marsh introduction and the DCNP stimulated fast accretion of surrounding flats. We also find that the Hengsha flat and the Jiudian shoal exhibit different morphological behaviours, which can be explained by upstream water and sediment partition, local tidal dynamics and bio-physical interactions.

For the whole study area, a sudden shift from accretion to erosion occurred in 1997 and 2007, corresponding to the deep channel erosion in the Hengsha flat and Jiudian shoal. The nearly instantaneous impact is mainly explained by local human interventions. Specifically, the DCNP initially led to erosion with heavy sedimentation occurred later, followed by years of significant erosion. Further analyses reveal that the disposed volume accounts for ~50% of the volume changes as quantified by bathymetric data and therefore needs to be an integral part of the interpretation of erosional and depositional changes.

Although future monitoring is still needed to confirm the results, our data suggest a lagging morphological response of the mouth zone in response to the reduction in sediment supply at a time scale of ~30 years. Local human interventions play an important role in masking the gradual effect. Our results provide further insight into interpreting morphodynamic changes in large-scale estuaries and deltas under different human activities.

Table 2.3: Volume changes of the study area during different periods

Period	Sediment volume change ¹ (million m ³)	Total dredging amount ² (million m ³)	Sediment disposed to the reclamation area ³ (million m ³)	Equivalent volume disposed to the reclamation area ⁴ (million m ³)	Net annual sediment deposition/erosion rate ⁵ (million m ³ /year)	Net annual sediment deposition/erosion rate ⁶ (million m ³ /year)	Annual sediment load (million ton/year)
1958-1973	824.86	0	0	0	54.99	54.99	478.06
1973-1986	570.17	0	0	0	43.86	43.86	448.00
1986-1997	799.40	0	0	0	72.67	72.67	347.83
1997-2002	-147.52	83.72	0	0	-29.50	-29.50	318.00
2002-2007	592.67	163.88	39.42	47.304	118.53	127.99	177.80
2007-2010	-263.77	187.84	76.50	91.80	-87.92	-57.32	142.50
2010-2013	-150.43	260.6	78.75	94.50	-50.14	-18.64	133.70
2013-2016	-154.93	212.68	60.23	72.28	-51.64	-27.55	126.25
1958-1997	2194.40	0	0	0	56.27	56.27	425.33
1997-2016	370.62	918.36	263.00	315.60	19.51	36.12	159.00
2007-2016	-574.86	659.01	216.00	259.20	-63.87	-35.07	132.00
1958-2016	2565.00	918.36	263.00	315.60	44.22	49.67	273.14

¹ without disposed sediment on flat (only interpreted from bathymetric maps)

^{2,3} correspond to Figure 2.3b

⁴ dry density of ~1200 kg/m³ for dredged sediment

⁵ without disposed sediment on flat (only interpreted from bathymetric maps)

⁶ with disposed sediment on flat

2.A. APPENDIX: SUPPLYMENTARY TABLES AND FIGURES

Table S2.1: Study periods and study areas in some literatures.

Study period	Study area		Reference
	Region ¹	Name	
1958-2010	a	inner estuary & mouth zone	Luan et al., 2016
1958-2016	a	inner estuary & mouth zone	Zhao et al., 2018
1958-1997	b	subaqueous delta	Yang et al., 2003
1958-2007	c	subaqueous delta	Yang et al., 2011
1958-2009	d	subaqueous delta	Dai et al., 2014
1979-2011	e	subaqueous delta	Yang et al., 2018
1998-2011	f	North Passage	Dai et al., 2013a
1958-2005	g	Jiudian shoal	Gao et al., 2010
1958-2009	g & h	Hengsha flat & Jiudian shoal	Wei et al., 2015
1998-2014	g	Jiudian shoal	Wei et al., 2016
1986-2013	g	Jiudian shoal	Li et al., 2016a
1958-2012	i	Nanhui shoal	Wei et al., 2015
1998-2013	part of i	Nanhui shoal	Wei et al., 2017
1842-2004	i	Nanhui shoal	Fan et al., 2017
1953-2016	black line with dots	mouth zone (including Hengsha flat & Jiudian shoal)	this study

¹ regions labelling from a to i are shown in Figure S2.1

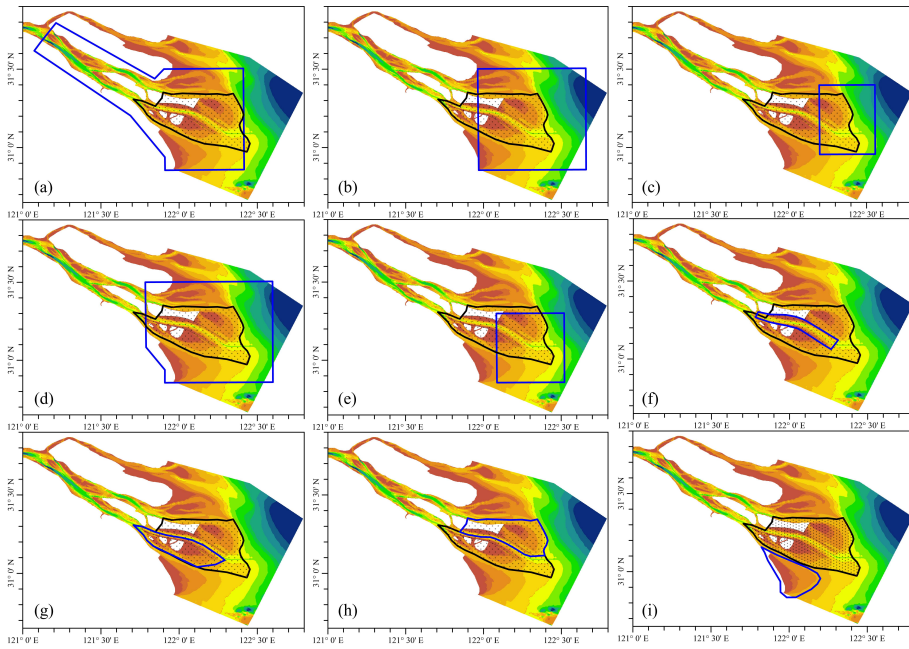


Figure S2.1: Study area of previous studies (see Table S2.1) and this study based on bathymetry in 2013.

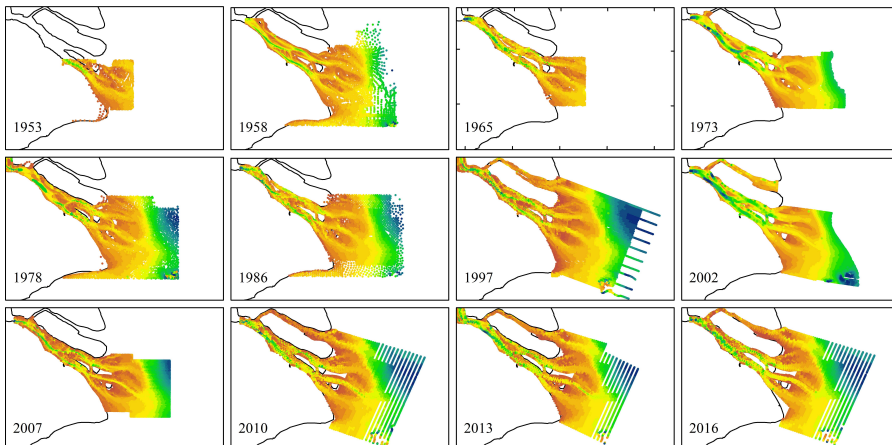


Figure S2.2: Bathymetric data points used in this study (scale 1:3,000,000) corresponding to Table 2.1.

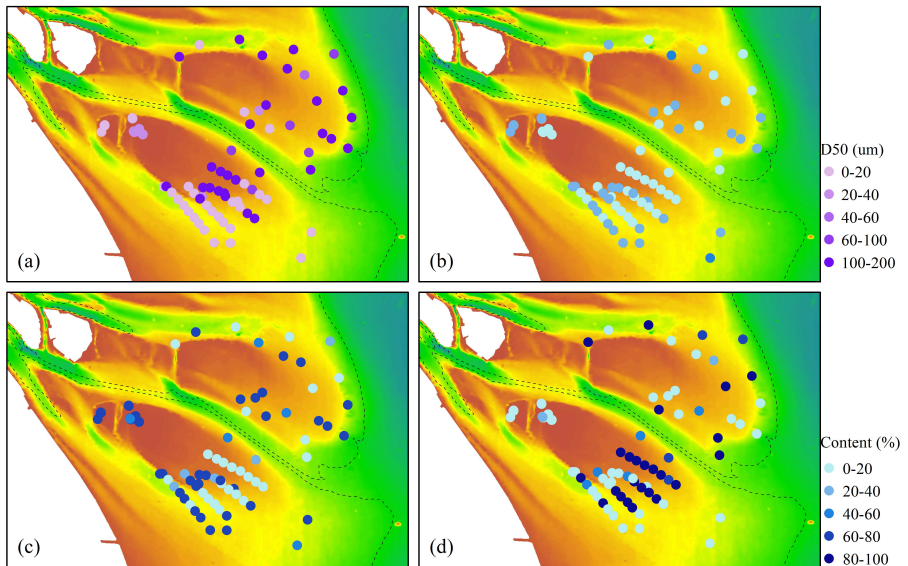
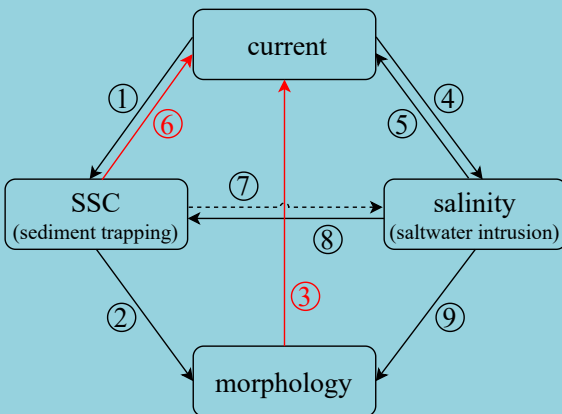


Figure S2.3: Spatial distribution of medium grain size (a), contents of clay (b), silt (c) and sand (d) in bed sediment. Reference position is shown by 5-m (dashed line) contour line. Sum of content of clay, silt and sand is 100%. More details about the data refer to (Liu et al., 2010).

3

EXPLORATION OF DECADAL TIDAL EVOLUTION IN RESPONSE TO MORPHOLOGICAL AND SEDIMENTARY CHANGES IN THE YANGTZE ESTUARY



*In fact, there is no road on the ground,
and there are more people to go,
and it will become a road.*
其实地上本没有路，
走的人多了，
也便成了路。

Lu Xun (Litterateur, 1881-1936)

This chapter focuses on the content in red and has been published in:

Zhu, C., Guo, L., van Maren, D.S., Wang, Z.B. and He, Q., 2021. Exploration of decadal tidal evolution in response to morphological and sedimentary changes in the Yangtze Estuary. *Journal of Geophysical Research-Oceans*, p.e2020JC017019.

Estuarine tidal dynamics are influenced by changes in morphology and friction. In this work, we quantified changes in tidal damping in the Yangtze Estuary and explored the impact of morphology and friction using a numerical model. In-depth analyses of tidal data reveal a strong reduction in tidal damping from 1990 to 2010, followed by a slightly enhanced damping from 2010 to 2020 in the South Branch. The reduced tidal damping in the South Branch from 1990 to 2010 is controlled by sediment decline which induces an increase in water depth (erosion), thereby strongly amplifying tides. However, the effective bottom roughness (Manning coefficient) is increased by 60%, which is probably related to the ~80% decrease in the suspended sediment concentration (SSC). Such an effect may enhance tidal damping, which counteracts the contribution of water depth increase on amplifying tides by ~75%. From 2010 to 2020, the tides in the South Branch became more damped, suggesting a dominance of the decrease in SSC over the morphological changes. In the mouth zone, tidal dissipation is enhanced from 1997 to 2010, which is mainly caused by an overall increase in effective bottom roughness. Local structures dominate the increase in effective bottom roughness; however, fluid mud formation may contribute to a decrease after 2010. Overall we argue that estuarine morphological and sedimentary changes in response to riverine sediment decline and local engineering works control the tidal evolution in the Yangtze Estuary, which is important for evaluation of human activities and estuarine management.



3.1. INTRODUCTION

ANTHROPOGENIC activities may strongly influence the morphology in varying coastal environments, particularly in tidal estuaries where hydro-morphodynamic feedback processes are important. Human interventions potentially influence tidal dynamics, in terms of tidal range, amplitudes, and wave shape, resulting in tidal amplification/damping, and deformation. These modifications in turn influence the intertidal area, salinity and freshwater availability, as well as the navigational depth. A thorough understanding of changes in tidal amplification/damping is therefore crucial for sustainable coastal management.

Tidal amplitudes and ranges have been observed to increase in many estuaries owing to channel deepening related to dredging (Woodworth, 2010; Talke and Jay, 2020). For instance, on the U.S. East Coast, the mean tidal range in the Cape Fear River Estuary in Wilmington (NC) had doubled to 1.55 m since the 1880s (Familkhalili and Talke, 2016). In Ria de Aveiro, Spain, an averaged increase of 0.245 m in the M_2 amplitude and an averaged 17.4° decrease in the M_2 phase were detected over 16 years (1987-2004) (Araújo et al., 2008). The amplitudes of the major tidal constituents exhibited a significant increase over the last century in the Venice Lagoon (Ferrarin et al., 2015). The tidal range in the upstream reaches of the Hudson River had more than doubled over 150 years (Ralston et al., 2019). Interestingly, decreases in tidal amplitudes are less documented, except in a few studies such as in Norfolk, Virginia; Washington DC; and Providence, Rhode Island where the mean tidal range has decreased by 8-9% since the mid-nineteenth century (Talke and Jay, 2020). Moreover, a decrease in tidal amplitude is found in the Yangshan Harbour and Yalu river estuary due to the dams and land reclamation (Guo et al., 2018b; Cheng et al., 2020).

Tidal amplitudes and ranges are strongly dependent on morphology, particularly on changes in water depth and channel width. Increasing water depth reduces the effects of bottom friction, causing a reduction in the effective hydraulic drag, resulting in an increase in amplitude and propagation speed of tidal waves (Ralston et al., 2019). The increase in tidal amplitude in many estuaries is found to be caused by the increase in water depth, some of which are caused by natural morphological changes (Jalón-Rojas et al., 2018) while others are associated with human-induced dredging activities, such as in the Rhine-Meuse Delta (Vellinga et al., 2014), Tampa Bay (Zhu et al., 2014); Elbe Estuary, Ems Estuary, and Loire Estuary (Winterwerp et al., 2013), upper Scheldt estuary (Wang et al., 2019b), Columbia Estuary (Jay et al., 2011) and Cape Fear River Estuary (Familkhalili and Talke, 2016).

The deepening of tidal channels usually results in a modification of both vertical and horizontal tides. Enlarged tidal currents lead to an increase in SSCs (de Jonge et al., 2014; Dijkstra et al., 2019b). High SSCs cause a reduction in the effective hydraulic drag due to buoyancy destruction (Winterwerp et al., 2009), which in turn cause a stronger tidal amplification in estuaries (Gabioux et al., 2005; Winterwerp and Wang, 2013; Winterwerp et al., 2013; Wang et al., 2014; Jalón-Rojas et al., 2016; Jalón-Rojas et al., 2018). A positive feedback was identified between channel deepening, increase in SSCs, reduction in bottom drag, and enhanced tidal amplification, which increases sediment trapping and SSC, and potentially induce a regime shift to hyper-turbid conditions (Winterwerp, 2011; Winterwerp and Wang, 2013; van Maren et al., 2015b; Dijkstra et al., 2019b,a). This

phenomenon has been documented for the Ems (de Jonge et al., 2014; Dijkstra et al., 2019b,a), and Loire estuaries (Winterwerp et al., 2013). In contrast, a decline in SSC owing to a reduction in sediment availability from the upstream river basin may increase bottom drag and affect tidal dynamics, which is probably the case of the Yangtze Estuary.

The Yangtze Estuary is a large-scale alluvial system undergoing changes within the estuary and at the boundary, driven by intensive human activities. The estuary is a highly turbid system with near-bottom SSC up to 100 kg/m^3 , forming near-bed fluid mud in the mouth zone (Wan et al., 2014b). The high SSC has a damping effect on the turbulence and thereby decreases the effective bed roughness (Geyer, 1993; Winterwerp et al., 2009). As a result, a very low friction parameter (e.g. a Manning coefficient n of $0.012 \text{ s/m}^{1/3}$, Hu et al., 2009) is needed to correctly simulate tidal wave propagation in the Yangtze Estuary. It is likely, however, that the effect of sediment on the bed roughness is changing over time. On the one hand, an increase in fluid mud thickness has been observed in the North Passage of the Yangtze Estuary (Liu et al., 2011; Song et al., 2013; Wan et al., 2014b), owing to enhanced stratification after the construction of the jetties and groins. This change potentially reduces the regional bed roughness. On the other hand, dam construction in the river basin causes a drastic decline in river-borne sediment supply since 2003 (Yang et al., 2011; Luan et al., 2016; Zhao et al., 2018; Guo et al., 2018a). As a result, the SSC in the Yangtze Estuary decreases accordingly in recent decades, although the degree of this reduction varies spatially (Liu, 2009; Zhu et al., 2015). Vertical SSC gradients dampen vertical mixing, leading to a hydraulically smoother bed (Winterwerp, 2001; Winterwerp et al., 2009; van Maren et al., 2015b). Therefore, a reduction in SSC is expected to strengthen bottom friction and subsequently deform the tidal wave. Additionally, the morphology of the Yangtze Estuary is changing as well. The construction of long jetties and a series of groins to regulate the navigational waterway, together with intensive dredging and land reclamation, has modified the estuarine morphology substantially. These human interventions influence the hydrodynamics (e.g. Hu and Ding, 2009; Zhu et al., 2017) in the short term and morphological changes in the long term (e.g. Jiang et al., 2012; Zhao et al., 2018; Zhu et al., 2019). Our understanding of the tidal dynamics in the Yangtze Estuary is progressively increasing in recent years concerning the temporal and spatial variations of tidal dynamics (Fu, 2013; Wan et al., 2014a; Lu et al., 2015) and river-tide interactions (Cai et al., 2014; Guo et al., 2015). However, to what degree the tides in the Yangtze Estuary have changed in response to the various human interventions remains insufficiently known.

In this contribution, we aim to examine the decadal changes in the tidal dynamics of the Yangtze Estuary using observational data and subsequently unravel the role of changes in morphology, sediment concentration and human interventions using a numerical model. The structure of this paper is as follows. The study area is described first, followed by an overview of available data and setup of the model and model scenarios. In the results section, we introduce the observed and computed tidal evolution, whereas the mechanisms contributing to this tidal evolution are interpreted in the discussion. We finalize with conclusions.

3.2. STUDY AREA

THE Yangtze River is one of the largest rivers in the world in terms of its river length (~6,300 km) and catchment area (~1.9 million km²). Datong station, ~490 km upstream of Xuliujing, is the tidal wave limit in the dry seasons. The yearly mean river discharge monitored at Datong is 28,200 m³/s (1951–2016), but monthly averaged values fluctuate between 10,000 and 80,000 m³/s. The annual suspended sediment load has declined from 424 million tons per year (1951–2002) to 134 million tons per year (2003–2018). The river flows south-eastward into the East China Sea via its four outlets in the Yangtze Estuary, i.e., the North Branch, the North Channel, the North Passage, and the South Passage (Figure 3.1). In this work, we mainly focus on the inner South Branch and the seaward mouth zone including the North Channel, North Passage, and its seaward area. Xuliujing station, the bifurcation point between the North Branch and the South Branch, is defined as the origin ($x=0$ km) of the axis. Tides in the Yangtze Estuary have a predominantly semi-diurnal regime with a form factor $(A_{O1}+A_{K1})/(A_{M2}+A_{S2})$ ranging between 0.15 and 0.25 (Yun, 2004; Lu et al., 2015) and the oceanic tides show no long-term changes other than the nodal tidal variations. In the landward direction, tidal waves are first slightly amplified from offshore to the nearshore (up to Niupijiao) owing to decreased water depth, and then predominantly damped further inside the estuary owing to the combined effect of bed friction and river discharge (Guo et al., 2015). The seasonal variations in tidal amplitude in the region upstream of Xuliujing are dominantly controlled by highly non-stationary river discharge.

In the past 60 years, both the reduction in riverine sediment input and large-scale human interventions influence the hydro-morphodynamics in the Yangtze Estuary. The annual river discharge at Datong has remained stable since 1954, but its seasonal variations are regulated by hydropower dams, i.e., increased river discharges in the dry season and reduced peak river discharges in the wet season (Guo et al., 2018a). The suspended sediment load has gradually decreased since the mid-1980s, and this reduction has accelerated since 2003 when the TGD began operation (Yang et al., 2011; Luan et al., 2016; Zhao et al., 2018; Guo et al., 2018a). Within the estuary, the Deep Channel Navigation Project (DCNP) was implemented in the North Passage from 1997 to 2010 with three phases (Figure 3.2). Phase I of the project (1998–2001) involved the construction of diversion works at the bifurcation between the North and South Passage, of the northern training jetty and groins (N1–N5), and the southern training jetty and groins (S1–S5). The navigation channel was deepened to 8.5 m with a 300 m width. Phase II of the project was undertaken between 2002 and 2005, including the extension of the two training jetties and construction of the groins N6–N10 and S6–S9. The navigational channel was deepened, reaching a depth of 10 m and a width of 300–400 m. Phase III of the project was carried out from 2006 to 2010, during which the navigational channel was deepened to 12.5 m with the construction of a 21-km long sediment-retention jetty and lengthening of the groins. Between 2007 and 2016, an average of 72 million m³ of sediment was annually dredged along the North Passage, of which approximately 30% was disposed on Hengsha flat to create land, and the remaining parts were disposed partly in the shallow areas between the groins and partly offshore (Zhu et al., 2019).

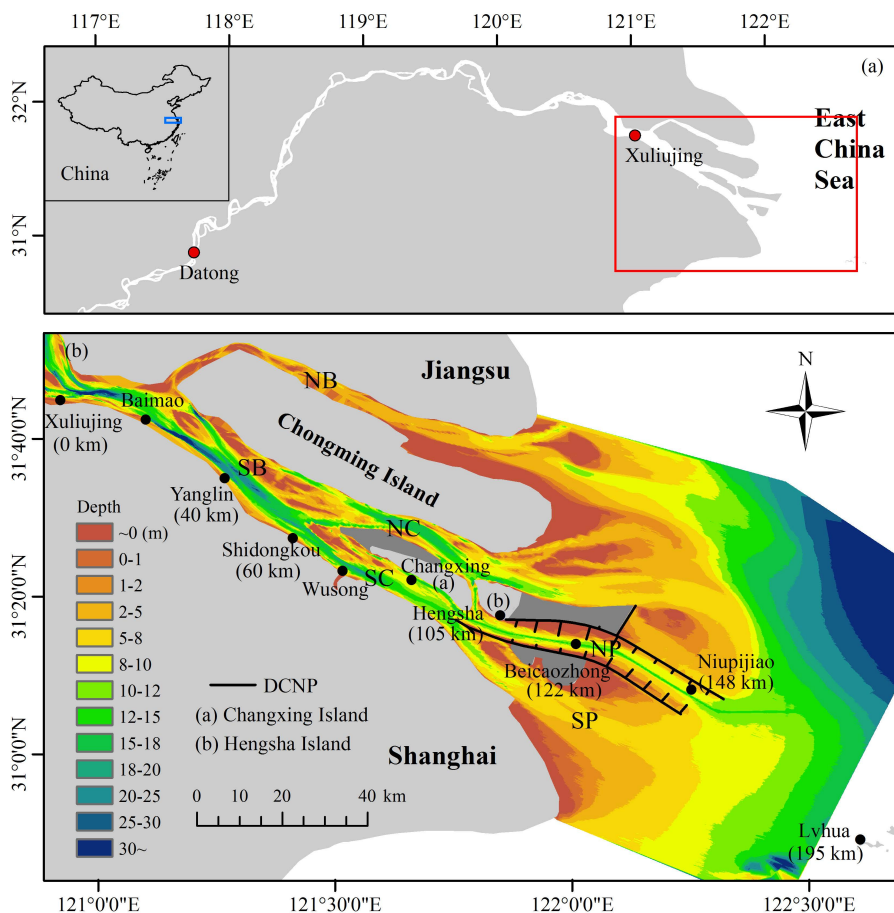


Figure 3.1: (a) The Yangtze Estuary and (b) the study area and the tidal gauge stations. The figures in brackets are distances downstream of Xuliujing ($x=0$ km). DCNP: Deep Channel Navigation Project. NB: North Branch; SB: South Branch; NC: North Channel; SC: South Channel; NP: North Passage; SP: South Passage.

3.3. MATERIAL AND METHODS

3.3.1. DATA

LONG time series of river discharges, sediment loads, and water levels in the Yangtze Estuary were provided by the Bureau of Hydrology, Changjiang Water Resources Commission (CWRC) for detailed analysis. Daily river discharges between 1958 and 2020 and annual sediment loads between 1951 and 2019 were collected at Datong. Hourly tidal water levels were provided for 1990-1991, 2009-2010, and 2019-2020 at Xuliujing and Yanglin ($x=40$ km) to reveal the tidal evolution in the South Branch. In addition, the yearly-averaged tidal ranges are obtained from the yearly-averaged high and low water levels from 1996 to 2011 (Fu, 2013) at seven stations, i.e. Shidongkou ($x=60$ km), Wusong ($x=70$ km), Changxing, Hengsha ($x=105$ km), Beicaozhong ($x=122$ km), Niupijiao

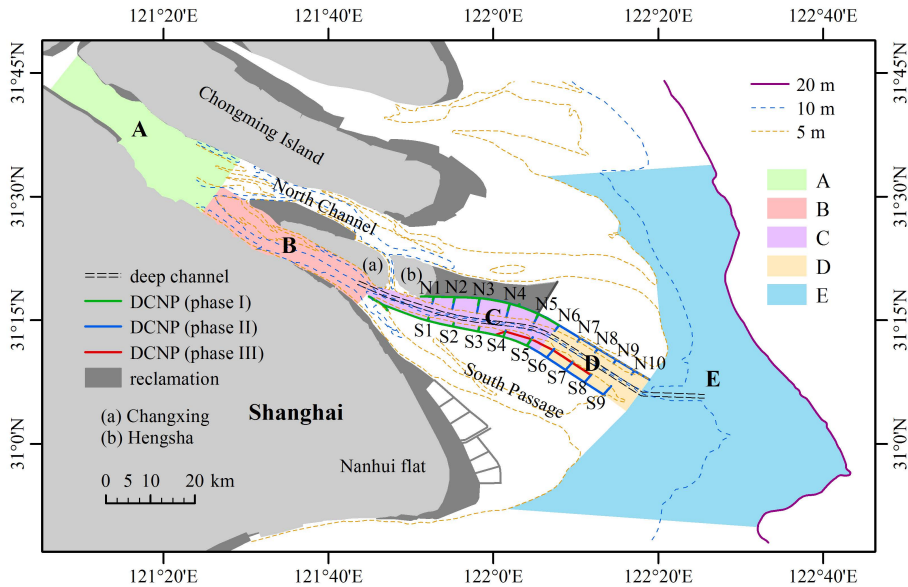


Figure 3.2: The three phases of the Deep Channel Navigation Project (DCNP), reclamation areas and the regions A, B, C, D and E in the Yangtze Estuary.

(except in 1996-2001) and Lvhu to quantify the decadal tidal evolution in the mouth zone. Time series of hourly water levels are available at Xuliujing and Wusong between 2006 and 2015.

Bathymetric data are available for 1986, 1997, 2002, 2007, 2010, and 2016; see [Zhu et al. \(2019\)](#) for details of the digitalization, accuracy, and description of the bathymetry maps. These bathymetries are further used to explore the effect of morphological changes using a numerical model.

3.3.2. DATA ANALYSIS

Tidal evolution is evaluated by changes in tidal amplitudes and ranges, phases, and tidal damping factors. The amplitudes and phases of the main tidal constituents are determined by harmonic tidal analysis with nodal corrections, by using the t-tide function ([Pawlowicz et al., 2002](#)). To evaluate the effect of seasonal river discharge variations, we also employed an enhanced harmonic analysis for non-stationary tides using the s-tide function to resolve the main tidal constituents ([Pan et al., 2018](#); [Wang et al., 2020](#)).

To eliminate natural tidal amplitude variations over time (e.g. the spring-neap variations), we define a damping factor per section of the estuary to quantify the amplification/damping rate of the tidal waves. A damping factor is the ratio of tidal range in the landward station to a more seaward station, equivalent to the amplification factor (see [Wang et al., 2014, 2019b](#); [Jalón-Rojas et al., 2018](#)). The tidal ranges are estimated similar to [Kukulka and Jay \(2003\)](#) and [Matte et al. \(2013\)](#), by high-pass filtering the hourly water levels to remove variations at subtidal frequencies, interpolating the data to 6 min intervals, and determining the minimum and maximum heights using a 25 h moving window

with a 1 h time step (Guo et al., 2015). We additionally compute the hydraulic head, which strongly depends on the river discharge but provides indications for changes in morphology (e.g. the water depth, storage width, and hydraulic drag, see Wang et al., 2019b). For a given time series of water levels, e.g., at Xuliujing and Yanglin, the hydraulic head is determined as the difference between the subtidal water levels at Xuliujing and Yanglin.

3.3.3. NUMERICAL MODELLING

MODEL SETUP

Since both morphology and SSC affect tidal amplification, it is technically difficult to identify the different controlling variables based on observations only. In numerical models, the contribution of morphological changes can be evaluated from simulations using historic bathymetries under the same forcing conditions (Lopes et al., 2013; Grasso and Le Hir, 2019). The effect of SSC changes on the tides on a decadal scale can be evaluated by varying bed roughness, e.g. the Manning coefficient n (Wang et al., 2014; van Maren et al., 2015b). Note that the bed roughness in numerical models is a combined result of bedforms, subgrid-scale morphology, near-bed turbulence, bed properties, and vegetation, etc. For instance, the apparent bed roughness is smaller in three-dimensional (3D) baroclinic models than two-dimensional (2D) models in case of suppression of turbulence near the bed resulting from steep concentrations or vertical salinity gradients induced by salinity or sediments (Winterwerp et al., 2009). Therefore, we developed a 2D barotropic model in which salinity but especially the role of sediments is parameterized in the bed roughness. The contribution of morphology, construction of structures, and bed roughness can then be evaluated individually. The required modifications in the bed roughness are subsequently interpreted in terms of changes in SSC and fluid mud occurrences.

In addition, the Yangtze Estuary is such a large estuary that patterns of tidal amplification/damping (and underlying mechanisms leading to these tidal changes) may vary spatially. Therefore, in this study, we quantify the decadal tidal evolution with the damping factor in different parts of the estuary based on water level data since the 1990s. The numerical model is subsequently applied to interpret the physical mechanisms responsible for the observed changes using historic bathymetries in 1986, 1997, 2002, 2007, 2010, and 2016.

The model was set up using the Delft3D model system (Lesser et al., 2004), which simulates flow, sediment transport, and morphological changes. The 2D model is simulated for a full year in 2006 to reach equilibrium and another full year in 2007 for further study with realistic forcing of river discharges measured at Datong. The jetties and groins in the North Passage (since 1998) are numerically implemented as structures completely blocking through- or overflow. The effect of the hydraulic drag is expressed in terms of the Manning coefficient n ($\text{s}/\text{m}^{1/3}$) which is initially converted from existing values of the Nikuradse roughness length varying from 0.002 to 0.008 m (Zhu et al., 2016) and the water depth:

$$n = h^{1/6} / \left[18 \log \left(\frac{12h}{k_s} \right) \right] \quad (3.1)$$

Where h is the water depth (m), k_s is the Nikuradse roughness length (m). The resulting Manning coefficient n ($\text{s}/\text{m}^{1/3}$) is then calibrated ranging from 0.013 to 0.022. Note that the Manning coefficient n is so frequently used in this paper that the unit is hereafter omitted. The Manning coefficient n (the reference n in Table 3.1) is relatively small in the estuary (0.013~0.018) and high in the river upstream of $x=0$ km (0.018~0.022) as well as seaward of $x=195$ km (0.018~0.02).

MODEL CALIBRATION

The model is calibrated against measured water levels for the whole year of 2007. The computed water level at the 8 stations agrees well with the measured data exemplified with August-September 2007 (see Figure S3.1). Both the modelled M_2 amplitude and tidal range are consistent with the observations from 15 August 2007 to 15 September 2007 (Figure 3.3a and b). From the mouth (Lvhua) to its upstream, the tides are amplified by 8% to $x=148$ km and then damped by 30% further upstream. For the M_2 constituent, the difference between the computed and measured amplitudes is less than 5%. Similarly, the difference between observed and modelled tidal ranges in the same period is also less than 5%. For a whole year, we computed tidal ranges at 9 stations (see Figure 3.1), to compare with the measurements (Figure 3.3c). We also calibrated damping factors in the reaches Xuliujing-Yanglin, Shidongkou-Hengsha, Hengsha-Beicaozhong, Beicaozhong-Niupijiao, Hengsha-Niupijiao, Niupijiao-Lvhua, and Hengsha-Lvhua (Figure 3.3d). The differences between the modelled and observed yearly-averaged tidal ranges as well as damping factors are less than 5%. This calibration suggests a high-performance level of the numerical tidal model which is subsequently used to study the impact of changing boundary conditions.

MODEL SCENARIOS

Three groups of simulations were executed (Table 3.1), based on the changes in topography (hindcast scenarios) and friction coefficients (as a sensitivity test and for detailed calibration):

- (1) Historic scenarios ('tpg1' - 'tpg6') are executed for the years 1986, 1997, 2002, 2007, 2010, and 2016 with different phases of jetties and groins constructed in 2002 (phase I), 2007 (phase I and II), 2010 (phase I and II) and 2016 (phase I and II). This group accounts for the effect of topography (including the morphological changes and the simulated engineering structures) on tidal evolution. To reveal the effect of bathymetry (and also roughness hereafter), all scenarios are run with the same river discharge, using the hydrograph of the year 2007. The sensitivity of tidal damping to the river discharged will be evaluated in more detail in the discussion.
- (2) The sensitivity of tidal dynamics to effective bottom roughness is explored with runs 'rgh0' - 'rgh5'. The effective bottom roughness is lowered to estimate the effect of fluid mud formation in the North Passage (following e.g., Winterwerp et al., 2013; Wang et al., 2014; van Maren et al., 2015b). We use a reduction of 10% to account for a reduced sediment supply (which is less than the 15-50% change introduced by the studies mentioned above). The effect of a 10% decrease in Manning coefficient n was evaluated for regions A, B, C, D, and E (see Figure 3.2), named '0.9A', '0.9B', '0.9C', '0.9D', and '0.9E', respectively.

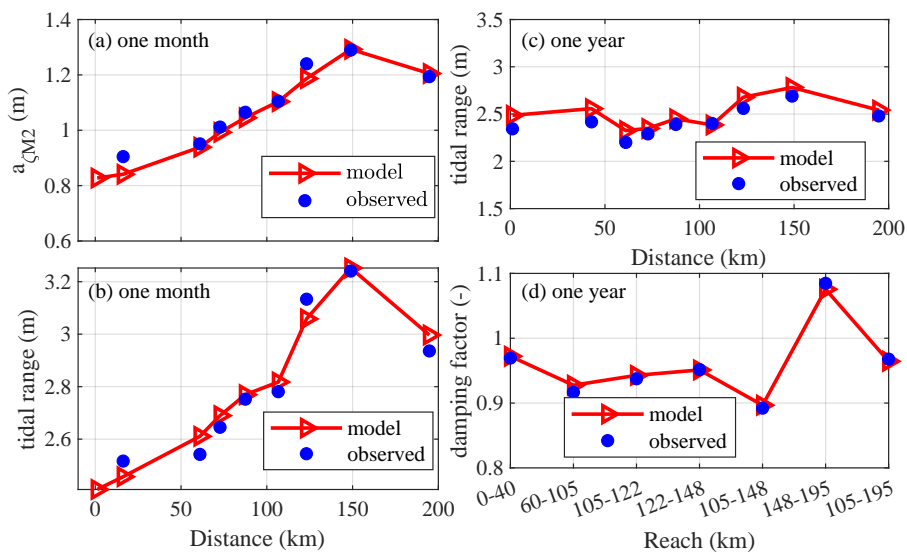


Figure 3.3: Comparison between observed and modelled (a) M_2 amplitude ($a_{\zeta M2}$) during 15 August – 15 September 2007; (b) tidal range during 15 August-15 September 2007; (c) yearly-averaged tidal range in 2007; and (d) yearly-averaged damping factor in the reaches Xuliujing-Yanglin (0-40 km), Shidongkou-Hengsha (60-105 km), Hengsha-Beicaozhong (105-122 km), Beicaozhong-Niupijiao (122-148 km), Hengsha-Niupijiao (105-148 km), Niupijiao-Lvhua (148-195 km), and Hengsha-Lvhua (105-195 km) in 2007.

- (3) The last group was calibrated to observed amplification/damping by changing the bed roughness in the historic scenarios, with ('cal_tpg1' - 'cal_tpg6') and without ('cal_mor1' - 'cal_mor6') the effect of local structures. This calibration was executed by iteratively modifying the roughness in parts of the model domain (using the 'rgh' series as an initial estimate) to fit modelled tidal damping factors to the observed tidal damping factors. The comparison between the simulations with and without local structures also indicates the effect of local structures on the calibrated roughness changes.

3.4. RESULTS

3.4.1. OBSERVED DECADEAL TIDAL EVOLUTION

IN the South Branch, the 2-year averaged amplitude of M_2 tide from $x=40$ km to $x=0$ km is reduced by 12% in 1990-1991 whereas the reduction is only 3% in the periods 2009-2010 and 2019-2020 (Table S3.1). Conversely, the 2-year averaged amplitude of the M_4 overtide decreases by 1% from $x=40$ km to $x=0$ km in 1990-1991 and 14% in the periods 2009-2010 and 2019-2020. As a result, the A_{M4}/A_{M2} amplitude ratio increased from 0.195 ($x=40$ km) to 0.219 ($x=0$ km) in 1990-1991 and decreased from 0.213 ($x=40$ km) to 0.189 ($x=0$ km) in 2009-2010. In 2019-2020, the A_{M4}/A_{M2} amplitude ratio decreased from 0.193 ($x=40$ km) to 0.171 ($x=0$ km). An increase and decrease in the A_{M4}/A_{M2} amplitude ratio implies more and less tidal distortion, respectively.

Table 3.1: List of scenarios implemented in the model. Local structures of phase I include jetties and groins (N1-N5, S1-S5) whereas phases I & II include N1-N10 and S1-S9 (see Figure 3.2). '0.9A', '0.9B', '0.9C', '0.9D', and '0.9E' represent a 10% decrease in the Manning coefficient n in the regions A, B, C, D, and E, respectively (see Figure 3.2) compared with the reference roughness in the calibrated case, similarly for the roughness in the other series.

Aim	Cases	Depth	Local structures (phase)	Roughness	Note
Sensitivity to topography	tgp1	1986	-	reference	-
	tgp2	1997	-	reference	-
	tgp3	2002	I	reference	-
	tgp4	2007	I & II	reference	calibrated
	tgp5	2010	I & II	reference	-
	tgp6	2016	I & II	reference	-
Sensitivity to roughness	rgh0	2007	I & II	reference	calibrated
	rgh1	2007	I & II	0.9A	-
	rgh2	2007	I & II	0.9B	-
	rgh3	2007	I & II	0.9C	-
	rgh4	2007	I & II	0.9D	-
	rgh5	2007	I & II	0.9E	-
Optimize roughness	cal_tgp1	1986	-	0.75A	recalibrated
	cal_tgp2	1997	-	1.1B0.75(CDE)	recalibrated
	cal_tgp3	2002	I	1.2B0.8D0.7E	recalibrated
	cal_tgp4	2007	I & II	reference	calibrated
	cal_tgp5	2010	I & II	1.2(ABC)0.7E	recalibrated
	cal_tgp6	2016	I & II	1.25A	recalibrated
	cal_mor1	1986	-	0.75A	recalibrated
	cal_mor2	1997	-	1.1B0.75(CDE)	recalibrated
	cal_mor3	2002	-	1.2B1.3C0.8D0.7E	recalibrated
	cal_mor4	2007	-	1.1C0.9D0.9E	recalibrated
	cal_mor5	2010	-	1.2(AB)1.3C0.9D0.7E	recalibrated
	cal_mor6	2016	-	1.25A	recalibrated

The damping factors and hydraulic head between $x=0$ and $x=40$ km are calculated for the three periods (1990-1991, 2009-2010, and 2019-2020, see Figure 3.4). The damping factors were overall smaller than 1, indicating predominantly landward damping. The mean damping factor was approximately 0.1 larger in the period 2009-2010 than 1990-1991 whereas the mean damping factor slightly decreased again from 2009-2010 to 2019-2020. Seasonal variations indicate a smaller damping factor under higher river discharge, which is more pronounced in 1990-1991 than the other two periods. Specifically, the damping factor in the dry season is ~ 0.08 higher than in the wet season in 1990-1991. The hydraulic head also suggests significant seasonal variations in the three periods, i.e. a larger hydraulic head under higher river discharge. From 1990-1991 to 2009-2010, the

hydraulic head from $x=0$ km to $x=40$ km decreased, with an abrupt increase at the end of 2009 which is attributed to an increase in river discharge. From 2009-2010 to 2019-2020, the hydraulic head slightly increased.

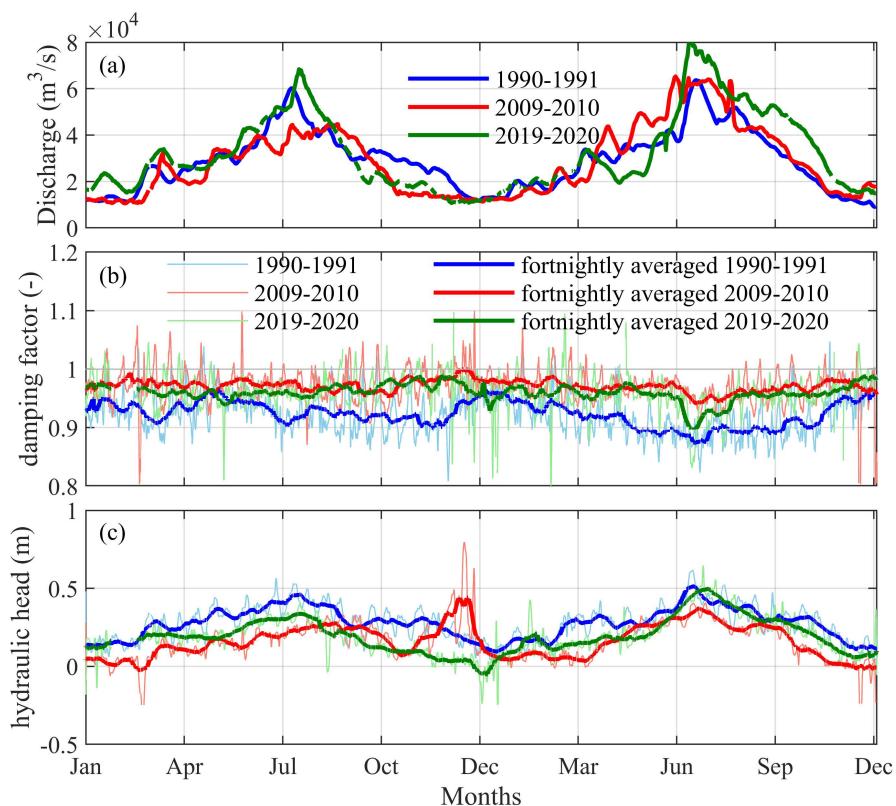


Figure 3.4: Variations of (a) river discharge at Datong, (b) damping factor and (c) hydraulic head between Xuliujing ($x=0$ km) and Yanglin ($x=40$ km) during 1990-1991, 2009-2010 and 2019-2020.

The observed yearly averaged damping factors in the lower estuary (sections for $x>60$ km) since 1997 are also provided per section (lines in Figure 3.5b and c). Unlike the weaker tidal damping in the South Branch (0-40 km), the damping factor in the South Channel (60-105 km) increased to 0.93 in 2004 and then decreased to 0.86 in 2011. In the North Passage (105-148 km), the observed damping was stronger from 1997 to ~ 2005 followed by weakened damping afterwards. Seaward of the North Passage (148-195 km), the damping factor (>1 , tidal amplification) show similar variations as the North Passage with the lowest damping factor of 1.05 observed in 2006; although the damping factor decreased after 2010.

3.4.2. COMPUTED TIDAL EVOLUTION

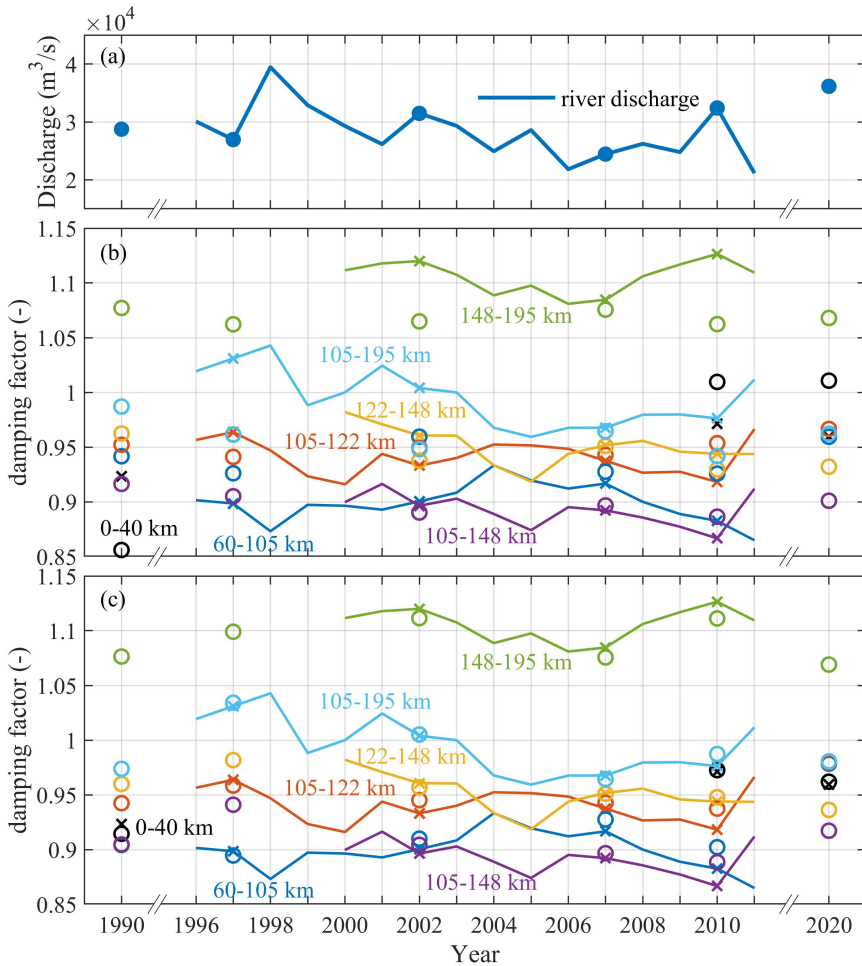


Figure 3.5: The yearly averaged (a) river discharge at Datong, (b) observed (solid lines for all years, crosses for years evaluated with the model) and computed ('tpg' series, circles) damping factors in the reaches Xuliujing-Yanglin (0-40 km), Shidongkou-Hengsha (60-105 km), Hengsha-Beicaozhong (105-122 km), Beicaozhong-Niupijiao (122-148 km), Hengsha-Niupijiao (105-148 km), Niupijiao-Lvhua (148-195 km) and Hengsha-Lvhua (105-195 km), and (c) same as (b) but the computed damping factors are from 'cal_tpg' series with optimized roughness. Colours refer to the reach.

HISTORIC SCENARIOS

The modelled tidal evolution ('tpg' series) over time is represented by the damping factors in different reaches in 1990, 1997, 2002, 2007, 2010, and 2020 (Figure 3.5b). In the South Branch (0-40 km), both the model results and observations suggest a decrease in tidal damping (~18% increase in the damping factor) from 1990 to 2010. However, the simulated change in tidal damping is ~13% larger than observations. In the lower estuary (all transects for $x > 60$ km), the simulated damping factor varies much less than the observed damping factors from 1997 to 2010. This suggests that tidal damping is less in-

fluenced by the topography, and therefore exemplified with more detailed comparisons of sections. In the South Channel (60-105 km), the modelled tidal damping is much lower than the observed damping. In the lower North Passage (122-148 km) and seaward of the North Passage (148-195 km), the modelled tidal damping is much stronger than the observed tidal damping.

Overall, in the South Branch, the observed and modelled tidal damping reasonably agree (reduced tidal damping), which is therefore primarily the result of topographic changes. Seaward of the South Branch, the observed and modelled changes disagree, implying that the tidal changes are less influenced by topographic changes. In the next section, we will explore the role of processes impacting the bed roughness (SSC, fluid mud) on tidal damping in more detail by varying the bed roughness in the model.

CHANGES IN BED ROUGHNESS

A local adjustment of the bed roughness only influences the regional damping factor (Figure 3.6a). A local 10% roughness reduction influences the damping factor more in regions A (2.1%) and B (2.5%) than in other regions (~1.7%). This sensitivity was used to develop a time- and spatial- varying roughness field with which we recalibrated the numerical model (Figure 3.5c, Figure 3.6c and d). The effect of local structures on the roughness change is estimated by comparing the differences in calibrated effective bottom roughness between simulations with local structures ('cal_tpg' series) and without local structures ('cal_mor' series) (Figure 3.6b). Specifically, the local structures mainly increase the roughness in the period of the construction, i.e., a 30% increase in the roughness in region B from 1997 to 2002 and an 11% increase in regions D and E from 2002 to 2007. After 2002 in region C and after 2007 in regions D and E, the roughness decreased or remained relatively stable, which implies that the effects of the local structures are short-term. In region A, the effective bottom roughness shows a strong increase from 1990 to 2010 followed by a slight increase until 2020 (Figure 3.6c). Further seaward, the bed roughness varies more strongly over time (Figure 3.6d). The effective bottom roughness decreased by 6.7% in region E but increased by 60%, 9%, 60% and 25% in regions A, B, C, and D, respectively from the 1990s to 2010. From 2010 to 2020, the effective bottom roughness slightly increased by 5% in region A.

3.5. DISCUSSION

3.5.1. MODEL LIMITATIONS: EFFECT OF RIVER DISCHARGE

GIVEN the changes in river discharge of the recent 30 years are limited, we assumed that variations in tidal damping are mainly attributed to changes in topography (morphology and local structures) and effective bottom roughness, but not to inter-annual river discharge changes. Note that the river discharge has changed at the seasonal time scales owing to dam constructions (Guo et al., 2018a). To evaluate the effect of river discharge magnitude, we resolved the damping factors based on the M_2 amplitude using the s-tide function. The damping factors are further averaged during the periods when the river discharge is from 5,000 to 60,000 m^3/s with an increment of 5,000 m^3/s , e.g., between 5,000 and 10,000 m^3/s , between 10,000 and 15,000 m^3/s . We see that the damping factor decreases with increasing river discharge in the reaches 0-40 km and 60-105 km (Figure 3.7a, b), but has negligible influence seaward of $x=105$ km (Figure 3.7c, d).

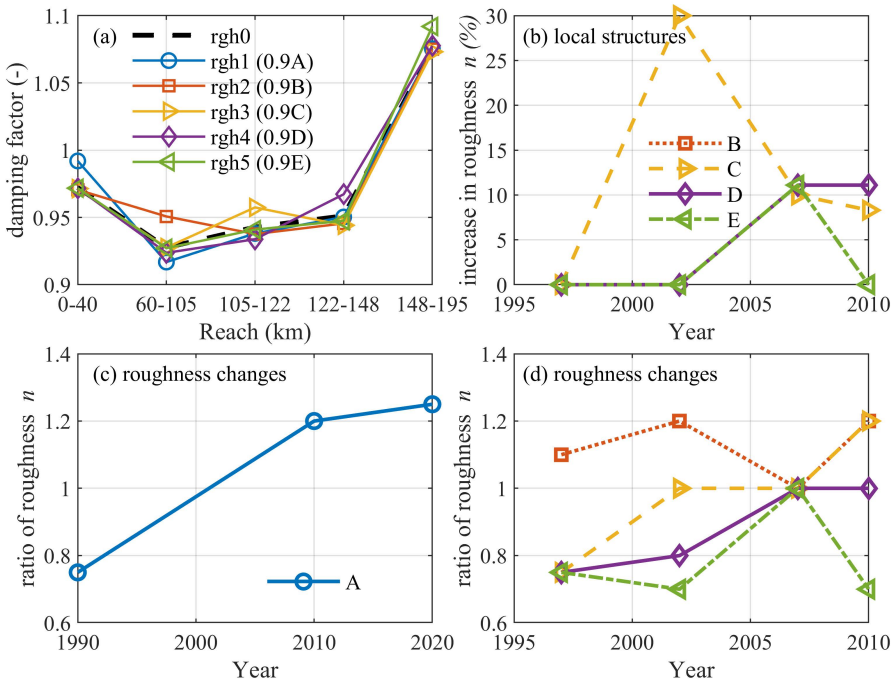


Figure 3.6: Modifications of the Manning coefficient n : (a) Model sensitivity to a 10% decrease in roughness ('rgh' series in Table 3.1) in the five regions-A, B, C, D, and E (see Figure 3.2), (b) the effect of simulated local structures on increasing the roughness, and changes in the effective bottom roughness in region A (c) and regions B, C, D, and E (d).

In the reach 0-40 km (South Branch), for equal river discharge, the damping factor in the period 1990-1991 is markedly lower than for the periods 2009-2010 and 2019-2020. This suggests that the impact of inter-annual changes in river discharge is much less important compared with the changes in morphology and bed roughness. The effect of river discharge is evaluated by rerunning the reference simulations with the river discharge of that particular year instead of using the 2007 hydrograph (as in the reference simulations). In the reaches 60-105 km, 105-148 km and 148-195 km, no significant changes in damping factors are detected under the changes in seasonal variations among the years 1997, 2002, and 2010 compared to the year 2007. Therefore, it can be concluded that the dependence of the damping factor on river discharge is limited in the downstream reaches but more pronounced in the upper reaches. However, changes in morphology still dominate tidal damping in the reach 0-40 km.

3.5.2. EFFECT OF MORPHOLOGICAL CHANGES

The morphological changes play a more important role in tidal damping in the reach 0-40 km (South Branch) than downstream of $x=40$ km (Figure 3.5b). Therefore, we mainly explore the effect of morphological changes in the South Branch. The longitudinal variation in width and water depth is derived from bathymetries of the years 1986, 1997,

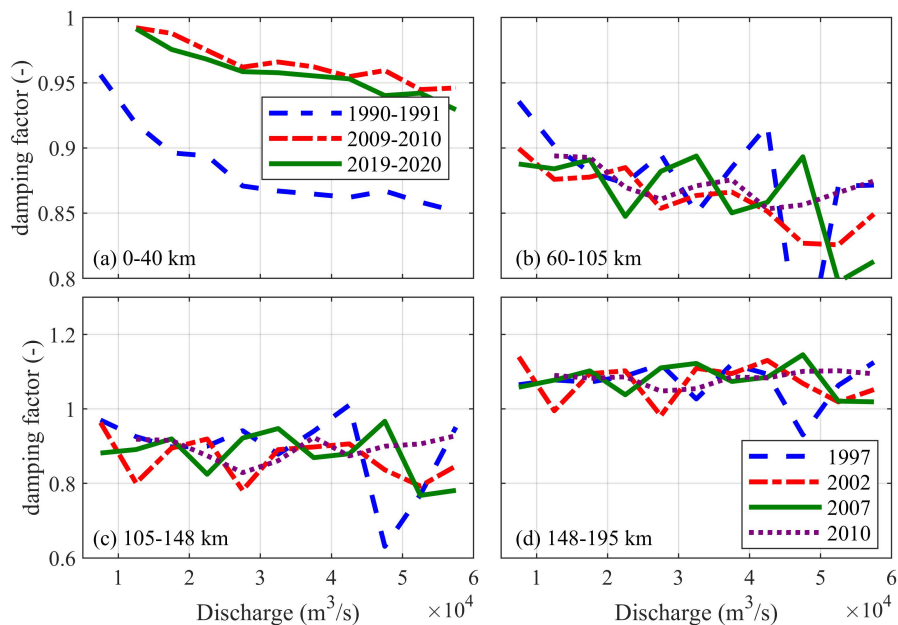


Figure 3.7: Observed damping factors (computed with non-stationary harmonic analysis) in the reach Xuliujing-Yanglin (0-40 km) with the river discharges measured at Datong during 1990-1991, 2009-2010 and 2019-2020 (a) and modelled damping factor in the reaches (b) Shidongkou-Hengsha (60-105 km), (c) Hengsha-Niupijiao (105-148 km) and (d) Niupijiao-Lvhua (148-195 km) with river discharges measured at Datong in 1997, 2002, 2007 and 2010 in the reference scenarios (see Table 3.1).

2002, 2007 2010 and 2016 (Figure 3.8). The longitudinal change in width is defined by the cross-sectionally averaged width under the high and low water levels. Note that the high water level (1.37 m) and low water level (-1.32 m) for all years is based on Niupijiao station ($x=148$ km) in the year 2007. The longitudinal changes of the water depth are defined as the cross-sectionally averaged depths below mean sea level (0 m).

From 1986 to 2010, the channel width decreased whereas the water depth increased. The increase in the water depth is primarily associated with the channel scouring caused by reduced riverine sediment supply since the mid-1980s (Wang et al., 2013). The decrease in channel width may be ascribed to deposition in shallow areas and land reclamations (see Figure 3.2). Typically, both the decrease in width (strengthening the estuarine funnel shape) and increase in water depth weaken tidal damping (Jay, 1991; Friedrichs and Aubrey, 1988, 1994; Dyer, 1997; Savenije, 2006). However, the decrease in the hydraulic head cannot be explained by the decrease in the storage width, but only by the increase in depth. As a result, the reduced tidal damping in the South Branch (0-40 km) from 1990 to 2010 is primarily the result of the water depth increase. From 2010 to 2020, both the channel width and depth do not significantly change (Figure 3.8) and the modelled damping induced by the topography could not explain the slight decreasing damping factor (Figure 3.5). The decrease after 2010 is therefore more strongly influenced by the bed roughness, which will be discussed in the next section.

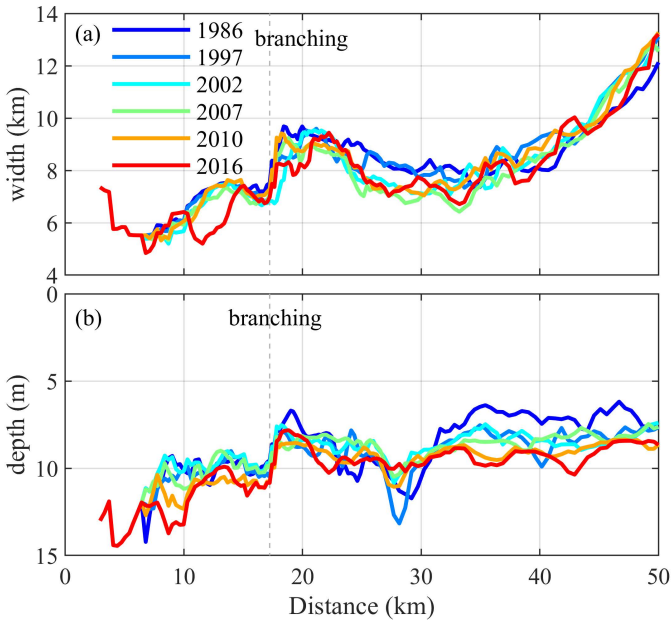


Figure 3.8: Longitudinal changes of (a) cross-sectional averaged width between high and low water levels and (b) cross-sectional averaged water depth in 1986, 1997, 2002, 2007, 2010 and 2016. The 'branching' indicates the location where the bifurcation between the North Branch and South Branch starts.

3.5.3. MECHANISMS RESPONSIBLE FOR CHANGES IN BED ROUGHNESS

We hypothesize that 4 factors may potentially influence the bed roughness, either through an increase (+), decrease (-) or both (see Table S3.2):

- The construction of local structures (+)
- The effect of the reduced riverine SSCs (+)
- The formation of fluid mud (-)
- The change of grain size of sediment (+) (-)

Firstly, the construction of jetties and groins in the DCNP may increase hydraulic friction. These frictional effects are at least partly incorporated in the model (accounting for energy losses resulting from jetties and groins). However, local structures generate strong shear and vortices which enhance turbulence mixing (Ma et al., 2011). These small-scale hydrodynamic effects may not be well simulated in a model with mesh sizes not sufficiently small to represent these phenomena but can cause important frictional effects which require an increase in the prescribed bed roughness.

Secondly, the changing roughness over time may be related to the changes in SSC, i.e. reduced hydraulic drag caused by the increase in the SSC (Winterwerp et al., 2009; Wang et al., 2014). The riverine SSC has been decreasing since the mid-1980s and even more pronounced after 2003 (Yang et al., 2011; Luan et al., 2016; Zhao et al., 2018; Guo et al.,

2018a; Zhu et al., 2019). However, the changes of SSC in response to the reduced riverine SSC in the Yangtze Estuary are complex. Previous studies suggest that SSC has been decreasing in the South Branch since 2009 (Zhu et al., 2015) but remained unchanged in the South Channel and mouth zone (Dai et al., 2013b; Zhu et al., 2015). Liu (2009) concluded that SSC in the South Branch and South Channel decreased and remained the same in the mouth zone but the assessment was based on 2-year observations only. We use five datasets of measured SSCs collected over similar periods (a spring-neap tidal cycle during the wet season), sampling methods, and locations in 2003, 2007, 2013, 2019, and 2020 (Figure 3.9). The observed tidally- and depth-averaged SSC confirms a significant decreasing trend in the South Branch and South Channel from 2003 to 2013 and in the South Passage from 2003 to 2020, i.e., reduced by 84%, 64% and 63%, respectively. The SSC does not show a clear trend until 2013 in the North Channel, North Passage and the seaward areas whereas a 24% and 51% decrease in SSC was observed between 2013 and 2020 in the North Channel and North Passage, respectively. Seaward of the channels, the decrease in SSC is only pronounced in the two most recent years (2019-2020) with an average of reduction 46% among the three branches. Therefore, the reduced SSC is likely to cause an increase in effective bottom roughness in the South Branch and South Channel. However, within and seaward of the North Passage, the reduction in SSC was not large enough over the investigated period and therefore insufficiently to induce the changes in effective bottom roughness from 1997 to 2010. However, it is expected that the continued reduction in SSC will progressively more influence tidal propagation.

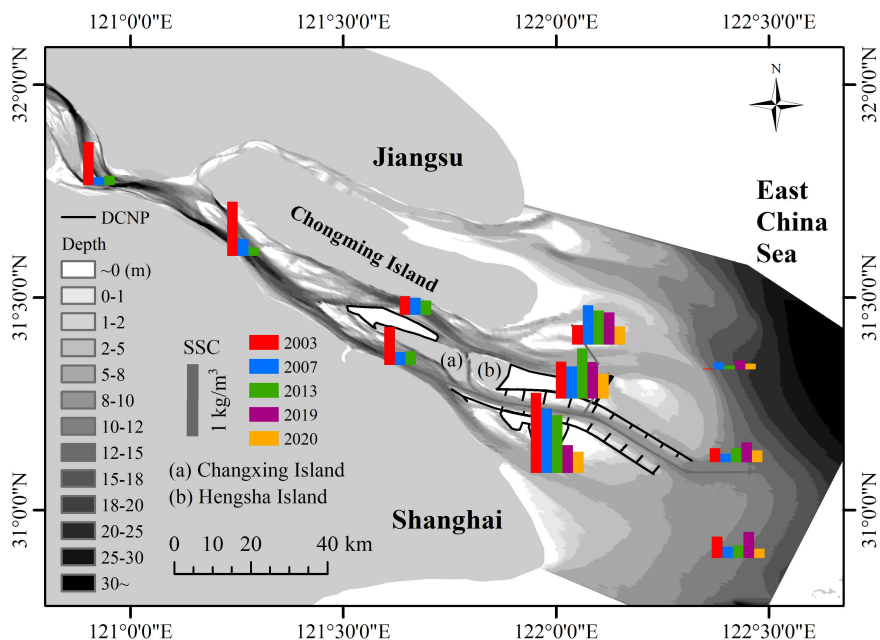


Figure 3.9: Tidal and depth-averaged suspended sediment concentrations (SSC) during the wet season in 2003, 2007, 2013, 2019 and 2020.

Thirdly, the formation of fluid mud, which is a layer of near-bed high SSC, is extremely important in the suppression of turbulence, reducing roughness and strengthening tidal amplification (Allen et al., 1980; Gabioux et al., 2005). Fluid mud with a thickness of up to 1 m has been detected within and seaward of the North Passage since the 1970s (Li et al., 2001). After the construction of the DCNP, the thickness of the fluid mud in the North Passage was 1-5 m and was more frequently observed as a result of reinforced stratification in the narrowed and deepened channels (Liu et al., 2011; Song et al., 2013; Wan et al., 2014b; Lin et al., 2021). This is also consistent with the high siltation rate and large dredging demand in the regulated North Passage, triggering research on controlling mechanisms of the fluid mud (Liu et al., 2011; Wu et al., 2012; Jiang et al., 2013a; Kuang et al., 2014). Therefore, enhanced fluid mud formation within and seaward of the North Passage has likely reduced the effective roughness.

Lastly, due to the upstream dam construction, the grain size of sediment may have changed in the Yangtze Estuary. The grain size of the suspended sediment has been reported to decrease, although varying with channels as well as hydrodynamic conditions (see Figure S3.2 adapted from Chen et al., 2016b, 2019; Yang et al., 2016). The effect of the grain size of suspended sediment on roughness may be complex since the relationship between the two may be non-linear (van Maren, 2007). Very fine sediments are uniformly distributed over the water column and therefore have limited sediment-induced density effects (and therefore tidal dynamics). Similarly, very coarse sediment remains close to the bed, therefore also having a minor impact on sediment-induced density effects. Median grained sediment has the most pronounced effect on vertical stratification and through its impact on the vertical exchange of turbulent momentum and viscous dissipation on the apparent hydraulic roughness. It is likely that over decadal timescales, dams primarily reduce the flux of these medium-grained sediments to the Yangtze Estuary (van Maren et al., 2013). Additionally, the grain size of bed sediments affects roughness through skin friction, but even more through its impact on estuarine bed forms (form friction). The combined relationship between grain size and apparent roughness is therefore very complex. After the operation of the TGD in 2003, the grain size of bed sediments did not significantly change in the South Branch, South Channel and North Passage (Luo et al., 2012; Qiao, 2019), whereas coarsening of bed sediments was observed seaward of the North Passage (Luo et al., 2012, 2017; Yang et al., 2018; Zhan et al., 2020): the averaged median grain size of the bed sediments in the seaward area coarsened from 8.0 μm in 1982 to 15.4 μm in 2012 (Yang et al., 2018). Although we still insufficiently understand the effect of sediment grain size on roughness, observations suggest a change in grain size of the bed sediment and the suspended load, which may contribute to the changes in roughness.

The changes in effective bottom roughness and the potential effects of the various factors are illustrated in different regions (Figure 3.10). Note that we derive the changes in effective bottom roughness in the reaches for $x > 40$ km after 2010 based on the changes in damping factor from 2010 to 2011. In the South Branch, the 60% increase in roughness from 1990 to 2010 is mainly attributed to the strongly reduced SSC; the 5% increase after 2010 results from minor changes in SSC thereafter. Although the local structures were constructed in the North Passage, they may play a role in increasing the effective bottom roughness not only in the North Passage but also in its upstream (South Channel) and

seaward area. The effect of local structures on raising the effective bottom roughness is also short-term (see the pronounced elevated bed roughness in the year 2002 in Figure 3.6b) and therefore such an effect may be limited after 2010. Moreover, the formation of fluid mud has been accelerated by the DCNP, which may play an increasing role in decreasing the effective bottom roughness in the North Passage and its seaward area. This effect may not strong enough to lead to a decrease in the effective bottom roughness in the North Passage during the DCNP construction (1997-2010) but may contribute to the decrease in the effective bottom roughness after 2010. The grain size of suspended and bed sediments is influenced by the dam constructions and engineering works, which may either increase or decrease the roughness throughout the estuary.

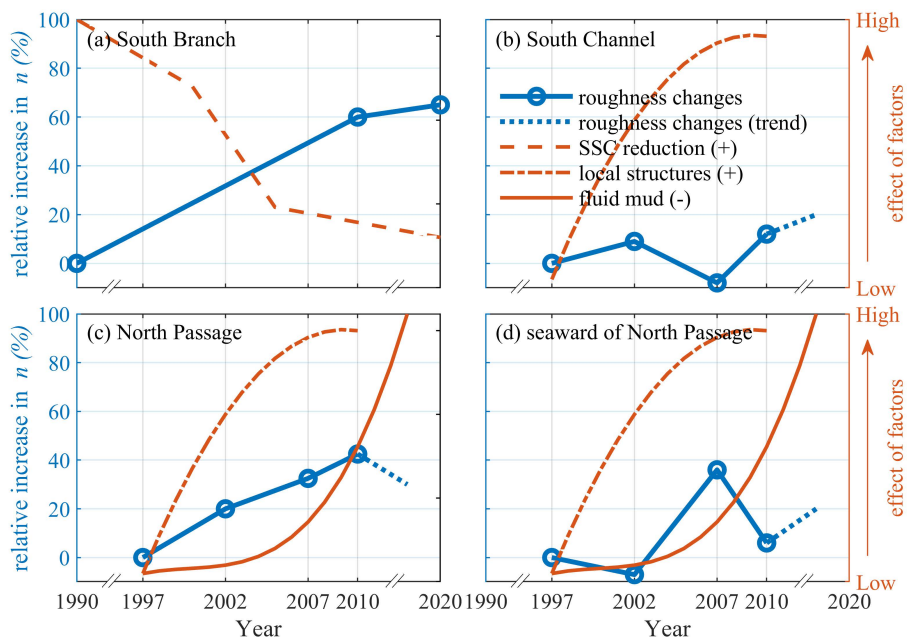


Figure 3.10: Sketch of the changing roughness (blue lines) in the (a) South Branch (region A), (b) South Channel (region B), (c) North Passage (regions C and D), and (d) seaward of the North Passage (region E) and the effects of the factors (red lines) on increasing (+) or decreasing (-) roughness. The factors include the reduction of suspended sediment concentrations (SSC), the construction of local structures from 1997 to 2010, and the increasing role of the fluid mud formation induced by the engineering works. The dashed blue lines indicate the increasing or decreasing trend of the roughness changes after 2010.

3.5.4. IMPLICATIONS FOR OTHER ESTUARIES

Deepening and narrowing have resulted in profound tidal amplification in many estuaries (Woodworth, 2010; Winterwerp et al., 2013; Talke and Jay, 2020). In the South Branch of the Yangtze Estuary, changes in tides are mainly ascribed to riverine sediment decline rather than local engineering works, which is confirmed with the gradual changes in the damping factor from 2006 to 2015 (Figure S3.3). The reduced sediment

supply may have two effects: 1) channel scouring (weakening tidal damping) and 2) reducing SSC and therefore increasing roughness (enhancing tidal damping). Sediment decline is a concern for the management of global deltas (e.g. Syvitski et al., 2009). In the South Branch, deepening and narrowing from 1990 to 2010 resulted in a predicted ~20% increase in the damping factor whereas the observed damping factor only increased ~5%. The ~75% contribution of deepening and narrowing on amplifying tides, i.e. ~15% increase in damping factor, was therefore counteracted by the increase in the effective bottom roughness due to reduced SSC. Specifically, our model suggests a 60% increase in the effective bottom roughness in the South Branch from 1990 to 2010, which may correspond to the observed ~80% decrease in the SSC from 2003 to 2013. The effect of sediment decline on tidal damping is so large that it may be relevant for other highly concentrated estuaries as well. However, most estuaries in which tidal amplification has been well documented have concentrations that are either too low to significantly influence tidal dynamics (such as in the Venice Lagoon, see Ferrarin et al., 2015 and Cape Fear River estuary, see Familkhalili and Talke, 2016); or are declining, but at a rate insufficient to counterbalance deepening effects (the Hudson river estuary, see Ralston et al., 2019) or are increasing (Elbe, Ems and Loire estuaries, see Winterwerp et al., 2013). In the Elbe, Ems, and Loir estuaries, a reduction in hydraulic roughness in response to increasing sediment concentrations was also observed in response to deepening, leading to tidal amplification (Winterwerp et al., 2013; van Maren et al., 2015b; Jalón-Rojas et al., 2016; Dijkstra et al., 2019b,a). Moreover, a positive feedback between tidal amplification and an increase in SSC may occur in these estuaries (Winterwerp and Wang, 2013; Winterwerp et al., 2013). However, these western European estuaries are examples of systems with a primarily marine source of sediment. Therefore, the change of tidal damping in the South Branch with a fluvial sediment source does not influence the SSC.

On the other hand, the tidal evolution in the mouth zone is controlled by the local engineering works which initially led to an increase in the effective bottom roughness, but later to a decrease as they also strengthened fluid mud formation. The fluid mud is likely to decrease the effective bottom roughness after 2010, resulting in less tidal damping, which is similar to the Elbe, Ems, and Loir estuaries. However, the changes in tides in the mouth zone were overall small in magnitude, which may not be strong enough to induce changes in SSC, particularly considering that the riverine sediment decline is prone to reduce the SSC. Such an effect in the mouth zone of the Yangtze Estuary may need future research.

3.6. CONCLUSIONS

THE tides in many estuaries are changing in response to natural and human factors operating concurrently. In this work, we analysed the tidal evolution in the Yangtze Estuary from the 1990s to 2020 using damping factors. Data analysis in the South Branch suggests a strong decrease in landward tidal damping from 1990 to 2010, but a minor increase in landward tidal damping from 2010 to 2020. Tidal damping increased in the mouth zone from 1997 to 2010.

A calibrated 2D hydrodynamic model is then used to investigate the effects of morphological changes, local structures and roughness. We found that reduced sediment supply controls the reduced tidal damping in the South Branch. Specifically, the tides

are amplified primarily due to the increase in water depth (channel scouring). However, we also estimate that the ~80% reduction in SSC has increased the effective bottom roughness (represented with a Manning coefficient) by 60%. This enhanced bed roughness reduces tidal damping, counteracting the impact of scouring by a reduced sediment supply on tidal amplification by ~75%. In the mouth zone, the effective bottom roughness overall increased until 2010, which is mainly attributed to the effects of local structures and partly counteracted by fluid mud formation. Fluid mud decreases the effective bed roughness, therefore weakening tidal damping after 2010. However, around the same period, the SSC declined, generating an opposite effect on apparent bed roughness and tidal damping. The changes in sediment grain size may also influence to some extent, either increasing or decreasing the apparent hydraulic roughness, adapting to both reduced sediment supply and local engineering works.

In conclusion, the tides in the Yangtze estuary responded to various human interventions on a local scale (fairway construction, land reclamations) and a larger scale (sediment load reduction). These interventions have influenced tidal dynamics through the impact on morphology (deepening) and roughness (involving complex feedback mechanism between hydrodynamics, sediment concentration and grain size, and fluid mud formation). As a result of the large number of mechanisms involved in spatial- and temporal-varying tidal damping, understanding the impact of such mechanisms on decadal tidal evolution is important for the management of turbid estuaries in general, exemplified in this study with the Yangtze Estuary.

3.A. APPENDIX: SUPPLYMENTARY TABLES AND FIGURES

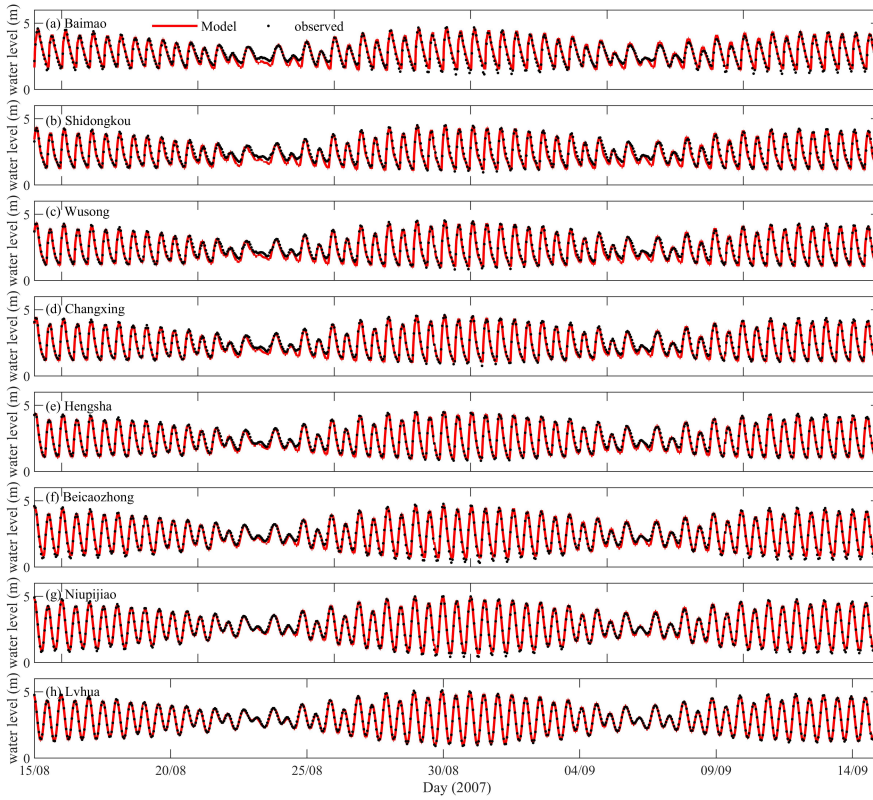


Figure S3.1: Model/data comparisons of water level variations at (a) Baimao, (b) Shidongkou, (c) Wusong, (d) Changxing, (e) Hengsha, (f) Beicaozhong, (g) Niupijiao and (h) Lvhua (see Figure 3.1 for the locations).

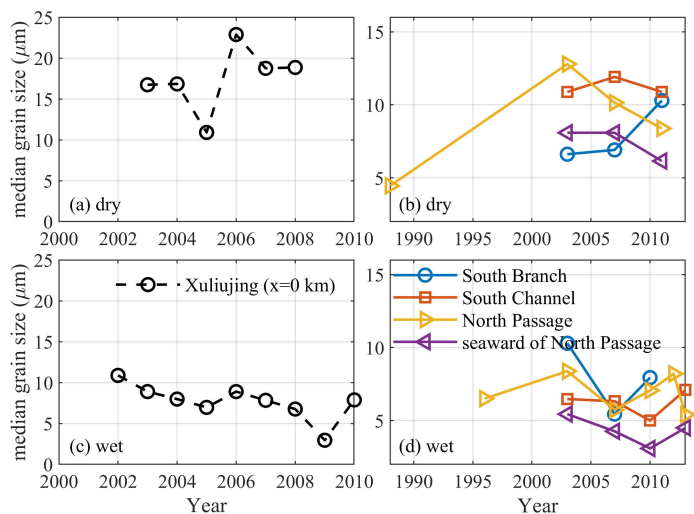


Figure S3.2: Variations of the depth-averaged median grain size of the suspended sediment averaged over spring and neap tides during (a, b) dry season and (c, d) wet season at (a, c) Xuliujing ($x=0$ km) and (b, d) downstream of $x=0$ km including the South Branch, South Channel, North Passage and its seaward area. Data are collected from [Chen et al. \(2016b, 2019\)](#); [Yang et al. \(2016\)](#).

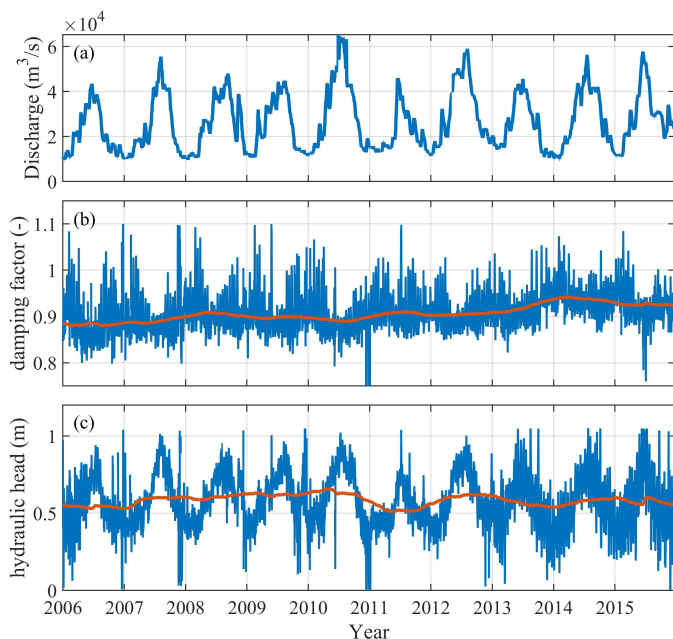


Figure S3.3: Variations of (a) river discharge at Datong between 2006 and 2016, (b) damping factor (blue) and (c) hydraulic head (blue) between Xuliujing ($x=0$ km) and Wusong ($x=70$ km) from 2006 to 2015. The red lines in (b) and (c) are yearly averaged.

Table S3.1: Two-year averaged tidal amplitudes (A) and phases (Φ) of major diurnal, semi-diurnal, and quarter-diurnal and subtidal frequencies at Xuliujing ($x=0$ km) and Yanglin ($x=40$ km) during 1990-1991, 2009-2010 and 2019-2020.

	Xuliujing						Yanglin						
	1990-1991		2009-2010		2019-2020		1990-1991		2009-2010		2019-2020		
	A (m)	Φ ($^{\circ}$)	A (m)	Φ ($^{\circ}$)	A (m)	Φ ($^{\circ}$)	A (m)	Φ ($^{\circ}$)	A (m)	Φ ($^{\circ}$)	A (m)	Φ ($^{\circ}$)	
Sub	Sa	0.447	201	0.458	207	0.512	198	0.326	205	0.345	206	0.404	203
	Ssa	0.115	333	0.062	325	0.114	308	0.111	329	0.078	340	0.085	334
	MSm	0.016	85	0.027	178	0.060	282	0.014	71	0.023	142	0.064	275
	Mim	0.049	12	0.029	18	0.044	35	0.027	4	0.021	6	0.044	49
	MSf	0.182	56	0.151	55	0.171	50	0.120	57	0.118	53	0.152	51
	Mf	0.039	23	0.047	25	0.052	51	0.029	17	0.043	15	0.042	39
D1	O ₁	0.148	195	0.145	194	0.126	194	0.148	174	0.147	178	0.124	177
	K ₁	0.206	248	0.209	247	0.191	244	0.219	226	0.220	228	0.204	224
D2	M ₂	0.842	80	0.877	79	0.885	70	0.957	41	0.905	42	0.914	37
	S ₂	0.367	130	0.371	128	0.378	115	0.431	91	0.389	90	0.408	82
	N ₂	0.146	60	0.153	59	0.157	47	0.167	22	0.160	25	0.164	17
D4	M ₄	0.185	81	0.166	76	0.151	61	0.187	360	0.193	1	0.176	349
	MS ₄	0.155	131	0.140	126	0.129	111	0.153	50	0.163	51	0.143	36
	MN ₄	0.062	60	0.058	55	0.062	45	0.063	340	0.066	342	0.054	333
M ₄ /M ₂	0.219		0.189		0.170		0.195		0.213		0.193		
2M ₂ -M ₄	79		81.22		52.23		82		83.18		301.05		

Table S3.2: The percentage of relative increase in Manning roughness (n) in different periods in regions A, B, C, D, and E (roughness changes based on Figure 3.6, regions see Figure 3.2) and the main causes.

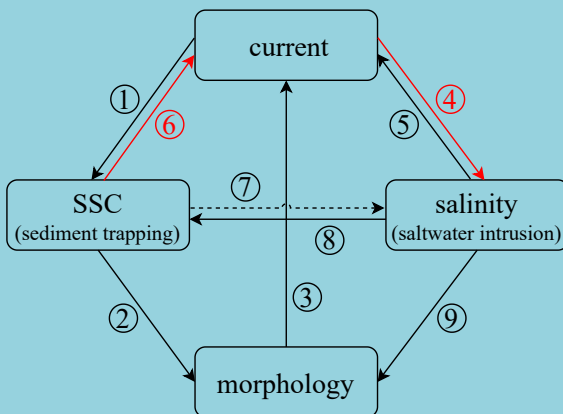
Region		Period	Roughness (n) changes	Main causes	
South Branch	A	1990-2010	+60%	SSC decreasing	changes in sediment grain size
		2010-2020	+5%	SSC decreasing	
South Channel	B	1997-2002	+9%	local structure	
		2002-2007	-17%	?	
		2007-2010	+20%	local structure	
North Passage	C	1997-2002	+33%	local structure	
		2002-2007	0	fluid mud	
		2007-2010	+20%	local structure	
	D	1997-2002	+7%	local structure	
		2002-2007	+25%	local structure	
		2007-2010	stable	-	
Seaward of North Passage	E	1997-2002	-7%	fluid mud	
		2002-2007	+43%	local structure	
		2007-2010	-30%	fluid mud	

4

EFFECTS OF SEDIMENT-INDUCED DENSITY GRADIENTS ON THE ESTUARINE TURBIDITY MAXIMUM IN THE YANGTZE ESTUARY

*There is no such thing as failure.
Failure is just life trying to move us in another direction.*

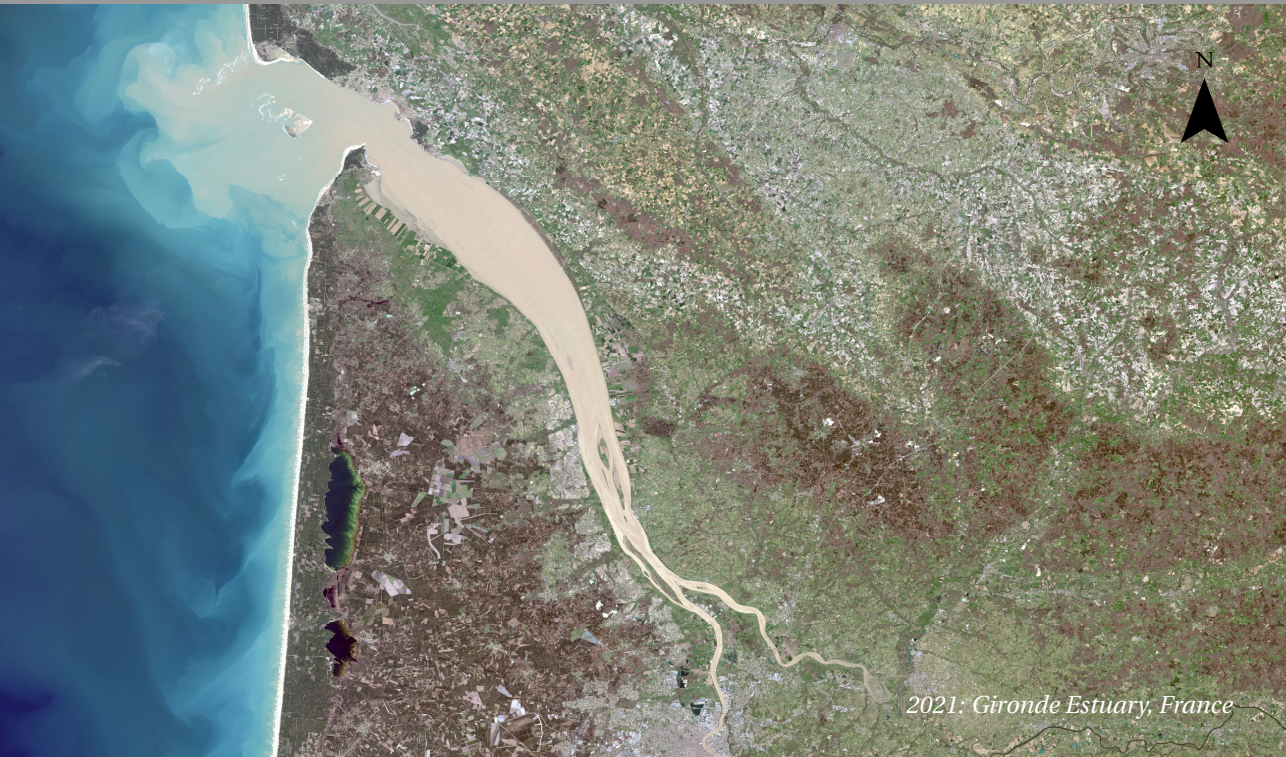
Oprah Winfrey
Commencement address
at Harvard University (30 May 2013)



This chapter focuses on the content in red and has been published in:

Zhu, C., van Maren, D.S., Guo, L., Lin, J., He, Q. and Wang, Z.B., 2021. Effects of sediment-induced density gradients on the estuarine turbidity maximum in the Yangtze Estuary. *Journal of Geophysical Research-Oceans*, doi: 10.1029/2020JC016927.

An estuarine turbidity maximum (ETM) is a region of elevated suspended sediment concentration (SSC) resulting from residual transport mechanisms driven by river flow, tides, and salinity-induced density gradients (SalDG). However, in energetic and highly turbid environments such as the Yangtze Estuary, sediment-induced density gradients (SedDG) may also substantially contribute to the formation and maintenance of the ETM. Since this mechanism is relatively poorly understood, we develop a three-dimensional model to explore the effect of SedDG on tidal dynamics and sediment transport. By running sensitivity simulations considering SalDG and/or SedDG, we conclude that the longitudinal SedDG leads to degeneration and landward movement of the ETM. Moreover, two effects of the vertical SedDG are identified to be responsible for sediment trapping: one by enhancing the vertical sediment concentration gradients, and another by additionally affecting hydrodynamics including the water levels, velocities and salinities. The longitudinal and vertical SedDG leads to seasonal and spring-neap variations of upstream migration of the salt wedge: vertical SedDG is more pronounced at neap tides in the wet season due to stronger stratification effects, whereas longitudinal SedDG is more pronounced at intermediate tides in the dry season due to weaker mixing and limited deposition. These findings imply that the SedDG contributes substantially to channel siltation and salt intrusion in highly turbid systems, and need to be accounted for when numerically modelling such phenomena.



4.1. INTRODUCTION

MANY estuaries have regions with locally elevated suspended sediment concentration (SSC), which are referred to as an Estuarine Turbidity Maximum (ETM) (Schubel, 1968; Dyer, 1986). ETMs are areas with a convergence of sediment transport, often corresponding to the landward limit of salt intrusion. With high SSCs, the ETMs lead to dynamic bed behavior and may influence tidal propagation through damping of turbulence (Geyer, 1993; Burchard and Baumert, 1998; Talke and Jay, 2020). Understanding the dynamics of ETMs is important for the management of navigation channels, freshwater resources and ecosystem services.

ETMs reflect trapping of sediment in the longitudinal direction, often as a result of (at least one of) two main mechanisms: tidal asymmetry and estuarine circulation. Tidal asymmetry is the distortion of the tidal wave resulting from non-linear interactions between the tide and channel morphology (Uncles et al., 1985; Dyer, 1988; Friedrichs and Aubrey, 1988; Brenon and Le Hir, 1999; Yu et al., 2014). Tidal wave distortion leads to stronger but shorter flood currents than ebb currents, resulting in a net transport of sediment in the landward direction. Estuarine circulation is characterized as a landward-directed bottom flow and a seaward directed surface flow, resulting from the baroclinic pressure gradient generated by longitudinal salinity differences (Festa and Hansen, 1978; Dyer, 1988; Burchard and Baumert, 1998; Geyer and MacCready, 2014). Sediment is transported seaward in the surface layer, gradually settling from suspension towards the bottom layer, which transports sediment back in the landward direction. This two-layer flow exists seaward of the salt-fresh water interface, and therefore a resultant ETM will develop in the tip of the salt wedge. Moreover, internal tidal asymmetry due to the flood-ebb asymmetry in turbulent mixing is typically stronger during flood than ebb tides (Jay and Musiak, 1994, 1996). The reduction of tidal mixing during ebb tide results in internal tidal asymmetry that generates a two-layer tidally-averaged residual circulation, which also contributes to estuarine circulation (Jay and Musiak, 1994, 1996). And finally, strain-induced tidal straining results from differential advection of a longitudinal density gradient (Simpson et al., 1990). During ebb tides, the water column is stratified via the straining of the density field which creates a vertically sheared velocity profile. During flood tides, this straining is reversed and the bottom water column becomes more mixed, intensifying the currents near the bottom. This asymmetric mixing leads to a residual flow strengthening the estuarine circulation (Jay and Musiak, 1994, 1996; Geyer and MacCready, 2014). Other than the above-mentioned mechanisms in inducing residual circulation in estuaries, in highly turbid estuaries, high SSC may result in extra density differences sufficiently large to dampen turbulent mixing, and therefore lead to rapid settling of suspended sediment, influencing the horizontal velocity structure (Winterwerp, 2001). Compared to the effect of salinity, the dynamics resulting from sediment-induced density differences have received much less scientific attention.

Sediment-induced density gradients (SedDG) may operate in both longitudinal and vertical directions and influence sediment trapping. Upstream of the location of the maximum SSC in the ETM, longitudinal salinity- and sediment-induced density gradients act together to enhance tidally-averaged circulation (Talke et al., 2009b). However, downstream of the maximum SSC in the ETM, the SedDG and salinity-induced density gradient (SalDG) may act in the opposite directions, leading to a three-layer circu-

lation with near-bed seaward flow and therefore weakened residual currents (Talke et al., 2009b). Additionally, SedDG promotes settling, resulting in larger gradients in the vertical SSC profile and more concentrated residual transport by depth-varying residual flows. And finally, vertical density gradients would suppress turbulence, reduce the apparent hydraulic roughness and lead to more amplified tides and enhanced tidal strength (Gabioux et al., 2005; Winterwerp et al., 2009; Wang et al., 2014), which in turn influence the ETM. Such a positive feedback may lead to an increase in SSC as a result of deepening and narrowing of navigation waterways in estuaries (Winterwerp, 2011; Winterwerp and Wang, 2013; Winterwerp et al., 2013; de Jonge et al., 2014; van Maren et al., 2015b). Moreover, the effect of sediment on the density causes variations in turbulence, and thereby mud-induced periodic stratification (Becker et al., 2018), leading to net upstream sediment transport, which is similar to the strain-induced periodic stratification (Simpson et al., 1990). Despite increasing phenomenological insight into the importance of sediment-induced effects, an integral study on the effects of the longitudinal and vertical SedDG on mixing, residual flows, and tidal propagation is still missing.

The Yangtze Estuary provides a case study in which all the above-mentioned dynamic processes play a role. It is an energetic and highly turbid estuary under strong fluvial and tidal forcing. An ETM stretching about 60 km in the mouth zone of the Yangtze Estuary occupies the region of the North and South Passages where bottom SSC can be $>10 \text{ kg/m}^3$ (Lin et al., 2019). The dynamics controlling the formation of ETM in the Yangtze have been extensively studied based on field observations (Li and Zhang, 1998; Wu et al., 2012; Song et al., 2013) and numerical models (Chu et al.; Song and Wang, 2013; Wan and Wang, 2017). Figure 1 provides an example of high near-bottom SSC of $\sim 30 \text{ kg/m}^3$ ($\sim 1 \text{ m}$ thick) lasting for 3-4 h in the middle of the North Passage (NP) (see Figure 4.2). The dynamics of these high concentration layers are regulated by the tidal variation in vertical mixing and horizontal advection, but their relative contribution remains poorly known. Even more, the impact of high near-bottom SSC on the hydrodynamics themselves (through its effect on the density, as elaborated above) remains poorly known. Earlier works suggest that the SedDG enhances stratification and strengthens the ETM (Song and Wang, 2013; Wan and Wang, 2017; Li et al., 2018b) and leads to a lower apparent roughness (Winterwerp et al., 2009). However, these studies do not account for longitudinal SedDG which may behave differently than the vertical SedDG. The interactions between sediments, salinity, mixing and residual flows require further detailed analysis.

In this contribution, we aim at identifying the contribution of longitudinal and vertical SedDG and SalDG on ETM dynamics. A three-dimensional (3D) model is used to account for the effects of SalDG and SedDG individually as well as the interactions between the sediments and salinity. We systematically analyze the changes in the estuarine hydrodynamics, e.g., the tidal propagation, residual flows, and stratification which contribute to the formation of the ETM. The setup of the model is described in section 4.2, and model results are presented in section 4.3. The model limitations, the effects of longitudinal and vertical SedDG, and the implications for other estuaries are discussed in section 4.4. Conclusions are drawn in section 4.5.

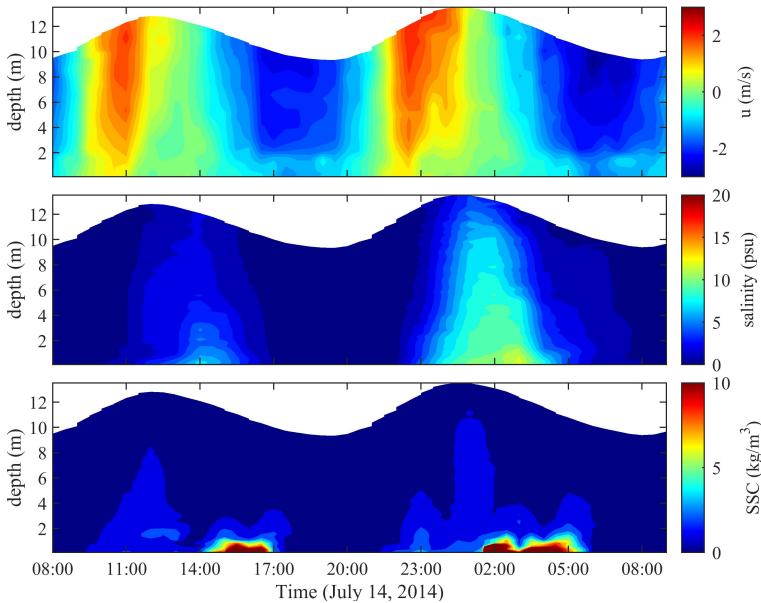


Figure 4.1: Observed variations of (a) longitudinal velocity u ; (b) salinity and (c) suspended sediment concentration (SSC) in the middle of the North Passage (see Figure 4.2 during 14–15 July, 2014. Positive u indicates the flood direction. See Lin et al. (2019) for details.

4.2. METHODOLOGY

4.2.1. STUDY AREA

THE Yangtze Estuary is a meso-tidal estuary (a mean tidal range of 2.6 m at the mouth but with spring tidal range up to 5.9 m) originating at Xuliujing (the estuary head, defined as km-0) with four main outlets called the North Branch, the North Channel, the NP and the South Passage (Figure 4.2). It has a predominantly semi-diurnal tidal regime with M_2 as the most important component, followed by S_2 , O_1 , and K_1 . The M_2 tidal amplitude increases in the first 50 km of the estuary due to the decreasing water depth and the convergent channel geometry. Further inside the estuary, the M_2 tidal amplitude decreases due to the damping effect of bottom friction and river discharge. The river discharge is high (monthly averaged value varying between 10,000–80,000 m^3/s at the tidal limit (Datong station, 640 km upstream of the mouth). Wind and waves are of secondary importance compared to the river and tidal forcing. The river also supplies a huge amount of sediment (364 million tons per year during 1950–2016, Zhu et al., 2019) to the estuary. The river-borne sediment is fine, with a median grain size of 4–11 μm (Guo and He, 2011), whereas the bottom sediment in the estuary is relatively coarser, with a median grain size of 8–120 μm (Hu et al., 2009). The ETM in the Yangtze Estuary encompasses the region of the NP, South Passage and the seaward segment of the North Channel (Li and Zhang, 1998; Jiang et al., 2013b). Generally, the spatial extent of ETM varies with the river discharge (Doxaran et al., 2009) and sediment input (Jiang et al., 2013b).

The NP, where the ETM of the Yangtze Estuary is most pronounced, typically has a surface SSC of 0.1–0.3 kg/m³ and a near-bottom SSC of 0.4–4 kg/m³ varying with spring and neap tides as well as over wet and dry seasons (Shi, 2004; Liu et al., 2011; Li et al., 2016b). The near-bottom SSC, however, may exceed 10 kg/m³ (see Figure 4.1, Lin et al., 2019) and even reach 100 kg/m³ (Wan et al., 2014b). Mixing and stratification periodically varies with the strength of river flow and tidal flow, leading to flood-ebb, spring-neap and seasonal variations (Shi, 2004; Wu et al., 2012; Song et al., 2013; Pu et al., 2015; Li et al., 2016b, 2018b). From 1998 to 2010, the NP was deepened and narrowed as part of the Deep Channel Navigation Project (DCNP) to accommodate larger ships. The DCNP was implemented with two long jetties and 19 groins to increase current velocity and mitigate sediment deposition in the main navigation channel. The main navigation channel was 350–400 m wide and 12.5 m, requiring an annual dredging volume of ~50–60 million m³ (Zhu et al., 2019). The high maintenance dredging costs fuels research on determining mechanisms controlling sediment trapping and siltation (Liu et al., 2011; Wu et al., 2012; Jiang et al., 2013a; Kuang et al., 2014). In this study, we focus on tidal propagation and sediment dynamics along the South Branch-South Channel-NP (see red dashed line in Figure 4.2).

4.2.2. MODEL SETUP

A 3D model was set up using the Delft3D model system, which simulates flow, sediment transport and morphological changes. The model solves the three-dimensional shallow water equations under the hydrostatic pressure assumption – see Lesser et al. (2004) for details. Vertical mixing is computed with a k - ϵ turbulence model. The model application domain is about 700 km long and 400 km wide, covering the entire tidal region of the Yangtze River, the Hangzhou Bay and a part of the adjacent Yellow Sea and East China Sea (Figure 4.2). The model has 1173×374 cells with a high resolution in the estuary (down to ~300 m in the NP) and coarsening towards the river and the open sea (up to 10 km). Ten equidistant σ layers are prescribed over the vertical. The model is set up with a bathymetry measured in 2010 and calibrated with data collected in 2007, assuming that the bathymetry did not significantly change between 2007 and 2010. This assumption is reasonable as the impact of the DCNP construction (1997–2010) was most pronounced in the period 1997–2007 (see Zhu et al., 2019). Here we briefly describe the setup of the model: more details on the governing equations and the calibration are in the Supporting information (SI).

HYDRODYNAMIC BOUNDARY CONDITIONS

The upstream boundary is at Datong where a daily river discharge is prescribed with strong seasonal variations. A constant discharge of 1,000 m³/s was defined at the head of Hangzhou Bay. At the seaward side, water levels are prescribed with 13 astronomic tidal constituents (M_2 , S_2 , N_2 , K_2 , K_1 , O_1 , P_1 , Q_1 , MF , M_4 , MS_4 , MN_4) derived from the TPXO 7.2 Global Inverse Tide Model (Egbert et al., 1994; Egbert and Erofeeva, 2002) as a non-reflective open boundary. The tidal waves can cross the open sea boundary unhampered and without reflections. The shallow water equations are solved by the steady-state solution which means the specified water level boundary acts as a nodal point. The salinity at the sea boundary is set constant and equal to 34 psu, whereas fresh

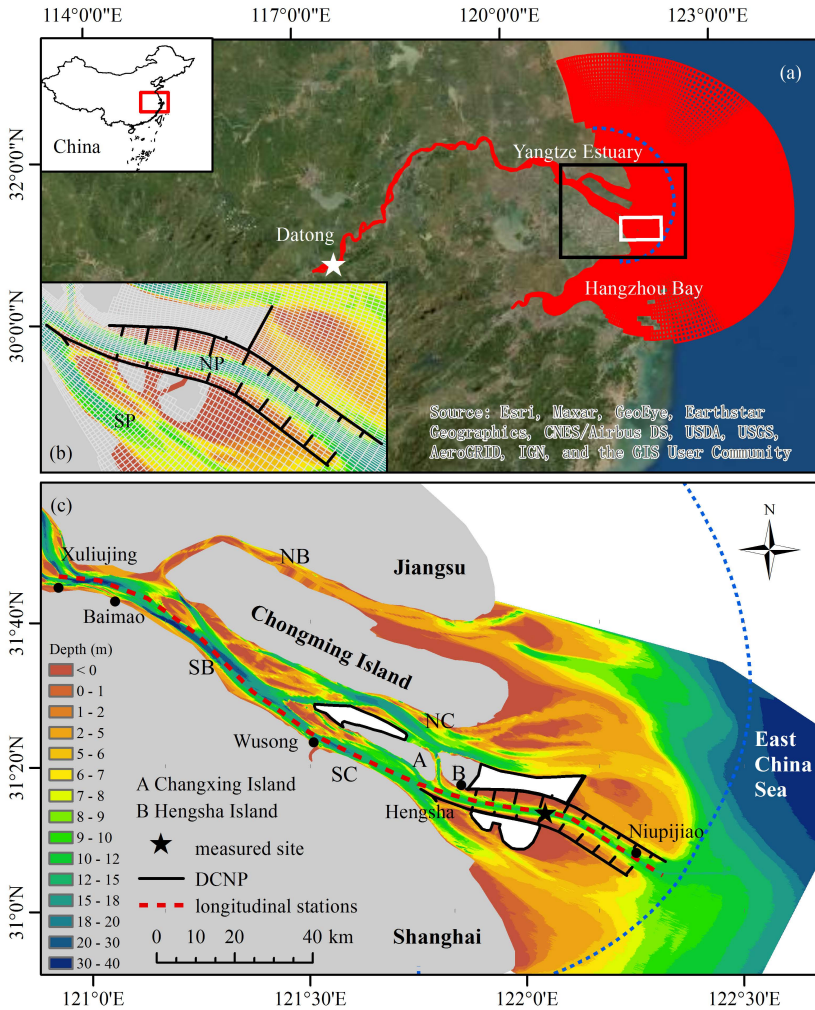


Figure 4.2: (a) Model domain; (b) highest grid resolution in the mouth zone of the Yangtze Estuary; (c) geometry and bathymetry of the Yangtze Estuary in 2010 and stations in the longitudinal direction (red dashed line). Seaward of the blue dashed line in (a) and (c) is prescribed as offshore settings. The white areas are the reclaimed regions. DCNP: Deep Channel Navigation Project. NB: North Branch; SB: South Branch; NC: North Channel; SC: South Channel; NP: North Passage; SP: South Passage.

water is prescribed at the upstream boundary. Although the Yangtze discharges a large amount of fresh water into the coastal seas, the model boundaries are sufficiently far away from the river mouth to allow a constant salinity value representing marine conditions. The model was first run for one year (2006) as a spin-up period, while the second year (2007) was used for calibration and detailed analysis. The 3D baroclinic model was calibrated with spatially varying Manning’s n coefficient. The initial Manning’s n [$\text{s/m}^{-1/3}$] was based on the roughness height in a calibrated hydrodynamic model (Zhu

Table 4.1: Parameter settings in the model (details refer to the Supporting information)

Parameter	Description	Value
Δt (min)	Time step	0.5
n ($s/m^{-1/3}$)	Manning coefficient	0.01 ~ 0.025 with spatial variation
$\omega_{s,0}$ (mm/s)	Settling velocity	0.5
c_{soil} (kg/m^3)	Reference density for hindered settling	200
ρ_s (kg/m^3)	Specific density for cohesive sediment	2650
τ_{cr} (N/m^2)	Critical erosion stress	0.1
M ($kg/m^2/s$)	Erosion parameter	0.001

et al., 2016), which is subsequently optimized through calibration. In 2010, jetties and groins were constructed in the DCNP. These jetties and groins are numerically implemented as structures completely blocking through- or overflow. The calibrated parameters are summarized in Table 4.1.

SEDIMENT TRANSPORT

The measured daily SSC, varying between 0.01 and 1 kg/m^3 , was prescribed as a sediment transport boundary condition at Datong. The sediment concentration at the head of Hangzhou Bay is prescribed as zero. This is justified as the river sediment input here is negligible compared to the Yangtze River and seldom reaches the Yangtze Estuary (Hu et al., 2000). The sediment is represented by a single cohesive sediment fraction with a settling velocity of 0.5 mm/s (Yun, 2004). Sediment is modelled as supply-limited: the model is not initialized with sediment on the bed, but sediment is transported into the model through the open boundaries. The model is run until the computed SSC is in dynamic equilibrium (i.e. the computed SSC remains constant if it is averaged over relevant hydrodynamic timescales such as spring-neap tidal cycles). The modelled ETM is therefore resulting from sediment transport convergence computed by the model, and the strength and location of the ETM are the results of subtle variations in the hydrodynamics. This will be discussed in more detail in section 4.3. The erosion flux E of cohesive sediment ($< 64 \mu m$) are calculated with Partheniades-Krone equation (Partheniades, 1965) and deposition D as a bed shear stress independent flux (Winterwerp, 2007):

$$E = M \left(\frac{\tau}{\tau_{cr}} - 1 \right) \quad (4.1)$$

$$D = \alpha \omega_s c \quad (4.2)$$

Where M is the erosion parameter ($kg/m^2/s$), τ is the bed shear stress, τ_{cr} is the critical bed shear stress for erosion, ω_s is the settling velocity, c is the SSC, and α is the 'reduced deposition' factor used to approximate complex and poorly understood physical processes that occur near the bed and become stronger at high SSC (see van Maren et al., 2020). These processes include hindered settling (reducing the rate at which particles settle on the bed), floc destruction in the bed boundary layer (leading to lower

settling velocities), and consolidation (the critical shear stress for erosion is not attained instantaneously, but a particle only gradually gains strength through consolidation after deposition and therefore they are easily immediately re-entrained). All these processes lead to reduced sediment deposition rates at high SSCs. We use a spatially varying α to account for different physical processes which are poorly represented in the model for various reasons. Specifically, $\alpha = 0.1$ is prescribed in the estuary to represent a reduced sediment flux into the bed (resulting from simplification of the consolidation and erosion processes at high concentrations, for instance, as elaborated above), leading to higher near-bottom SSCs; $\alpha = 0$ in the groin field to imply additional sediment availability from the groin field (no deposition, to account for lateral gravity flows and dredging works), and $\alpha = 1$ in the offshore (seaward of the dashed blue line in Figure 4.2a and c) where the majority of sediment supplied to the coastal zone deposits on the inner shelf. The critical shear stresses for erosion is prescribed as 0.1 N/m^2 in the estuary, following earlier sediment transport models developed for the Yangtze Estuary (Chu et al.; Wan and Wang, 2017) and as 0.5 N/m^2 offshore. The small critical shear stress for erosion is characteristic of non-consolidated sediments, which can be easily eroded and re-suspended.

MODEL CALIBRATION AND SCENARIOS SETUP

The model is calibrated in fully baroclinic mode, a standard scenario called Full, which includes both salinity- and sediment-induced density effects (see SI for details). The modelled averaged salinity and SSC show a similar pattern (magnitude and location of the ETM) as observation (Figure 4.3). The simulated depth-averaged and near-bottom SSC in the ETM reach 1.5 and 5 kg/m^3 , respectively, which can sufficiently influence the density of the suspension to reduce vertical mixing rates and corresponding sediment-induced density effects (Winterwerp, 2001). A sensitivity study on the effect of the settling velocity (see SI) reveals that lower settling velocity results in a less pronounced ETM whereas higher settling velocity does not reproduce seasonal variations of SSC. A comparison of the effect of turbulence model parameterizations (see also SI) shows that a k - L turbulence model or additional background vertical viscosity and diffusivity in the k - ϵ turbulence model could induce more mixing effects, which underestimates the effects of the vertical density gradients on suppressing turbulence. The standard model therefore better represents the seasonal and spatial distributions of the SSC.

We set up four scenarios to investigate the impact of SalDG and SedDG on tidal dynamics and sediment transport (Table 4.2). Three other scenarios are set up stepwise excluding the SalDG and SedDG, with scenarios defined as Sal (salinity density effect only), Sed (sediment density effect only), and Barot (neither salinity nor sediment density effect, in other words, a barotropic model). Note that the Sal and Barot scenarios exclude the SedDG by excluding the effect of SSC in calculating the density of water (see SI). The differences in the estuarine dynamics between these four scenarios provide the individual effects of salinity and sediment on the ETM.

4.2.3. DENSITY PARAMETERS

The effect of density differences on hydrodynamics is evaluated by computing the residual flow and the pressure gradient. In the longitudinal momentum equation, the

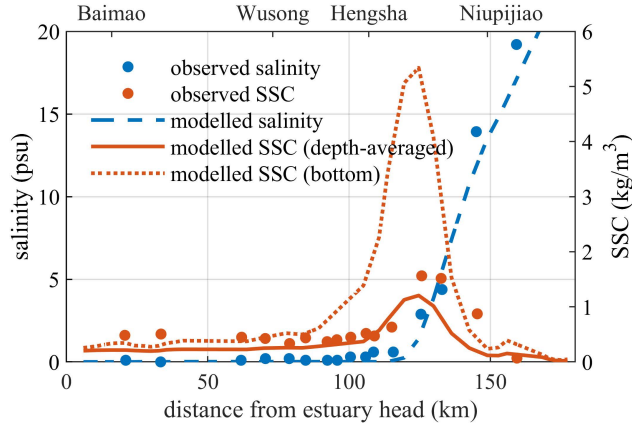


Figure 4.3: Comparison between modelled (lines) and observed (dots) longitudinal distribution of depth-averaged and bottom suspended sediment concentration (SSC, red) and depth-averaged salinity (blue). The observed data are tidal period and depth-averaged during 12-16 August 2007 from Wan et al. (2014a). The modelled salinity and SSC are averaged during the wet season (May-October). The estuary head is at Xuliujing (see Figure 4.2).

Table 4.2: Overview of model scenarios. SalDG: salinity-induced density gradient; SedDG: sediment-induced density gradient. * indicates the fully baroclinic scenario based on which the model is calibrated.

No.	Scenarios	SalDG	SedDG
1	Full*	Yes	Yes
2	Sal	Yes	No
3	Sed	No	Yes
4	Barot	No	No

pressure is a function of the barotropic and baroclinic pressure gradient terms:

$$\frac{\partial p}{\partial x} = g\rho_0 \frac{\partial \xi}{\partial x} + g \left(\int_z^\xi \frac{\partial \rho}{\partial x} dz' \right) \quad (4.3)$$

Where x is the along-channel direction, ξ is water surface elevation, ρ_0 is the depth-averaged density, ρ is the density of saltwater containing suspended sediments, g is the gravitational acceleration, and p is the fluid pressure. The first term on the right side is the barotropic pressure gradient and the second term on the right side is the baroclinic pressure gradient F . The baroclinic pressure gradient F , which is estimated from the longitudinal density gradient, is closely related to the residual flow induced by the SalDG and SedDG.

The vertical density effects are expressed using three parameters: the vertical salinity difference, the vertical SSC difference, and the gradient Richardson number. The vertical salinity difference Δs is a simple measure for stratification and is defined as the difference between the bottom and surface salinities ($\Delta s = s_{\text{bottom}} - s_{\text{surface}}$). Similarly, the

vertical SSC difference Δc is obtained from the difference between the bottom and surface SSCs ($\Delta c = c_{\text{bottom}} - c_{\text{surface}}$). The gradient Richardson number Ri_g is a dimensionless ratio of buoyancy and velocity shear, expressing the stability of the water column:

$$Ri_g = \frac{g \frac{\partial \rho}{\partial z}}{\rho \left(\frac{\partial u}{\partial z} \right)^2} \quad (4.4)$$

Where $\frac{\partial \rho}{\partial z}$ and $\frac{\partial u}{\partial z}$ are the vertical gradient of density and horizontal velocity, respectively. Miles (1961) suggest the existence of a critical Ri_g value of 0.25 above which a stable salinity stratification tends to occur, while below which the stratification tends to be unstable and hence tidal mixing is likely to occur. In this work, we calculated the instantaneous Ri_g in which the maximum value over the water column is focused on to indicate the most pronounced changes. The median and interquartile range of the maximum Ri_g over a year in different scenarios are then compared to suggest the changes in stratification.

4.3. RESULTS

4.3.1. TIDAL DYNAMICS

THE tidal propagation is evaluated by analyzing changes in the M_2 amplitude, M_4 to M_2 amplitude ratio and the phase difference between M_2 and M_4 (Figure 4.4). The M_2 amplitude landward of km-150 is approximately 0.08, 0.06 and 0.01 m larger in the Full, Sal and Sed scenarios compared to the Barot scenario (representing the combined density effects, and individual SalDG and SedDG effect on tidal amplification, respectively). SalDG (Sal scenario) therefore contributes more to tidal amplification than SedDG (Sed scenario). However, the difference in tidal amplification in the combined scenario (Full scenario) is larger than the sum of the individual effects of SalDG and SedDG, indicating a feedback mechanism between salinity and sediments. Similarly, the effect of SedDG is also stronger on tidal asymmetry (the M_4 to M_2 amplitude ratio and phase difference) when combined with salinity, compared to the individual SedDG (Sed scenario). Specifically, both the amplitude ratio and the phase difference computed with the Sed scenario are very similar to the Barot scenario but strongly differ between the Full and the Sal scenario. It suggests that the effect of the interaction between salinity and sediments is also pronounced in tidal asymmetry. The M_4 to M_2 amplitude ratio and phase difference of scenarios with salinity (Full and Sal) are smaller than in the barotropic scenario (Barot) landward of km-150 (but larger seaward of this point for the phase difference). This suggests that the salinity gradients decrease the degree of tidal wave deformation and behave differently in the regions upstream and downstream of km-150 whereas individual SedDG (Sed scenario) limitedly influences tidal asymmetry. Overall, both SalDG and SedDG lead to slightly larger tidal amplification and deformation; however, the effect of SedDG is only pronounced with the consideration of salinity gradients. It also indicates that salt intrusion, partly as a result of tidal amplification, may be influenced by the effect of SedDG as elaborated later.

The effect of the density gradients on changing flow fields is illustrated with the velocity amplitude of the M_2 tide (Figure 4.5). The SalDG strongly modifies the flow field,

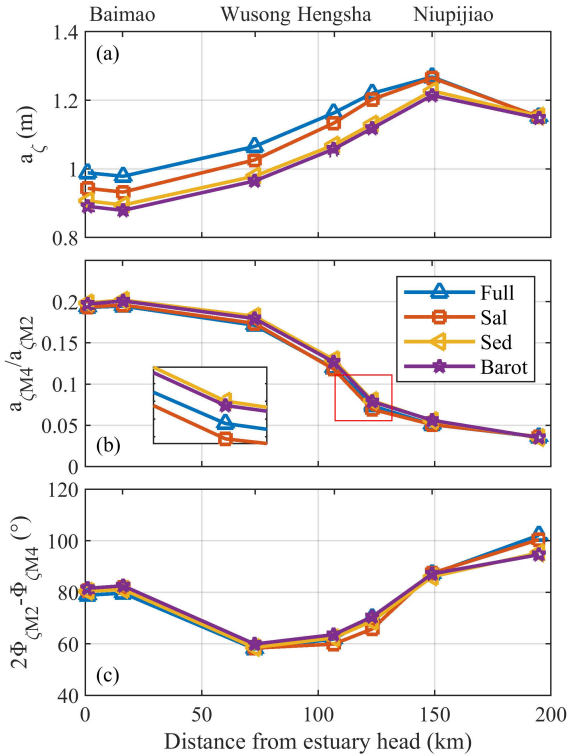


Figure 4.4: Modelled longitudinal variations (red dashed line in Figure 4.2) of (a) water level amplitude M_2 $a_{\zeta M_2}$, (b) amplitude ratio of M_4 to M_2 ($a_{\zeta M_4}/a_{\zeta M_2}$) and (c) phase difference between M_2 and M_4 for water levels ($2\phi_{\zeta M_2} - \phi_{\zeta M_4}$) in scenarios- Full, Sal, Sed, and Barot (see Table 4.2). The estuary head is at Xuliujing (see also Figure 4.2).

i.e., enlarging the flow velocity in the upper water column up to 30% relative to the barotropic scenario (particularly in the ETM), whereas the SedDG does not substantially influence the flow field. This implies that the effect of the SedDG on flow velocities is limited. Again, the differences between the Full and Sal scenarios (representing the effect of sediment in combination) are larger than the effect of sediment alone (the difference between Sed and Barot), allowing us to identify the baroclinic effect of the SedDG in the following sections.

4.3.2. ETM LOCATION AND EXTENSION

The location and extension of the ETM vary in the four scenarios (Figure 4.6). No significant ETM develops in the Barot scenario, and both surface and bottom along-estuary SSCs are $<0.5 \text{ kg/m}^3$ as insufficient sediment trapping mechanisms exist counterbalancing seaward sediment transport by river flow. The Sed scenario exhibits relatively higher bottom SSC at km-90. In the Sal scenario, a significant ETM with maximum bottom SSC $<1 \text{ kg/m}^3$ is obtained and the maximum SSC in the ETM occurs between km-100 and km-

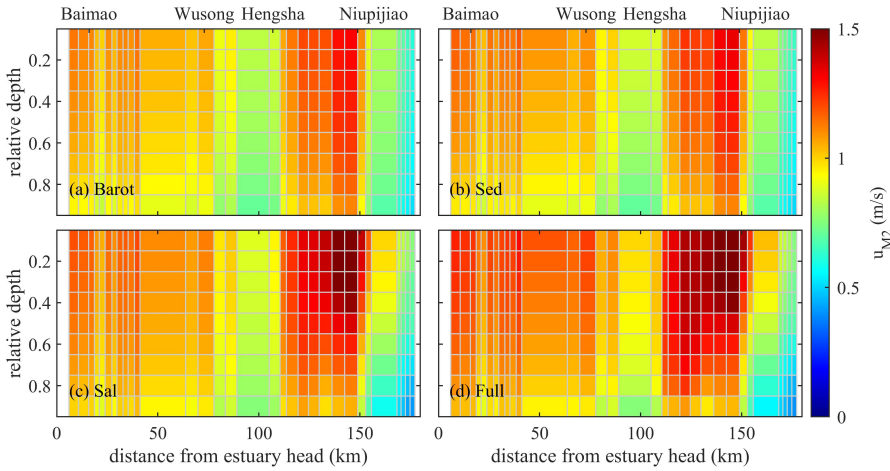


Figure 4.5: Modelled M_2 amplitude of the longitudinal velocity during a year in the scenarios of (a) Barot, (b) Sed, (c) Sal, and (d) Full (see Table 4.2). The estuary head is at Xuliujing (see Figure 4.2).

150 which is in agreement with observations (see SI). This suggests the important role of the salinity-induced gravitational circulation on sediment trapping in the Yangtze Estuary. When adding sediment-induced density effects, the near-bottom SSC in the ETM becomes an order of magnitude larger and the extension of the ETM is much wider into the landward side in the Full scenario. The ETM extends further upstream than the observed ETM region identified by Li and Zhang (1998). This longitudinal extent may be the result of the constant settling velocity prescribed in our model whereas in reality the settling velocity is spatially varying, with higher settling velocities in the ETM resulting from salinity effects and high concentrations. Additionally, the salinity is more vertically stratified and the salt front propagates further upstream, i.e., an upstream shift of the near-bed 1 and 5 psu isohalines of ~ 15 and ~ 2 km, respectively.

4.3.3. DENSITY GRADIENTS

LONGITUDINAL DENSITY GRADIENTS

The effects of yearly-averaged longitudinal density gradients are analyzed by depicting the longitudinal baroclinic pressure gradient (Figure 4.7a) and residual current (Figure 4.8). In the Barot scenario, the longitudinal density gradients are zero as no density effects are considered. In the Sed scenario, the longitudinal density gradients are small and show alternately positive and negative values, implying irregularly directed sediment transport. In the Full and Sal scenarios, the baroclinic pressure gradients are always positive seaward of km-90 because of salinity effects, leading to significant landward sediment transport. Interestingly, the baroclinic pressure gradients increase upstream of km-120 and decrease downstream of km-120 in the Full scenario compared with the Sal scenario (interpreted as the effect of sediment in combination with salinity). This suggests that the combined density effects by salt and sediment (Full scenario) are not a sum of the individual effect of the SalDG (Sal scenario) and SedDG (Sed scenario).

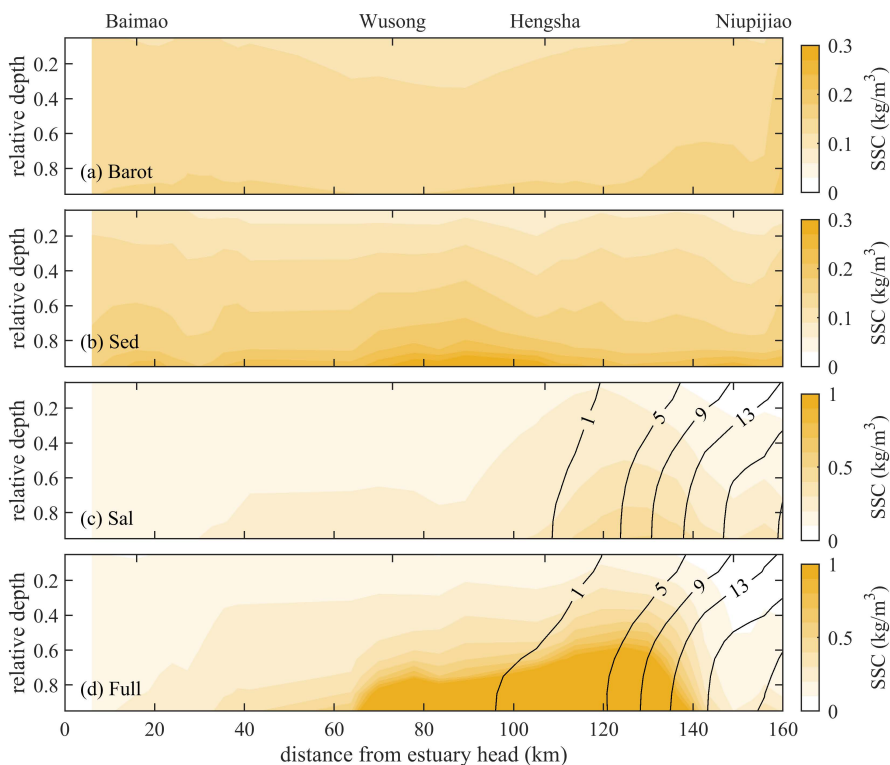


Figure 4.6: Modelled longitudinal distribution (red dashed line in Figure 4.2) of salinity (black contour lines) and SSC (color shading) of the scenarios of (a) Barot, (b) Sed, (c) Sal, and (d) Full (see Table 4.2) averaged from 1 Jan 2007 to 1 Jan 2008. The estuary head is at Xuliujing (see also Figure 4.2).

This is caused by the interaction between salinity and sediments: the distributions of SSC (and therefore the effect of the SedDG) are completely different with and without SalDG (see Figure 4.6). In other words, when sediment interacts with salinity, the SedDG enhances or strengthens the SalDG in the region landward and seaward of km-120, respectively. This will be discussed in more detail hereafter.

Without density effects, the barotropic residual currents are persistently directed seaward due to the large river flow with a magnitude decreasing from 0.4 m/s at km-0 to 0.2 m/s at km-150 (Figure 4.8a). Therefore, the density-induced residual current patterns are obtained by subtracting the residual current in the Barot scenario from the Sed, Sal, and Full scenarios (Figure 4.8b, c, d). The residual currents induced by SedDG are small and mostly directed seaward except the South Branch landward of km-50 (Figure 4.8b). Salinity drives a classical residual flow downstream of km-100, with a landward flow (0-0.13 m/s) near the bottom and seaward flow (0-0.23 m/s) near the surface (Figure 4.8c). Such a residual circulation causes a net landward sediment transport as sediment concentrations are higher near the bed, suggesting that the SalDG is important for the convergence of sediment. Landward of km-100, the residual current in the deep chan-

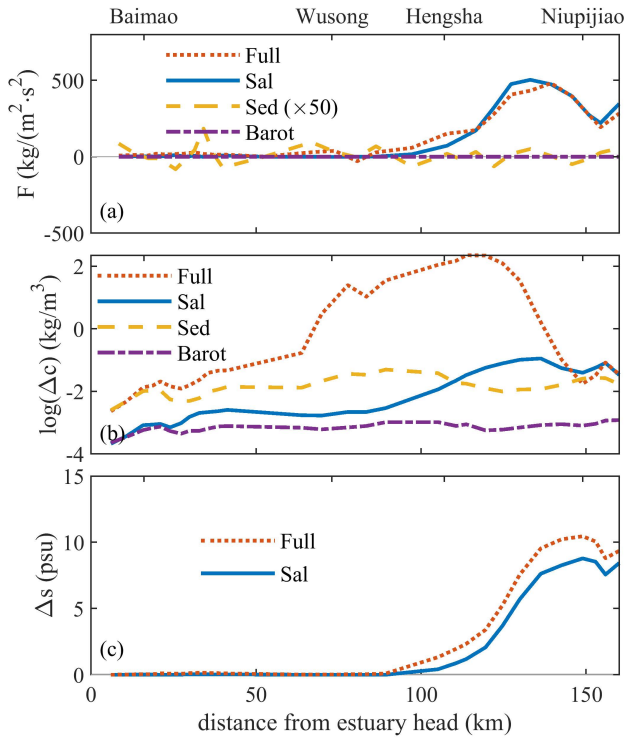


Figure 4.7: Modelled longitudinal changes (red dashed line in Figure 4.2) of yearly-averaged (a) baroclinic pressure gradient F , (b) vertical suspended sediment concentration (SSC) difference Δc (logarithmic scale), and (c) vertical salinity difference Δs in the scenarios-Full, Sal, Sed, and Barot (see Table 4.2). The estuary head is at Xuliujing (see also Figure 4.2).

nel is directed landward (0-0.02 m/s) relative to the barotropic flow in the Sal scenario. This landward flow in the South Channel is compensated by stronger seaward flow in the North Channel (Figure 4.9a, c). Further seaward, in the NP, salinity drives a more classical salinity-induced circulation cell with near-bed inflow and near-surface outflow (Figure 4.9b, d), as also evident in Figure 4.8c.

Also in the fully baroclinic scenario (Full, also including sediments), a residual circulation exists between km-100 and km-150 (Figure 4.8d). However, the near-surface outflow velocity is approximately 0.01-0.03 m/s stronger whereas the near-bed inflow increases by 0.01-0.05 m/s (relative to the Sal scenario) between km-100 and km-140. The differences correspond to the changes in surface and bottom residual flow in the South Channel and NP (Figure 4.9). Moreover, in the South Channel, sediment leads to a reduction of the landward flow in the main channel (as also visible in Figure 4.8c, d) accompanied by more landward flow over shallow areas. This landward flow is compensated by a seaward flow in the North Channel, especially near-surface.

The spatial patterns of residual flow in Figure 4.9 illustrate that salinity and sediment not only drive the longitudinal and vertical flows but also lateral flows. However, in the

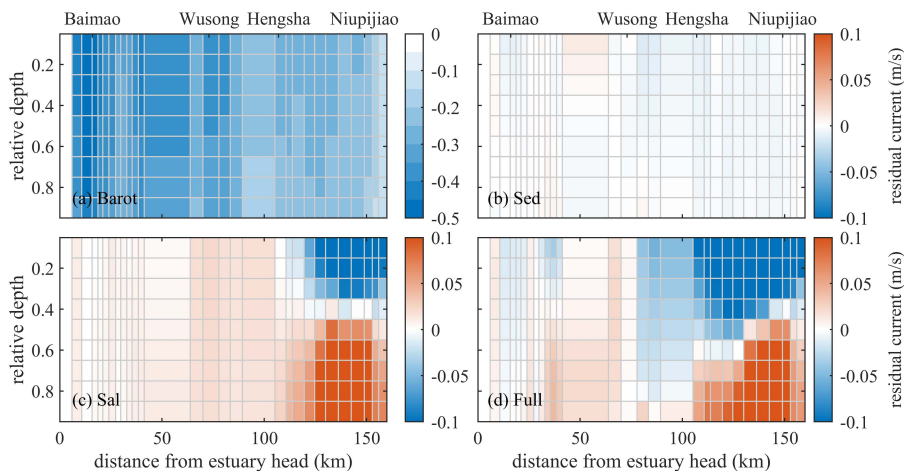


Figure 4.8: Modelled longitudinal distribution (red dashed line in Figure 4.2) of yearly-averaged residual currents in the scenarios of the barotropic simulation (a, Barot) and differences of the various baroclinic model runs with the barotropic model (b-d). The sediment-only barotropic run is provided in (b) Sed, salinity-only in (c) Sal, and fully baroclinic model in (d) Full (see Table 4.2). Positive and negative indicates flood (landward) and ebb (seaward) direction, respectively. The estuary head is at Xuliujing (see also Figure 4.2).

remainder of this paper, we will primarily address the vertical and longitudinal density effects as we consider these to be the main drivers of sediment transport convergence and divergence which are influenced by sediments. The lateral density effects need to be addressed in greater detail as part of future work.

VERTICAL DENSITY GRADIENTS

We interpret the vertical density gradients first using the vertical SSC difference (Figure 4.7b) and the vertical salinity difference (Figure 4.7c). The vertical SSC difference is smaller than 1 kg/m^3 in all the scenarios except the Full scenario. The maximum vertical SSC difference (0.3 kg/m^3) is at km-80 in the Sed scenario, which may be considered an ETM location resulting from sediment-induced transport processes. On the other hand, the maximum vertical SSC difference (0.4 kg/m^3) locates near the landward limit of the salt wedge in the Sal scenario, corresponding to the role of the SalDG in trapping sediment due to the landward near-bed residual current (see Figure 4.8c). Similar to the longitudinal density gradients, the effect of SedDG plays an important role only in combination with salinity effects, leading to a pronounced higher near-bed SSC in the Full scenario (in the area in-between the Sal ETM and the Sed ETM). Interestingly, the vertical salinity gradient in the Full scenario is $\sim 1.5 \text{ psu}$ larger than that in the Sal scenario downstream of km-90, suggesting that SedDG strengthens the vertical salinity gradient.

We subsequently interpret the vertical density gradients with the maximum gradient Richardson number, quantifying the stability of the water column (Figure 4.10). The water column is stably stratified for $Ri_g > 0.25$, whereas mixing prevails for $Ri_g < 0.25$. The whole channel is stably stratified in the Sed scenario with the largest values upstream of km-120. Mixing prevails upstream of km-120 in the Sal scenario, but stratified condi-

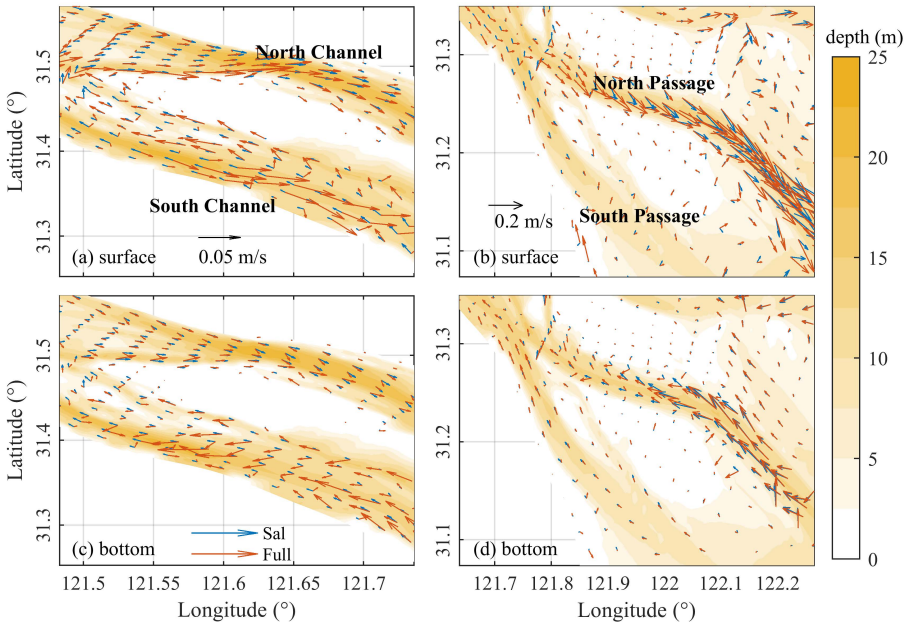


Figure 4.9: Comparison of the modelled yearly-averaged (a, b) surface and (c, d) bottom residual currents (relative to the barotropic model) in the (a, c) South Channel and (b, d) North Passage between the Sal and Full scenarios (see Table 4.2).

tions prevail further seaward. The Ri_g in the Full scenario is close to a superposition of the Ri_g values in the Sed and Sal scenarios. However, Ri_g in the Full scenarios is over 2 times stronger than the value in the Sed scenario downstream of km-60 and the strongest stratification takes place slightly upstream of the Ri_g peak in the Sal scenario.

4.3.4. SEASONAL AND SPRING-NEAP VARIATIONS

The effect of the SedDG on sediment transport and salt intrusion displays strong seasonal and spring-neap variations owing to changes in river discharge and tidal strength (Figure 4.11). The seasonal variation of the tidal range offshore varies only 10% between the wet and dry season at Niupijiao (see Guo et al., 2015), and therefore the seasonal variability is only evaluated for river discharge. In both the Sal and Full scenarios, the SSC is the largest at intermediate tides during the dry season (Figure 4.11c, e) whereas the SSC is the largest at neap tides during the wet season (Figure 4.11d, f). In the Sal scenario, the location of the maximum SSC in the ETM is more landward in the dry season than in the wet season. Interestingly, the movement of the ETM does not entirely follow the salt front in the Full scenario during the dry season, suggesting an impact of sediment-induced effects on ETM location (superimposed on salinity effects). Furthermore, the SSC in the upper estuary (landward of km-100) is larger during the wet season than dry season due to the larger sediment input.

The spring-neap variation of the vertical salinity gradient is more pronounced when

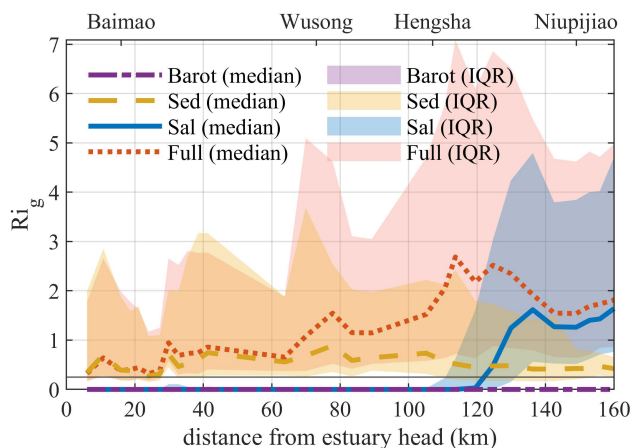


Figure 4.10: Modelled longitudinal changes (red dashed line in Figure 4.2) of the median and interquartile range (IQR) of the maximum gradient Richardson number Ri_g over the water column from 1 Jan 2007 to 1 Jan 2008 in the scenarios of Barot (purple), Sed (yellow), Sal (blue), and Full (red) (scenarios see Table 4.2). The values over 0.25 (grey solid line) suggest more stratification effect. The estuary head is at Xuliujing (see also Figure 4.2).

including sediment-induced density effects, and stronger during the wet season than during the dry season (Figure 4.11g, h). During the wet season, the effect of sediment on salinity gradients is most pronounced during neap tide whereas it is strong at both neap and spring tides during the dry season. This suggests different controlling mechanisms in the dry season compared with the wet season.

The salt front intrudes further landward movement under the influence of SedDG (Figure 4.11i, j), moving up to 20 km landward in the Full scenario compared with the Sal scenario. During the wet season, the salt intrusion moves 5-15 km more landward during neap tides and 0-10 km during spring tides due to the SedDG. During the dry season, the salt intrusion moves farthest landward (10-20 km) at intermediate tides and <5 km (or even seaward) during spring and neap tides due to the SedDG. In addition, the landward movement of the salt wedge due to the SedDG strongly varies with tidal cycles, for instance, the high water and low water can also lead to a maximum of 20 km movement of the salt front induced by the SedDG.

4.4. DISCUSSION

4.4.1. MODEL LIMITATIONS

THE sediment transport dynamics in the Yangtze Estuary have been extensively studied using numerical models (Hu et al., 2009; Chu et al.; Pang et al., 2010; Song and Wang, 2013). The suspended transport in these models was largely determined by bed erosion and sediment suspension, with highest sediment concentrations occurring in areas with highest flow velocities. This so-called erosion-limited approach (or local sediment source approach, see Brouwer et al., 2018; Dijkstra et al., 2018; van Maren et al.,

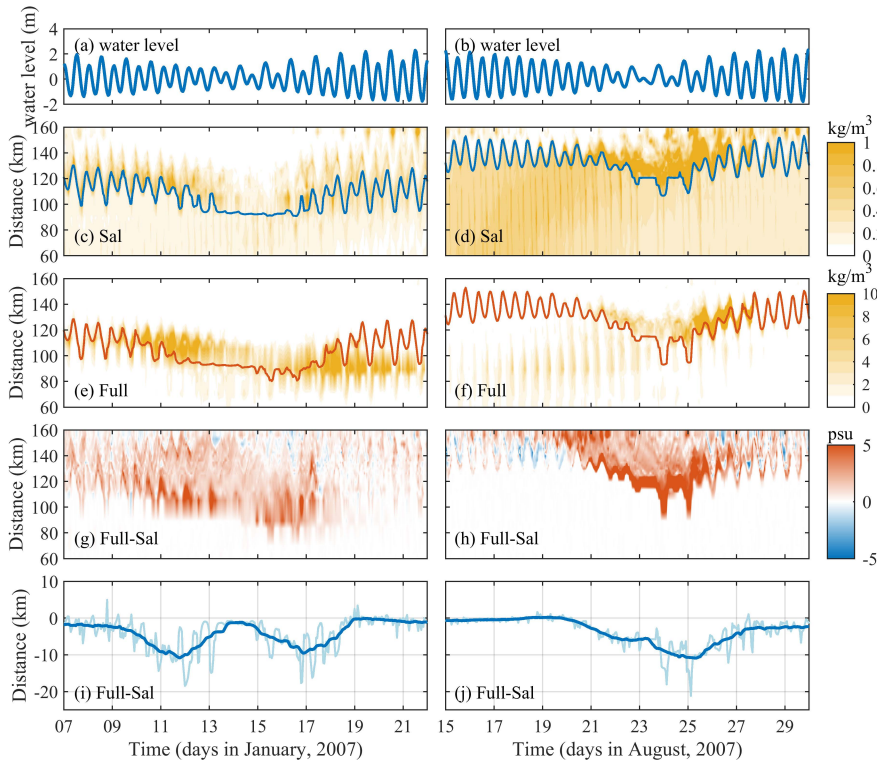


Figure 4.11: Time evolution of the modelled (a, b) tidal water level at Niupijiao; bottom suspended sediment concentration (SSC) in the scenarios of (c, d) Sal, and (e, f) Full; (g, h) difference of the vertical salinity gradients between the Sal and Full scenarios (Full- Sal) and (i, j) difference of the instantaneous (thin light blue) and tidally averaged (thick dark blue) salt front locations (Full- Sal) in a spring-neap cycle during (a, c, e, g, i) dry season and (b, d, f, h, j) wet season. The blue and red lines in (c, d) and (e, f) represent the tidally-averaged salinity front location which is defined as the 3-psu bottom salinity limit, in the Sal and Full scenarios, respectively (scenarios refer to Table 4.2).

2020) leads to a strong relation between bed shear stress and turbidity and is less sensitive to variations of residual flows, and therefore altering sediment convergence zones. Instead, we assume that the ETM results from density-driven processes and thus the ETM is more dynamic (supply-limited approach, or reduced deposition approach, availability-limited state; see Brouwer et al., 2018; Dijkstra et al., 2018; Hesse et al., 2019; van Maren et al., 2020). The sediment dynamics following a supply-limited approach are sensitive to the subtle variations in the hydrodynamic forcing. Using a supply-limited approach (as adopted for our study) allows detailed investigations on the formation of the ETM in response to residual sediment transport processes, such as estuarine circulation and tidal asymmetries (van Maren et al., 2011; Hesse et al., 2019). The supply-limited approach has been used in several cases and can result in equilibrium transport for sediment trapping (van Maren et al., 2015b; Brouwer et al., 2018; Dijkstra et al., 2018; Hesse et al., 2019). One limitation of this approach is the difficulty in calibrating the large-scale

model against observations, particularly for the near-bed SSC. Seaward of the NP, the depocenter of the Yangtze subaqueous delta (a ~40 m thick mud belt, Liu et al., 2007, maintains a high deposition rate (10 cm/yr during 1958-2009, Dai et al., 2014) probably as a result of the alongshore current. The simulated ETM formation is also influenced by the deposition zone seaward of the NP (see SI). Moreover, the simulated near-bed SSC and salt intrusion are difficult to be well reproduced simultaneously considering the identified interaction between SSC and salinity; however, it does not negate the main findings in this work.

The modelled depth-averaged SSC corresponds well with data (Figure 4.3), and the near-bed SSC is substantially larger than averaged over depth (see also Figure 4.3). However, if we compare the computed near-bed SSC in Figure 4.3 with an alternative dataset (Figure 4.1), the model seems to underestimate the high concentrations occurring close to the bed ($>10 \text{ kg/m}^3$). We attribute this underestimation to (1) flocculation: the settling velocity varies over time and space resulting from flocculation processes influenced by hydrodynamic shear, salinity, and the sediment concentration, which is not numerically accounted for; (2) high SSCs occur as thin layers very close to the bed. The thickness of the near-bed layers is too large (1 m) to resolve such fluid mud layers. These layers result in high SSC concentration gradients, which in turn dampen turbulent mixing, strengthening sediment concentration gradients; (3) consolidation processes are not accounted for which may result in spatially and temporally varying critical bed shear stress. Additionally, the sediment within and seaward of the NP is finer, with lower critical shear stress for erosion. Both consolidation and spatial segregation of sediments may lead to discrepancies of observed and modelled sediment convergence; and (4) The jetties and groins are implemented as blocked thin dams which limit the water and sediment exchanges (Zhu et al., 2017) whereas in reality, the jetties overflow around high water. As a result, the model underestimates lateral inflow of suspended sediment, especially under high tides and storm events when water levels and SSC are high.

Despite the near-bed SSC underestimation in the ETM, the model does differentiate the effects of longitudinal and vertical SedDG. In reality, the relative effect of the SedDG is expected to be more pronounced, resulting in more pronounced effects on sediment transport and tidal propagation.

4.4.2. ETM DEVELOPMENT BY SEDDG

EFFECT OF THE SEDDG

The effect of the SedDG is completely different with and without salinity effects. Without salinity, no ETM develops and the effect of SedDG is limited. With salinity effects, a pronounced ETM develops with a shape, strength and location strongly influenced by the SedDG. This dependence implies a nonlinear interaction between salinity and SSC, which we address by analyzing the differences between the Sal and Full scenarios. In the following analysis, we differentiate the longitudinal and vertical sediment-induced density effects.

Longitudinal salinity-induced effects trap sediment and therefore generate a pronounced ETM (Figure 4.6 and Figure 4.7). In contrast, the longitudinal sediment-induced effects lead to divergence of sediment (I in Figure 4.12) with sediment transport directed from the middle of the ETM to both the landward and seaward direction. This implies

that the longitudinal SedDG strengthens the longitudinal SalDG landward of the ETM, but weakens the longitudinal SalDG seaward of the ETM (corresponding to the increased and decreased baroclinic pressure gradients in the Full scenario compared to the Sal scenario in upstream and downstream of km-120, respectively, see Figure 4.7). Therefore, the ETM extends further upstream and the longitudinal distribution of SSC is more asymmetric when accounting for sediment-induced density effects (see Figure 4.6).

Salinity stratification reduces vertical mixing rates and therefore mitigating tidal damping. This effect is reflected in increasing tidal amplitudes from simulations with salinity (Figure 4.4). Vertical SedDG influences ETM in two ways. The first (IIa in Figure 4.12) excludes interaction with the large-scale hydrodynamics (only local turbulent mixing), in which the SedDG increases the vertical concentration gradient (lower surface SSCs and higher bottom SSCs) because of the reduced vertical mixing. These sediment-induced effects become stronger at higher sediment concentrations, leading to progressive sediment trapping in high concentration areas. Even more, strong vertical SSC gradients strengthen the effect of salinity-driven residual circulation on ETM formation. Secondly, this vertical distribution also influences the large-scale hydrodynamics (water levels, velocities and salinities, see IIb in Figure 4.12). The vertical SedDG has the same effect as the SalDG on amplifying and deforming tides as vertical density gradients reduce the effective hydraulic drag due to buoyancy destruction (Winterwerp et al., 2009). The drag reduction will subsequently strengthen tidal amplification (Gabioux et al., 2005; Winterwerp and Wang, 2013; Wang et al., 2014) and tidal deformation (van Maren et al., 2015b). The tides are deformed as friction transfers energy among tidal frequencies and changes the propagation speed at high and low water levels (Parker, 1984; Friedrichs and Aubrey, 1994; Savenije, 2006). More importantly, our work demonstrates that the vertical salinity and sediment effects strengthen each other, introducing a positive feedback mechanism promoting ETM formation.

Overall, this work demonstrates that the longitudinal SedDG leads to sediment transport divergence. This is an important confirmation of the analytical model results of Talke et al. (2009b) but also the first time the vertical and longitudinal sediment-induced density effects are differentiated in a complex numerical modelling environment. Particularly the interaction between salinity and SSC indicates that the effect of the vertical SedDG is even more complicated than mechanisms identified earlier (focusing on the individual contribution of sediment), such as sediment-induced damping of turbulence (Winterwerp, 2001), reduction of hydraulic drag (Winterwerp et al., 2009), and tidal deformation (van Maren et al., 2015b).

FLUVIAL AND TIDAL EFFECTS

The effect of the vertical SedDG is closely related to the seasonal and spring-neap variations of stratification and mixing. Typically, a higher river discharge leads to more stratification compared to a lower discharge, and stronger tidal flow leads to stronger mixing (Dyer, 1986); the river discharge itself leads to tidal damping (Horrevoets et al., 2004). As a result, the SedDG most strongly influences the vertical distribution of the sediment concentration and salinity at neap tides during the wet season, corresponding to the spring-neap variations of the migration of the salt wedge (Figure 4.11h, j). In contrast, in the dry season, the spring-neap variations of the migration of the salt wedge induced by the SedDG are much less related to the enhanced vertical salinity gradients

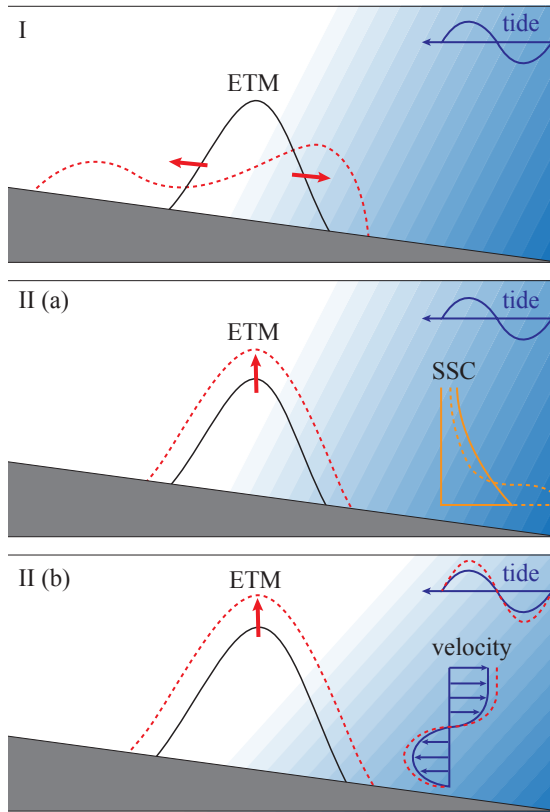


Figure 4.12: Schematic effects of the longitudinal and vertical sediment-induced density gradients (SedDG) on sediment trapping. I: effect of the longitudinal SedDG; II(a): effect of the vertical SedDG with changes only in suspended sediment concentration (SSC) (no sediment-induced changes on hydrodynamics); II(b): effect of the vertical SedDG with changes including hydrodynamics, i.e. water level, velocity and salinity. Solid and dashed lines are the situation without and with the effect of the SedDG, respectively.

(Figure 4.11g, i). This is probably caused by the spring-neap variation in mixing and deposition which additionally modulates the SSC variation: during the dry season, the near-bed SSC of the salinity-driven ETM (Figure 4.11c) is smaller at spring tides due to stronger tidal mixing. At neap tides, however, the bottom sediments tend to deposit into the bed, resulting in the lower bottom SSC (as for spring tides, but for a different reason). As a result, vertical SSC differences are low around spring tides and neap tides, but more pronounced in-between.

The strength of the longitudinal SedDG depends on the trapping efficiency as explained above and therefore the expansion of the ETM is most pronounced at intermediate tides during the dry season. Similarly, the strongest effect of the longitudinal SedDG occurs at neap tides during the wet season; however, the divergence of the ETM is not significant. Note that, although the vertical convergence of the ETM is stronger during the wet season than during the dry season, the near-bed SSC is higher during the

dry season. Probably, the high river discharge also leads to stronger seaward flushing of sediment, which is more efficiently trapped during the dry season.

4.4.3. IMPLICATIONS FOR OTHER ESTUARIES

ETM DEVELOPMENT

Our work reveals that the SedDG promotes the formation and longitudinal dispersion of the ETM of the Yangtze. These findings are probably relevant for ETM dynamics in other systems as well. ETMs can be classified into three types with respect to their location relative to the salt wedge controlled by different mechanisms (Table 4.3): near the landward limit of the salt wedge, far into the freshwater zone, and within the estuarine salinity gradient (Burchard et al., 2018). An ETM may switch location due to river discharges and tide-induced sediment transport. In particular, sediment may play important roles in highly turbid systems. In the Ems estuary, for example, successive channel deepening resulted in the upstream movement of the ETM into the freshwater zone (Chernetsky et al., 2010; de Jonge et al., 2014), which was attributed to positive feedback mechanisms triggered by high SSCs in response to deepening (Winterwerp, 2011; Winterwerp and Wang, 2013; van Maren et al., 2015b; Dijkstra et al., 2019b,a). In addition to these vertical sediment-induced density effects, Talke et al. (2009b) suggested longitudinal sediment-induced density effects to generate up-estuary sediment transport in the Ems. In the river-dominated systems, although the ETM is rarely observed to migrate into the freshwater region, ETM dispersion still occurs. For instance, the ETM is weakened from neap tides to spring tides in the Amazon Estuary, which was primarily ascribed to the tidally varying vertical stratification in salinity and sediment (Geyer, 1993). Moreover, the expansion of the ETM is more pronounced in the dry season than the wet season in the Mekong Estuary, which was attributed to the seasonal variation in erosion and deposition processes (Wolanski et al., 1996, 1998). However, the role of sediments in ETM dynamics has received little scientific attention and we believe that the SedDG may be also important for ETM dispersion in other systems.

SALT INTRUSION

The landward migration of the salt intrusion induced by SedDG is important for freshwater intake. Approximately 70% of the freshwater supply in Shanghai is taken from the Yangtze Estuary, which is endangered by salinity intrusion (Zhu et al., 2018). Analytical solutions (Savenije, 1993; Kuijper and Van Rijn, 2011; Zhang et al., 2011; Cai et al., 2015) and numerical models (Xue et al., 2009; Gong and Shen, 2011) are often used to predict salt intrusion in estuaries. However, these models do not consider sediment-induced effects on salt intrusion. Our model suggests a 5-km yearly-averaged (0-20 km considering seasonal and spring-neap variations) landward movement of the salt intrusion as a result of the SedDG. Note that as our model under-predicts the near-bed SSC, the impact of sediment on salt intrusion may be even larger in reality.

The effect of sediments on salinity is important since the SSC has been changing in many estuaries worldwide. A decrease in riverine sediment flux has been widely reported in many large river deltas due to dam construction and soil conservation (Vörösmarty et al., 2003; Syvitski and Saito, 2007; Walling, 2009). Although the response time of an estuary to such a riverine sediment decline may be slow (and is often not known), a

Table 4.3: Examples of estuarine turbidity maximums (ETM) with the main formation mechanisms. ETM1, ETM2, and ETM3 refer to the ETMs locating within the estuarine salinity gradient, near the landward tip of the salt wedge, and far into the freshwater zone, respectively.

Type	Main formation mechanisms	Estuaries
ETM1	<ul style="list-style-type: none"> • topographic trapping (e.g., transition of topography) • under certain conditions (e.g., high river flow) 	USA: Chesapeake Bay (North and Houde, 2001; Fugate et al., 2007), Columbia River estuary (Jay and Musiak, 1994; Fain et al., 2001; Hudson et al., 2017), Delaware estuary (Sommerfield and Wong, 2011), Hudson estuary (Geyer et al., 2001; Ralston et al., 2012), San Francisco Bay (Schoellhamer, 2000), York River estuary (Lin and Kuo, 2001) Germany: Elbe estuary (Kappenberg and Grabemann, 2001) UK: Humber estuary (Mitchell et al., 1998; Uncles et al., 2006)
ETM2	<ul style="list-style-type: none"> • gravitational circulation (salinity-driven transport) • tide-induced sediment transport 	USA: Chesapeake Bay (Schubel, 1968; Sanford et al., 2001), Columbia River estuary (Jay and Smith, 1990; Jay and Musiak, 1994), Delaware estuary (Sommerfield and Wong, 2011), York River estuary (Lin and Kuo, 2001) Germany: Elbe estuary (Postma, 1961), Weser estuary (Grabemann et al., 1997) France: Gironde estuary (Allen et al., 1980), Seine estuary (Avoine, 1987; Grasso et al., 2018; Grasso and Le Hir, 2019) UK: Humber estuary (Uncles et al., 2006), Tamar estuary (Grabemann et al., 1997) Brazil: Amazon Estuary (Geyer, 1993) Vietnam: Mekong Estuary (Wolanski et al., 1996, 1998) China: Yangtze Estuary (Li and Zhang, 1998; Shi, 2004; Wu et al., 2012; Li et al., 2016b)
ETM3	<ul style="list-style-type: none"> • tide-induced sediment transport • under certain conditions (e.g., low river flow) 	Netherlands: Ems estuary (Talke et al., 2009b; Chernetsky et al., 2010; de Jonge et al., 2014) France: Gironde estuary (Allen et al., 1980; Castaing and Allen, 1981) UK: Humber estuary (Mitchell et al., 1998; Uncles et al., 2006), Tamar estuary (Grabemann et al., 1997)

Note: Talke et al. (2009b) and this study focuses on the sediment-driven transport in the Ems and the Yangtze Estuary, respectively.

future decrease in SSC in the estuary may prevent salt intrusion (for instance, resulting from a reduction in river discharge or deepening). However, other estuaries experience an increase in SSC due to local human interventions, such as narrowing and deepening, dredging and dumping activities etc. (Winterwerp, 2011; Winterwerp et al., 2013; Winterwerp and Wang, 2013; van Maren et al., 2015a,b). Such an effect, which may be more profound in small estuaries where marine sediment supply dominates the ETMs, could strengthen salt intrusion. Our results on sediment-induced density effects are important for sediment management and management of freshwater supply in turbid estuaries. These findings stress the importance of understanding the effect of human activities within the estuary, in the upstream basin, or through global climate change on estuarine SSC. A change in SSC does not only negatively impact maintenance dredging or estuarine ecology, but also influences salt intrusion through sediment-induced density effects and therefore threatens freshwater availability.

4.5. CONCLUSIONS

MANY estuaries are characterized by ETMs generated by salinity-induced density currents and tide-induced transport mechanisms. In this work, we reveal that high sediment concentrations also influence the stability and position of the ETM. The strength and position of ETMs are investigated using a model accounting for the effects of sediment and salinity on longitudinal variations of tidal propagation and sediment transport. Using the Yangtze Estuary as a case study, the model shows that the density effects of salinity and sediment cause ~ 0.1 m increase in tidal amplitudes. Salinity- and sediment-induced density gradients play different roles in the distribution of SSC along the estuary. Salinity-induced density gradients are the primary drivers for ETM formation leading to the pronounced sediment convergence whereas longitudinal sediment-induced density gradients lead to sediment transport divergence (although depending on the strength of the ETM, which depends on the strength of salinity-driven residual currents). Vertical sediment-induced density gradients introduce a behavior opposite to the longitudinal sediment-induced density gradients on two levels: they 1) enhance the vertical SSC gradients, leading to more efficient salinity-driven residual transport and 2) additionally influence the tidal amplitude, salinity structure, and therefore residual flows, generating a positive feedback mechanism for ETM formation. Summarizing, the strength of the ETM depends on the convergence of the salinity-driven sediment transport, enhanced by the effects of vertical sediment-induced density gradients but weakened by the divergence of sediment resulting from longitudinal sediment-induced density gradients.

We further conclude that sediment-induced density effects vary seasonally and throughout the spring-neap tidal cycles. During the wet season, the vertical salinity gradient is stronger, and therefore the impact of sediment on salt intrusion and ETM formation is more pronounced. The impact is the strongest at neap tides, as during these conditions the water column is more salinity-stratified. During the dry season, in contrast, salt intrusion and ETM displacement are the largest at intermediate tides. This is probably the result of higher near-bed sediment concentrations during that period, resulting from weak vertical mixing while sediment deposition remains limited.

In conclusion, sediment-induced density effects are important for longitudinal tidal

propagation, sediment transport, and salt intrusion and should therefore be accounted for in the management of salt intrusion and mitigation of sediment deposition in highly turbid estuaries.

4.A. APPENDIX: PARAMETERS IN THE SEDIMENT TRANSPORT MODEL

The governing equation to solve suspended sediment concentration (SSC) is the 3D advection-diffusion (mass-balance) equation:

$$\frac{\partial c}{\partial t} + \frac{\partial(uc)}{\partial x} + \frac{\partial(vc)}{\partial y} + \frac{\partial}{\partial z} [c(\omega + \omega_s)] = \frac{\partial}{\partial x} \left(\varepsilon_x \frac{\partial c}{\partial x} \right) + \frac{\partial}{\partial y} \left(\varepsilon_y \frac{\partial c}{\partial y} \right) + \frac{\partial}{\partial z} \left(\varepsilon_z \frac{\partial c}{\partial z} \right) \quad (\text{S4.1})$$

Here, t is the time; u , v and ω are the x , y and z components of velocity, respectively; c is the SSC; $h = h_0 + \zeta$ is the water depth, where h_0 is the bottom topography (water depth at reference level) and ζ is the surface elevation; ε_x , ε_y and ε_z are the sediment diffusion coefficients in the horizontal x and y directions and vertical z direction, respectively. ω_s is the settling velocity. In high concentration mixtures, the settling velocity of a single particle is reduced due to the presence of other particles. In order to account for this hindered settling effect, we follow [Richardson and Zaki \(1954\)](#) and determine the settling velocity in a fluid-sediment mixture as a function of the sediment concentration and the non-hindered settling fall velocity:

$$\omega_s = \omega_{s,0} \left(1 - \frac{c}{c_{soil}} \right)^5 \quad (\text{S4.2})$$

Where c_{soil} is the reference density for hindered settling, and $\omega_{s,0}$ is the settling velocity for a sediment particle. The interaction of sediment, turbulence and hydrodynamics is modelled by including the effect of sediment on water density, which subsequently reduces turbulence mixing through the k - ε model:

$$\rho = \rho_w + \left(1 - \frac{\rho_w}{\rho_s} \right) c \quad (\text{S4.3})$$

Where ρ_w is the clear sea-water density, and ρ_s is the sediment density.

4.B. APPENDIX: MODEL CALIBRATION FOR HYDRODYNAMICS AND SEDIMENT TRANSPORT

The fully baroclinic model (or the Full scenario) was validated against measured tidal water levels at 8 tidal stations- Baimao, Shidongkou, Wusong, Changxing, Hengsha, Beicaozhong, Niupijiao and Lvhua (see [Figure S4.1](#) and [Table S4.1](#) for the locations). The model results at the 8 stations agree well with the measured data in August-September 2007 ([Figure S4.2](#)). The amplitudes and phases of three main tidal constituents (M_2 , S_2 and M_4) were also calculated to compare with the observations using t-tide harmonic analysis ([Pawlowicz et al., 2002](#)), see [Figure S4.3](#). From the seaward station (Lvhua) to the up-estuary station shown here (Baimao), the tides (observed as well as computed) are amplified by 8% at the location of the ETM and then decrease 30% in the upstream direction. For the dominant M_2 constituent, the differences between the computed and measured values are less than 5% in amplitude and less than 10 degrees in phase. The

largest error between the model and observations occurs at Baimao station for the amplitude of S_2 constituent, but the error is less than 15%. The amplitude of M_4 increases from Lvhu to Wusong and then decreases to Baimao, which is consistent with the observed data.

The model was further validated against flow velocity measured at six levels (surface, 0.2h, 0.4h, 0.6h, 0.8h and bottom) on 14-18 August, 2007. The modelled depth-averaged flow velocity was compared with observations at selected mooring stations (see Figure S4.1 and Table S4.1 for the locations) in August 2007 (Figure S4.4). The model performance is quantitatively evaluated against observed data by computing Root Mean Square Error (RMSE), Correlation Coefficient (CC) and Skill Score (SS) at different layers (Figure S4.5). The averaged RMSE of the magnitude of depth-averaged flow velocity is 0.34 m/s whereas that of CC and SS are 0.98 and 0.9, respectively. For reference concerning SS, an evaluation of a hydrodynamic and ecosystem model in the southern North Sea categorized an $SS > 0.65$ as excellent, 0.5–0.65 as very good, 0.2–0.5 as good, and < 0.2 as poor (Allen et al., 2007). The model performs thus well. Moreover, the simulated salinity is plotted together with observations in Figure S4.6. Despite some discrepancies in the South Passage and relative lower simulated salinity in the North Passage, the model can be utilized to investigate the effect of density gradients.

Seasonal variations of river discharge have a large impact on salt intrusion and sediment trapping. The model is also run for 2009 to validate the model against the measurements of surface SSC in 2009 (Figure S4.7). In 2009, the mean river discharge during the flood season (May-October) is 33,498 m³/s, which is 2 times that during dry season (November-April). At Hengsha, the surface SSC is smaller during flood season than that during dry season, whereas the surface SSC is larger during flood season than that during dry season at Xuliujing. Note that the measurements are sampled twice a day at Xuliujing and Hengsha (Li et al., 2012) and the modelled results are in an interval of 1 hour. Therefore, the magnitude of modelled time series of SSC is larger than the observed times series of SSC. Overall, the model is suitable for modelling seasonal variations of sediment transport.

4.C. APPENDIX: SENSITIVITY STUDIES ON ETM FORMATION

The model is calibrated in fully baroclinic mode and the effects of the deposition zone, turbulence model and sediment settling velocities are evaluated from scenarios 'R1'-'R5' (see Table S4.2 and Figure S4.8). R1 only limitedly allow deposition offshore by specifying reduced deposition efficiency α of 0.1 and critical bed shear stress for erosion 0.1 N/m². Therefore, a second ETM is identified offshore (seaward of km-150). In addition, the sediments are accumulated more in the R1 scenario than the Full scenario as the Full scenario reduces the offshore sediment supply compared with the R1 scenario. For very fine sediments (settling velocity of 0.1 mm/s, R2), less sediments can be trapped in the estuary and most of the fine sediments are flushed into the sea. For coarser sediments (settling velocity of 2 mm/s, R3), strong accumulation is found in the ETM; however, sediments are less influenced by the river and tide forcing. Specifically, the surface sediments at Hengsha during the dry season in the R3 scenario are fairly low and the seasonal variations are even opposite to the Full scenario (Figure S4.9). In the R3 and R4 scenarios, we tested the behavior of the turbulence closure model, i.e., additional

background vertical eddy viscosity $0.001 \text{ m}^2/\text{s}$ and background vertical eddy diffusivity $0.001 \text{ m}^2/\text{s}$ in the $k-\epsilon$ model (R3), and the k-L model (R4). Both the two scenarios suggest stronger mixing effect and less effect on the convergence of the sediments than our calibrated model.

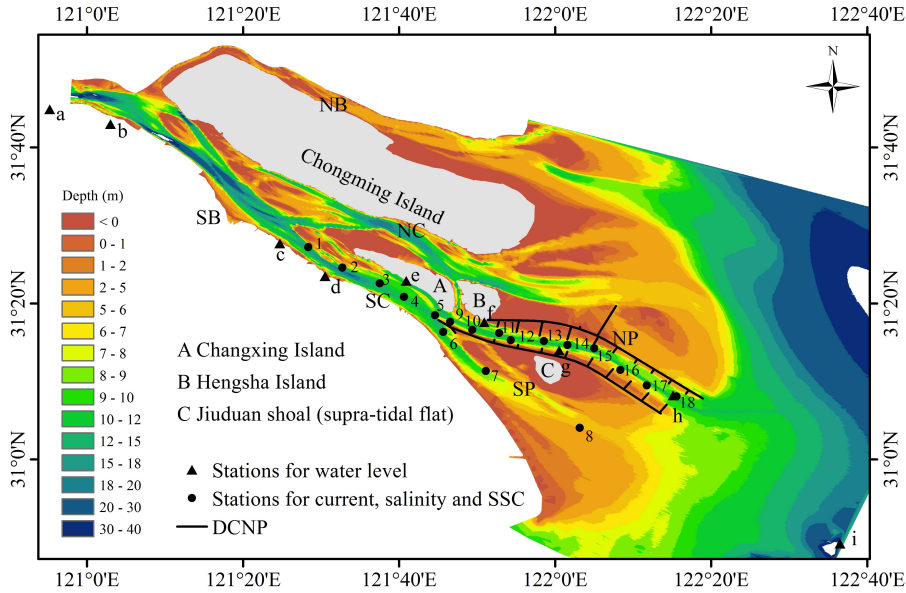


Figure S4.1: Stations for validation of water level, current, salinity and suspended sediment concentration (SSC). Names of stations are shown in Table S4.1. DCNP: Deep Channel Navigation Project. NB: North Branch; SB: South Branch; NC: North Channel; SC: South Channel; NP: North Passage; SP: South Passage.

Table S4.1: Name of stations for validation in Figure S4.1.

Stations for water level		Stations for current, salinity and SSC			
No.	Name	No.	Name	No.	Name
a	Xuliujing	1	NGN1	10	CS0
b	Baimao	2	NGN2	11	CS1
c	Shidongkou	3	NGN3	12	CB2
d	Wusong	4	NGN4	13	CS2
e	Changxing	5	NG3	14	CS6
f	Hengsha	6	NC1	15	CSW
g	Beicaozhong	7	NC2	16	CS3
h	Niupijiao	8	NC4	17	CS7
i	Lvhua	9	CB1	18	CS4

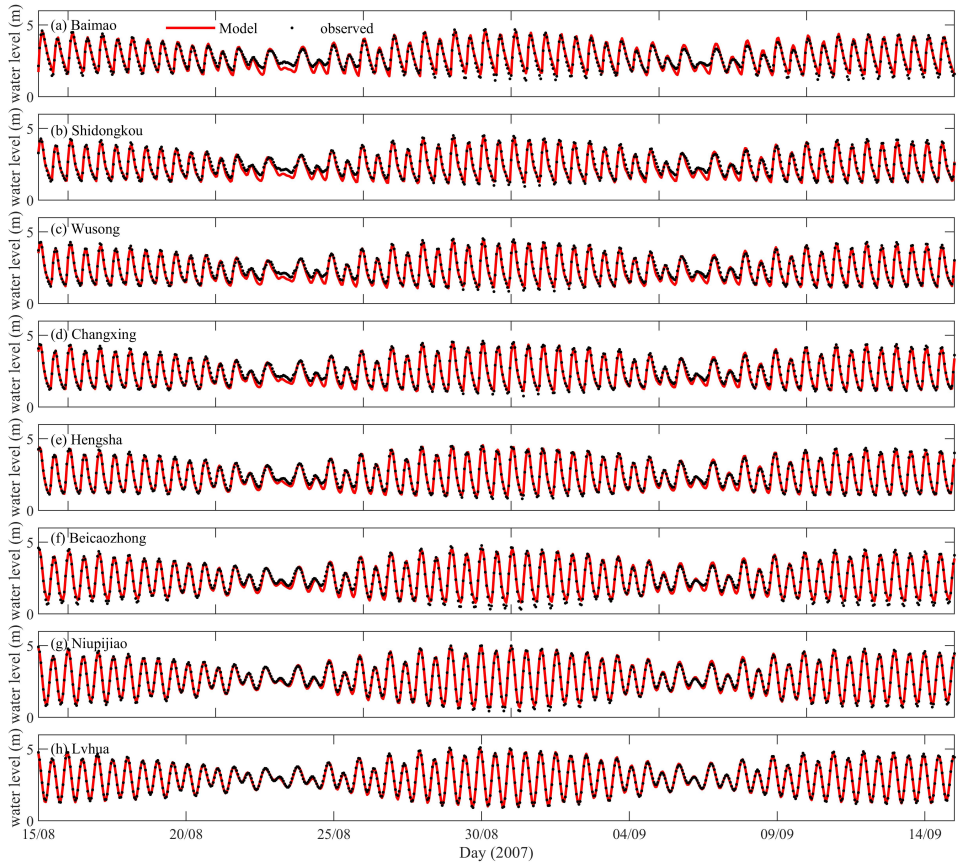


Figure S4.2: Model-data comparisons for water level variations at (a) Baimao, (b) Shidongkou, (c) Wusong, (d) Changxing, (e) Hengsha, (f) Beicaozhong, (g) Niupijiao and (h) Lvhu (see Figure S4.1 and Table S4.1 for the locations).

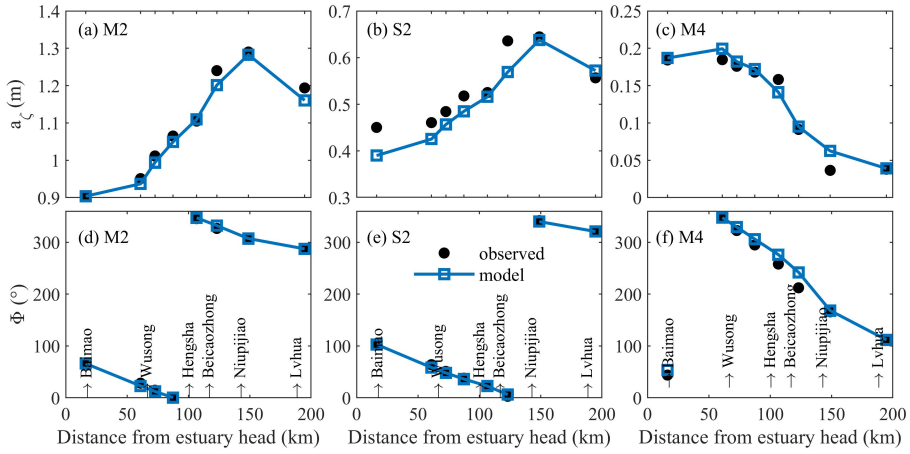


Figure S4.3: Comparison between the modelled (solid line) and observed (dots) results in terms of tidal amplitude and (upper panel) phases (lower panel) of M₂ (a, d) S₂ (b, e) and M₄ (c, f) along the estuary (see Figure S4.1 for the locations). The estuary head is at Xuliujing (see also Figure S4.1 and Table S4.1).

Table S4.2: Overview of model scenarios for sensitivity study. SalDG: salinity-induced density gradient; SedDG: sediment-induced density gradient.

Case No.	Settling velocity (mm/s)	SalDG	SedDG	Mixing model	Note
Full	0.5	Yes	Yes	$k-\epsilon$	calibrated
R1	0.5	Yes	Yes	$k-\epsilon$	limited deposition offshore
R2	0.1	Yes	Yes	$k-\epsilon$	-
R3	2	Yes	Yes	$k-\epsilon$	-
R4	0.5	Yes	Yes	$k-\epsilon$	background vertical eddy viscosity 0.001 m ² /s; background vertical eddy diffusivity 0.001 m ² /s
R5	0.5	Yes	Yes	$k-L$	-

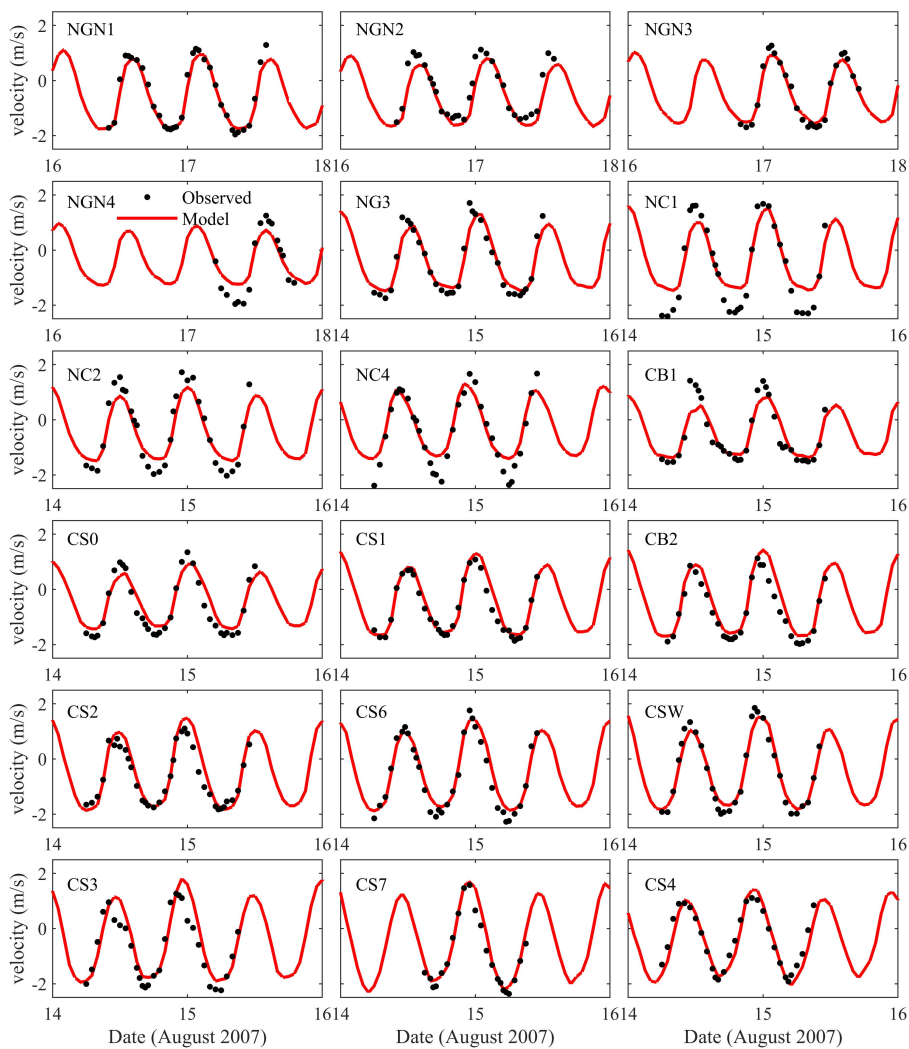


Figure S4.4: Model-data comparisons of depth-averaged along estuary velocity at 18 stations in 2007 (see Figure S4.1 and Table S4.1 for the locations), positive value indicates landward direction.

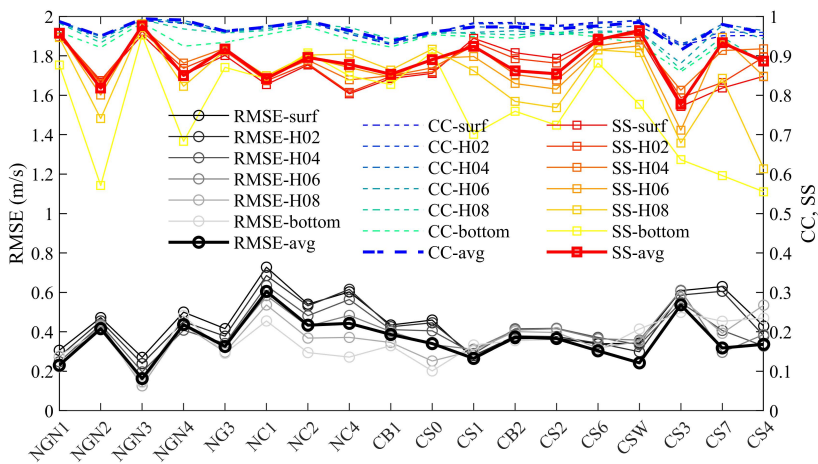


Figure S4.5: Root Mean Square Error (RMSE), Correlation Coefficient (CC) and Skill Score (SS) of the magnitude of flow velocity at 18 mooring stations (see Figure S4.1 and Table S4.1 for the locations). The surf, H02, H04 H06, H08, bottom and avg represent the layers at surface, 0.2h, 0.4h, 0.6h, 0.8h, bottom and depth-averaged, respectively.

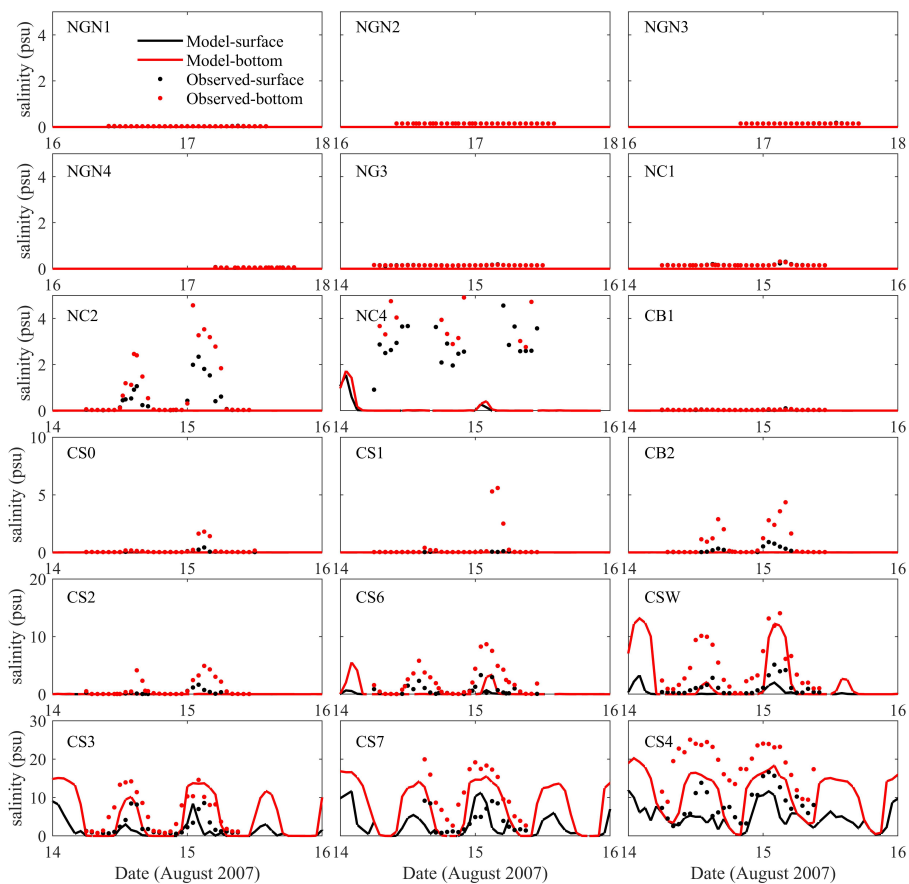


Figure S4.6: Model-data comparisons of salinity variations at 18 stations in 2007 (see Figure S4.1 and Table S4.1 for the locations).

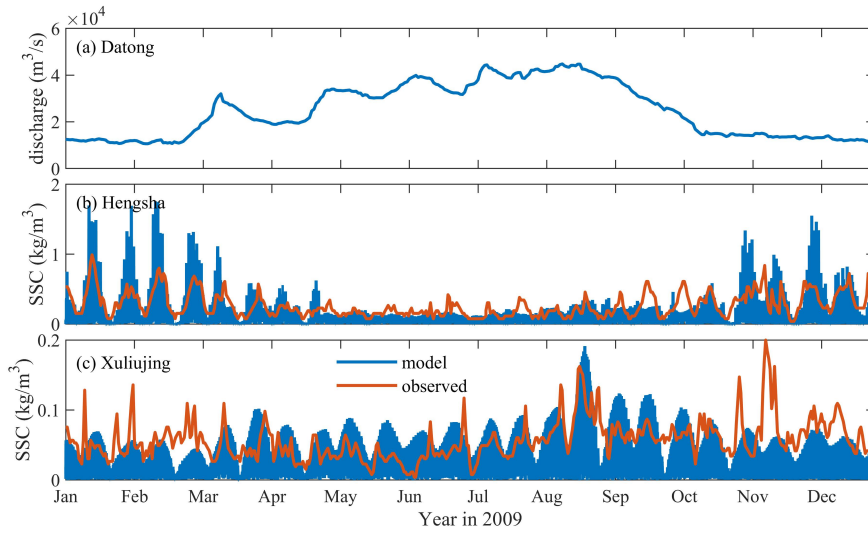


Figure S4.7: Variations of (a) measured water discharge at Datong in 2009 and modelled (blue) and observed (red) surface suspended sediment concentration (SSC) at (b) Hengsha and (c) Xuliujing in 2009. Data of observed surface SSC is from [Li et al. \(2012\)](#). Locations of Hengsha and Xuliujing refer to [Figure S4.1](#) and [Table S4.1](#).

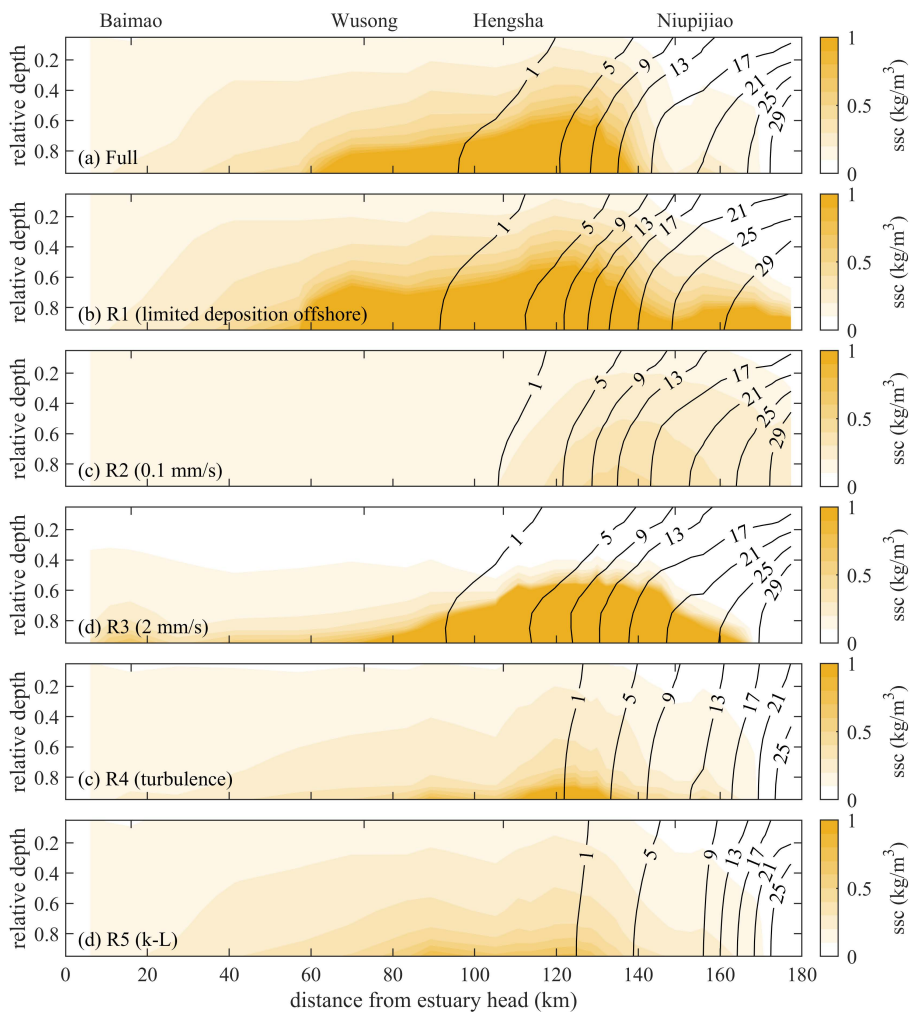


Figure S4.8: Modelled longitudinal distribution of salinity (black contour lines) and SSC (color shading) in the scenarios of (a) Full, (b) R1, (c) R2, (d) R3, (e) R4, and (f) R5 (scenarios see Table S4.2) averaged from 1 Jan, 2007 to 1 Jan, 2008. The estuary head is at Xuliujing (see also Figure S4.1 and Table S4.1).

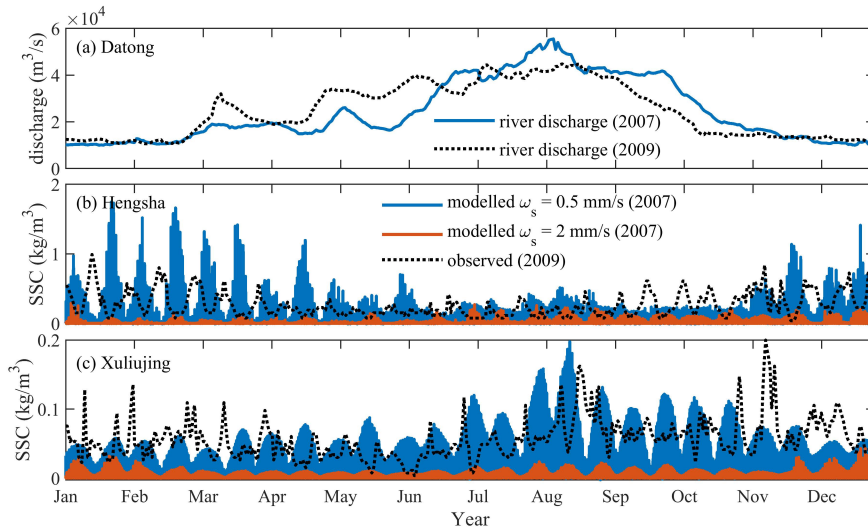


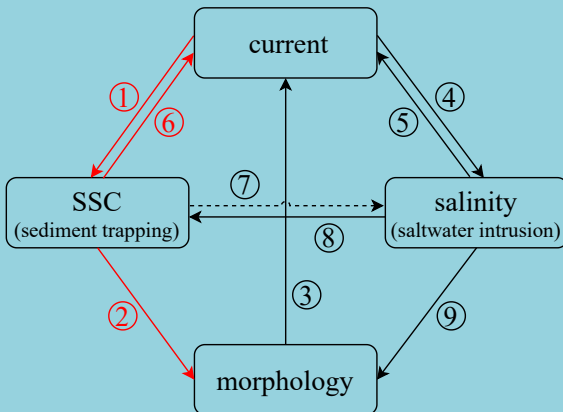
Figure S4.9: Variations of (a) measured water discharge at Datong in 2007 and comparisons between the modelled surface suspended sediment concentration (SSC) with settling velocity ω_s of 0.5 mm/s (scenario-Full) and 2 mm/s (scenario-R3, scenarios see Table S4.2) at (b) Hengsha and (c) Xuliujing in 2007. Locations of Hengsha and Xuliujing refer to Figure S4.1 and Table S4.1.

5

FEEDBACK EFFECTS OF SEDIMENT SUSPENSION ON TRANSPORT MECHANISMS IN ESTUARINE TURBIDITY MAXIMUM

*God does not care about our mathematical difficulties.
He integrates empirically.*

Albert Einstein (Mathematician, Physicist 1879-1955)
In L. Infield. *Quest*



This chapter focuses on the content in red and has been under review in:
Zhu, C., van Maren, D.S., Guo, L., Lin, J., He, Q. and Wang, Z.B., Feedback effects of sediment suspension on transport mechanisms in estuarine turbidity maximum. *Journal of Geophysical Research-Oceans*.

The mechanisms controlling the formation of an estuarine turbidity maximum (ETM) in estuaries have been extensively investigated, but one aspect that has received much less scientific attention is the feedback role of sediment suspensions themselves on ETM formation. Particularly in highly turbid estuaries, sediment suspensions influence ETM development through a combination of horizontal sediment-induced density currents, reduction in turbulent mixing, and water-bed exchange processes. In this study, we developed a schematic model resembling the Yangtze Estuary where the ETM is controlled by tidal pumping, estuarine circulation, and advection operating simultaneously. Model results suggest that without sediment-induced density effects, stronger flood tidal dominance leads to more pronounced sediment trapping through tidal pumping. Depending on the type of tidal asymmetry, sediment-induced density effects lead to ETM strengthening or ETM dispersion due to enhanced or weakened landward tidal pumping, respectively. Higher near-bed sediment concentrations as a result of water-bed exchange processes, in turn, strengthen the effect of estuarine circulation but simultaneously strengthen the divergence of sediment by tidal pumping. Overall, the contribution of sediment-induced effects is comparable to the contribution of tidal asymmetry for ETM formation and should be properly accounted for in studies on ETM dynamics in turbid estuaries.

5



5.1. INTRODUCTION

MANY estuaries trap sediments in regions called the Estuarine Turbidity Maximum (ETM), resulting in locally elevated suspended sediment concentrations (SSC) (Schubel, 1968). ETM dynamics have been extensively studied through in-situ measurements (e.g. Fettweis et al., 1998; Mitchell et al., 2017; Jalón-Rojas et al., 2015, 2016) and numerical modelling (e.g. Festa and Hansen, 1978; Geyer, 1993; Brenon and Le Hir, 1999; Yu et al., 2014; Kumar et al., 2017; Grasso et al., 2018). ETMs are the result of converging sediment transport, where the seaward directed transport in the upper estuary (predominantly driven by fluvial processes) is balanced by landward directed transport components of marine origin. The most important landward transport components are 1) tidal asymmetry, commonly by a stronger but shorter flood velocity and weaker but longer ebb velocity (Uncles et al., 1985; Dyer, 1988; Friedrichs and Aubrey, 1988; Brenon and Le Hir, 1999; Yu et al., 2014) and 2) gravitational circulation, with longitudinal salinity gradients generating a landward residual flow close to the bed (Festa and Hansen, 1978; Dyer, 1988; Burchard and Baumert, 1998; Geyer and MacCready, 2014). Other mechanisms such as internal tidal asymmetry (Jay and Musiak, 1994, 1996) and tidal straining (Simpson et al., 1990) strengthen the sediment trapping effect as well.

Other factors such as sediment properties, sediment-induced density effects, and water-bed exchange processes additionally influence the ETM formation. Asymmetries in sediment properties (settling velocity, critical shear stress for erosion) generate settling and scour lags (Van Straaten and Kuenen, 1957; Postma, 1961; Friedrichs, 2011), which in combination with spatial or temporal hydrodynamic asymmetries contribute to sediment trapping. The settling lag and scour lag lead to net sediment transport in the direction of decreasing current velocity or water depth. Coarser (fast-settling) particles are more sensitive to maximum flow asymmetry (a difference in maximum ebb and flood flow velocities) whereas finer (slow-settling) particles are more sensitive to an asymmetry in the slack tidal period (the difference between the duration of high and low water slack, at which the flow velocity is below a critical velocity threshold, see Friedrichs, 2011).

Especially for relatively high SSC, the presence of suspended sediments influences hydrodynamics (and therefore residual transport) through sediment-induced density effects (SedDE) in two ways. First, horizontal sediment-induced density gradients enhance (weaken) estuarine circulation upstream (downstream) of the maximum SSC in the ETM. As a result, the SedDE leads to a divergence of sediment (Talke et al., 2009b). Secondly, vertical SedDE leads to the suppression of turbulence and therefore promote settling of sediments (Winterwerp, 2001), resulting in sediment trapping (Winterwerp and van Kessel, 2003; van Maren et al., 2020) but also in a reduction of the hydraulic drag (Winterwerp et al., 2009). Smoothing of the bed leads to tidal amplification in estuaries (Gabioux et al., 2005; Wang et al., 2014; Jalón-Rojas et al., 2016; Jalón-Rojas et al., 2018), resulting in a positive feedback mechanism with progressively more sediment trapping and potentially a regime shift towards hyper-turbid conditions (Winterwerp, 2011; Winterwerp and Wang, 2013; van Maren et al., 2015b; Dijkstra et al., 2019b,a). Although these sediment effects have been addressed individually, and partly combined (e.g., the effect of tidal asymmetry and settling lag by Chernetsky et al., 2010 and the effect of asymmetry in the water motion and SSC by Kumar et al., 2017); few have explored

the effect of asymmetry in tides and sediment properties together with the SedDE on the formation of the ETM.

The near-bed sediment concentration is influenced by water-bed exchange processes related to 1) settling flux of sediment onto the bed by suppression of turbulence (as elaborated above) and the settling velocity of the particles, and 2) resuspension processes related to the critical shear stress for erosion of freshly deposited sediments. In sediment-laden flows, the near-bed sediment concentration is larger due to the reduced deposition flux and stronger resuspension processes for the following reasons (see [van Maren et al., 2020](#) for more details). The deposition flux is damped as the settling velocity is reduced by floc breakup in the highly sheared near-bed region ([Hill et al., 2001](#)) and by hindered settling. At high SSC, flocs are larger (and hence the floc breakup mechanism more important), and therefore the near-bed reduction in settling velocity is more prominent at high concentrations. Hindered settling leads to an overall reduction in the settling velocity at high SSC. In addition, the net deposition of sediments is reduced at high SSC by erosion/consolidation processes. Consolidation scales quadratically with the thickness of the consolidating layer, and therefore particles depositing at high SSC only slowly consolidate and consequently only slowly attain critical shear stress for erosion. This means that particles transported at high concentrations in a decelerating tidal flow are kept in suspension (close to the bed) for a longer time. These water-bed exchange processes lead to relatively high near-bed sediment concentrations, which influence hydrodynamics and also directly influence the relative role of residual flows (as estuarine circulation) or resuspension processes (such as tidal asymmetry) on residual transport.

As a result of the large variation range of hydrodynamic and sedimentary processes, the location of the ETM may greatly vary; an estuary may even have multiple ETMs reflecting the range in transport mechanisms. Depending on the relative contribution of the various transport processes, the ETM may be located near the landward limit of the salt wedge, far into the freshwater zone, and within the estuarine salinity gradient ([Burchard et al., 2018](#)). The location of the ETM may also shift in time (e.g. due to human interventions). For instance, the ETM of the Ems estuary moved from the landward limit of the salt wedge (resulting from the classic salinity-induced circulation) upstream into the freshwater zone due to stronger tidal asymmetry in response to deepening ([Chernet-sky et al., 2010](#)) and stronger horizontal sediment-induced density gradients ([Talke et al., 2009b](#)).

The great variability in hydrodynamic and sedimentary processes and the resulting range in ETM locations fuels the need for a systematic study determining the contribution of transport processes on sediment trapping and ETM location. For this purpose, we develop a schematized model reflecting the hydrodynamics and sediment dynamics of the Yangtze Estuary, providing a well-studied example of an estuary where all the above mentioned hydrodynamic and sedimentary processes play a role (e.g. [Li and Zhang, 1998](#); [Liu et al., 2011](#); [Song et al., 2013](#); [Li et al., 2018b](#)). Our goal here is not to provide a realistic simulation for this particular estuary, but rather to gain insights into the roles of tidal asymmetries, sediment properties, sediment-induced density effects, and higher near-bed SSCs on ETM dynamics. The model setup, effects of sediments, and the methods for decomposing the net sediment flux are described in section 5.2. Model results in terms of the distribution of SSC and ETM locations are presented in section 5.3.

Transport mechanisms are discussed in section 5.4 and conclusions drawn in section 5.5.

5.2. METHODS

5.2.1. BASIC MODEL SETUP

WE construct a schematized three-dimensional (3D) estuarine model based on the open-source Delft3D code (Lesser et al., 2004). This modelling system simulates hydrodynamics and sediment transport and has been widely validated and used in varying estuarine and coastal environments. The generation, transport, and dissipation of turbulence are resolved with a $k-\epsilon$ model, in which turbulent mixing is modified by sediment-induced buoyancy effects through the equation of state.

The model has a planform geometry comparable to that of the Yangtze Estuary in which the origin of the axis is defined at the river boundary (km-0) (Figure 5.1). It consists of a 560-km long basin with a width diverging from 3 km at the landward limit to 50 km at the mouth. The basin has a deep channel and shallow areas with a width accounting for one-third and two-thirds of each cross-sectional width, respectively. The channel depth increases linearly from 20 m at the landward head (km-0) to 25 m at the mouth, after which the depth increases more rapidly to 50 m at the seaward boundary (km-710). The depth of the shallow areas increases linearly from 5 m at the origin to 10 m at the mouth. The banks of the estuary are non-erodible.

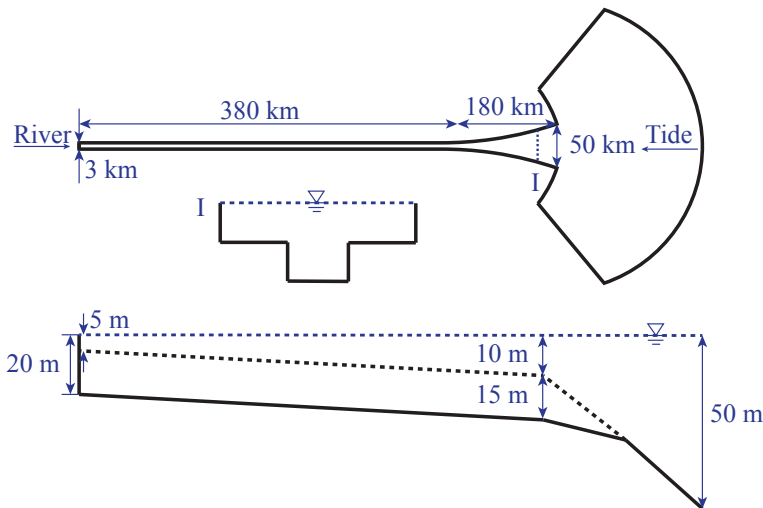


Figure 5.1: The planform and bathymetry of the schematic model. The x-axis is defined in the longitudinal seaward direction starting from the river boundary (km-0).

The model is forced with a simplified river discharge and tidal elevation. River discharge is prescribed with a constant value of $30,000 \text{ m}^3/\text{s}$, which is the approximate annual mean river discharge of the Yangtze River. Tidal water level constituents (M_2 , S_2 , M_4 , and MS_4) are prescribed at the seaward boundary (amplitudes of 1.5, 1, 0.15 and 0.15 m, respectively) with different water level phase relations to explore the effect of tidal

asymmetry: (1) symmetric tide (no M_4 and MS_4 component); (2) asymmetric tide with water level phase differences of 90° (with $2\phi_{\zeta M_2} - \phi_{\zeta M_4} = 90^\circ$ and $2\phi_{\zeta S_2} - \phi_{\zeta MS_4} = 90^\circ$); (3) asymmetric tide with water level phase differences of 180° (with $2\phi_{\zeta M_2} - \phi_{\zeta M_4} = 180^\circ$, $2\phi_{\zeta S_2} - \phi_{\zeta MS_4} = 180^\circ$).

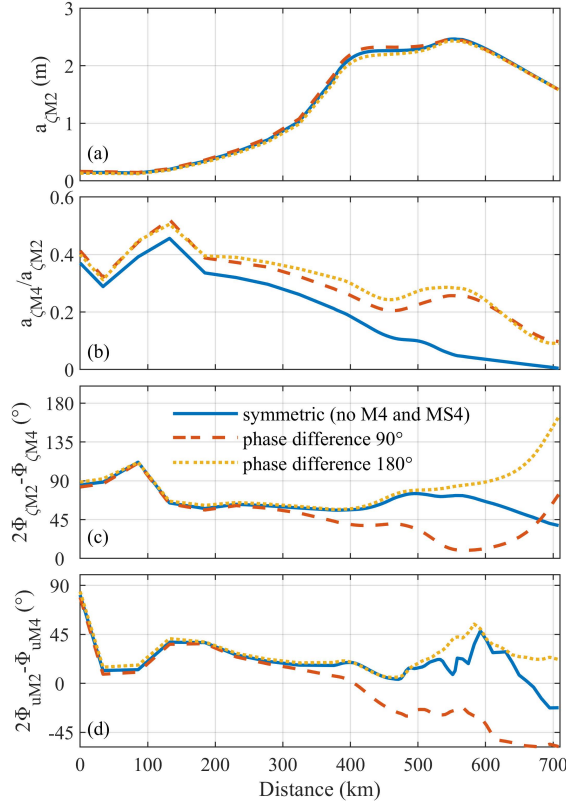


Figure 5.2: Tidal propagation in the scenarios with the symmetric tide (no M_4 and MS_4), asymmetric tide with phase differences of 90° and 180° , respectively: (a) water level amplitude of M_2 ($a_{\zeta M_2}$), (b) amplitude ratio of M_4 to M_2 ($a_{\zeta M_2}/a_{\zeta M_4}$), (c) phase difference between M_2 and M_4 for water levels ($2\phi_{\zeta M_2} - \phi_{\zeta M_4}$), and (d) phase difference between M_2 and M_4 for depth-averaged flow velocity ($2\phi_{uM_2} - \phi_{uM_4}$).

Note that the type of tidal asymmetry varies throughout the estuary by deformation of the landward propagating tide (Figure 5.2). The type of tidal asymmetry is determined by the phase lag in the velocity of M_2 and M_4 components ($\theta_u = 2\phi_{uM_2} - \phi_{uM_4}$). For $\theta_u = -90^\circ \sim 90^\circ$, the peak flood flow velocity is larger than the peak ebb flow velocity (with maximum flood-dominance at $\theta_u = 0^\circ$), see Friedrichs and Aubrey, 1988, which leads to landward transport. For $\theta_u = 0^\circ \sim 180^\circ$ (maximal at flood-dominance at $\theta_u = 90^\circ$), the duration of high water (HW) slack is longer than that of low water (LW) slack. Sediment transported landward during flood therefore has a longer period to settle at HW slack tide than at LW slack tide, resulting in net landward transport (Dronkers, 1986). The computed velocity phase difference θ_u for offshore water level phase dif-

ferences of 90° is approximately -30° at km-560, and therefore the tide at the mouth is mainly flood dominant due to peak flow asymmetry with an additional minor LW slack tide asymmetry. Similarly, for an offshore water level phase difference of 180° , $\theta_u = 45^\circ$ at the mouth and therefore the tide is flood dominant because of peak flow asymmetry with a bit HW slack tide asymmetry.

The sediment dynamics are computed using the Partheniades equation (Partheniades, 1965) for erosion E , and a permanent deposition flux D (Sanford and Halka, 1993):

$$E = M \left(\frac{\tau}{\tau_{cr}} - 1 \right) \quad (5.1)$$

$$D = \alpha \omega_s c \quad (5.2)$$

Where M is the erosion rate ($\text{kg}/\text{m}^2/\text{s}$), τ is the bed shear stress, τ_{cr} the critical bed shear stress for erosion, ω_s the settling velocity (m/s), c the SSC (kg/m^3), and α is a reduced deposition factor introduced by Van Kessel and Vanlede (2010) to approximate complex and poorly understood water-bed exchange processes but are not part of the model setup or formulations (see more details hereafter).

Finally, the model is initialised without sediment on the bed and no morphological changes. All sediment enters the domain through the upstream river boundary, and the model is run until the computed SSC reaches dynamic equilibrium (i.e., a condition where the SSC only varies over the tidal and spring-neap tidal cycle but does no longer display a trend).

5.2.2. EFFECTS OF SEDIMENTS

Sediments influence the hydrodynamics by damping of turbulence (computed with a $k-\varepsilon$ model) and through horizontal density gradients driving longitudinal and lateral flows. Both result from the contribution of sediment to the water density which is computed as:

$$\rho = \rho_w + \left(1 - \frac{\rho_w}{\rho_s} \right) c \quad (5.3)$$

Where ρ_w is the clear sea-water density, and ρ_s is the sediment density. The effect of sediment on density is evaluated by comparing model simulations with (scenario 'Full') and without (scenario 'Sal') the sediment density coupling. To separate the interaction with salinity, we additionally run a completely barotropic simulation ('Barot', without salinity effects and sediment effects) and a sediment-only scenario ('Sed', with sediment-induced density effects but without salinity-induced effects).

The sediment concentration itself also introduces several feedback mechanisms related to the settling and erosion of sediments, influencing the exchange of sediments between the water column and bed. At high sediment concentrations, the following processes become increasingly important (van Maren et al., 2020, see also section 5.1): (1) hindered settling reduces the rate at which the particles settle on the bed; (2) the reduction in settling velocity by floc breakup in the sheared near-bed layer, and (3) slow consolidation of deposited sediment results in easily erodible sediments. The water-bed

exchange processes described above lead to higher near-bed SSC at high sediment concentrations. However, they are either not sufficiently understood from a physical point of view (floc destruction in the near-bed boundary layer, strength development of soils at short time scales) or cannot be represented in large-scale numerical models from a computational point of view (a sufficiently high vertical resolution to account for the hindered settling effects, floc destruction in the near-bed boundary layer). Note that the hindered settling effect is accounted for by prescribing a reference density (200 kg/m^3) above which the settling velocity is reduced following [Richardson and Zaki \(1954\)](#) but additional effects may still occur due to the water-bed exchange processes. The combined effect of these processes is parameterized by the reduced deposition factor α introduced earlier ([Van Kessel and Vanlede, 2010](#); [van Maren et al., 2020](#)).

With the current state of knowledge, it is not clear which mechanism is more important. However, their combined effect is a reduced sediment flux into the bed and/or increased resuspension, leading to higher near-bed sediment concentrations which are more pronounced at high SSC environments, e.g. ETMs. The combined effect of these water-bed exchange processes is evaluated through scenarios in which the deposition efficiency is varied (using $\alpha = 1, 0.5, 0.3,$ and 0.1 representing no to strongly reduced deposition).

5

5.2.3. NET SEDIMENT FLUX

To explore the relative importance of various physical processes, the net sediment flux averaged over a tidal cycle at the specified stations can be quantified as follows ([Dyer, 1988, 1997](#)):

$$F = \frac{1}{T} \int_0^T \int_0^1 h u c z dz dt$$

$$= \underbrace{h_0 \bar{u}_0 \bar{c}_0}_{F1} + \underbrace{\bar{c}_0 \langle h_t \bar{u}_t \rangle}_{F2} + \underbrace{\bar{u}_0 \langle h_t \bar{c}_t \rangle}_{F3} + \underbrace{h_0 \langle \bar{u}_t \bar{c}_t \rangle}_{F4} + \underbrace{\langle h_t \bar{u}_t \bar{c}_t \rangle}_{F5} + \underbrace{h_0 \overline{u'_0 c'_0}}_{F6} + \underbrace{h_0 \langle u'_t c'_t \rangle}_{F7} \quad (5.4)$$

Where h is the water depth; z is relative depth, $0 \leq z \leq 1$; c is the SSC, u is the current velocity, T is the tidal period, the subscript 0 means tidally averaged, the subscript t denotes tidally fluctuating and the quotation marks denote a depth-depending term. Angled brackets ($\langle \rangle$) and overbars ($\bar{}$) signify the means over the tidal cycles and the depth, respectively.

Each decomposed term represents a particular contribution related to a certain physical process. The first term ($F1$) is the non-tidal drift, called the Eulerian flux whereas the second term ($F2$) is the flux induced by the Stokes' drift. The two terms ($F1 + F2$) represent the residual flow of water and the tidally and vertically averaged SSC to provide the advective sediment flux (the Lagrangian flux). The terms $F3$, $F4$ and $F5$ are produced by the tidal phase differences between the depth-averaged SSC, the depth-averaged velocity and the tidal elevation. Term $F6$ indicates the tidally averaged vertical circulation, which can be interpreted as density-driven estuarine circulation; Term $F7$ arises from the changing forms in the vertical distribution of velocity and SSC. Typically, the terms $F3$, $F4$ and $F5$ are tidal pumping terms ([Dyer, 1988](#)); however, term $F7$ is also regarded as tidal pumping in some studies ([Burchard et al., 2018](#); [Dijkstra et al., 2019a](#)). [Burchard](#)

et al. (2018) described tidal pumping as tidal covariance transport due to the correlation between SSC and current velocities, e.g., up-estuarine transport due to higher depth-mean SSC during flood than during ebb. Term $F7$ represents the combined vertical and temporal covariance transport which may result from internal asymmetries in mixing and settling velocity (Burchard et al., 2018). In this study, we adopt the tidal pumping terms as the sum of the terms $F3$, $F4$, $F5$ and $F7$ to clarify the mechanisms. The decomposition method has been applied widely to the study of sediment flux patterns (Uncles et al., 1985; Uncles and Stephens, 1993; Li and Zhang, 1998; Liu et al., 2011; Li et al., 2018b). By comparing the values of the decomposed terms, the relative importance of different processes can be accessed, which is helpful to understand the formation mechanism of ETM.

5.3. RESULTS

5.3.1. IMPACT OF SEDIMENT PROPERTIES

THE location and strength of the ETM are influenced by sediment properties, tidal asymmetry and sediment-induced effects. The effect of sediment properties is exemplified using an asymmetric tide with phase differences of 180° , including sediment-induced effects. These simulations reveal that the location of the ETM is mainly influenced by the settling velocity whereas the strength of the ETM (the SSC) is primarily regulated by the critical bed shear stress (Figure 5.3). Low critical shear stress for erosion results in higher resuspension rates, and therefore higher SSC in the ETM. Sediment with a large settling velocity (2 mm/s) is more efficiently transported up-estuary just landward of the tip of the salt wedge, whereas the ETM remains confined within the salt wedge for sediment with a small settling velocity (0.1 mm/s). The ETM of the Yangtze Estuary is located at the tip of the salt wedge (as for $\omega_s = 2$ mm/s) with a peak SSC of several kg/m^3 (as for $\tau_{cr} = 0.1$ Pa) (e.g. Liu et al., 2011; Lin et al., 2019). To reproduce the basic ETM dynamics in the Yangtze Estuary, we will therefore prescribe sediment with $\tau_{cr} = 0.1$ Pa and $\omega_s = 2$ mm/s for further analysis of sediment-induced density effects and tidal asymmetry.

5.3.2. LONGITUDINAL SSC DISTRIBUTION

Reduced deposition, in combination with sediment-induced density effects (SedDE), leads to a pronounced increase in SSC, especially in combination with tidal asymmetry (both types of asymmetry, see Figure 5.4). The effect of SedDE is limited without reduced deposition ($\alpha = 1$) but may lead to a 10-fold increase in near-bed SSC for conditions with a strongly reduced deposition ($\alpha = 0.1$). This is because reduced deposition increases vertical SSC gradients, which suppress turbulence mixing, leading to further settling of sediments. As these sediments only limitedly deposit on the bed because of reduced deposition, the near-bed SSC becomes very high. The SedDE without reduced deposition ($\alpha = 1$) also leads to an increase and decrease in SSC in the ETM for asymmetric tides with phase differences of 90° and 180° , respectively, suggesting different SedDE under different types of tidal asymmetry. The location of the ETM appears to migrate landward at decreasing α mostly pronounced for phase differences of 180° and seaward in absence of offshore tidal asymmetry - this will be explored in the next section.

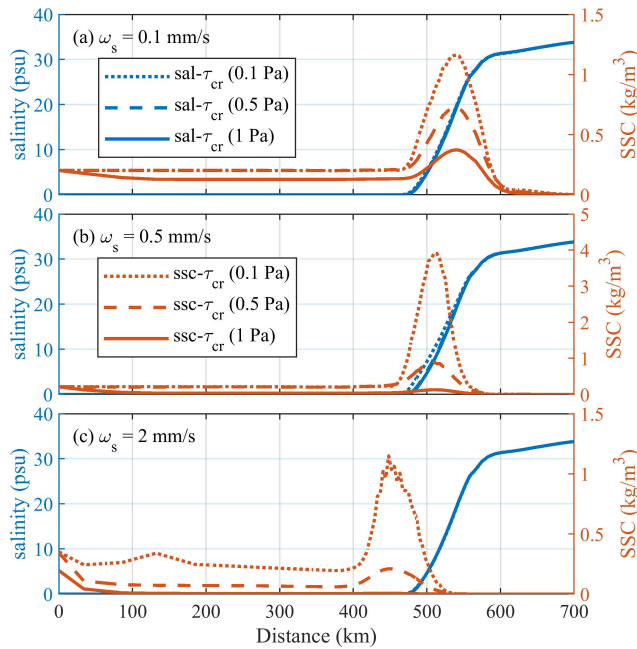


Figure 5.3: Modelled longitudinal distribution of mean near-bed suspended sediment concentration (SSC, red) and salinity (blue) over a spring-neap tidal cycle with settling velocity ω_s of (a) 0.1 mm/s; (b) 0.5 mm/s; (c) 2 mm/s and bed sediment with critical shear stress for erosion τ_{cr} of 0.1 Pa (dotted line), 0.5 Pa (dashed lined) and 1 Pa (solid line). The model is prescribed with water level phase differences of 180° with the sediment-induced density gradient.

5.3.3. ETM LOCATION

An important metric resulting from the model simulations is the longitudinal location of the ETM. Here we define the ETM position as the location where the 90th percentile of the longitudinal near-bed SSC is the highest (Figure 5.5). Without sediment effects (no SedDE and $\alpha = 1$), the most landward and seaward ETM positions occur ~ 2 days before spring and neap tides, respectively for all types of tidal asymmetry (Figure 5.5d-f). The time lags between the occurring time of maximum seaward (landward) location and neap (spring) tides may be ascribed to the spring-neap variations of the strength of flood-dominance. With the SedDE, the ETM location for asymmetric tides with phase differences of 90° moves ~ 20 km landward (Figure 5.5e). In contrast, the ETM migrates ~ 40 km landward when applying SedDE for phase differences of 180° and reaches its maximum seaward location near the neap tide (Figure 5.5f), implying that the effect of sediment-induced density gradient depends on the type of tidal asymmetry. With decreasing α , the ETM location for symmetric tides and for asymmetric tides with phase differences of 90° becomes less dependent on SedDE (Figure 5.5g, j, m and Figure 5.5h, k, n). Only for asymmetric tides with phase differences of 180° , both the ETM location and the spring-neap variability strongly differ for simulations with and without SedDE.

The combined impact of tidal asymmetry, SedDE and reduced deposition on ETM location becomes more clear when averaging over a spring-neap tidal cycle (Figure 5.6).

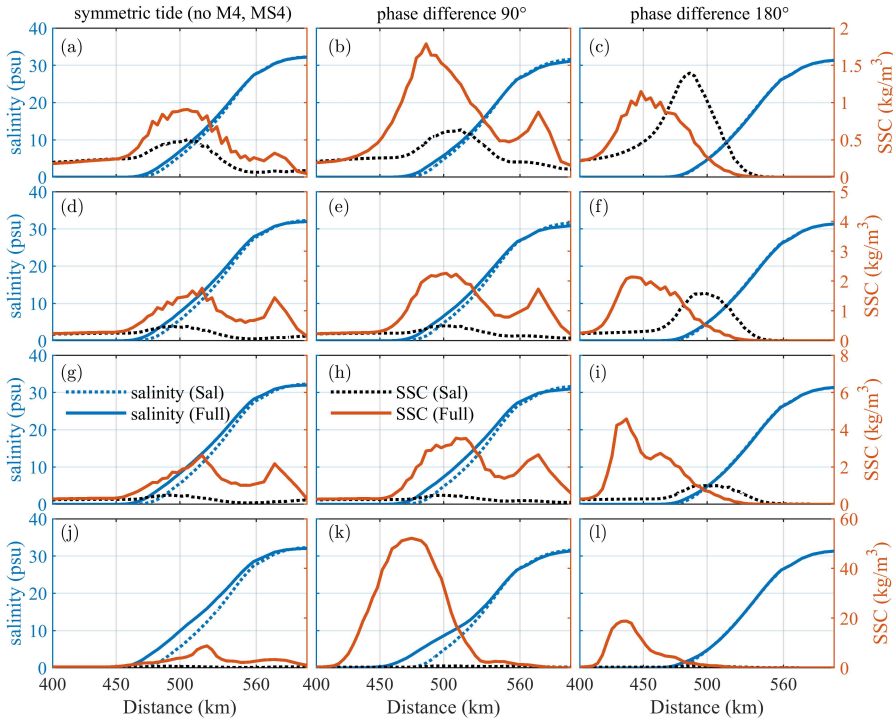


Figure 5.4: Comparison between the modelled longitudinal distribution of suspended sediment concentration (SSC) and salinity with (Full, solid line) and without (Sal, dashed line) sediment-induced density effect (SedDE) averaged over a spring-neap tidal cycle. Left, middle and right panels refer to scenarios with the symmetric tide (no M_4 and MS_4), asymmetric tide with water level phase differences of 90° and 180° , respectively. Top to bottom panels are scenarios with reduced deposition factor of 1 (a-c), 0.5 (d-f), 0.3 (g-i), and 0.1 (j-l). Note that the horizontal axes have different scales as in Figure 5.3.

For symmetric tides without the SedDE, reduced deposition leads to landward movement of the ETM. However, accounting for the SedDE, reduced deposition leads to ~ 20 km seaward movement. For asymmetric tides, the SedDE mainly leads to a landward migration of the ETM (with the largest landward migration of ~ 35 km for phase differences of 180° when $\alpha = 1$). This landward migration is also strengthened by reduced deposition, particularly under the strongest reduced deposition ($\alpha = 0.1$) with a distance of ~ 15 km.

5.4. DISCUSSION

5.4.1. EFFECT OF TIDAL ASYMMETRY

TO analyse and explain the computed ETM dynamics, the residual sediment transport is decomposed into the contribution of advection, tidal pumping, and estuarine circulation (following the procedure described in section 5.2.3). In shallow areas, both with and without the SedDE, seaward advective transport is balanced by landward tidal

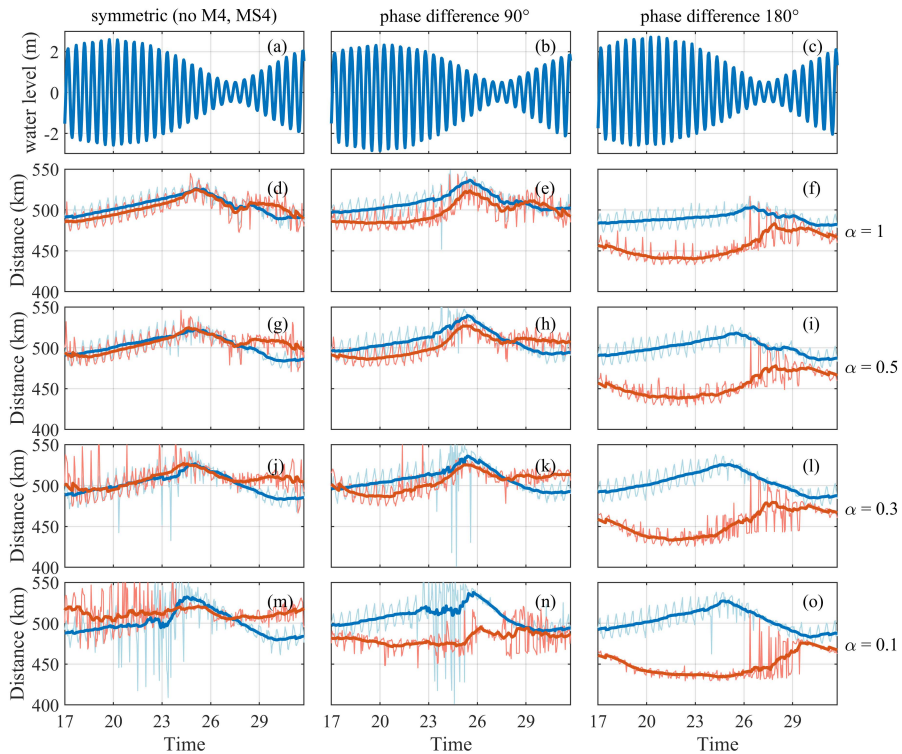


Figure 5.5: Comparison between modelled instantaneous (light colour, with dark colour daily averaged) locations of the ETM with (red) and without (blue) sediment-induced density effect (SedDE) over a spring-neap tidal cycle (a-c). Left, middle and right panels refer to scenarios with the symmetric tide (no M_4 and MS_4), asymmetric tide with phase differences of 90° and 180° , respectively. Top to bottom panels are scenarios with reduced deposition factor of 1 (d-f), 0.5 (g-i), 0.3 (j-l), and 0.1 (m-o).

pumping whereas estuarine circulation is less important (Figure 5.7). In addition, the residual sediment flux in shallow areas is an order of magnitude smaller than that in the deep channel, suggesting that sediment transport mainly takes place in the deep channel. The weak residual sediment flux and the strong influence of tidal pumping in the shallow areas are consistent with earlier observations by Sommerfield and Wong (2011). Therefore, unless explicitly mentioned otherwise, in the following section we elaborate on the effects of tidal asymmetry, SedDE and reduced deposition in the deep channel.

Without the SedDE, estuarine circulation leads to landward sediment transport in the channel (Figure 5.7a), typical for an estuary with a pronounced longitudinal salinity gradient and vertical concentration gradient. The contribution of the tidal pumping term varies with the type of tidal asymmetry, i.e., symmetric tide and asymmetry tide with phase differences of 90° lead to seaward sediment transport but asymmetric tides with phase differences of 180° lead to landward sediment transport. The internally generated tidal asymmetry for the offshore symmetric tide is flood dominant ($\theta_u = 20^\circ$) but very weak (see Figure 5.2) and therefore not able to transport sediment landward. Sim-

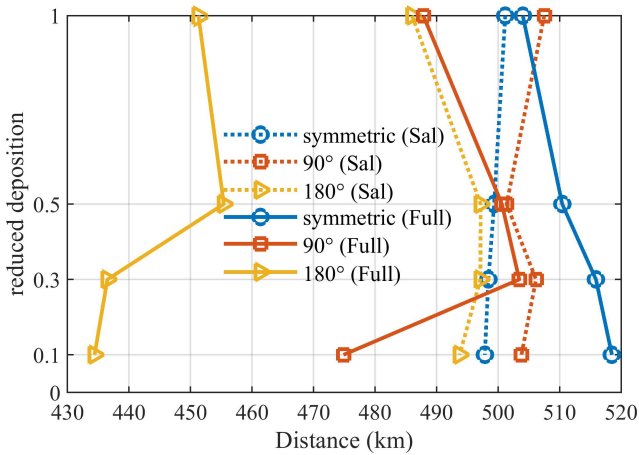


Figure 5.6: Modelled location of the ETM averaged during a spring-neap tidal cycle (see Figure 5.4) influenced by the reduced deposition with the symmetric tide (no M_4 and MS_4) and asymmetric tide with phase differences of 90° and 180° , and with (Full, solid line) / without (Sal, dashed line) sediment-induced density effect (SedDE).

ulations with phase differences of 90° are flood dominant in terms of peak flow velocity, but slightly ebb-asymmetric in terms of slack tide asymmetry. Apparently, the slack tide asymmetry contributes more to residual transport than the peak flow asymmetry.

Whether slack tide asymmetry or peak flow asymmetry contributes more to transport depends on the type of transported sediment. Rapidly settling sediment with a large critical shear stress for erosion (sand), especially when available in great quantities, is very susceptible to peak flow asymmetry. However, sediment transported in our Yangtze river prototype is more susceptible to slack tide asymmetry. We prescribe sediments with a low critical shear stress for erosion, and with $\omega_s = 2$ mm/s (typically for a grain size of $50 \mu\text{m}$, corresponding to 7.2 m/hour). This means that for a short slack tidal period (~ 0.5 hrs) only a small amount of sediment settles, whereas the majority of sediment settles for a long slack tidal period (~ 1.5 hrs). The conditions in the deep channel therefore favour a seaward and landward sediment transport for the asymmetric tides with phase differences of 90° (little LW slack tide dominant) and 180° (little HW slack tide dominant), respectively.

The largest impact of adding sediment-induced effects (Figure 5.7b) is a much stronger contribution of estuarine circulation to landward sediment transport. Also, the asymmetric tides with 90° phase differences now lead to up-estuary transport. The mechanism responsible for these patterns will be evaluated in more detail hereafter.

5.4.2. EFFECT OF SEDIMENT: SEDIMENT-INDUCED DENSITY EFFECTS

Horizontal SedDE leads to dispersion of the ETM whereas vertical SedDE promotes ETM formation (Zhu et al., 2021). In this study, we further elaborate on density effects through its interaction with tidal asymmetry. Without density gradients (Barot scenario), sediment converges at the mouth (km-540) for asymmetric tides with phase differences

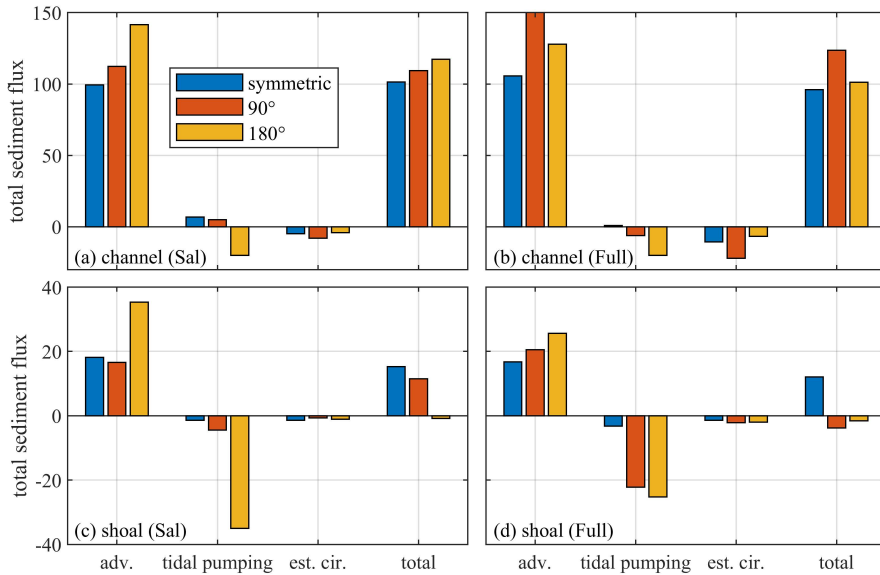


Figure 5.7: Total decomposed residual sediment flux (kg/m/s) along the estuary in the scenarios without reduced deposition ($\alpha = 1$) in the (a, b) deep channel and (c, d) shallow shoals (a, c) without (Sal) and (b, d) with (Full) the sediment-induced density effect (SedDE) induced by advective transport, tidal pumping, estuarine circulation and the total contribution. Positive values indicate the ebb direction and negative values indicate the flood direction.

of 180° probably because of the stronger tidal asymmetry at the mouth (peak flow asymmetry in combination with HW slack tide asymmetry) compared to the other two types. In this scenario, the convergence of sediment is mainly due to the landward sediment transport by tidal pumping (Figure 5.8). The individual SedDE (Sed scenario) leads to dispersion of the barotropic ETM for asymmetric tides with phase differences of 180° whereas sediments are transported to seaward of km-560 in the other two. With salinity-induced density gradients (Sal scenario), an ETM is formed landward of km-560 due to the tidal processes in transporting sediments upstream for all types of tidal asymmetry. The combined effect of salinity and sediment-induced density effects (Full scenario) lead to a more pronounced ETM (50% higher SSC for symmetric tides and asymmetric tides with phase differences of 90° – see Figure 5.8a, b) or landward shift (asymmetric tides with phase differences of 180° , see Figure 5.8c).

Including the SedDE, both the effects of tidal pumping and estuarine circulation on landward sediment transport are enhanced for asymmetric tides with phase differences of 90° (Figure 5.8h and k), which primarily result in the strengthening of the ETM. For asymmetric tides with phase differences of 180° , the effect of tidal pumping is reduced whereas that of estuarine circulation is slightly increased (Figure 5.8i and l), leading to a dispersion of ETM. This suggests that the peak flow asymmetry in combination with HW slack tide asymmetry leads to the most pronounced ETM mainly for conditions without the SedDE (see also section 5.4.1). In addition, with the SedDE, the ETM promotion and dispersion mainly result from the enhanced and weakened tidal pumping, respec-

tively (Figure 5.7 and Figure 5.8), which depends on the types of tidal asymmetry. It also implies that the vertical SedDE on ETM promotion and horizontal SedDE on ETM dispersion are associated with the types of tidal asymmetry, i.e. pronounced for asymmetric tides with phase differences of 90° and 180° , respectively.

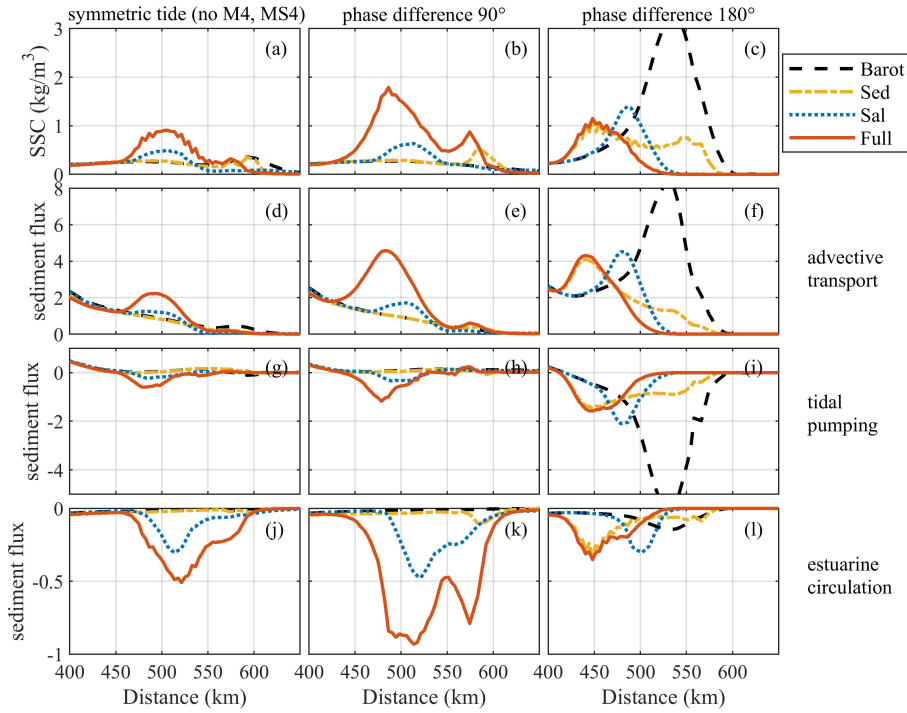


Figure 5.8: Modelled longitudinal distribution of (a, b, c) suspended sediment concentration (SSC) and decomposed residual sediment flux (kg/m/s) for cases without both salinity- and sediment-induced density effect (Barot), with only sediment-induced density effect (SedDE) (Sed), with only salinity-induced density effect (Sal) and with both (Full). The residual sediment flux is decomposed into (d, e, f) advective transport, (g, h, i) tidal pumping, and (j, k, l) estuarine circulation. Left, middle and right panels refer to scenarios with the symmetric tide (no M_4 and MS_4), asymmetric tide with water level phase differences of 90° and 180° , respectively. Positive values indicate the ebb direction and negative values indicate the flood direction. The reduced deposition in these scenarios is not considered.

5.4.3. EFFECT OF SEDIMENT: WATER-BED EXCHANGE

Water-bed exchange processes regarding deposition and higher suspension lead to higher near-bed SSC, which to a large extent increases the contribution of SedDE (see the ETM formation and migration in Figure 5.4 and Figure 5.6). For symmetric tides, the contribution of advective term migrates seaward (Figure 5.9), controlling the seaward shift of ETM (Figure 5.6) whereas landward sediment transport driven by tidal pumping and estuarine circulation becomes important for asymmetry tides. For asymmetric tides, the most important impact of the higher near-bed SSC due to water-bed exchange processes is (1) strengthening and upstream migration of the ETM, and (2) a

progressively larger contribution of the landward transport component driven by estuarine circulation (Figure 5.9). The large contribution of estuarine circulation is the result of high near-bed concentrations, which are most sensitive to the landward current near the bed generated by the longitudinal salinity gradients. It also reflects the positive feedback between sediment and salinity as identified in [Zhu et al. \(2021\)](#): the higher near-bed SSC and SedDE increase the vertical SSC gradient which influences the velocity and salinity distribution and leads to stronger salt intrusion, which further promotes sediment trapping. Therefore, estuarine circulation becomes progressively more important for ETM dynamics with higher near-bed SSC. Particularly for asymmetric tide with phase differences of 180° , when $\alpha > 0.5$, the contribution of tidal pumping to up-estuary transport exceeds that of estuarine circulation, whereas the contribution of estuarine circulation is greater than that of tidal pumping $\alpha < 0.5$ (Figure 5.10).

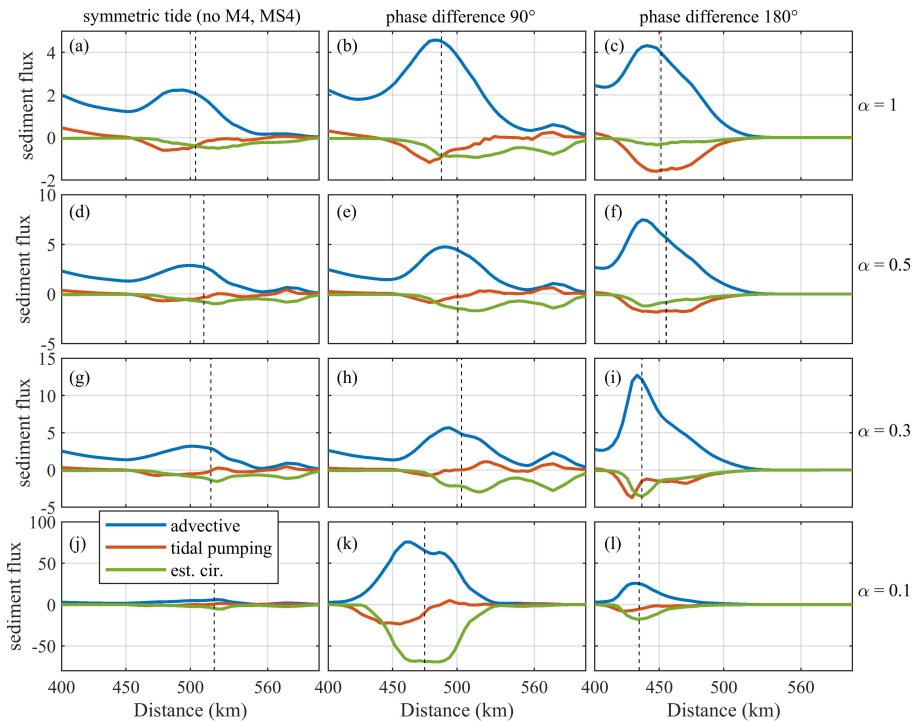


Figure 5.9: Decomposed residual sediment flux ($\text{kg}/\text{m}/\text{s}$) in scenarios with the sediment-induced density effect (SedDE) induced by advective transport, tidal pumping and estuarine circulation. Left, middle and right panels refer to scenarios with the symmetric tide (no M_4 and MS_4), asymmetric tide with water level phase differences of 90° and 180° , respectively. Top to bottom panels are scenarios with reduced deposition factor of 1, 0.5, 0.3, and 0.1, respectively. The vertical dashed lines indicate the location of the ETM (see Figure 5.4). Positive values indicate the ebb direction and negative values indicate the flood direction. The relative contribution of the four mechanisms in panel j are not visible to keep scaling consistent with panels k and l, but the longitudinal patterns are comparable with panels k and l.

Interestingly, with the increased contribution of estuarine circulation dominating the up-estuary sediment transport (for all types of tidal asymmetry), tidal pumping may re-

sult in lateral spreading near the concentration peaks in the ETM (evident as a transport flux changing direction in the along-estuary direction, Figure 5.9). Correspondingly, a weakened contribution of tidal pumping could be identified with reduced deposition (Figure 5.10). Moreover, the contributions of advection and estuarine circulation with the highest near-bed SSC ($\alpha = 0.1$, near-bed SSC of $\sim 50 \text{ kg/m}^3$ in Figure 5.4k) for asymmetric tide with phase differences of 90° are quite large probably because fluid mud is formed in which non-Newtonian behaviour may play a role.

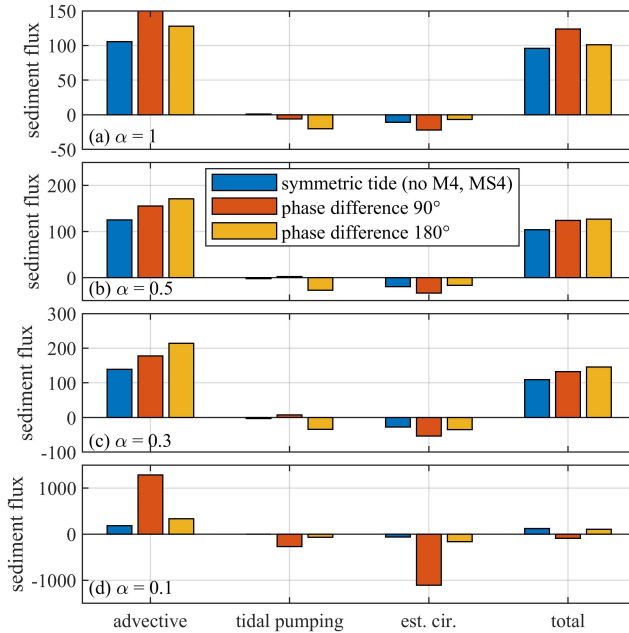


Figure 5.10: Total decomposed residual sediment flux (kg/m/s) along the estuary in scenarios with the sediment-induced density effect (SedDE) induced by advective transport, tidal pumping and estuarine circulation with reduced deposition factor (a) $\alpha = 1$; (b) $\alpha = 0.5$; (c) $\alpha = 0.3$ and (d) $\alpha = 0.1$. Positive values indicate the ebb direction and negative values indicate the flood direction.

5.4.4. A SYNTHESIS

ETMs are the result of various trapping mechanisms working simultaneously as introduced earlier. To clarify the relative roles of mechanisms more clearly, we group them into three main mechanisms summarized and modified from [Dijkstra \(2019\)](#): estuarine circulation, tidal pumping and other processes (Table 5.1). Estuarine circulation refers to classical processes due to different effects of salinity with ETMs firstly found near the limit of the salt intrusion. Tidal pumping is a more general term that includes multiple mechanisms associated with the interaction between current and sediments. Interestingly, the above-mentioned sediment-induced effects (SedDE and water-bed exchange processes) is important for understanding the relative roles of estuarine circulation and tidal pumping (especially with estuarine circulation becoming more important

at stronger SedDE) and is therefore elaborated in more detail below.

The location of ETM influenced by estuarine circulation is constrained by the salt limit; however, tidal pumping may lead to more variable changes in the location. Our results suggest that the variability in the location also depends on sediment concentration effects, either resulting from the SedDE or higher near-bed SSC due to water-bed exchange processes. The SedDE and higher near-bed SSC lead to landward movement of the ETM, especially for asymmetric tide with phase differences of 180° (Figure 5.8). The increase of SSC within the ETM as a result of sediment-related transport processes introduce positive feedback mechanisms which may lead to a progressive increase in SSC and tidal amplification over time. As such positive feedback mechanisms including SSC take time (Winterwerp and Wang, 2013; Wang et al., 2015), the ETM movement induced by the SedDE and tidal asymmetries may lead to different locations of ETM with regards to the salt intrusion (Figure 5.4).

The role of sediment-induced density effects on ETM dynamics through horizontal density-driven currents was first explored by Talke et al. (2009b); the role of sediment-induced density effects on both horizontal flows and vertical mixing was elaborated in greater detail by Zhu et al. (2021). In this study, we further extend their analysis by also including near-bed sediment effects (reduced deposition) and systematically explore the role of hydrodynamic asymmetries. These results can subsequently be used to interpret earlier observations. For instance, in the Ems estuary, the ETM was observed to migrate in the landward direction, into the freshwater zone (Talke et al., 2009b). The water level phase difference is 170° at the mouth in the upper Ems estuary, suggesting mainly HW slack tide dominance (Chernetsky et al., 2010; van Maren et al., 2015b); an asymmetry where stronger sediment-induced effects lead to a landward migration of the ETM (Figure 5.4). In the Yangtze Estuary, the water level phase difference at the mouth is 80° (Guo et al., 2015; Lu et al., 2015). Our results suggest that for such an asymmetry, sediment-induced effects lead to an increasing SSC within the ETM, rather than an upstream migration in the ETM (Figure 5.4). This may be the reason that siltation rates in the Yangtze Estuary navigation channel are so strong, and the ETM remains stationary (Liu et al., 2011; Jiang et al., 2013a).

The predominance of estuarine circulation or tidal pumping as the main up-estuary transport component is often considered to be related to the magnitude of the tidal range compared to the freshwater flow (Dyer, 1986). In some estuaries with a high tidal range, tidal pumping is widely accepted to dominate sediment trapping, such as in the Gironde Estuary (Allen et al., 1980), Seine Estuary (Brenon and Le Hir, 1999; Le Hir et al., 2001; Grasso et al., 2018), and Hudson River Estuary (Geyer et al., 2001). However, for some estuaries, the dominant trapping mechanisms remain under discussion with both estuarine circulation and tidal pumping identified as the main up-estuary transport component. A typical example of such a system is the upper Chesapeake Bay. Based on field observations, estuarine circulation was first identified as the dominant mechanism favouring landward sediment transport (Schubel, 1968), Sanford et al. (2001) later concluded tidal pumping to be dominant. Observational data in the Yangtze Estuary alternately suggest tidal pumping (Li and Zhang, 1998; Wu et al., 2012; Song et al., 2013) or estuarine circulation (Liu et al., 2011; Jiang et al., 2013a; Pu et al., 2015; Li et al., 2016b, 2018b) be the dominant transport mechanisms. These inconsistent findings from mea-

measurements may be caused by different methods, spatial and temporal scales.

Table 5.1: Classification of the main mechanisms summarized and modified from [Dijkstra \(2019\)](#).

Main mechanisms	Names or processes	References
Estuarine circulation	gravitational circulation	Festa and Hansen, 1978
	turbulence damping by salinity gradients	Geyer, 1993
	strain-induced stratification or SIPS	Simpson et al., 1990 ; Burchard and Baumert, 1998 ; Scully and Friedrichs, 2003
Tidal pumping	tidal asymmetry	Friedrichs, 2011
	flocculation	Winterwerp, 2011
	mixing asymmetry/ internal tidal asymmetry	Jay and Musiak, 1994, 1996
	mud-induced periodic stratification or MIPS	Becker et al., 2018
	scour lag	Dyer, 1997
	spatial settling lag	Postma, 1954 ; Van Straaten and Kuenen, 1957
	temporal settling lag	Groen, 1967
Other processes	wind-induced tidal straining	Scully et al., 2005 ; Burchard and Hetland, 2010
	along-channel non-linear advective processes	Li and O' Donnell, 2005
	flow generated by channel curvature	Chant and Stoner, 2001 ; Chant, 2002
	flow generated by Earth's rotation	Huijts et al., 2006 Winterwerp, 1999 ;
	sediment-induced density effect	Talke et al., 2009b ; Zhu et al., 2021
	eddy viscosity-shear covariance (ESCO) circulation	Burchard et al., 2013 ; Dijkstra et al., 2017
	along-channel differences in sediment properties (e.g., settling velocity)	Donker and de Swart, 2013

Numerical models additionally suggest the different dominant roles of estuarine circulation and tidal pumping in the Chesapeake Bay under different river flow conditions ([Park et al., 2008](#)) and the Yangtze Estuary under different tidal conditions ([Song and Wang, 2013](#); [Wan and Wang, 2017](#)). However, numerical models introduce additional uncertainties influencing the dominant transport term, such as the role of sediments (through water-bed exchange processes and density effects), input parameters (such as the critical shear stress for erosion and settling velocity, influencing the relative role of

tidal pumping and estuarine circulation) and vertical discretisation (a high vertical resolution will lead to larger vertical gradients, and hence the effect of sediments; van Maren et al., 2020). Our results suggest that water-bed exchange processes influence the relative contribution of estuarine circulation and tidal pumping on ETM formation, which is important in interpreting the numerical results. Such an effect has also been identified by Yu et al. (2014) who observed that ETM formation mechanisms may be erroneously interpreted if the effects of advection induced by the horizontal SSC gradient and fine bed sediment supply are ignored.

Despite its geometric simplicity, our model provides a useful instrument to analyse ETM formation processes in response to tidal asymmetries in combination with sediment-induced effects (related to the turbulent mixing, horizontal density gradients, and near-bed effects). Especially the applied formulations for the near-bed exchange processes are strongly simplified and need to be further investigated as part of future research. Nevertheless, our results do reveal that the uncertainties in the near-bed exchange process have a major impact on ETM dynamics.

5

5.5. CONCLUSIONS

USING a schematized model reflecting the dynamics of the Yangtze Estuary, we explored the roles of tidal asymmetries, sediment properties (critical shear stress and settling velocity), sediment-induced density effects and high near-bed SSC due to water-bed exchange processes on ETM dynamics. The critical shear stress for erosion mainly influences the magnitude of the maximum SSC of the ETM, whereas the settling velocity influences the location of the ETM. Without sediment-induced density effects, estuarine circulation leads to an up-estuary sediment transport for all types of tidal asymmetry whereas the net landward sediment transport due to tidal pumping is controlled by the strength of flood tidal dominance. With sediment-induced density effects, tidal asymmetry leads to a progressively larger contribution of estuarine circulation. Sediment-induced density effects also lead to pronounced high SSC and landward migration mainly due to the contribution of enhanced and weakened tidal pumping, respectively, which depends on the type of tidal asymmetry. Higher near-bed SSC due to water-bed exchange processes additionally increases the sediment-induced density gradients due to the enhanced vertical SSC gradients and strongly influences the relative contribution of tidal pumping and estuarine circulation. Higher near-bed SSC increases the effect of estuarine circulation on landward sediment transport and the tidal pumping term could even become a diffusive term leading to a longitudinal divergence of sediment. The enhanced estuarine circulation is closely related to the positive feedback between sediments and salinity. Our study therefore suggests that sediment-induced effects (density effects and water-bed exchange processes) interacting with tidal asymmetries strongly influence ETM dynamics, which is essential for understanding and interpreting ETM formation mechanisms in future studies.

6

FUTURE CHANGES IN SALTWATER INTRUSION IN THE YANGTZE ESTUARY: THE IMPORTANCE OF SEDIMENT DYNAMICS

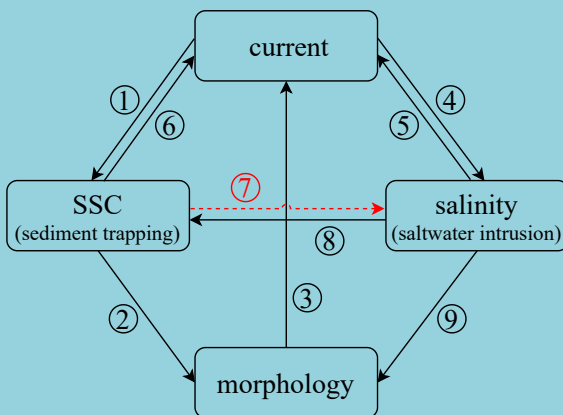
Do it all at once, second time tired, third time exhausted.

一鼓作气 再而衰 三而竭

Zuo Qiuming (Confucian, 556 B.C.-451 B.C.)

In *Cao Gui debate*

Cao Gui (Military theorist)



This chapter focuses on the content in red.

Saltwater intrusion in estuaries threatens freshwater supply in coastal regions. In highly-turbid estuaries, saltwater intrusion is not only controlled by the primary river and tidal forcing conditions but probably also by sediment dynamic owing to the interaction and feedback mechanisms between hydro- and sediment dynamics, which is, however, insufficiently understood. In this work, we explore the variations of saltwater intrusion in the Yangtze Estuary in response to changes in river discharge (and the associated change in riverine sediment supply) and sea-level rise (SLR) utilizing a well-calibrated hydrodynamics and sediment transport model. We found that the changes in river discharge and SLR affect sediment trapping efficiency and location, influencing saltwater intrusion. Higher sediment trapping efficiency leads to larger effects of sediment, which enhances salinity-induced stratification and saltwater intrusion. Model results suggest that the period of possible freshwater intake for the Qingcaosha reservoir is shortened due to the effect of sediments. The decrease is days if sediment concentration is low ($\sim 2 \text{ kg/m}^3$) and months if sediment concentration is high ($>10\text{-}30 \text{ kg/m}^3$). A 70% decline of sediment input leads to a seaward shift of saltwater intrusion of $\sim 3 \text{ km}$ and an extension of possible freshwater intake at Qingcaosha Reservoir for over 2 months. This work highlights the importance of considering sediment transport dynamics in predicting saltwater intrusion under changing river and oceanic forcing and has broad implications for freshwater resources management in estuaries.



6.1. INTRODUCTION

Saltwater intrusion is influenced by tidal forcing and river flow and strongly dependent on geometry and bathymetry. The degree of saltwater intrusion directly influences estuarine ecology (Watanabe et al., 2014) and freshwater supply to densely populated deltas, but also indirectly through its impact on sediment dynamics (Wolanski et al., 1996; Wan and Zhao, 2017; van Maanen and Sottolichio, 2018). Sediment dynamics additionally influence the ecological state of the estuary through its impact on the light climate (Talke et al., 2009a), but also drives siltation in tidal channels, often resulting in dredging requirements in urbanized delta systems (Hossain et al., 2004; Jeuken and Wang, 2010; van Maren et al., 2015a; Wu et al., 2016).

Saltwater intrusion is mainly controlled by river discharge, tide, wind, sea-level rise (SLR), and morphological changes. A high river discharge results in a reduced saltwater intrusion. The relationship between saltwater intrusion length and river discharge follows a power law with an exponent coefficient varying in different estuaries (Monismith et al., 2002; Banas et al., 2004). The effect of tides on saltwater intrusion is closely related to the degree of tidal mixing. For a well-mixed or salt wedge estuary, salt intrudes more landward during spring tides than during neap tides (Uncles and Stephens, 1996; Brockway et al., 2006; Xue et al., 2009; Ralston et al., 2010), whereas in partially mixed estuaries, the upstream salt flux is largest during neap tides (Monismith et al., 2002; Banas et al., 2004; Ralston et al., 2008; Lerczak et al., 2009). SLR increases water depth and benefits inland tidal propagation, which may strengthen estuarine circulation (Chua and Xu, 2014) and enhance saltwater intrusion (Rice et al., 2012; Prandle and Lane, 2015; Robins et al., 2016). Persistent northerly wind may enhance saltwater intrusion in the Yangtze Estuary by landward Ekman currents (Xue et al., 2009; Wu et al., 2010; Li et al., 2020b). Strong wind events may also induce water level setup, an increase in flood current velocity, and a decrease in ebb-directed current velocity and freshwater inflow, enhancing saltwater intrusion (Zhang et al., 2019). Moreover, various human interventions have influenced the degree of saltwater intrusion, especially morphological changes resulting from channel deepening (Wu et al., 2016) or modifications in river discharge (Gong and Shen, 2011) or bed load transport (Eslami et al., 2019). In the future, such anthropogenic influences will become more pronounced as a result of climatic change-induced shifts in precipitation patterns and SLR (Rice et al., 2012; Chen et al., 2016a; van Maanen and Sottolichio, 2018; Talke and Jay, 2020), river discharge changes (Alferi et al., 2015; Robins et al., 2016; Talke and Jay, 2020) and tidal channel deepening (Wu et al., 2016; van Maren et al., 2015b).

Sediment transport dynamics are controlled by hydrodynamics and sediment dynamics may also exert feedback to the hydrodynamics, thus probably affecting saltwater intrusion, particularly in highly turbid estuaries. High sediment concentrations would suppress turbulence mixing, reduce hydraulic drag and then affect tidal propagation. Many estuaries have regions of elevated suspended sediment concentrations (a so-called Estuarine Turbidity Maximum or ETM) resulting from converging sediment transport (Dyer, 1997). The residual sediment transport is strongly influenced by the salinity-induced density gradient (Festa and Hansen, 1978) and tidally varying stratification (Simpson et al., 1990). Therefore, ETMs are often located at the landward limit of saltwater intrusion. In turn, sediments also influence saltwater intrusion due to feed-

back between suspended sediment concentration (SSC), velocity, water level, salinity, and tidal amplification (Zhu et al., 2021) with higher SSC leading to stronger saltwater intrusion. Many rivers have experienced a decline in their sediment load resulting from the construction of upstream reservoirs (Syvitski et al., 2009; Dunn et al., 2019; Besset et al., 2019; Li et al., 2020a), which probably causes a reduction in sediment concentration in estuaries, and then influence saltwater intrusion. However, the role of sediment dynamics on salinity intrusion has so far remained unexplored.

The Yangtze Estuary is a strongly engineered system with altered river flow, sediment loads, and local geometry. Saltwater intrusion in the Yangtze Estuary has been modelled both analytically (Zhang et al., 2011; Cai et al., 2015; Zhang et al., 2019) and numerically (Xue et al., 2009; Wu et al., 2010; Chen et al., 2016a; Zhu et al., 2018). Moreover, saltwater intrusion in the Yangtze Estuary has been studied for natural effects and climate change, i.e., the effect of wind (Xue et al., 2009; Wu et al., 2010; Zhu et al., 2018; Zhang et al., 2019; Li et al., 2020b) and SLR (Chen et al., 2016a) as well as human interventions, i.e., Three Gorges Dam (TGD), Deep Channel Navigation Project (DCNP) and Water Diversion Project (WDP), see Zhu et al. (2018). However, the contribution of sediment dynamics on the impact of such interventions on saltwater intrusion has not yet been investigated. This study aims to numerically explore the effect of the changes in river discharge and sediment supply as well as SLR on altering the sediment dynamics and saltwater intrusion in the Yangtze Estuary.

6.2. STUDY AREA

THE Yangtze Estuary is a 650 km long estuary conveying large river discharge and sediment load supplied by the Yangtze River. The river discharge and sediment transport of the Yangtze River are highly variable, with river discharge ranging from 8300 to over 90000 m³/s and SSC ranging from 0.01 to >3 kg/m³. In the Yangtze River basin, two large projects regulate the river discharge and sediment load into the estuary: the TGD and WDP (Figure 6.1a). The TGD was constructed between 1993 and 2009 and put into operation in 2003 to store and flush water seasonally (Guo et al., 2018a). Apart from the TGD, thousands of hydropower dams were built in the Yangtze River basin, altering the river flow regime and decreasing sediment supply. Specifically, the high river discharge in the wet season decreases profoundly by ~30% while the low river discharge in the dry season slightly increases by ~10% due to the regulation whereas the sediment discharge is reduced by 70% (Guo et al., 2018a). The ongoing South-to-North WDP is a strategic project to mitigate water shortage in northern China. It includes three water transfer plans: the western, middle, and eastern route project. Since 2014, the WDP annually withdraws 18.3 billion m³ of surface water from the Yangtze River basin, but when completed the total diversion capacity will be 44.8 billion m³ per year (approximately 5% of the annual mean Yangtze river discharge) (Guo et al., 2018a). Moreover, extremely high flood occurred in 1954 (92,600 m³/s), 1998 (82,300 m³/s) and 2020 (84,500 m³/s), over ~30% higher than the peak high river discharge in normal years. Relatively low river discharges are approximately 6,500-10,000 m³/s, e.g., in 1972 (7,060 m³/s), 1979 (6,470 m³/s), and 2006 (9,660 m³/s), 10%~40% lower than the average low river discharge.

The Yangtze Estuary has three orders of bifurcation and four outlets into the sea. Approximately 5% of river discharge is flushed through the North Branch and the other

major portion of river flow is discharged in the South Branch and the seaward channels (Figure 6.1b). The Yangtze River supplies freshwater to Shanghai through three reservoirs, i.e., Dongfengxisha Reservoir, Chenhang Reservoir, and Qingcaosha Reservoir. The Qingcaosha Reservoir was built in 2010 along northwestern Changxing Island (Figure 6.1c), which is the largest one supplying more than 70% of the freshwater for the 13 million inhabitants of Shanghai. The salinity in the Yangtze Estuary near the intake of Qingcaosha Reservoir is therefore crucial for freshwater availability and used in this study as a metric to evaluate the impact of sediment dynamics on saltwater intrusion. Saltwater intrusion in the North Channel can affect water intake of the Qingcaosha Reservoir from the seaside, while salt spillover in the North Branch adds additional influence from the landward side (Chen et al., 2016a; Zhu et al., 2018).

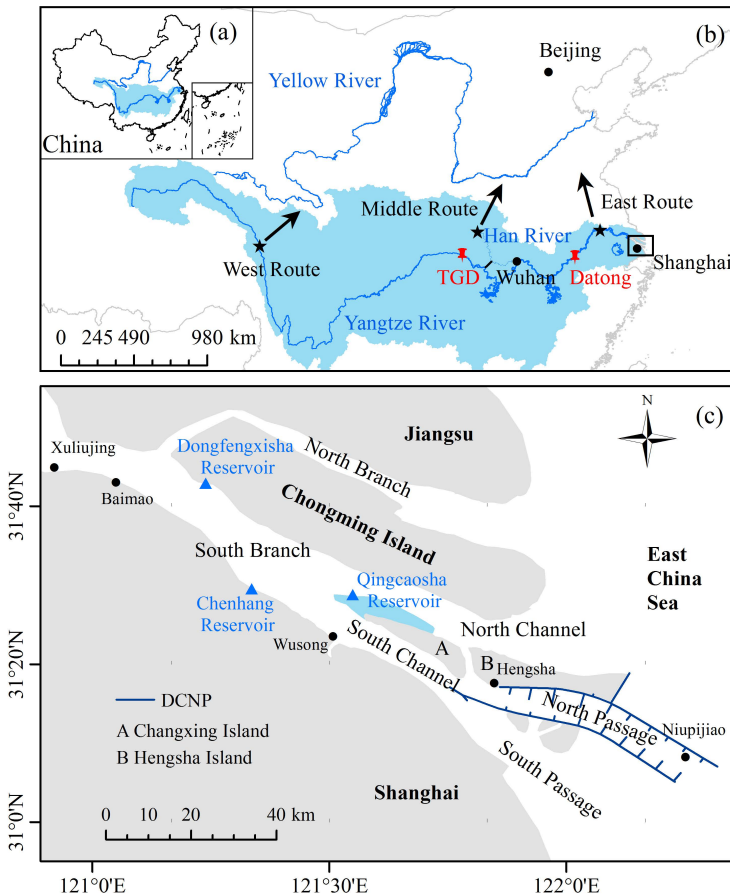


Figure 6.1: Map of (a) China, (b) South to North Water Diversion Project (WDP) and the Three Gorges Dam (TGD) in the Yangtze River basin (shade in blue), and (c) location of the freshwater reservoirs and saltwater intrusion paths in the Yangtze Estuary. DCNP: Deep Channel Navigation Project.

6.3. METHODS

SALTWATER intrusion is typically predicted using analytical and numerical models. Analytical models have been used to predict saltwater intrusion length and longitudinal salinity distribution in estuaries. Such analytical models are sufficient for simplified estuaries with prismatic and convergent channels (Prandle, 2004; Savenije, 2006) and can also account for tidal mixing under river and tidal forcing (Nguyen et al., 2012; Cai et al., 2015). More in-depth understanding of the mechanisms underlying saltwater intrusion in realistic geometries is obtained from three-dimensional (3D) numerical models (Jeong et al., 2010; Ralston et al., 2010; Gong and Shen, 2011; Cheng et al., 2012; Wang et al., 2019a). In this study, we use a well-calibrated 3D numerical model accounting for sediment-induced effects in a turbid system, the Yangtze Estuary.

The 3D sediment transport model is set up using the Delft3D model system (Lesser et al., 2004). The model application consists of hydrodynamic and sediment transport modules (see Figure 4.2, Zhu et al., 2021). The hydrodynamics are computed for one full year (2007) with a realistic river discharge hydrograph and tidal forcing to capture the convergence of sediment. The sediment transport module is supply-limited, with an ETM arising from sediment supplied from the model boundaries rather than initial bed conditions (see van Maren et al., 2011; Brouwer et al., 2018; Dijkstra et al., 2018; Hesse et al., 2019; van Maren et al., 2020). This approach allows the establishment of equilibrium sediment response to subtle variations in hydrodynamic conditions (in contrast with an alluvial bed approach, where the amount and location of bed sediment dominated ETM dynamics and location). The model keeps track of erosion and deposition rates through sediment availability, but to focus on the impact of hydrodynamic processes on residual transport the model is run in morphostatic mode. The sediment concentration contributes to the water density through the equation of state, thereby generating sediment-induced density effects (SedDE). The main SedDE results from horizontal density gradients (leading to a gravitational circulation comparable to that of salt) and suppression of turbulence mixing by vertical concentration gradients (see Zhu et al., 2021 for details). The SedDE can be optionally switched off, as will be done to understand the effect of sediments.

To eliminate the impact of the variability in river and sediment discharges, we impose simplified river discharge and sediment hydrographs, based on typical river discharge and sediment load observations (Figure 6.2). We assume that 1) there is only one significant flood peak each year and the hydrograph is symmetric and 2) there is a linear relationship between the river discharge and SSC and therefore the seasonal variation of the SSC is the same to that of the river discharge. We simplify two hydrographs with the same annual fluxes (878 billion m^3 of total river discharge) representing the pre-TGD ('QA') and post-TGD situations ('QB'). The post-TGD ('QB') accounts for the effect of dam constructions on reducing the seasonal variability of the river discharge compared to the pre-TGD ('QA'). i.e., the peak high river discharge is reduced by 30%, and the peak low river discharge is increased by 10%. Two types of hydrographs for sediment with the annual sediment loads of 486 Mt yr^{-1} and 146 Mt yr^{-1} (70% reduction) respectively represent the sediment supply in the pre-TGD ('SA') and post-TGD ('SB') periods.

To explore the effect of changes in river discharge, SLR, and sediment supply on saltwater intrusion, the various boundary conditions are combined into a series of scenarios

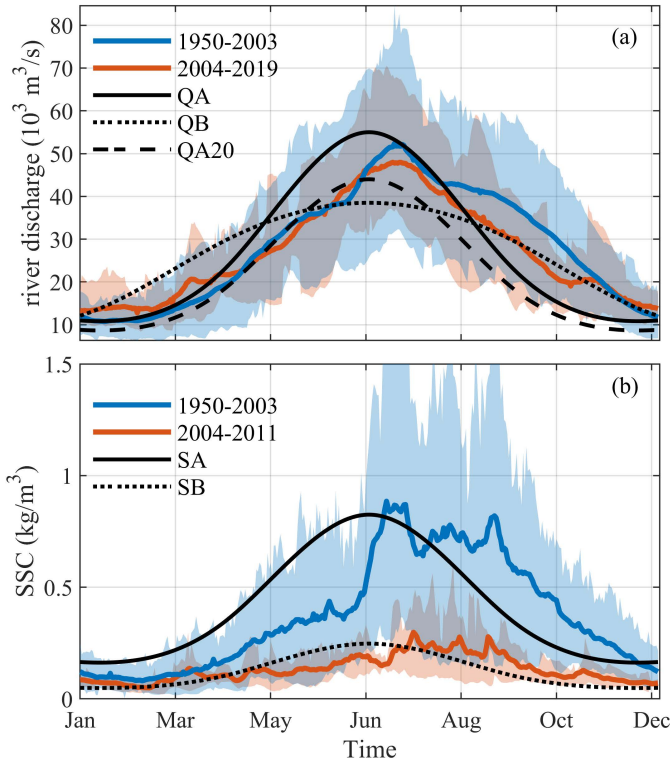


Figure 6.2: Simplified hydrographs of (a) river discharge (QA, QB, QA20) and (b) suspended sediment concentration (SSC) (SA, SB) at Datong according to the measurement in the pre-TGD (1950-2003) and post-TGD (2004-2015) periods. The blue and red lines are the mean values of the pre- and post-TGD periods whereas the shades indicate the variation range.

(Table 6.1). Additional modification of the ‘QA’ hydrograph with an increase/decrease in the total river discharge is represented by a scenario with a reduction in 20% river discharge proportional to QA (‘QA20’). A 1-m SLR is included to evaluate the effect of SLR in the future. Note that using the same SSC hydrograph for different annual discharge distribution leads to variable annual sediment loads while keeping the same annual sediment loads requires a new SSC hydrograph derived from the river discharge hydrograph. However, a sensitivity analysis on this effect revealed that this variability negligibly affected model results, and therefore the former approach is used to simplify the analysis.

The saltwater intrusion in winter threatens the freshwater supply to the city of Shanghai. Typically, a salinity level of 0.25 psu is the limit for freshwater intake (Li and Chen, 2019). Observed data suggested ~68 days without freshwater supply at Chenhong Reservoir in 2007 (Tang et al., 2011) whereas a well-calibrated numerical model indicated 54 maximum continuous days without freshwater supply at Qingcaosha Reservoir in 2008 (Zhu et al., 2013). Note that only >4 hours in a day with salinity lower than the limit is suitable for water intake (Zhu et al., 2013). Using a critical salinity level of 0.75 psu, our

Table 6.1: List of model scenarios. Hydrographs for river discharge (QA, QB, and QA20) and suspended sediment concentrations (SSC) (SA and SB) refer to Figure 6.2. ‘QA20’ represents a 20% reduction in river discharge proportional to hydrograph ‘QA’. SedDE: sediment-induced density effect. SLR: sea-level rise.

No.	Cases	River discharge hydrograph	SSC hydrograph	SLR (m)	SedDE
Reference	Ref	QA	SA	0	Y
Changes in boundary conditions	Q1030	QB	SA	0	Y
	Q20	QA20	SA	0	Y
	SLR1m	QA	SA	1	Y
	S70	QA	SB	0	Y
Without sediment effects	Ref-hydro	QA	SA	0	N
	Q1030-hydro	QB	SA	0	N
	Q20-hydro	QA20	SA	0	N
	SLR1m-hydro	QA	SA	1	N
	S70-hydro	QA	SB	0	N

6

model (scenario Ref) reproduces the observed number of days with sufficient freshwater. Using 0.75 psu, the model predicts 71 days without freshwater supply at Chenhang Reservoir and 54 continuous days without freshwater supply at Qingcaosha Reservoir in 2007.

6.4. RESULTS

6.4.1. RESPONSES OF SSC AND SALINITY

The changes in river flow, SLR, and sediment supply alter the sediment trapping and saltwater intrusion (Figure 6.3). For all scenarios, the highest bottom SSC of the ETM locates at approximately km-120 (originating at Xuliujing, defined at km-0), corresponding to the landward limit of saltwater intrusion. Under equal annual river discharge and sediment load, the seasonal variations of river discharge strongly influence the longitudinal distribution of salinity. Model results suggest that the strongest saltwater intrusion occurs for a reduction in river discharge (‘QA20’ hydrograph) and the weakest for the scenario with reduced seasonal variability of the river discharge (‘QB’ hydrograph). The two scenarios with the change in river discharge result in a landward and seaward migration of saltwater intrusion by ~5 km compared to the reference scenario, respectively. Among all the scenarios, a SLR of 1 m results in the most pronounced saltwater intrusion, with a landward migration of approximately 10 km (compared to the reference scenario). On the other hand, a reduced sediment supply leads to less saltwater intrusion and lower near-bed SSC. Specifically, a 70% reduced sediment load leads to a seaward migration of saltwater intrusion of ~3 km compared to the reference scenario. Moreover, sediment trapping is constrained near-bed and between km-90 and km-140.

The longitudinal variations of bottom SSC and depth-averaged salinity also indicate

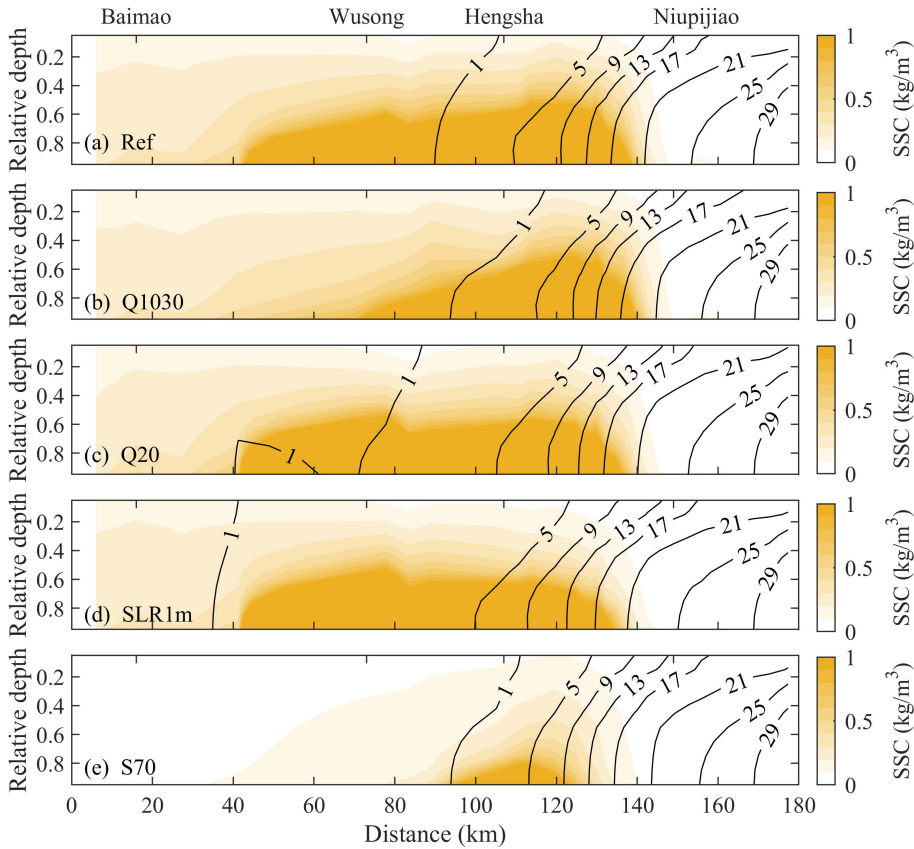


Figure 6.3: Modelled longitudinal distribution of salinity (black contour lines) and SSC (color shading) in scenarios (a) Ref, (b) Q1030, (c) Q20; (d) SLR1m, and (e) S70 (see Table 6.1).

strong differences between the dry and wet seasons (Figure 6.4). The changes in river discharge and SLR lead to more pronounced changes in both the magnitude and location of the maximum SSC in the dry season, whereas in the wet season only the magnitude changes. In the dry season, the discharge redistribution ('QB') leads to seaward movement of the ETM (relative to the reference) whereas a discharge reduction ('QA20') and SLR lead to landward movement of the ETM (Figure 6.4a). In the wet season, the changes in river discharge ('QB' and 'QA20') as well as SLR enhance sediment trapping, with strongest sediment trapping occurring for SLR of 1 m with a maximum SSC of $>30 \text{ kg/m}^3$ (Figure 6.4b). A 70% reduced sediment supply ('SB' hydrograph) results in an order of magnitude of lower SSC trapped in the ETM, and the maximum SSC in the ETM is slightly larger in the dry season ($\sim 2 \text{ kg/m}^3$) than in the wet season ($\sim 1 \text{ kg/m}^3$).

Considering the changes in river discharge, stronger saltwater intrusion corresponds to the lower river discharges, i.e. the 'QA', 'QB' and 'QA20' hydrographs have an average discharge of 13,934, 20,221, 11,148 m^3/s in the dry season, resulting in the weakest salt-

water intrusion for ‘QB’ and the strongest for ‘QA20’ (Figure 6.4c). Similarly, the ‘QA’, ‘QB’ and ‘QA20’ hydrographs have an average river discharge of 41,697, 35,444, 33,358 m³/s in the wet season with the strongest saltwater intrusion for ‘QA20’ (Figure 6.4d). However, the effect of the changes in river discharge on saltwater intrusion is not as pronounced as that in the dry season. Moreover, SLR of 1-m leads to stronger saltwater intrusion than the changes in river discharge in both the dry and wet seasons. A 70% reduction in sediment supply causes weaker saltwater intrusion mainly in the wet season.

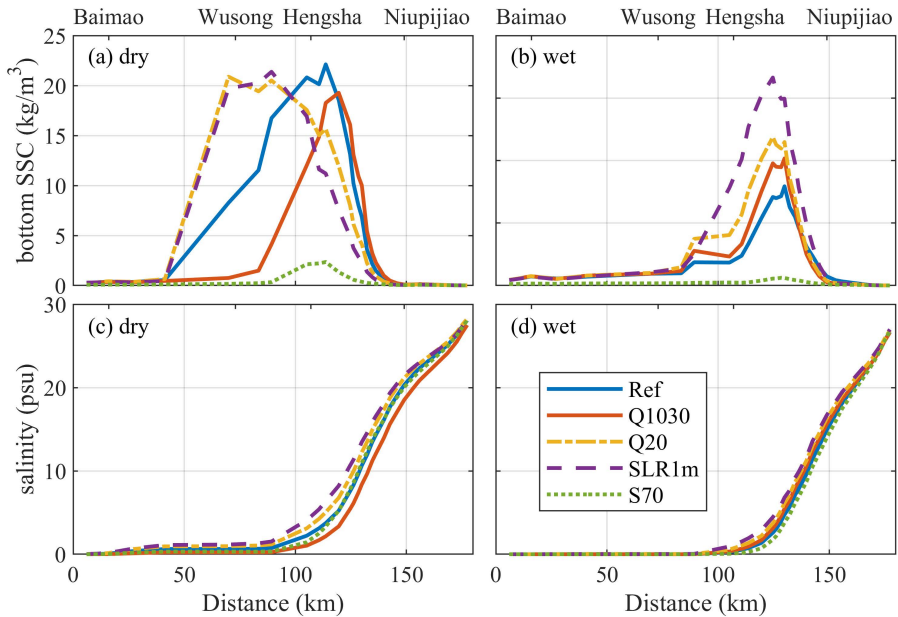


Figure 6.4: Modelled longitudinal variations of the (a, b) bottom suspended sediment concentration (SSC) and (c, d) depth-averaged salinity in the scenarios with the effects of sediment (scenarios see Table 6.1) averaged over the year 2007. The distance indicates the locations along the South Branch-South Channel-North Passage originating at Xuliujing defined as km-0 (see red dashed line in Figure 4.2) if not otherwise specified.

6.4.2. EFFECT OF SEDIMENTS

To evaluate the effect of sediments, various model scenarios have been executed without feedback between sediments and hydrodynamics (the SedDE). We then explored the variations of surface and bottom salinity induced by changes in boundary conditions by subtracting the salinities in the scenarios without the SedDE from those considering the effects of sediment (Figure 6.5). The effects of sediments on the role of changing river discharge, SLR and sediment supply vary in the surface and bottom salinity. In the dry season, the surface salinity increases upstream of km-110 and downstream of km-160 (and decreases in between) by including the effect of sediments (Figure 6.5c). The increase in surface salinity driven by the changes in boundary conditions is largest when sediment trapping is the most pronounced. Specifically, the surface salinity in-

increases up to ~ 0.5 psu upstream of km-110 for the 'QA20' hydrograph and SLR of 1-m where the maximum SSC is the largest with $>30 \text{ kg/m}^3$. The weakest increase in surface salinity by ~ 0.1 psu occurs for the 70% reduced sediment supply ('SB' hydrograph) with a maximum SSC in the ETM of $\sim 2 \text{ kg/m}^3$. However, the decrease in surface salinity between km-110 and km-160 does not show a close relationship with the sediment trapping efficiency. Such a larger influence on the surface salinity by the effects of sediment plays an important role in the freshwater intake as elaborated later. In the wet season, the effects of sediment on changing the surface salinity is limited upstream of km-110 and varies downstream of km-110 (Figure 6.5d). The decrease in surface salinity downstream of km-110 is more pronounced with stronger sediment trapping (e.g., for SLR of 1-m) whereas the increase in surface salinity downstream of km-110 is more pronounced with less sediment trapping (e.g., reduced sediment supply with 'SB' hydrograph). In contrast, the bottom surface is overall increased throughout the estuary with the maximum increase at km-110 in the dry season and km-140 in the wet season (Figure 6.5e, f). In the dry season, the increase in bottom salinity is up to ~ 2 psu with 'QA' hydrograph and 1-m SLR whereas 'SB' hydrograph with a 70% reduction in sediment supply leads to the smallest increase in bottom salinity, i.e. the most pronounced increase occurs at km-110 by ~ 1 psu. The increase in salinity induced by the SedDE is stronger downstream of km-90 in the wet season than the dry season, probably because of the landward movement of the sediment trapping location in the wet season compared to the dry season. The maximum increase in bottom salinity is ~ 3 psu with 'QA' hydrograph and 1-m SLR.

The different response of the surface and bottom salinity induced by the SedDE suggest an impact on stratification, which is illustrated by the changes in the salinity threshold of 0.75 psu and its variability (Figure 6.6). Under equal annual river discharge and sediment supply, with the effects of sediment, the 'QA', 'QB' and 'QA20' hydrographs lead to seaward movement of the median isohaline by ~ 2 -3 km in the surface and landward movement of the median isohaline by ~ 4 km in the bottom in the dry season (Figure 6.6a, c, e). In the wet season, only landward movement of the median isohaline in the bottom induced by the SedDE is pronounced in the wet season, by ~ 8 km with the 'QA', 'QB' and 'QA20' hydrographs (Figure 6.6b, d, f). It therefore suggests that salinity-induced stratification is enhanced by the effect of sediments under changes in river discharge both in the dry and wet seasons. Similarly, SLR of 1-m enhances stratification with a larger landward shift of the bottom isohaline with ~ 8 km in both the dry and wet season (Figure 6.6g, h). Note that increase in stratification due to the SedDE is closely related to the sediment trapping efficiency, and therefore the landward movement of the bottom isohaline is larger than the surface isohaline considering the higher near-bed SSC in the ETM in all the scenarios. For 70% reduced sediment supply ('SB' hydrograph) with the same river and tidal conditions, the sediment trapping is significantly reduced with a maximum SSC an order of magnitude smaller ($\sim 2 \text{ kg/m}^3$). Consequently, the landward movement of the bottom isohaline due to the effects of sediment is only ~ 1 km in the dry and wet season, which is much smaller than for the other scenarios (Figure 6.6i, j).

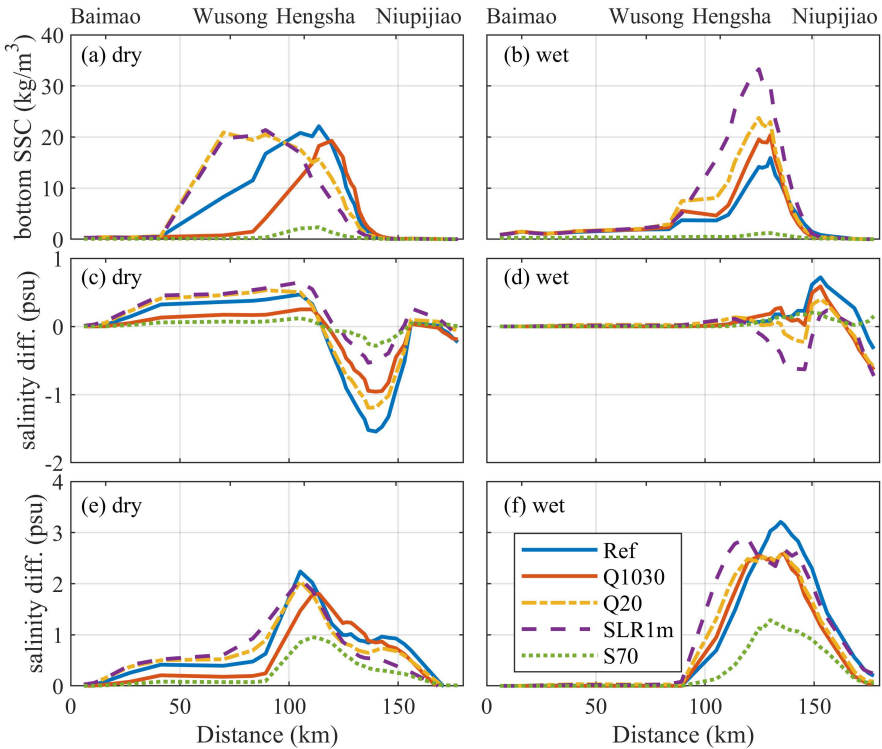


Figure 6.5: Modelled longitudinal variations of the bottom suspended sediment concentration (SSC) with influence of sediment on hydrodynamics (a, b) and salinity differences (c-f) between the scenarios including and excluding the sediment-induced density effects (SedDE) in the surface (c, d) and bottom (e, f) layers in the dry (left) and wet (right) seasons (scenarios see Table 6.1). Positive value indicates an increase in salinity with the effects of sediment than without.

6.4.3. EFFECT ON FRESHWATER SUPPLY

The changes in spatial and seasonal variations of the surface salinity due to the changes in boundary conditions (with the effect of sediments) are further explored comparing it with the reference scenario (Figure 6.7). Typically, a higher river discharge leads to a decrease in salinity, weakening saltwater intrusion. Specifically, before April 26 and after September 6, the 'QB' hydrograph has a lower river discharge the reference scenario with 'QA' hydrograph, resulting in the increase in salinity in this period. Moreover, the increase in salinity in this period upstream of km-110 indicates strong spring-neap variations. The reduced river discharge of 'QA20' hydrograph has similar spring-neap variations except an increase in salinity throughout the year. Note that although the river and sediment hydrographs are symmetric in the year, the tidal boundary conditions are not. Thus the increase in salinity under the changes in river discharge are not symmetric, particularly considering the non-linear interactions between river and tides, and between hydrodynamics and sediment transport. On the other hand, the 1-m SLR scenario leads to an overall increase in the surface salinity and enhances saltwater intru-

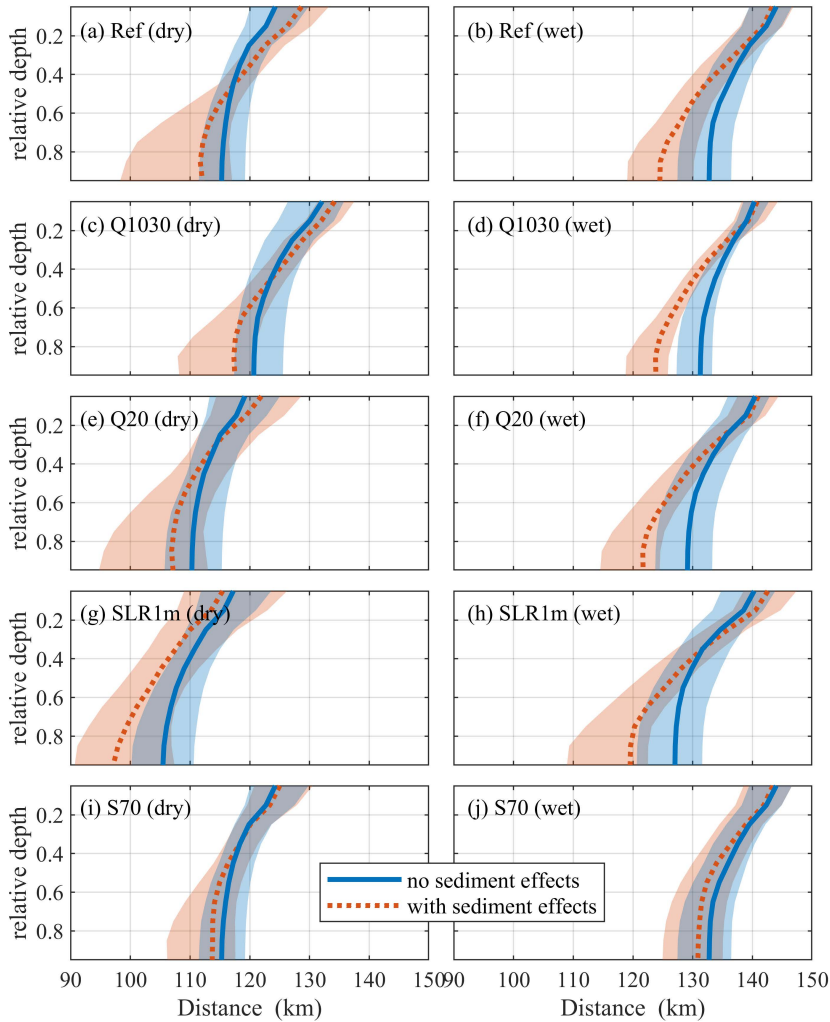


Figure 6.6: Comparison of the modelled vertical variation of the median location and variability of the salt limit (defined as the intersection of the 0.75 psu isohaline from the surface to bottom) between the scenarios without the sediment effects (in blue) and with the sediment effects (in bed) in the dry (left) and wet season (right). Scenarios include (a, b) Ref, (c, d) Q1030, (e, f) Q20, (g, h) SLR1m, and (i, j) S70 (see Table 6.1). The shades indicate the interquartile range of the location. The range in distance displayed here is different from the other figures to indicate the clear changes in stratification.

sion under lower river discharges. Under higher river discharges, the saltwater intrusion enhanced by SLR is constrained downstream of km-150 with pronounced spring-neap variations, i.e., an increase of >1 psu during spring tides and a decrease of >1 psu during neap tides. The effect of reduced sediment supply also results in different responses in the longitudinal direction of the channel and in the seasonal variation. Specifically, an

increase in surface salinity occurs in the ETM in spring tides in the dry season whereas the decrease in surface salinity is pronounced in other areas and periods. This suggests that the effect of changes in sediment supply on surface salinity needs to be carefully considered especially in the ETM. However, with reduced sediment supply ('SB' hydrograph) compared with 'SA' hydrograph, the bottom salinity is overall reduced therefore the saltwater intrusion is weakened (see Figure 6.5) and more sufficient freshwater is available considering the surface salinity upstream of the ETM.

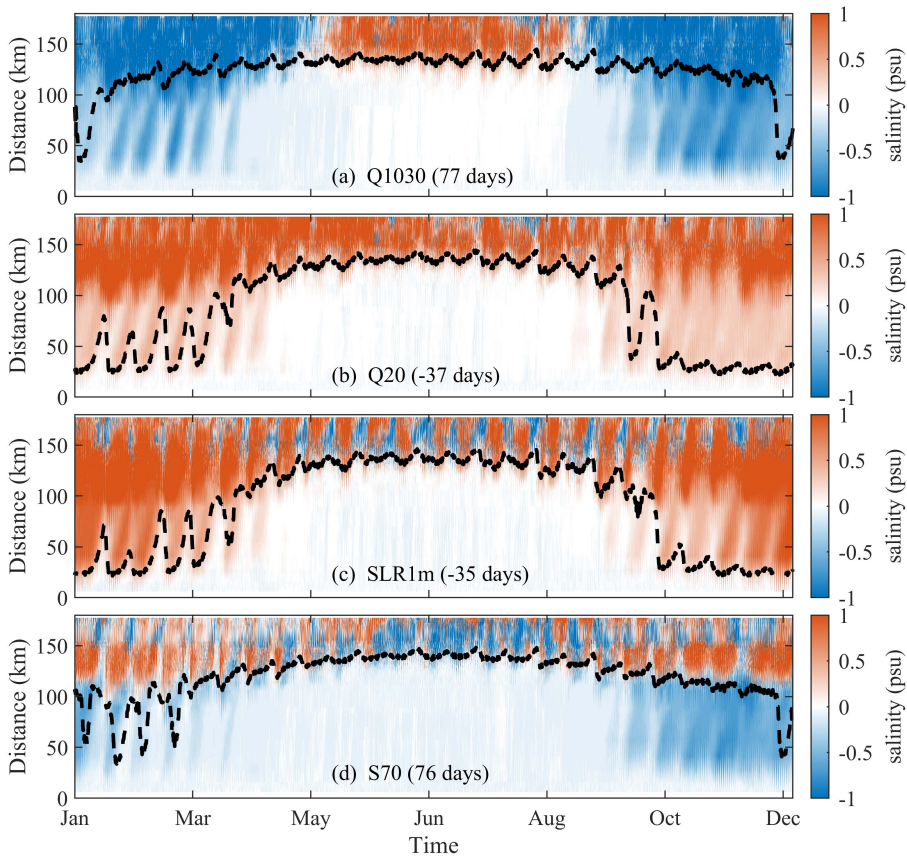


Figure 6.7: Time evolution of the modelled difference of surface salinity in the scenarios of (a) Q1030, (b) Q20; (c) SLR1m, and (d) S70 compared to the reference case (see Table 6.1). The dashed black lines represent the tidally-averaged location of surface salinity of 0.75 psu throughout the year. The days in brackets indicate the increased freshwater supply days in a year at Qingcaosha Reservoir (km-75, see Figure 6.1) compared to the reference case.

To quantify the effect of sediments on the roles of changes in boundary conditions on freshwater supply, we analyzed freshwater supply days based on surface salinity of <0.75 psu at km-75 (see section 6.3) under the changes in river discharge, SLR, and sediment supply (Table 6.2). Note that without the effect of sediments, scenarios 'Ref-hydro'

Table 6.2: Comparisons between averaged surface salinity at Qingcaosha Reservoir (km-75) during the wet season, dry season, and a full year, and the freshwater supply days in a series of scenarios (see Table 6.1). Negative freshwater supply days in brackets are the difference between scenarios with and without sediment effects.

Category	Scenarios	Salinity at km-75 (psu)			Freshwater supply days	Days relative to the reference
		Wet	Dry	Year		
With sediment effects	Ref	0.009	0.718	0.365	275 (-79)	—
	Q1030	0.002	0.356	0.180	352 (-13)	77
	Q20	0.054	1.051	0.554	238 (-60)	-37
	SLR	0.036	1.317	0.678	240 (-43)	-35
	S70	0.001	0.397	0.200	351 (-3)	76
Without sediment effects	Ref-hydro	0.001	0.320	0.161	354	—
	Q1030-hydro	0.001	0.320	0.161	365	11
	Q20-hydro	0.011	0.545	0.279	298	-56
	SLR-hydro	0.012	0.688	0.351	283	-71
	S70-hydro	0.001	0.320	0.161	354	0

and 'S70-hydro' are the same. Without the effect of sediments, a redistribution in river discharge ('QB' hydrograph) increases the number of days with freshwater supply by 11 days whereas 'QA20' hydrograph and 1-m SLR decrease the number of days with sufficient freshwater by approximately two months (56 and 71 days, respectively). With the SedDE, the freshwater supply days are shortened by 79, 13, 60, 43, and 3 days (the difference of freshwater supply days between with and without sediment effects) in the scenarios 'Ref', 'Q1030', 'Q20', 'SLR', and 'S70', respectively. Moreover, compared to the reference scenario (Ref), the freshwater supply days are decreased by approximately one month in scenarios considering reduced river flow (scenario Q20) and SLR (scenario SLR1m). In contrast, the 70% reduced sediment supply strongly alleviate saltwater intrusion with over 2 months more freshwater supply.

6.5. DISCUSSION

Throughout the world, estuaries are impacted by the consequence of climate change, upstream dam construction, and the deepening of waterways. These interventions influence the river discharge (average as well as seasonal variability), tidal dynamics, and the sediment load, which modifies estuarine sediment dynamics and in turn have an impact on saltwater intrusion and therefore freshwater supply (Figure 6.8). The effect of changes in river discharge, tides, water levels and sediments are discussed below.

CHANGING RIVER DISCHARGE

The changes in river discharge determine freshwater supply primarily through a critical river discharge above which the saltwater is unable to intrude into a particular location in the estuary. This critical freshwater discharge is closely associated with the geometry of the estuary and tidal water levels, which can be estimated from analytical

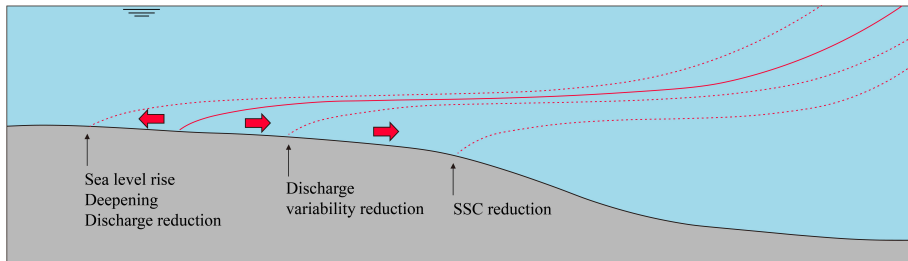


Figure 6.8: Sketch of the average isohalines for various scenarios. Sea-level rise, deepening, and discharge reduction lead to a landward migration of the saltwater intrusion (red line) whereas a reduction in seasonal variability of river discharge leads to a seaward migration of comparable magnitude (within our scenario space). A 70% reduction in suspended sediment concentration (SSC), however, leads to a much more pronounced seaward migration of the saltwater intrusion.

solutions (Cai et al., 2015). However, the changes in river discharge alter the trapping locations mainly in the dry season and the trapping efficiency mainly in the wet season. In the dry season, river discharges lead to more upstream sediment trapping, additionally enhancing saltwater intrusion by the effect of sediment. In the wet season, river discharges lead to larger trapping efficiency, additionally strengthening saltwater intrusion by the effect of sediments. Therefore, the lower river discharge enhances saltwater intrusion not only from the hydrodynamic effect itself but also by the additional feedback effect of sediment on hydrodynamics. The feedback effect of sediment dynamics is also reflected by the critical freshwater discharge. For instance, in this study, the critical river discharges, defined as the minimum river discharge allowing saline water of 0.75 psu to reach the Qingcaosha Reservoir are approximately 16,010, and 13,323 m^3/s in scenarios Ref and S70, respectively under the same river discharge. The $\sim 3,000 \text{ m}^3/\text{s}$ decrease in the critical river discharge is caused by the reduced sediment trapping efficiency (an order of magnitude lower near-bed SSC) under 70% reduction in sediment supply.

In the future, changes in the river discharge are not only influenced by human interventions, e.g., dam construction and water diversions, but also by climate change-induced modifications in precipitation which are not uniform across regions. For instance, precipitation is predicted to increase 4.4–11.1% in most regions of China when global temperature increase by 1.5°C (Li et al., 2018a). It may therefore to some degree alleviate saltwater intrusion. In contrast, the mean river discharge of many European rivers is projected to decrease (Alfieri et al., 2015). In these systems, saltwater intrusion may therefore be more pronounced when accounting for the effects of sediment.

CHANGING TIDES AND WATER LEVELS

SLR causes inundation of land and loss of wetlands, affecting the geometries of estuaries and altering tidal properties (Talke and Jay, 2020). Recent probabilistic assessments suggest a global sea-level rise of 0.45–0.82 m by 2100 for very high anthropogenic greenhouse gas emissions (IPCC, 2014), much larger than the rise of approximately 0.14–0.19 m during the 20th century (Church and White, 2011; Hay et al., 2015). According to our model results, a SLR of 1 m strengthens saltwater intrusion even more when accounting for the effect of sediments. Specifically, the changes in residual current indi-

cates that SLR increases the seaward surface current and landward bottom current by ~ 1 m/s, enhancing gravitational circulation (see Figure 6.9). The increase in gravitational circulation therefore leads to stronger salinity-induced stratification (Chua and Xu, 2014; Chen et al., 2016a). Moreover, the increase in gravitational circulation leads to more sediment trapping (Festa and Hansen, 1978; Burchard and Baumert, 1998; Geyer and MacCready, 2014), further increasing the SedDE and therefore strengthening saltwater intrusion (Zhu et al., 2021, as elaborated later).

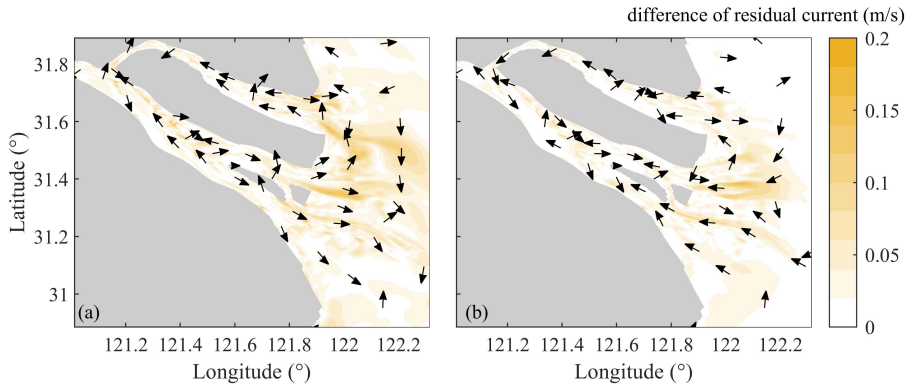


Figure 6.9: Difference of the residual current in the scenario ‘SLR1m’ compared to the reference case ‘Ref’ (scenarios see Table 6.1) in the surface (a) and bottom (b). Color in shading represents the magnitude and arrows indicate the direction.

In addition to SLR, many estuaries are deepened and narrowed, such as in the Rhine-Meuse Delta (Vellinga et al., 2014), Tampa Bay (Zhu et al., 2014), Elbe Estuary, Ems Estuary, and Loire Estuary (Winterwerp et al., 2013), upper Scheldt estuary (Wang et al., 2019b), Columbia Estuary (Jay et al., 2011) and Cape Fear River Estuary (Famikhali and Talke, 2016), leading to tidal amplification (Ralston and Geyer, 2019; Zhang et al., 2021). The tidal amplification is more likely to enhance saltwater intrusion as a result of enhanced stratification in partially-mixed estuaries (Monismith et al., 2002; Lerczak et al., 2009; Eslami et al., 2019) but may also alleviate saltwater intrusion due to the stronger mixing effect (Uncles and Stephens, 1996; Brockway et al., 2006; Ralston et al., 2010) in the future.

CHANGING SEDIMENT

Reduced sediment supply has been widely reported in major deltas and estuaries (Syvitski et al., 2009; Dunn et al., 2019; Besset et al., 2019; Li et al., 2020a). Although reduced sediment supply raises concern for delta erosion and coastline recession, our results suggest that a 70% reduction in sediment load leads to a seaward migration of the saltwater intrusion by ~ 3 km over a full year, a decrease in surface salinity of 0.32 psu at Qingcaosha Reservoir (km-75) in the dry season and a lengthened period with sufficient freshwater availability by over 2 months (76 days). This impact of sediment is so large because of positive feedbacks between sediment-induced stratification (due to the SedDE), salinity-induced stratification, and tidal dynamics.

As demonstrated by [Zhu et al. \(2021\)](#), the SedDE has contrasting vertical and horizontal density effects. On the one hand, it increases vertical sediment concentration gradients due to reduced vertical mixing. On the other hand, the SedDE increases salinity-induced stratification and amplifies and deforms tides, enhancing ETM formation and saltwater intrusion which in turn leads to stronger SedDE. Moreover, a positive feedback also exists between SSC and tidal amplification due to the effect of high near-bed SSC on reducing the apparent hydraulic roughness ([Winterwerp and Wang, 2013](#)). Predicting the impact of upstream interventions, changes in local geometry, or SLR in estuaries with high SSC therefore requires a 3D model properly accounting for the SedDE. Such an effect may reduce freshwater availability from days to months, depending on sediment trapping. For instance, the SedDE decreases the freshwater supply months in scenarios Ref, Q1030, Q20, and SLR1m with a near-bed SSC over $10\text{--}30\text{ kg/m}^3$ and only days in the scenario S70 with the near-bed SSC in the ETM an order of magnitude smaller (Table 6.2). Typically, more sediment trapping efficiency leads to stronger SedDE on enhancing saltwater intrusion and thereby decreasing freshwater supply days. However, sediment trapping location is also influenced by the divergence of horizontal SedDE ([Zhu et al., 2021](#)), which may also play a role in the migration of saltwater intrusion. The positive feedbacks introduced above are, however, only valid for fine-grained sediment (as evaluated in the current work). When the sediment load is primarily composed of sandy sediment, the most prominent impact of a sediment load reduction may be an erosion of the river bed. This effectively deepens the river bed, promoting saltwater intrusion and amplifying the tides. This has been observed, for instance, in the Mekong river ([Es-lami et al., 2019](#)).

The changes in the fraction of sediment may also change sediment trapping and stratification, influencing saltwater intrusion. Typically, very fine sediments are easily flushed out to the sea, and because of their vertically uniform SSC distribution only limitedly influence vertical mixing (and hence do not set in motion positive feedback mechanisms strengthening saltwater intrusion and tidal amplification). Very coarse sediments tend to deposit rapidly, and therefore also generate minor sediment-induced density effects. The intermediate grain size of sediments (mainly silt and fine sand) has the most pronounced SedDE and sediment trapping. In the Yangtze Estuary, the TGD mostly traps sand and silt whereas clay is flushed through the reservoir. The shortage of sand may be partly compensated by the bed erosion downstream of the Yangtze River ([Luo et al., 2012](#); [Yang et al., 2014](#)) and therefore it is especially the intermediate silt fraction that is reduced in the estuary ([van Maren and Winterwerp, 2013](#)). Since especially silt promotes the SedDE and then promotes saltwater intrusion, the shortage of silt resulting from the upstream dams reduces saltwater intrusion.

6.6. CONCLUSIONS

Using a numerical model, we explored the effect of changes in river discharge, SLR, and sediment supply on saltwater intrusion in the Yangtze Estuary, particularly focusing on the role of sediment dynamics. Reduced seasonal variability of river discharge reduces saltwater intrusion in the dry season but enhances in the wet season whereas reduced river discharge and SLR strengthen saltwater intrusion. These changes in river discharge and SLR also lead to stronger sediment trapping over the year and migration

mainly in the dry season. On the other hand, reduced sediment supply reduces sediment concentrations and alleviates saltwater intrusion. Concerning the simulated scenarios including reduced seasonal variability of the river discharge ('QB' hydrograph), 20% reduced river discharge ('QA20' hydrograph), 1-m SLR, and 70% reduced sediment supply ('SB' hydrograph), the saltwater intrusion moves approximately -5, 5, 10, and -3 km landward respectively over a full year. The movement of saltwater intrusion correspond to an increase in freshwater supply (salinity level of <0.75 psu at Qingcaosha Reservoir comparable to observations) by 77, -37, -35 and 76 days, respectively. These effects are influenced by the sediment-induced density effects which enhance saltwater intrusion by decreasing freshwater supply from days if sediment concentration is low ($\sim 2 \text{ kg/m}^3$) to months if sediment concentration is high ($>10\text{-}30 \text{ kg/m}^3$). Future changes in precipitation will alter the total river discharge and its seasonal distribution, influencing saltwater intrusion and the response is further complicated by local human interventions, global sea level rise, and changes in the sediment load and sediment grain size. Particularly saltwater intrusion may be enhanced by deepening as a result of its interactions with tidal amplification and sediment trapping but may also be counteracted by the decreasing sediment supply.

Overall, we conclude that although saltwater intrusion is influenced by a large number of potential future scenarios influencing the hydrodynamics (SLR, changes in total discharge and variability by precipitation changes and reservoirs, as well as local intervention), a previously overlooked aspect that is crucial for turbid estuaries is the role of sediments. Sediments influence saltwater intrusion through complex feedback mechanisms, making future saltwater intrusion even more difficult to predict. But even more, the biggest projected impact on saltwater intrusion is a reduction in fluvial sediment supply. In turbid estuaries, studies on (changes in) saltwater intrusion should adequately address the effect of sediment concentration, and it is advised to closely monitor estuarine suspended sediment concentrations.

7

CONCLUSIONS AND RECOMMENDATIONS

*Long, long had been my road and far, far was the journey;
I would go up and down to seek my heart's desire*

路漫漫其修远兮
吾将上下而求索

Qu Yuan (Poet, Politician, 340 B.C.-278 B.C.)
In *Li Sao*



THIS dissertation aims to identify if human-driven regime shifts have occurred in the Yangtze Estuary and to understand how SSC-related effects influence on hydrodynamics, sediment dynamics, and saltwater intrusion in the past and in the future. First, the five research questions formulated in Chapter 1 are answered (section 7.1). Then, an evaluation is given how the two overarching goals are achieved (section 7.2). We finalise with recommendations for further research (section 7.3).

7.1. ANSWERS TO THE RESEARCH QUESTIONS

- (1) *What are the decadal morphological changes in the mouth zone of the Yangtze Estuary in response to a reduced sediment supply?*

Although sediment supply has been decreasing since the mid-1980s, two shoals in the mouth zone, i.e. Hengsha flat and Jiudian shoal, accreted at different rates until 2010 followed by erosion. The Hengsha flat expanded more horizontally than it accreted vertically whereas the Jiudian shoal accreted more vertically than it expanded horizontally. This different behavior can be explained by upstream water and sediment partition, local tidal dynamics and bio-physical interactions. Accretion and expansion of the two shoals until 2010 are closely related to local human intervention, such as salt marsh introduction, land reclamation and the construction of a navigation channel. The erosion of both shoals since 2010 is attributed to dredging activities and a shortage of sediments due to upstream dam construction. For the two shoals and the North Passage as a whole in the mouth zone, a sudden shift from accretion to erosion occurred in 1997 and 2007. The short-term erosion is mainly explained by the local navigation project and may not be fully explained by impacts of fluvial sediment decline. Specifically, the disposed volume, used for land reclamation from dredging activities, accounts for ~50% of the volume changes (interpreted as erosion) as quantified by bathymetric data. Considering the continuous erosion after 2010 during which local interventions may still play a role, we identified a morphodynamic response time lag of ~30 years in the mouth zone to riverine sediment decrease (**Chapter 2**).

- (2) *What is the tidal evolution in response to morphological and sedimentary changes in the Yangtze Estuary?*

Tidal evolution in the Yangtze Estuary exhibits spatial variations (**Chapter 3**). Data analysis in the South Branch suggests a strongly reduced tidal damping during 1990-2010 and a slightly weakened tidal damping during 2010-2020. The yearly averaged tidal ranges in the mouth zone show an overall stronger tidal damping from 1997 to 2010. A calibrated 2D hydrodynamic model further suggests that the reduced damping in the South Branch is controlled by sediment decline which results in an increase in water depth and a 70% reduced SSC. The reduced SSC induces a 60% increase in the effective bottom roughness, counteracting over 50% of the reduced tidal damping from the water depth increase during 1990-2010. During 2010-2020, the effect of morphological changes is limited and the decreasing SSC increased effective bottom roughness by ~5% which controls the slightly enhanced tidal damping in the South Branch. Moreover, in the mouth zone, an overall increase in effective bottom roughness dominates the increased tidal damping

from 1997 to 2010. The increase in effective bottom roughness is mainly caused by local structures and partly counteracted by the enhanced fluid mud. The enhanced fluid mud may decrease the roughness after 2010; however, the SSC is decreasing recently (2019-2020) which may increase the roughness. Therefore, future changes in fluid mud and sediments influenced by the combined effect of sediment decline and local engineering works need close monitoring.

- (3) *How does high suspended sediment concentration interact with hydrodynamics and in turn influence the estuarine turbidity maximum?*

A calibrated 3D sediment transport model in the Yangtze Estuary reveals that high sediment concentrations influence the stability and position of the ETM (**Chapter 4**). Salinity-induced vertical density effects are the primary drivers for ETM formation, leading to a pronounced sediment convergence whereas longitudinal sediment-induced density effects lead to sediment transport divergence. Vertical sediment-induced density effects introduce a behavior opposite to the longitudinal sediment-induced density effects on two levels: 1) they enhance the vertical SSC gradients, leading to more efficient salinity-driven residual transport and 2) they additionally amplify tides, increase salinity-induced stratification, and therefore increase residual flow, favoring net landward sediment transport and generating a positive feedback mechanism to promote ETM formation.

- (4) *What are the roles of tidal asymmetry and sediment-induced density effects on the formation of estuarine turbidity maximum?*

The roles of tidal asymmetry and sediment-induced effects (density effects and high near-bed SSC due to water-bed exchange processes) are reflected from a schematic model with different types of offshore tidal asymmetry and strength of sediment-induced effects (**Chapter 5**). Sediment properties in terms of the critical shear stress for erosion mainly influences the magnitude of the maximum SSC of the ETM, whereas the settling velocity influences the location of the ETM. Sediment-induced density effects in combination with tidal asymmetry lead to a progressively larger contribution of estuarine circulation; however, they may lead to either pronounced ETM promotion or pronounced ETM dispersion due to the contribution of tidal pumping. Higher near-bed SSC due to water-bed exchange processes additionally increases the sediment-induced density effects due to the enhanced vertical SSC gradients and strongly influences the relative contribution of tidal pumping and estuarine circulation. Higher near-bed SSC increases the effect of estuarine circulation on landward sediment transport and the tidal pumping term could even become a diffusive term leading to a longitudinal divergence of sediment.

- (5) *How do sediment-induced density effects influence the predicted impact of global change?*

Sediment-induced effects play an important role in the formation of an ETM, but also on saltwater intrusion. With a 3D hydrodynamics and sediment transport model, we found that sediment-induced density effects vary seasonally and throughout the spring-neap tidal cycles (**Chapter 4**). During the wet season, the verti-

cal salinity gradient is stronger, and therefore the ETM formation is more pronounced, enhancing saltwater intrusion. During the dry season, the effect of longitudinal sediment gradient is more pronounced, resulting in the ETM dispersion and enhancing saltwater intrusion. Natural and human interventions alter the ETM strength and location, influencing saltwater intrusion which is especially important for freshwater resources (**Chapter 6**). The saltwater intrusion is limitedly influenced when near-bed sediment concentration is $\sim 2 \text{ kg/m}^3$ whereas the saltwater intrusion is strongly enhanced when near-bed sediment concentration is over $20\text{--}30 \text{ kg/m}^3$, i.e., the freshwater availability is decreased by months. Particularly, when the sediment load declines by 70%, estuarine sediment concentration is largely reduced, thereby mitigating saltwater intrusion. Overall, the effects of sediment dynamics are of critical importance for understanding and predicting saltwater intrusion in the future.

7.2. GENERAL CONCLUSIONS

FURTHER summarizing the results of this thesis, the general conclusion is formulated in answer to the main aims of this thesis, which are

- **To identify if human interventions have triggered regime shifts in the Yangtze Estuary**

In Chapter 1, regime shifts are described as ‘a shift from one dynamic regime (morphodynamic equilibrium state) to another, which is influenced by global environmental changes and human interferences’ and ‘is characterized by a tipping point in the forcing factors beyond which the estuary loses its natural characteristics, thereby endangering the environmental sustainability’. Specifically, regime shifts are evidenced by 1) a shift in morphology to a new morphodynamic equilibrium, and 2) a shift in sediment concentration to a low-turbidity conditions with weak tidal amplification due to declined fluvial sediment load.

Based on the observations of water levels, sediment concentrations and morphological changes, we have identified human-driven changes in the Yangtze Estuary. In this section we evaluate to what extent these changes can be considered a regime shift. Data suggest strong spatial variations, i.e. response of tidal evolution and sediment concentrations to reduced sediment supply in the South Branch is relatively faster than those in the mouth zone.

In the South Branch, depths became deeper and sediment concentrations became lower (bed becomes rougher) after decline in fluvial sediment load; and tides became less damped during 1990-2010 and slightly more damped during 2010-2020. These changes in morphology, sediment concentrations and tides in the South Branch are mainly caused by reduced sediment supply (**Chapter 2 and 3**). The South Branch has altered from net sedimentation to net erosion since 1958 due to reduced sediment load and the net erosion maintained at $50 \text{ million m}^3/\text{year}$ in volume and 50 mm/year in thickness after 1986 (Wang et al., 2013; Luan et al., 2016; Zhao et al., 2018). Almost no net change has been detected since 1986, which can be referred as dynamic equilibrium of type II (see section 1.2.2). Therefore, the

regime shift in morphology has been identified in the South Branch. Considering the regime shift in sediment concentration, the positive feedback between the sediment concentration and tidal damping (less turbid with less tidal amplification) seems not to occur during 1990-2010. Although a less turbid with less tidal amplification condition occurred from 2010 to 2020 (**Chapter 3**), the SSC is controlled by riverine sediment supply. The changes in tides will not trigger further decrease of SSC and therefore is not considered a regime shift in the South Branch.

In the mouth zone, morphology evolves from accretion to erosion (**Chapter 2**), sediment concentrations maintain unchanged for a long time except for a decreasing trend in recent years (2019-2020), and tides are more damped in the period 1997-2010 with a trend of less tidal damping after 2010 (**Chapter 3**). We have identified the strong effect of local engineering works and a ~30 years of morphological response time lag to riverine sediment decline (**Chapter 2**). However, whether the morphological changes in the mouth zone reach a new equilibrium state is still unknown. On the other hand, although the sediment concentrations do not significantly change for a relatively long time, the near-bed SSC (fluid mud) was increased due to local engineering works, partly counteracting the effect of local structures on increasing the effective roughness and thereby enhancing tidal damping. However, the positive feedback between sediment concentrations and tidal damping still cannot be sufficiently built during 1997-2010. Specifically, the effect of enhanced near-bed SSC does not lead to less tidal damping but more tidal damping due to local structures. After 2010, tides are less damped with probably higher near-bed SSC. However, the depth-averaged SSC has decreased in recent years. Therefore, we are still not able to identify the regime shift in the mouth zone of the Yangtze Estuary yet and whether a potential regime shift occurs needs to be investigated by close monitoring on the changes in tides, SSC and morphology.

- **To understand the effect of SSC on hydrodynamics (including saltwater intrusion) under current and future conditions**

Understanding the feedbacks between SSC and hydrodynamics (including saltwater intrusion), and ETM development is important for turbid estuaries worldwide. The main findings of the SSC-related effects in this thesis are summarized as follows:

- Effects of SSC-induced density gradients strengthen salinity-induced stratification and the longitudinal and vertical SSC-induced density gradients have opposite effects on the ETM formation (**Chapter 4**).
 - ◇ Effects of SSC-induced longitudinal density gradients cause longitudinal dispersion of the salinity-induced turbidity maximum.
 - ◇ Effects of SSC-induced vertical density gradients strengthen salinity stratification and thereby the salinity-induced horizontal density currents and associated sediment trapping.
 - ◇ Effects of longitudinal SSC density gradients are more pronounced under weak salinity stratification conditions, and those of vertical SSC density gradients under strong salinity stratification conditions.

- Effects of SSC-induced density gradients are influenced by tidal asymmetry and influence the mechanisms controlling sediment trapping (**Chapter 5**).
 - ◇ Without sediment-induced density effects, sediment trapping is primarily controlled by the strength of flood dominance.
 - ◇ Sediment-induced density effects lead to strengthening or dispersion of the ETM, depending on the type of tidal asymmetry.
 - ◇ Higher near-bed sediment concentrations strengthen the role of estuarine circulation and thereby sediment trapping.
- Effects of SSC-induced density gradients influence saltwater intrusion, and future changes in sediment loads are therefore crucial for predicting saltwater intrusion (**Chapter 6**).
 - ◇ Sediment dynamics influence the effect of river discharge changes and sea-level rise on saltwater intrusion.
 - ◇ The decline in riverine sediment supply may weaken sediment-induced effects, thereby reducing saltwater intrusion.

7.3. RECOMMENDATIONS FOR FUTURE RESEARCH

Monitoring and tracking estuarine changes Estuarine responses times are long and influenced by multiple drivers operating on different scales and time periods. Understanding estuarine response therefore requires long-term monitoring of hydrodynamics, sediments and morphology. Our findings indicate that the Yangtze Estuary has not moved to a new dynamic equilibrium (particularly in the mouth zone) and is likely still under transition. It is thus essential to keep monitoring and tracking the data to understand how and why the changes in the hydrodynamics, SSC and morphology in this stage. For instance, in the mouth zone, the tidal data should be gathered at a higher frequency to identify more convincing trend changes. Moreover, although the depth-averaged SSC was detected to decrease in 2019-2020, the changes in near-bed SSC which comes at high cost has been limited explored. The recent morphological evolution using latest bathymetric maps should be evaluated for whether the local effects of engineering works has been finished.

Effects of other human interventions Various human interventions occur within estuaries, such as water diversion, dredging and dumping activities, saltmarsh introduction, land reclamation etc. These human interventions have been widely studied for their local effects but have been seldom evaluated for the effects on the development of the large-scale estuary. For instance, in the Yangtze Estuary, channels bifurcate and interconnect in the branching channel network. Therefore, water and sediment exchanges occur between channel and shoals. The diversion of water and sediment discharges may also have different effects in branching channels. To what extent the human interventions within an estuary influence tides, sediment transport and morphology in a large spatial scale also needs to be addressed.

Sediment effects on lateral processes This thesis has limitedly evaluated the sediment

effects on lateral circulation. However, lateral circulation and sediment transport also interact with those in the longitudinal direction (Lerczak and Rockwell Geyer, 2004; Huijts et al., 2006; Zhu et al., 2017; Zhou et al., 2019, 2021). Moreover, the lateral processes may be influenced by blocking jetties and groins, dredging and dumping activities. Therefore, the sediment effects on lateral processes and probably the interaction with longitudinal processes may be essential as well. Further research is required to understand the interactions between hydrodynamics and sediments in the lateral direction and to what extent the lateral processes due to sediment effects affect the longitudinal processes should also be addressed.

The impact of sediment composition The models used in this thesis consider a single sediment fraction but our sensitivity scenarios suggest different behavior of different types of sediments on forming ETM and influencing saltwater intrusion (Chapter 4 and 5). Moreover, the sediment grain size distribution has changed due to the dam construction in the river basin. Previous studies have documented the effect of grain size on shaping tidal flats (van Maren et al., 2013; Zhou et al., 2015). We have also identified that two shoals in the mouth zone eroded after ~2010 which is probably due to the shortage of the silt sediments (Chapter 2). In addition, the sediment grain size may either increase or decrease the effective bottom roughness, which is essential for understanding sediment effects. These effects need to be further investigated.

Water-bed exchange processes An ETM may result from density-driven processes (supply-limited) and local resuspension (erosion-limited). This thesis has mainly focused on the density-driven processes. However, the water-bed exchanges processes are essential to understand delta responses in terms of tides, SSC and morphology. Moreover, the effect of complex near-bed exchange was explored with the 'reduced deposition' concept. Strong 'reduced deposition' leads to higher near-bed sediment concentrations, strengthening the effect of sediment-induced density gradients and influencing the relative role of estuarine circulation and tidal pumping on importing sediments (Chapter 5). Therefore, the water-bed exchange processes relevant for the 'reduced deposition' concept are important. However, this concept integrates a number of insufficiently known processes into one model parameter, and more in-depth research on these processes is recommended.

REFERENCES

- Alferi, L., Burek, P., Feyen, L., and Forzieri, G.: Global warming increases the frequency of river floods in Europe, *Hydrology and Earth System Sciences*, 19, 2247–2260, 2015.
- Allen, G. P., Salomon, J., Bassoullet, P., Du Penhoat, Y., and De Grandpre, C.: Effects of tides on mixing and suspended sediment transport in macrotidal estuaries, *Sedimentary Geology*, 26, 69–90, 1980.
- Allen, J., Somerfield, P., and Gilbert, F.: Quantifying uncertainty in high-resolution coupled hydrodynamic-ecosystem models, *Journal of Marine Systems*, 64, 3–14, 2007.
- Anderson, P. J. and Piatt, J. E.: Community reorganization in the Gulf of Alaska following ocean climate regime shift, *Marine Ecology Progress Series*, 189, 117–123, 1999.
- Araújo, I., Dias, J., and Pugh, D.: Model simulations of tidal changes in a coastal lagoon, the Ria de Aveiro (Portugal), *Continental Shelf Research*, 28, 1010–1025, 2008.
- Avoine, J.: Sediment exchanges between the Seine estuary and its adjacent shelf, *Journal of the Geological Society*, 144, 135–148, 1987.
- Banas, N., Hickey, B., MacCready, P., and Newton, J.: Dynamics of Willapa Bay, Washington: A highly unsteady, partially mixed estuary, *Journal of Physical Oceanography*, 34, 2413–2427, 2004.
- Beaugrand, G.: The North Sea regime shift: evidence, causes, mechanisms and consequences, *Progress in Oceanography*, 60, 245–262, 2004.
- Becker, M., Maushake, C., and Winter, C.: Observations of mud-induced periodic stratification in a hyperturbid estuary, *Geophysical Research Letters*, 45, 5461–5469, 2018.
- Besset, M., Anthony, E. J., and Bouchette, F.: Multi-decadal variations in delta shorelines and their relationship to river sediment supply: An assessment and review, *Earth-Science Reviews*, 193, 199–219, doi:10.1016/j.earscirev.2019.04.018, 2019.
- Blott, S. J., Pye, K., van der Wal, D., and Neal, A.: Long-term morphological change and its causes in the Mersey Estuary, NW England, *Geomorphology*, 81, 185–206, doi:10.1016/j.geomorph.2006.04.008, 2006.
- Brenon, I. and Le Hir, P.: Modelling the turbidity maximum in the Seine estuary (France): Identification of formation processes, *Estuarine Coastal and Shelf Science*, 49, 525–544, doi:10.1006/ecss.1999.0514, 1999.

- Brockway, R., Bowers, D., Hogue, A., Dove, V., and Vassele, V.: A note on salt intrusion in funnel-shaped estuaries: Application to the Incomati estuary, Mozambique, *Estuarine, Coastal and Shelf Science*, 66, 1–5, doi:<https://doi.org/10.1016/j.ecss.2005.07.014>, URL <http://www.sciencedirect.com/science/article/pii/S0272771405002635>, 2006.
- Brouwer, R. L., Schramkowski, G. P., Dijkstra, Y. M., and Schuttelaars, H. M.: Time Evolution of Estuarine Turbidity Maxima in Well-Mixed, Tidally Dominated Estuaries: The Role of Availability- and Erosion-Limited Conditions, *Journal of Physical Oceanography*, 48, 1629–1650, doi:10.1175/jpo-d-17-0183.1, 2018.
- Burchard, H. and Baumert, H.: The formation of estuarine turbidity maxima due to density effects in the salt wedge. A hydrodynamic process study, *Journal of Physical Oceanography*, 28, 309–321, doi:10.1175/1520-0485(1998)028<0309:Tfoetm>2.0.Co;2, 1998.
- Burchard, H. and Hetland, R. D.: Quantifying the Contributions of Tidal Straining and Gravitational Circulation to Residual Circulation in Periodically Stratified Tidal Estuaries, *Journal of Physical Oceanography*, 40, 1243–1262, doi:10.1175/2010jpo4270.1, 2010.
- Burchard, H., Hetland, R. D., Schulz, E., and Schuttelaars, H. M.: Drivers of residual estuarine circulation in tidally energetic estuaries: Straight and irrotational channels with parabolic cross section, *Journal of Physical Oceanography*, 41, 548–570, 2011.
- Burchard, H., Schuttelaars, H. M., and Geyer, W. R.: Residual sediment fluxes in weakly-to-periodically stratified estuaries and tidal inlets, *Journal of physical oceanography*, 43, 1841–1861, 2013.
- Burchard, H., Schuttelaars, H. M., and Ralston, D. K.: Sediment Trapping in Estuaries, *Ann Rev Mar Sci*, 10, 371–395, doi:10.1146/annurev-marine-010816-060535, 2018.
- Buschman, F. A., van der Vegt, M., Hoitink, A. J. E., and Hoekstra, P.: Water and suspended sediment division at a stratified tidal junction, *Journal of Geophysical Research: Oceans*, 118, 1459–1472, doi:10.1002/jgrc.20124, 2013.
- Cai, H., Savenije, H., and Toffolon, M.: Linking the river to the estuary: influence of river discharge on tidal damping, *Hydrology and Earth System Sciences*, 18, 287–304, 2014.
- Cai, H., Savenije, H. H., Zuo, S., Jiang, C., and Chua, V. P.: A predictive model for salt intrusion in estuaries applied to the Yangtze estuary, *Journal of Hydrology*, 529, 1336–1349, 2015.
- Castaing, P. and Allen, G. P.: Mechanisms controlling seaward escape of suspended sediment from the Gironde: a macrotidal estuary in France, *Marine Geology*, 40, 101–118, 1981.
- Chaalali, A., Beaugrand, G., Boët, P., and Sautour, B.: Climate-caused abrupt shifts in a European macrotidal estuary, *Estuaries and Coasts*, 36, 1193–1205, 2013.

- Chant, R. J.: Secondary circulation in a region of flow curvature: Relationship with tidal forcing and river discharge, *Journal of Geophysical Research: Oceans*, 107, 14–1–14–11, 2002.
- Chant, R. J. and Stoner, A. W.: Particle trapping in a stratified flood-dominated estuary, *Journal of Marine Research*, 59, 29–51, doi:Doi10.1357/002224001321237353, URL <GotoISI>://WOS:000167772100002, 2001.
- Chen, J., Zhu, H., Dong, Y., and Sun, J.: Development of the Changjiang Estuary and its subaqueous delta, *Processes of dynamics and geomorphology of the Changjiang Estuary*, pp. 48–62, 1988.
- Chen, J. Y., Zhu, H. F., Dong, Y. F., and Sun, J. M.: Development of the Changjiang Estuary and Its Submerged Delta, *Continental Shelf Research*, 4, 47–56, 1985.
- Chen, S.-L., Zhang, G.-A., Yang, S.-L., and Shi, J. Z.: Temporal variations of fine suspended sediment concentration in the Changjiang River estuary and adjacent coastal waters, China, *Journal of Hydrology*, 331, 137–145, 2006.
- Chen, W., Chen, K., Kuang, C., Zhu, D. Z., He, L., Mao, X., Liang, H., and Song, H.: Influence of sea level rise on saline water intrusion in the Yangtze River Estuary, China, *Applied Ocean Research*, 54, 12–25, doi:https://doi.org/10.1016/j.apor.2015.11.002, URL <http://www.sciencedirect.com/science/article/pii/S0141118715001364>, 2016a.
- Chen, Y., He, Q., Zhang, D., and Guo, C.: Grain size distribution of suspended sediment in Yangtze River Estuary turbidity maximum in dry season, *Journal of sediment research*, 1, 24–30 (in Chinese with Abstract in English), 2016b.
- Chen, Y., He, Q., Zhang, Y., and Lin, J.: Grain size distribution of suspended sediment in Yangtze River Estuary turbidity maximum in wet season, *Journal of sediment research*, 5, 48–55 (in Chinese with Abstract in English), 2019.
- Cheng, P., Valle-Levinson, A., and de Swart, H. E.: A numerical study of residual circulation induced by asymmetric tidal mixing in tidally dominated estuaries, *Journal of Geophysical Research*, 116, doi:10.1029/2010jc006137, 2011.
- Cheng, X.-j., Zhan, W., Guo, Z.-r., and Yuan, L.-r.: A modeling study on saltwater intrusion to western four watercourses in the Pearl River estuary, *China Ocean Engineering*, 26, 575–590, doi:10.1007/s13344-012-0044-y, URL <https://doi.org/10.1007/s13344-012-0044-y>, 2012.
- Cheng, Z., Jalon-Rójas, I., Wang, X. H., and Liu, Y.: Impacts of land reclamation on sediment transport and sedimentary environment in a macro-tidal estuary, *Estuarine, Coastal and Shelf Science*, 242, 106 861, 2020.
- Chernetsky, A. S., Schuttelaars, H. M., and Talke, S. A.: The effect of tidal asymmetry and temporal settling lag on sediment trapping in tidal estuaries, *Ocean Dynamics*, 60, 1219–1241, doi:10.1007/s10236-010-0329-8, 2010.

- Chevillot, X., Pierre, M., Rigaud, A., Drouineau, H., Chaalali, A., Sautour, B., and Lobry, J.: Abrupt shifts in the Gironde fish community: an indicator of ecological changes in an estuarine ecosystem, *Marine Ecology Progress Series*, 549, 137–151, 2016.
- Chu, A., Wang, Z., De Vriend, H., and Stive, M.: A process-based approach to sediment transport in the Yangtze Estuary, in: 32nd International Conference on Coastal Engineering, ICCE 2010, June 30–July 5 2010, Shanghai, China.
- Chua, V. P. and Xu, M.: Impacts of sea-level rise on estuarine circulation: An idealized estuary and San Francisco Bay, *Journal of Marine Systems*, 139, 58–67, doi: <https://doi.org/10.1016/j.jmarsys.2014.05.012>, URL <http://www.sciencedirect.com/science/article/pii/S0924796314001419>, 2014.
- Church, J. A. and White, N. J.: Sea-Level Rise from the Late 19th to the Early 21st Century, *Surveys in Geophysics*, 32, 585–602, doi:10.1007/s10712-011-9119-1, URL <https://doi.org/10.1007/s10712-011-9119-1>, 2011.
- Cloern, J. E. and Jassby, A. D.: Drivers of change in estuarine-coastal ecosystems: Discoveries from four decades of study in San Francisco Bay, *Reviews of Geophysics*, 50, 2012.
- Dai, Z., Liu, J. T., Fu, G., and Xie, H.: A thirteen-year record of bathymetric changes in the North Passage, Changjiang (Yangtze) estuary, *Geomorphology*, 187, 101–107, doi: 10.1016/j.geomorph.2013.01.004, 2013a.
- Dai, Z., Liu, J. T., Wei, W., and Chen, J.: Detection of the Three Gorges Dam influence on the Changjiang (Yangtze River) submerged delta, *Sci Rep*, 4, 6600, doi: 10.1038/srep06600, 2014.
- Dai, Z.-J., Chu, A., Li, W.-H., Li, J.-F., and Wu, H.-L.: Has Suspended Sediment Concentration Near the Mouth Bar of the Yangtze (Changjiang) Estuary Been Declining in Recent Years?, *Journal of Coastal Research*, 289, 809–818, doi:10.2112/jcoastres-d-11-00200.1, 2013b.
- Davis, J.: A morphogenic approach to world shorelines, *Zeitschrift für geomorphologie*, pp. 127–142, 1964.
- de Jonge, V. N., Schuttelaars, H. M., van Beusekom, J. E. E., Talke, S. A., and de Swart, H. E.: The influence of channel deepening on estuarine turbidity levels and dynamics, as exemplified by the Ems estuary, *Estuarine, Coastal and Shelf Science*, 139, 46–59, doi:10.1016/j.ecss.2013.12.030, 2014.
- De Vriend, H. J., Wang, Z. B., Ysebaert, T., Herman, P. M., and Ding, P.: Eco-morphological problems in the Yangtze Estuary and the Western Scheldt, *Wetlands*, 31, 1033–1042, 2011.
- Dijkstra, Y.: Regime shifts in sediment concentrations in tide-dominated estuaries, *Thesis*, 2019.

- Dijkstra, Y. M., Schuttelaars, H. M., and Burchard, H.: Generation of exchange flows in estuaries by tidal and gravitational eddy viscosity-shear covariance (ESCO), *Journal of Geophysical Research: Oceans*, 122, 4217–4237, 2017.
- Dijkstra, Y. M., Schuttelaars, H. M., and Winterwerp, J. C.: The hyperturbid state of the water column in estuaries and rivers: the importance of hindered settling, *Ocean Dynamics*, 68, 377–389, 2018.
- Dijkstra, Y. M., Schuttelaars, H. M., and Schramkowski, G. P.: A Regime Shift From Low to High Sediment Concentrations in a Tide-Dominated Estuary, *Geophysical Research Letters*, 46, 4338–4345, 2019a.
- Dijkstra, Y. M., Schuttelaars, H. M., Schramkowski, G. P., and Brouwer, R. L.: Modeling the transition to high sediment concentrations as a response to channel deepening in the Ems River Estuary, *Journal of Geophysical Research: Oceans*, 124, 1578–1594, 2019b.
- Donker, J. J. and de Swart, H. E.: Effects of bottom slope, flocculation and hindered settling on the coupled dynamics of currents and suspended sediment in highly turbid estuaries, a simple model, *Ocean dynamics*, 63, 311–327, 2013.
- Doxaran, D., Froidefond, J.-M., Castaing, P., and Babin, M.: Dynamics of the turbidity maximum zone in a macrotidal estuary (the Gironde, France): Observations from field and MODIS satellite data, *Estuarine, Coastal and Shelf Science*, 81, 321–332, doi:10.1016/j.ecss.2008.11.013, 2009.
- Dronkers, J.: Tidal Asymmetry and Estuarine Morphology, *Netherlands Journal of Sea Research*, 20, 117–131, doi:10.1016/0077-7579(86)90036-0, URL <GotoISI>://WOS:A1986E116200004, 1986.
- Dunn, F. E., Darby, S. E., Nicholls, R. J., Cohen, S., Zarfl, C., and Fekete, B. M.: Projections of declining fluvial sediment delivery to major deltas worldwide in response to climate change and anthropogenic stress, *Environmental Research Letters*, 14, 084 034, 2019.
- Dyer, K.: Coastal and estuarine sediment dynamics, JOHN WILEY AND SONS, CHICHESTER, SUSSEX(UK), 1986, 358, 1986.
- Dyer, K. R.: Fine sediment particle transport in estuaries, pp. 295–310, Springer, 1988.
- Dyer, K. R.: Estuaries: a physical introduction, 2nd edition, eds. John Wiley Sons, 1997.
- Egbert, G. D. and Erofeeva, S. Y.: Efficient inverse modeling of barotropic ocean tides, *Journal of Atmospheric and Oceanic Technology*, 19, 183–204, 2002.
- Egbert, G. D., Bennett, A. F., and Foreman, M. G.: TOPEX/POSEIDON tides estimated using a global inverse model, *Journal of Geophysical Research: Oceans*, 99, 24 821–24 852, 1994.
- Eidam, E. F., Nittrouer, C. A., Ogston, A. S., DeMaster, D. J., Liu, J. P., Nguyen, T. T., and Nguyen, T. N.: Dynamic controls on shallow clinoform geometry: Mekong Delta, Vietnam, *Continental Shelf Research*, 147, 165–181, doi:10.1016/j.csr.2017.06.001, 2017.

- Eslami, S., Hoekstra, P., Nguyen Trung, N., Ahmed Kantoush, S., Van Binh, D., Duc Dung, D., Tran Quang, T., and van der Vegt, M.: Tidal amplification and salt intrusion in the Mekong Delta driven by anthropogenic sediment starvation, *Scientific Reports*, 9, 18 746, doi:10.1038/s41598-019-55018-9, URL <https://doi.org/10.1038/s41598-019-55018-9>, 2019.
- Fain, A. M., Jay, D. A., Wilson, D. J., Orton, P. M., and Baptista, A. M.: Seasonal and tidal monthly patterns of particulate matter dynamics in the Columbia River estuary, *Estuaries*, 24, 770–786, 2001.
- Fairbridge, R.: The estuary: its definition and geochemical role. *Chemistry and biogeochemistry of estuaries*. E. Olausson and I. Cato, New York, Wiley, 1, 35, 1980.
- Familkhalili, R. and Talke, S. A.: The effect of channel deepening on tides and storm surge: A case study of Wilmington, NC, *Geophysical research letters*, 43, 9138–9147, 2016.
- Fan, D., Wu, Y., Zhang, Y., Burr, G., Huo, M., and Li, J.: South Flank of the Yangtze Delta: Past, present, and future, *Marine Geology*, 392, 78–93, doi:10.1016/j.margeo.2017.08.015, 2017.
- Ferrarin, C., Tomasin, A., Bajo, M., Petrizzo, A., and Umgieser, G.: Tidal changes in a heavily modified coastal wetland, *Continental Shelf Research*, 101, 22–33, 2015.
- Festa, J. F. and Hansen, D. V.: Turbidity maxima in partially mixed estuaries: A two-dimensional numerical model, *Estuarine and Coastal Marine Science*, 7, 347–359, 1978.
- Fettweis, M., Sas, M., and Monbaliu, J.: Seasonal, neap-spring and tidal variation of cohesive sediment concentration in the Scheldt Estuary, Belgium, *Estuarine Coastal and Shelf Science*, 47, 21–36, doi:10.1006/ecss.1998.0338, URL [WOS:000074901500002](https://www.wosid.org/doi/10.1006/ecss.1998.0338), 1998.
- Folke, C., Carpenter, S., Walker, B., Scheffer, M., Elmqvist, T., Gunderson, L., and Holling, C. S.: Regime shifts, resilience, and biodiversity in ecosystem management, *Annu. Rev. Ecol. Evol. Syst.*, 35, 557–581, 2004.
- Friedrichs, C. and Aubrey, D.: Uniform bottom shear stress and equilibrium hypsometry of intertidal flats, *Mixing in estuaries and Coastal seas*, pp. 405–429, 1996.
- Friedrichs, C. T.: Tidal flat morphodynamics: a synthesis, pp. 137–170, doi:10.1016/b978-0-12-374711-2.00307-7, 2011.
- Friedrichs, C. T. and Aubrey, D. G.: Non-Linear Tidal Distortion in Shallow Well-Mixed Estuaries - a Synthesis, *Estuarine Coastal and Shelf Science*, 27, 521–545, doi:10.1016/0272-7714(88)90082-0, 1988.
- Friedrichs, C. T. and Aubrey, D. G.: Tidal propagation in strongly convergent channels, *Journal of Geophysical Research*, 99, 3321, doi:10.1029/93jc03219, 1994.

- Fu, G.: Recent changes of tidal characteristics in the Yangtze Estuary, *Port and Waterway Engineering*, 11, 61–69 (Chinese with Abstract in English), 2013.
- Fugate, D. C., Friedrichs, C. T., and Sanford, L. P.: Lateral dynamics and associated transport of sediment in the upper reaches of a partially mixed estuary, Chesapeake Bay, USA, *Continental Shelf Research*, 27, 679–698, doi:<https://doi.org/10.1016/j.csr.2006.11.012>, URL <http://www.sciencedirect.com/science/article/pii/S0278434306003682>, 2007.
- Gabioux, M., Vinzon, S. B., and Paiva, A. M.: Tidal propagation over fluid mud layers on the Amazon shelf, *Continental Shelf Research*, 25, 113–125, 2005.
- Galloway, W. E.: Process framework for describing the morphologic and stratigraphic evolution of deltaic depositional systems, 1975.
- Gao, A., Yang, S. L., Li, G., Li, P., and Chen, S. L.: Long-Term Morphological Evolution of a Tidal Island as Affected by Natural Factors and Human Activities, the Yangtze Estuary, *Journal of Coastal Research*, 261, 123–131, doi:10.2112/08-1052.1, 2010.
- Gao, Z. and Zhang, L.: Multi-seasonal spectral characteristics analysis of coastal salt marsh vegetation in Shanghai, China, *Estuarine, Coastal and Shelf Science*, 69, 217–224, 2006.
- Ge, J., Ding, P., and Chen, C.: Impacts of Deep Waterway Project on local circulations and salinity in the Changjiang Estuary, China, vol. 32, 2010.
- Geyer, W. R.: The Importance of Suppression of Turbulence by Stratification on the Estuarine Turbidity Maximum, *Estuaries*, 16, 113–125, doi:10.2307/1352769, 1993.
- Geyer, W. R. and MacCready, P.: The Estuarine Circulation, *Annual Review of Fluid Mechanics*, 46, 175–197, doi:10.1146/annurev-fluid-010313-141302, 2014.
- Geyer, W. R., Woodruff, J. D., and Traykovski, P.: Sediment transport and trapping in the Hudson River estuary, *Estuaries*, 24, 670–679, 2001.
- Gong, W. and Shen, J.: The response of salt intrusion to changes in river discharge and tidal mixing during the dry season in the Modaomen Estuary, China, *Continental Shelf Research*, 31, 769–788, 2011.
- Grabemann, I., Uncles, R. J., Krause, G., and Stephens, J. A.: Behaviour of Turbidity Maxima in the Tamar (U.K.) and Weser (F.R.G.) Estuaries, *Estuarine, Coastal and Shelf Science*, 45, 235–246, doi:<https://doi.org/10.1006/ecss.1996.0178>, URL <http://www.sciencedirect.com/science/article/pii/S027277149690178X>, 1997.
- Grasso, F. and Le Hir, P.: Influence of morphological changes on suspended sediment dynamics in a macrotidal estuary: diachronic analysis in the Seine Estuary (France) from 1960 to 2010, *Ocean Dynamics*, 69, 83–100, 2019.

- Grasso, F., Verney, R., Le Hir, P., Thouvenin, B., Schulz, E., Kervella, Y., Khojasteh Pour Fard, I., Lemoine, J., Dumas, E., and Garnier, V.: Suspended sediment dynamics in the macrotidal Seine Estuary (France): 1. Numerical modeling of turbidity maximum dynamics, *Journal of Geophysical Research: Oceans*, 123, 558–577, 2018.
- Groen, P.: On the residual transport of suspended matter by an alternating tidal current, *Netherlands Journal of Sea Research*, 3, 564–574, 1967.
- Guo, L. and He, Q.: Freshwater flocculation of suspended sediments in the Yangtze River, China, *Ocean Dynamics*, 61, 371–386, 2011.
- Guo, L., van der Wegen, M., Jay, D. A., Matte, P., Wang, Z. B., Roelvink, D., and He, Q.: River-tide dynamics: Exploration of nonstationary and nonlinear tidal behavior in the Yangtze River estuary, *Journal of Geophysical Research-Oceans*, 120, 3499–3521, doi: 10.1002/2014jc010491, 2015.
- Guo, L., Su, N., Zhu, C., and He, Q.: How have the river discharges and sediment loads changed in the Changjiang River basin downstream of the Three Gorges Dam?, *Journal of Hydrology*, 560, 259–274, doi:10.1016/j.jhydrol.2018.03.035, 2018a.
- Guo, W., Wang, X. H., Ding, P., Ge, J., and Song, D.: A system shift in tidal choking due to the construction of Yangshan Harbour, Shanghai, China, *Estuarine, Coastal and Shelf Science*, 206, 49–60, 2018b.
- Hare, S. R. and Mantua, N. J.: Empirical evidence for North Pacific regime shifts in 1977 and 1989, *Progress in oceanography*, 47, 103–145, 2000.
- Hay, C. C., Morrow, E., Kopp, R. E., and Mitrovica, J. X.: Probabilistic reanalysis of twentieth-century sea-level rise, *Nature*, 517, 481–484, 2015.
- Hayes, M. O.: Morphology of sand accumulation in estuaries: an introduction to the symposium, pp. 3–22, Elsevier, 1975.
- Hesse, R. F., Zorndt, A., and Fröhle, P.: Modelling dynamics of the estuarine turbidity maximum and local net deposition, *Ocean Dynamics*, 69, 489–507, 2019.
- Hill, P. S., Voulgaris, G., and Trowbridge, J. H.: Controls on floc size in a continental shelf bottom boundary layer, *Journal of Geophysical Research: Oceans*, 106, 9543–9549, 2001.
- Hori, K., Saito, Y., Zhao, Q. H., and Wang, P. X.: Architecture and evolution of the tide-dominated Changjiang (Yangtze) River delta, China, *Sedimentary Geology*, 146, 249–264, doi:10.1016/S0037-0738(01)00122-1, 2002.
- Horrevoets, A., Savenije, H., Schuurman, J., and Graas, S.: The influence of river discharge on tidal damping in alluvial estuaries, *Journal of Hydrology*, 294, 213–228, 2004.
- Hossain, S., Eyre, B. D., and McKee, L. J.: Impacts of dredging on dry season suspended sediment concentration in the Brisbane River estuary, Queensland, Australia, *Estuarine, Coastal and Shelf Science*, 61, 539–545, doi:10.1016/j.ecss.2004.06.017, 2004.

- Hu, K. and Ding, P.: The Effect of Deep Waterway Constructions on Hydrodynamics and Salinities in Yangtze Estuary, China, *Journal of Coastal Research*, pp. 961–965, 2009.
- Hu, K., Ding, P., Wang, Z., and Yang, S.: A 2D/3D hydrodynamic and sediment transport model for the Yangtze Estuary, China, *Journal of Marine Systems*, 77, 114–136, doi:10.1016/j.jmarsys.2008.11.014, 2009.
- Hu, K. L., Ding, P. X., Zhu, S. X., and Cao, Z. Y.: 2-D current field numerical simulation integrating Yangtze Estuary with Hangzhou Bay, China *Ocean Engineering*, 14, 89–102, 2000.
- Huang, H. and Zhang, L.: A study of the population dynamics of *Spartina alterniflora* at Jiuduansha shoals, Shanghai, China, *Ecological Engineering*, 29, 164–172, doi:10.1016/j.ecoleng.2006.06.005, 2007.
- Hudson, A. S., Talke, S. A., and Jay, D. A.: Using satellite observations to characterize the response of estuarine turbidity maxima to external forcing, *Estuaries and Coasts*, 40, 343–358, 2017.
- Huijts, K. M. H., Schuttelaars, H. M., de Swart, H. E., and Valle-Levinson, A.: Lateral entrapment of sediment in tidal estuaries: An idealized model study, *Journal of Geophysical Research*, 111, doi:10.1029/2006jc003615, 2006.
- IPCC: Climate change 2014: synthesis report. Contribution of Working Groups I, II and III to the fifth assessment report of the Intergovernmental Panel on Climate Change [Core Writing Team, R.K. Pachauri and L.A. Meyer (eds.)], Report, 2014.
- Jahan, R. and Choi, J. K.: Climate regime shift and phytoplankton phenology in a macrotidal estuary: long-term surveys in Gyeonggi Bay, Korea, *Estuaries and coasts*, 37, 1169–1187, 2014.
- Jalón-Rojas, I., Schmidt, S., and Sottolichio, A.: Turbidity in the fluvial Gironde Estuary (southwest France) based on 10-year continuous monitoring: sensitivity to hydrological conditions, *Hydrology and Earth System Sciences*, 19, 2805, 2015.
- Jalón-Rojas, I., Schmidt, S., Sottolichio, A., and Bertier, C.: Tracking the turbidity maximum zone in the Loire Estuary (France) based on a long-term, high-resolution and high-frequency monitoring network, *Continental Shelf Research*, 117, 1–11, 2016.
- Jalón-Rojas, I., Sottolichio, A., Hanquiez, V., Fort, A., and Schmidt, S.: To what extent multidecadal changes in morphology and fluvial discharge impact tide in a convergent (turbid) tidal river, *Journal of Geophysical Research: Oceans*, 123, 3241–3258, 2018.
- Jay, D. A.: Green's law revisited: Tidal long-wave propagation in channels with strong topography, *Journal of Geophysical Research: Oceans*, 96, 20 585–20 598, 1991.
- Jay, D. A. and Musiak, J. D.: Particle trapping in estuarine tidal flows, *Journal of Geophysical Research*, 99, 20 445, doi:10.1029/94jc00971, 1994.

- Jay, D. A. and Musiak, J. D.: Internal tidal asymmetry in channel flows: Origins and consequences, *Coastal and Estuarine Studies*, pp. 211–249, 1996.
- Jay, D. A. and Smith, J. D.: Circulation, density distribution and neap-spring transitions in the Columbia River Estuary, *Progress in Oceanography*, 25, 81–112, 1990.
- Jay, D. A., Leffler, K., and Degens, S.: Long-term evolution of Columbia River tides, *Journal of waterway, port, coastal, and ocean engineering*, 137, 182–191, 2011.
- Jeong, S., Yeon, K., Hur, Y., and Oh, K.: Salinity intrusion characteristics analysis using EFDC model in the downstream of Geum River, *Journal of Environmental Sciences*, 22, 934–939, doi:[https://doi.org/10.1016/S1001-0742\(09\)60201-1](https://doi.org/10.1016/S1001-0742(09)60201-1), URL <http://www.sciencedirect.com/science/article/pii/S1001074209602011>, 2010.
- Jeppesen, E., Søndergaard, M., Pedersen, A. R., Jürgens, K., Strzelczak, A., Lauridsen, T. L., and Johansson, L. S.: Salinity induced regime shift in shallow brackish lagoons, *Ecosystems*, 10, 48–58, 2007.
- Jeuken, M. C. J. L. and Wang, Z. B.: Impact of dredging and dumping on the stability of ebb–flood channel systems, *Coastal Engineering*, 57, 553–566, doi:10.1016/j.coastaleng.2009.12.004, 2010.
- Jia, J., Gao, J., Cai, T., Li, Y., Yang, Y., Wang, Y. P., Xia, X., Li, J., Wang, A., and Gao, S.: Sediment accumulation and retention of the Changjiang (Yangtze River) subaqueous delta and its distal muds over the last century, *Marine Geology*, 401, 2–16, doi:10.1016/j.margeo.2018.04.005, 2018.
- Jiang, C., Li, J., and de Swart, H. E.: Effects of navigational works on morphological changes in the bar area of the Yangtze Estuary, *Geomorphology*, 139–140, 205–219, doi:10.1016/j.geomorph.2011.10.020, 2012.
- Jiang, C., de Swart, H. E., Li, J., and Liu, G.: Mechanisms of along-channel sediment transport in the North Passage of the Yangtze Estuary and their response to large-scale interventions, *Ocean Dynamics*, 63, 283–305, doi:10.1007/s10236-013-0594-4, 2013a.
- Jiang, X., Lu, B., and He, Y.: Response of the turbidity maximum zone to fluctuations in sediment discharge from river to estuary in the Changjiang Estuary (China), *Estuarine, Coastal and Shelf Science*, 131, 24–30, doi:10.1016/j.ecss.2013.07.003, 2013b.
- Kappenberg, J. and Grabemann, I.: Variability of the mixing zones and estuarine turbidity maxima in the Elbe and Weser estuaries, *Estuaries*, 24, 699–706, 2001.
- Kerner, M.: Effects of deepening the Elbe Estuary on sediment regime and water quality, *Estuarine, Coastal and Shelf Science*, 75, 492–500, doi:10.1016/j.ecss.2007.05.033, 2007.
- Kirby, R.: Practical implications of tidal flat shape, *Continental Shelf Research*, 20, 1061–1077, doi:10.1016/S0278-4343(00)00012-1, 2000.

- Kuang, C.-p., Chen, W., Gu, J., and He, L.-l.: Comprehensive analysis on the sediment siltation in the upper reach of the deepwater navigation channel in the Yangtze Estuary, *Journal of Hydrodynamics*, 26, 299–308, doi:10.1016/s1001-6058(14)60033-0, 2014.
- Kuijper, K. and Van Rijn, L. C.: Analytical and numerical analysis of tides and salinities in estuaries; Part II: Salinity distributions in prismatic and convergent tidal channels, *Ocean Dynamics*, 61, 1743–1765, 2011.
- Kukulka, T. and Jay, D. A.: Impacts of Columbia River discharge on salmonid habitat: 1. A nonstationary fluvial tide model, *Journal of Geophysical Research: Oceans*, 108, doi:10.1029/2002jc001382, 2003.
- Kumar, M., Schuttelaars, H. M., and Roos, P. C.: Three-dimensional semi-idealized model for estuarine turbidity maxima in tidally dominated estuaries, *Ocean Modelling*, 113, 1–21, doi:10.1016/j.ocemod.2017.03.005, 2017.
- Lane, A.: Bathymetric evolution of the Mersey Estuary, UK, 1906–1997: causes and effects, *Estuarine Coastal and Shelf Science*, 59, 249–263, doi:10.1016/j.ecss.2003.09.003, 2004.
- Le Hir, P., Roberts, W., Cazaillet, O., Christie, M., Bassoullet, P., and Bacher, C.: Characterization of intertidal flat hydrodynamics, *Continental Shelf Research*, 20, 1433–1459, doi:10.1016/S0278-4343(00)00031-5, 2000.
- Le Hir, P., Ficht, A., Jacinto, R. S., Lesueur, P., Dupont, J.-P., Lafite, R., Brenon, I., Thouvenin, B., and Cugier, P.: Fine sediment transport and accumulations at the mouth of the Seine estuary (France), *Estuaries*, 24, 950–963, 2001.
- Lees, K., Pitois, S., Scott, C., Frid, C., and Mackinson, S.: Characterizing regime shifts in the marine environment, *Fish and fisheries*, 7, 104–127, 2006.
- Lehman, P.: The influence of climate on phytoplankton community biomass in San Francisco Bay Estuary, *Limnology and Oceanography*, 45, 580–590, 2000.
- Lerczak, J. A. and Rockwell Geyer, W.: Modeling the lateral circulation in straight, stratified estuaries, *Journal of Physical Oceanography*, 34, 1410–1428, 2004.
- Lerczak, J. A., Geyer, W. R., and Ralston, D. K.: The temporal response of the length of a partially stratified estuary to changes in river flow and tidal amplitude, *Journal of Physical Oceanography*, 39, 915–933, 2009.
- Lesser, G. R., Roelvink, J. A., van Kester, J. A. T. M., and Stelling, G. S.: Development and validation of a three-dimensional morphological model, *Coastal Engineering*, 51, 883–915, doi:10.1016/j.coastaleng.2004.07.014, 2004.
- Li, C. and O’Donnell, J.: The effect of channel length on the residual circulation in tidally dominated channels, *Journal of Physical Oceanography*, 35, 1826–1840, 2005.
- Li, H., Chen, H., Wang, H., and Yu, E.: Future precipitation changes over China under 1.5 C and 2.0 C global warming targets by using CORDEX regional climate models, *Science of the Total Environment*, 640, 543–554, 2018a.

- Li, J., He, Q., Xiang, W., Wan, X., and Shen, H.: Fluid mud transportation at water wedge in the Changjiang Estuary, *Science in China Series B: Chemistry*, 44, 47–56, 2001.
- Li, J. F. and Zhang, C.: Sediment resuspension and implications for turbidity maximum in the Changjiang Estuary, *Marine Geology*, 148, 117–124, doi:10.1016/S0025-3227(98)00003-6, 1998.
- Li, L., He, Z., Xia, Y., and Dou, X.: Dynamics of sediment transport and stratification in Changjiang River Estuary, China, *Estuarine, Coastal and Shelf Science*, 213, 1–17, 2018b.
- Li, L., Ni, J., Chang, F., Yue, Y., Frolova, N., Magritsky, D., Borthwick, A. G. L., Ciais, P., Wang, Y., Zheng, C., and Walling, D. E.: Global trends in water and sediment fluxes of the world's large rivers, *Science Bulletin*, 65, 62–69, doi:10.1016/j.scib.2019.09.012, 2020a.
- Li, L., Zhu, J., Chant, R. J., Wang, C., and Pareja-Roman, L. F.: Effect of dikes on salt-water intrusion under various wind conditions in the Changjiang Estuary, *Journal of Geophysical Research: Oceans*, 125, e2019JC015685, 2020b.
- Li, M. and Chen, Z.: An Assessment of Saltwater Intrusion in the Changjiang (Yangtze) River Estuary, China, pp. 31–43, Elsevier, 2019.
- Li, P., Yang, S. L., Milliman, J. D., Xu, K. H., Qin, W. H., Wu, C. S., Chen, Y. P., and Shi, B. W.: Spatial, Temporal, and Human-Induced Variations in Suspended Sediment Concentration in the Surface Waters of the Yangtze Estuary and Adjacent Coastal Areas, *Estuaries and Coasts*, 35, 1316–1327, doi:10.1007/s12237-012-9523-x, 2012.
- Li, X., Liu, J. P., and Tian, B.: Evolution of the Jiuduansha wetland and the impact of navigation works in the Yangtze Estuary, China, *Geomorphology*, 253, 328–339, doi: 10.1016/j.geomorph.2015.10.031, 2016a.
- Li, X., Zhu, J., Yuan, R., Qiu, C., and Wu, H.: Sediment trapping in the Changjiang Estuary: Observations in the North Passage over a spring-neap tidal cycle, *Estuarine, Coastal and Shelf Science*, 177, 8–19, doi:10.1016/j.ecss.2016.05.004, 2016b.
- Lin, J. and Kuo, A. Y.: Secondary turbidity maximum in a partially mixed microtidal estuary, *Estuaries*, 24, 707–720, 2001.
- Lin, J., He, Q., Guo, L., van Prooijen, B. C., and Wang, Z. B.: An integrated optic and acoustic (IOA) approach for measuring suspended sediment concentration in highly turbid environments, *Marine Geology*, p. 106062, 2019.
- Lin, J., van Prooijen, B. C., Guo, L., Zhu, C., He, Q., and Wang, Z. B.: Regime shifts in the Changjiang (Yangtze River) Estuary: The role of concentrated benthic suspensions, *Marine Geology*, 433, 106403, 2021.
- Liu, G., Zhu, J., Wang, Y., Wu, H., and Wu, J.: Tripod measured residual currents and sediment flux: Impacts on the silting of the Deepwater Navigation Channel in the Changjiang Estuary, *Estuarine, Coastal and Shelf Science*, 93, 192–201, doi:10.1016/j.ecss.2010.08.008, 2011.

- Liu, H.: Sediment mixing and exchange processes in the Yangtze Estuary, Thesis, East China Normal University, 2009.
- Liu, H., He, Q., Wang, Z., Weltje, G. J., and Zhang, J.: Dynamics and spatial variability of near-bottom sediment exchange in the Yangtze Estuary, China, *Estuarine, Coastal and Shelf Science*, 86, 322–330, doi:10.1016/j.ecss.2009.04.020, 2010.
- Liu, J. P., Xu, K. H., Li, A. C., Milliman, J. D., Velozzi, D. M., Xiao, S. B., and Yang, Z. S.: Flux and fate of Yangtze River sediment delivered to the East China Sea, *Geomorphology*, 85, 208–224, doi:10.1016/j.geomorph.2006.03.023, 2007.
- Liu, Y. and Scavia, D.: Analysis of the Chesapeake Bay hypoxia regime shift: insights from two simple mechanistic models, *Estuaries and coasts*, 33, 629–639, 2010.
- Lopes, C. L., Plecha, S., Silva, P. A., and Dias, J. M.: Influence of morphological changes in a lagoon flooding extension: case study of Ria de Aveiro (Portugal), *Journal of Coastal Research*, 65, 1158–1163, 2013.
- Lu, S., Tong, C., Lee, D.-Y., Zheng, J., Shen, J., Zhang, W., and Yan, Y.: Propagation of tidal waves up in Yangtze Estuary during the dry season, *Journal of Geophysical Research: Oceans*, 120, 6445–6473, doi:10.1002/2014jc010414, 2015.
- Luan, H. L., Ding, P. X., Wang, Z. B., Ge, J. Z., and Yang, S. L.: Decadal morphological evolution of the Yangtze Estuary in response to river input changes and estuarine engineering projects, *Geomorphology*, 265, 12–23, doi:10.1016/j.geomorph.2016.04.022, 2016.
- Luo, X., Yang, S., and Zhang, J.: The impact of the Three Gorges Dam on the downstream distribution and texture of sediments along the middle and lower Yangtze River (Changjiang) and its estuary, and subsequent sediment dispersal in the East China Sea, *Geomorphology*, 179, 126–140, 2012.
- Luo, X. X., Yang, S. L., Wang, R. S., Zhang, C. Y., and Li, P.: New evidence of Yangtze delta recession after closing of the Three Gorges Dam, *Sci Rep*, 7, 41 735, doi:10.1038/srep41735, 2017.
- Ma, G., Shi, F., Liu, S., and Qi, D.: Hydrodynamic modeling of Changjiang Estuary: Model skill assessment and large-scale structure impacts, *Applied Ocean Research*, 33, 69–78, doi:10.1016/j.apor.2010.10.004, 2011.
- Matte, P., Jay, D. A., and Zaron, E. D.: Adaptation of Classical Tidal Harmonic Analysis to Nonstationary Tides, with Application to River Tides, *Journal of Atmospheric and Oceanic Technology*, 30, 569–589, doi:10.1175/jtech-d-12-00016.1, 2013.
- Miles, J. W.: On the stability of heterogeneous shear flows, *Journal of Fluid Mechanics*, 10, 496–508, 1961.
- Mitchell, S., West, J., Arundale, A., Guymer, I., and Couperthwaite, J.: Dynamics of the turbidity maxima in the upper Humber estuary system, UK, *Marine Pollution Bulletin*, 37, 190–205, 1998.

- Mitchell, S. B., Green, M. O., MacDonald, I. T., and Pritchard, M.: Field studies of estuarine turbidity under different freshwater flow conditions, Kaipara River, New Zealand, *Estuarine, Coastal and Shelf Science*, 198, 542–554, 2017.
- Monismith, S. G., Kimmerer, W., Burau, J. R., and Stacey, M. T.: Structure and flow-induced variability of the subtidal salinity field in northern San Francisco Bay, *Journal of Physical Oceanography*, 32, 3003–3019, doi:Doi10.1175/1520-0485(2002)032<3003:Safivo>2.0.Co;2, URL <GotoISI>://WOS:000178834000003, 2002.
- Morris, J. T., Sundareshwar, P., Nietch, C. T., Kjerfve, B., and Cahoon, D. R.: Responses of coastal wetlands to rising sea level, *Ecology*, 83, 2869–2877, 2002.
- Nguyen, D. H., Umeyama, M., and Shintani, T.: Importance of geometric characteristics for salinity distribution in convergent estuaries, *Journal of Hydrology*, 448–449, 1–13, doi:https://doi.org/10.1016/j.jhydrol.2011.10.044, URL <http://www.sciencedirect.com/science/article/pii/S0022169412003654>, 2012.
- North, E. W. and Houde, E. D.: Retention of white perch and striped bass larvae: biological-physical interactions in Chesapeake Bay estuarine turbidity maximum, *Estuaries*, 24, 756–769, 2001.
- Paerl, H. W., Hall, N. S., Hounshell, A. G., Luettich, R. A., Rossignol, K. L., Osburn, C. L., and Bales, J.: Recent increase in catastrophic tropical cyclone flooding in coastal North Carolina, USA: Long-term observations suggest a regime shift, *Scientific reports*, 9, 1–9, 2019.
- Pan, H., Lv, X., Wang, Y., Matte, P., Chen, H., and Jin, G.: Exploration of Tidal-Fluvial Interaction in the Columbia River Estuary Using S_TIDE, *Journal of Geophysical Research: Oceans*, 123, 6598–6619, 2018.
- Pang, C., Zhao, E., and Yang, Y.: Numerical simulation on the process of saltwater intrusion and its impact on the suspended sediment concentration in the Changjiang (Yangtze) estuary, *Chinese Journal of Oceanology and Limnology*, 28, 609–619, doi:10.1007/s00343-010-9254-4, 2010.
- Park, K., Wang, H. V., Kim, S.-C., Oh, J.-H. J. E., and Coasts: A model study of the estuarine turbidity maximum along the main channel of the upper Chesapeake Bay, 31, 115–133, 2008.
- Parker, B. B.: Frictional effects on the tidal dynamics of a shallow estuary, *Journal article*, 1984.
- Partheniades, E.: Erosion and deposition of cohesive soils, *Journal of the Hydraulics Division*, 91, 105–139, 1965.
- Pawlowicz, R., Beardsley, B., and Lentz, S.: Classical tidal harmonic analysis including error estimates in MATLAB using T-TIDE, *Computers & Geosciences*, 28, 929–937, doi:10.1016/S0098-3004(02)00013-4, 2002.

- Petersen, J. K., Hansen, J. W., Laursen, M. B., Clausen, P., Carstensen, J., and Conley, D. J.: Regime shift in a coastal marine ecosystem, *Ecological Applications*, 18, 497–510, 2008.
- Postma, H.: Hydrography of the Dutch Wadden sea, *Archives néerlandaises de Zoologie*, 10, 405–511, 1954.
- Postma, H.: Transport and accumulation of suspended matter in the Dutch Wadden Sea, *Netherlands Journal of Sea Research*, 1, 148–190, 1961.
- Prandle, D.: Saline intrusion in partially mixed estuaries, *Estuarine, Coastal and Shelf Science*, 59, 385–397, doi:<https://doi.org/10.1016/j.ecss.2003.10.001>, URL <http://www.sciencedirect.com/science/article/pii/S027277140300307X>, 2004.
- Prandle, D. and Lane, A.: Sensitivity of estuaries to sea level rise: Vulnerability indices, *Estuarine, Coastal and Shelf Science*, 160, 60–68, doi:<https://doi.org/10.1016/j.ecss.2015.04.001>, URL <http://www.sciencedirect.com/science/article/pii/S0272771415001250>, 2015.
- Prichard, D.: Estuarine circulation patterns, *Proc. Amer. Soc. Civil Eng.*, 81, 1–11, 1955.
- Pritchard, D. W.: What is an estuary: physical viewpoint, *American Association for the Advancement of Science*, 1967.
- Pu, X., Shi, J. Z., Hu, G.-D., and Xiong, L.-B.: Circulation and mixing along the North Passage in the Changjiang River estuary, China, *Journal of Marine Systems*, 148, 213–235, 2015.
- Qiao, Y.: Erodibility of bed sediments in the Yangtze Estuary, Master thesis, East China Normal University, 2019.
- Ralston, D. K. and Geyer, W. R.: Response to Channel Deepening of the Salinity Intrusion, Estuarine Circulation, and Stratification in an Urbanized Estuary, *Journal of Geophysical Research: Oceans*, 124, 4784–4802, 2019.
- Ralston, D. K., Geyer, W. R., and Lerczak, J. A.: Subtidal Salinity and Velocity in the Hudson River Estuary: Observations and Modeling, *Journal of Physical Oceanography*, 38, 753–770, doi:[10.1175/2007jpo3808.1](https://doi.org/10.1175/2007jpo3808.1), 2008.
- Ralston, D. K., Geyer, W. R., and Lerczak, J. A.: Structure, variability, and salt flux in a strongly forced salt wedge estuary, *Journal of Geophysical Research: Oceans*, 115, 2010.
- Ralston, D. K., Geyer, W. R., and Warner, J. C.: Bathymetric controls on sediment transport in the Hudson River estuary: Lateral asymmetry and frontal trapping, *Journal of Geophysical Research: Oceans*, 117, doi:[10.1029/2012JC008124](https://doi.org/10.1029/2012JC008124), 2012.
- Ralston, D. K., Talke, S., Geyer, W. R., Al-Zubaidi, H. A., and Sommerfield, C. K.: Bigger tides, less flooding: Effects of dredging on barotropic dynamics in a highly modified estuary, *Journal of Geophysical Research: Oceans*, 124, 196–211, 2019.

- Reid, P. C., Hari, R. E., Beaugrand, G., Livingstone, D. M., Marty, C., Straile, D., Barichivich, J., Goberville, E., Adrian, R., Aono, Y., et al.: Global impacts of the 1980s regime shift, *Global change biology*, 22, 682–703, 2016.
- Renaud, F. G., Syvitski, J. P. M., Sebesvari, Z., Werners, S. E., Kremer, H., Kuenzer, C., Ramesh, R., Jeuken, A., and Friedrich, J.: Tipping from the Holocene to the Anthropocene: How threatened are major world deltas?, *Current Opinion in Environmental Sustainability*, 5, 644–654, doi:10.1016/j.cosust.2013.11.007, 2013.
- Rice, K. C., Hong, B., and Shen, J.: Assessment of salinity intrusion in the James and Chickahominy Rivers as a result of simulated sea-level rise in Chesapeake Bay, East Coast, USA, *Journal of Environmental Management*, 111, 61–69, doi:https://doi.org/10.1016/j.jenvman.2012.06.036, URL <http://www.sciencedirect.com/science/article/pii/S0301479712003519>, 2012.
- Richardson, J. and Zaki, W.: The sedimentation of a suspension of uniform spheres under conditions of viscous flow, *Chemical Engineering Science*, 3, 65–73, 1954.
- Roberts, W., Le Hir, P., and Whitehouse, R.: Investigation using simple mathematical models of the effect of tidal currents and waves on the profile shape of intertidal mudflats, *Continental Shelf Research*, 20, 1079–1097, 2000.
- Robins, P. E., Skov, M. W., Lewis, M. J., Giménez, L., Davies, A. G., Malham, S. K., Neill, S. P., McDonald, J. E., Whitton, T. A., Jackson, S. E., and Jago, C. F.: Impact of climate change on UK estuaries: A review of past trends and potential projections, *Estuarine, Coastal and Shelf Science*, 169, 119–135, doi:https://doi.org/10.1016/j.ecss.2015.12.016, URL <http://www.sciencedirect.com/science/article/pii/S02727771415301669>, 2016.
- Sanford, L. P. and Halka, J. P.: Assessing the paradigm of mutually exclusive erosion and deposition of mud, with examples from upper Chesapeake Bay, *Marine Geology*, 114, 37–57, 1993.
- Sanford, L. P., Suttles, S. E., and Halka, J. P.: Reconsidering the physics of the Chesapeake Bay estuarine turbidity maximum, *Estuaries*, 24, 655–669, 2001.
- Sassi, M. G., Hoitink, A. J. F., de Brye, B., Vermeulen, B., and Deleersnijder, E.: Tidal impact on the division of river discharge over tributary channels in the Mahakam Delta, *Ocean Dynamics*, 61, 2211–2228, doi:10.1007/s10236-011-0473-9, 2011.
- Savenije, H. H.: Predictive model for salt intrusion in estuaries, *Journal of Hydrology*, 148, 203–218, 1993.
- Savenije, H. H.: *Salinity and tides in alluvial estuaries*, Elsevier, 2006.
- Scheffer, M. and Carpenter, S. R.: Catastrophic regime shifts in ecosystems: linking theory to observation, *Trends in ecology & evolution*, 18, 648–656, 2003.
- Scheffer, M., Carpenter, S., Foley, J. A., Folke, C., and Walker, B.: Catastrophic shifts in ecosystems, *Nature*, 413, 591–596, 2001.

- Scheffer, M., Bascompte, J., Brock, W. A., Brovkin, V., Carpenter, S. R., Dakos, V., Held, H., Van Nes, E. H., Rietkerk, M., and Sugihara, G.: Early-warning signals for critical transitions, *Nature*, 461, 53–59, 2009.
- Schoellhamer, D. H.: Influence of salinity, bottom topography, and tides on locations of estuarine turbidity maxima in northern San Francisco Bay, vol. 3, pp. 343–357, Elsevier, 2000.
- Schrottke, K., Becker, M., Bartholomä, A., Flemming, B. W., and Hebbeln, D.: Fluid mud dynamics in the Weser estuary turbidity zone tracked by high-resolution side-scan sonar and parametric sub-bottom profiler, *Geo-Marine Letters*, 26, 185–198, 2006.
- Schubel, J. and Carter, H.: The estuary as a filter for fine-grained suspended sediment, pp. 81–105, Elsevier, 1984.
- Schubel, J. R.: Turbidity maximum of the northern Chesapeake Bay, *Science*, 161, 1013–5, doi:10.1126/science.161.3845.1013, URL <http://www.ncbi.nlm.nih.gov/pubmed/17812801>, 1968.
- Scully, M. E. and Friedrichs, C. T.: The influence of asymmetries in overlying stratification on near-bed turbulence and sediment suspension in a partially mixed estuary, *Ocean Dynamics*, 53, 208–219, 2003.
- Scully, M. E., Friedrichs, C., and Brubaker, J.: Control of estuarine stratification and mixing by wind-induced straining of the estuarine density field, *Estuaries*, 28, 321–326, 2005.
- Shen, F., Zhou, Y., Zhang, J., Wu, J., and Yang, S.: Remote-sensing analysis on spatial-temporal variation in vegetation on Jiuduansha wetland, *Oceanologia et Limnologia Sinica*, 37, 504, 2006.
- Shen, H., Gu, G., and Li, J.: Characteristics of the tidal wave propagation and its effect on channel evolution in the Yangtze Estuary, *Dynamic Process and Geomorphic Development of Changjiang Estuary*, Chen JY, Shen HT, Yun CX (eds.), Shanghai Scientific Technological Press, Shanghai, 1988.
- Sherwood, C. R., Jay, D. A., Harvey, R. B., Hamilton, P., and Simenstad, C. A.: Historical Changes in the Columbia River Estuary, *Progress in Oceanography*, 25, 299–352, doi:10.1016/0079-6611(90)90011-P, 1990.
- Shi, Z.: Behaviour of fine suspended sediment at the North passage of the Changjiang Estuary, China, *Journal of Hydrology*, 293, 180–190, doi:10.1016/j.jhydrol.2004.01.014, 2004.
- Simpson, J. H., Brown, J., Matthews, J., and Allen, G.: Tidal Straining, Density Currents, and Stirring in the Control of Estuarine Stratification, *Estuaries*, 13, 125–132, doi:10.2307/1351581, 1990.
- SOA: Bulletin of Chinese sea level rise, URL http://www.coi.gov.cn/gongbao/haipingmian/201603/t20160328_33812.html, 2015.

- Sommerfield, C. K. and Wong, K.-C.: Mechanisms of sediment flux and turbidity maintenance in the Delaware Estuary, *Journal of Geophysical Research*, 116, doi:10.1029/2010jc006462, 2011.
- Song, D. and Wang, X. H.: Suspended sediment transport in the Deepwater Navigation Channel, Yangtze River Estuary, China, in the dry season 2009: 2. Numerical simulations, *Journal of Geophysical Research: Oceans*, 118, 5568–5590, doi:10.1002/jgrc.20411, 2013.
- Song, D., Wang, X. H., Cao, Z., and Guan, W.: Suspended sediment transport in the Deepwater Navigation Channel, Yangtze River Estuary, China, in the dry season 2009: 1. Observations over spring and neap tidal cycles, *Journal of Geophysical Research: Oceans*, 118, 5555–5567, doi:10.1002/jgrc.20410, 2013.
- Syvitski, J. P. and Saito, Y.: Morphodynamics of deltas under the influence of humans, *Global and Planetary Change*, 57, 261–282, 2007.
- Syvitski, J. P., Kettner, A. J., Overeem, I., Hutton, E. W., Hannon, M. T., Brakenridge, G. R., Day, J., Vörösmarty, C., Saito, Y., Giosan, L., and Nicholls, R. J.: Sinking deltas due to human activities, *Nature Geoscience*, 2, 681–686, 2009.
- Talke, S. A. and Jay, D. A.: Changing tides: the role of natural and anthropogenic factors, *Annual review of marine science*, 12, 121–151, 2020.
- Talke, S. A., de Swart, H. E., De Jonge, V. J. E., and coasts: An idealized model and systematic process study of oxygen depletion in highly turbid estuaries, 32, 602–620, 2009a.
- Talke, S. A., de Swart, H. E., and Schuttelaars, H. M.: Feedback between residual circulations and sediment distribution in highly turbid estuaries: An analytical model, *Continental Shelf Research*, 29, 119–135, doi:10.1016/j.csr.2007.09.002, 2009b.
- Tang, J., Xu, J., Zhao, S., and Liu, W.: Research on saltwater intrusion of the south branch of the Changjiang Estuary based on measured data, *Resources and Environment in the Yangtze Basin*, 20, 677–684 (in Chinese), 2011.
- Thomas, C., Spearman, J., and Turnbull, M.: Historical morphological change in the Mersey Estuary, *Continental Shelf Research*, 22, 1775–1794, 2002.
- Uncles, R. and Stephens, J.: Nature of the turbidity maximum in the Tamar Estuary, UK, *Estuarine, Coastal and Shelf Science*, 36, 413–431, 1993.
- Uncles, R. and Stephens, J.: Salt intrusion in the Tweed Estuary, *Estuarine, Coastal and Shelf Science*, 43, 271–293, 1996.
- Uncles, R., Stephens, J., and Harris, C.: Runoff and tidal influences on the estuarine turbidity maximum of a highly turbid system: the upper Humber and Ouse Estuary, UK, *Marine Geology*, 235, 213–228, 2006.
- Uncles, R. J., Elliott, R. C. A., and Weston, S. A.: Observed Fluxes of Water, Salt and Suspended Sediment in a Partly Mixed Estuary, *Estuarine Coastal and Shelf Science*, 20, 147–167, doi:10.1016/0272-7714(85)90035-6, 1985.

- Van Kessel, T. and Vanlede, J.: Impact of harbour basins on mud dynamics Scheldt estuary, the framework of LTV. Report, 1200253, 2010.
- van Maanen, B. and Sottolichio, A.: Hydro- and sediment dynamics in the Gironde estuary (France): Sensitivity to seasonal variations in river inflow and sea level rise, *Continental Shelf Research*, 165, 37–50, doi:<https://doi.org/10.1016/j.csr.2018.06.001>, URL <http://www.sciencedirect.com/science/article/pii/S0278434317302480>, 2018.
- van Maren, D.: Grain size and sediment concentration effects on channel patterns of silt-laden rivers, *Sedimentary Geology*, 202, 297–316, 2007.
- van Maren, D., Vroom, J., Fettweis, M., and Vanlede, J.: Formation of the Zeebrugge coastal turbidity maximum: The role of uncertainty in near-bed exchange processes, *Marine Geology*, p. 106186, 2020.
- van Maren, D. S. and Winterwerp, J. C.: The role of flow asymmetry and mud properties on tidal flat sedimentation, *Continental Shelf Research*, 60, S71–S84, doi:10.1016/j.csr.2012.07.010, 2013.
- van Maren, D. S., Winterwerp, J. C., Decrop, B., Wang, Z. B., and Vanlede, J.: Predicting the effect of a Current Deflecting Wall on harbour siltation, *Continental Shelf Research*, 31, S182–S198, doi:<https://doi.org/10.1016/j.csr.2010.12.005>, URL <http://www.sciencedirect.com/science/article/pii/S0278434310003687>, 2011.
- van Maren, D. S., Yang, S.-L., and He, Q.: The impact of silt trapping in large reservoirs on downstream morphology: the Yangtze River, *Ocean Dynamics*, 63, 691–707, doi:10.1007/s10236-013-0622-4, 2013.
- van Maren, D. S., van Kessel, T., Cronin, K., and Sittoni, L.: The impact of channel deepening and dredging on estuarine sediment concentration, *Continental Shelf Research*, 95, 1–14, doi:10.1016/j.csr.2014.12.010, 2015a.
- van Maren, D. S., Winterwerp, J. C., and Vroom, J.: Fine sediment transport into the hyper-turbid lower Ems River: the role of channel deepening and sediment-induced drag reduction, *Ocean Dynamics*, 65, 589–605, doi:10.1007/s10236-015-0821-2, 2015b.
- van Maren, D. S., Oost, A. P., Wang, Z. B., and Vos, P. C.: The effect of land reclamations and sediment extraction on the suspended sediment concentration in the Ems Estuary, *Marine Geology*, 376, 147–157, doi:10.1016/j.margeo.2016.03.007, 2016.
- Van Rijn, L. C.: Principles of sediment transport in rivers, estuaries and coastal seas, vol. 1006, Aqua publications Amsterdam, 1993.
- Van Straaten, L. and Kuenen, P. H.: Accumulation of fine grained sediments in the Dutch Wadden Sea, *Netherlands Journal of Geosciences*, 19, 329–354, 1957.

- Vellinga, N., Hoitink, A., van der Vegt, M., Zhang, W., and Hoekstra, P.: Human impacts on tides overwhelm the effect of sea level rise on extreme water levels in the Rhine–Meuse delta, *Coastal engineering*, 90, 40–50, 2014.
- Vörösmarty, C. J., Meybeck, M., Fekete, B., Sharma, K., Green, P., and Syvitski, J. P. M.: Anthropogenic sediment retention: major global impact from registered river impoundments, *Global and Planetary Change*, 39, 169–190, doi:10.1016/s0921-8181(03)00023-7, 2003.
- Walling, D. E.: *The impact of global change on erosion and sediment transport by rivers: current progress and future challenges*, Unesco, 2009.
- Wan, Y. and Wang, L.: Numerical investigation of the factors influencing the vertical profiles of current, salinity, and SSC within a turbidity maximum zone, *International Journal of Sediment Research*, 32, 20–33, doi:10.1016/j.ijsrc.2016.07.003, 2017.
- Wan, Y. and Zhao, D.: Observation of saltwater intrusion and ETM dynamics in a stably stratified estuary: the Yangtze Estuary, China, *Environmental monitoring assessment*, 189, 89, 2017.
- Wan, Y., Gu, F., Wu, H., and Roelvink, D.: Hydrodynamic evolutions at the Yangtze Estuary from 1998 to 2009, *Applied Ocean Research*, 47, 291–302, doi:10.1016/j.apor.2014.06.009, 2014a.
- Wan, Y., Roelvink, D., Li, W., Qi, D., and Gu, F.: Observation and modeling of the storm-induced fluid mud dynamics in a muddy-estuarine navigational channel, *Geomorphology*, 217, 23–36, doi:10.1016/j.geomorph.2014.03.050, 2014b.
- Wang, D., Pan, H., Jin, G., and Lv, X.: Seasonal variation of the principal tidal constituents in the Bohai Sea, *Ocean Science*, 16, 1–14, 2020.
- Wang, J., Bai, S., Liu, P., Li, Y., Gao, Z., Qu, G., and Cao, G.: Channel sedimentation and erosion of the Jiangsu reach of the Yangtze River during the last 44 years, *Earth Surface Processes and Landforms*, 34, 1587–1593, 2009.
- Wang, J., Li, L., He, Z., Kalhor, N. A., and Xu, D.: Numerical modelling study of seawater intrusion in Indus River Estuary, Pakistan, *Ocean Engineering*, 184, 74–84, doi:https://doi.org/10.1016/j.oceaneng.2019.05.029, URL <http://www.sciencedirect.com/science/article/pii/S0029801819302574>, 2019a.
- Wang, Y., Dong, P., Oguchi, T., Chen, S., and Shen, H.: Long-term (1842–2006) morphological change and equilibrium state of the Changjiang (Yangtze) Estuary, China, *Continental Shelf Research*, 56, 71–81, doi:10.1016/j.csr.2013.02.006, 2013.
- Wang, Z. B., Winterwerp, J. C., and He, Q.: Interaction between suspended sediment and tidal amplification in the Guadalquivir Estuary, *Ocean Dynamics*, 64, 1487–1498, doi:10.1007/s10236-014-0758-x, 2014.

- Wang, Z. B., Van Maren, D. S., Ding, P. X., Yang, S. L., Van Prooijen, B. C., De Vet, P. L. M., Winterwerp, J. C., De Vriend, H. J., Stive, M. J. F., and He, Q.: Human impacts on morphodynamic thresholds in estuarine systems, *Continental Shelf Research*, 111, 174–183, doi:10.1016/j.csr.2015.08.009, 2015.
- Wang, Z. B., Vandenbruwaene, W., Taal, M., and Winterwerp, H.: Amplification and deformation of tidal wave in the Upper Scheldt Estuary, *Ocean Dynamics*, pp. 1–11, 2019b.
- Watanabe, K., Kasai, A., Antonio, E. S., Suzuki, K., Ueno, M., and Yamashita, Y.: Influence of salt-wedge intrusion on ecological processes at lower trophic levels in the Yura Estuary, Japan, *Estuarine, Coastal and Shelf Science*, 139, 67–77, doi: <https://doi.org/10.1016/j.ecss.2013.12.018>, URL <http://www.sciencedirect.com/science/article/pii/S0272771413005428>, 2014.
- Wei, W., Tang, Z., Dai, Z., Lin, Y., Ge, Z., and Gao, J.: Variations in tidal flats of the Changjiang (Yangtze) Estuary during 1950s–2010s: future crisis and policy implication, *Ocean & Coastal Management*, 108, 89–96, 2015.
- Wei, W., Mei, X., Dai, Z., and Tang, Z.: Recent morphodynamic evolution of the largest uninhibited island in the Yangtze (Changjiang) estuary during 1998–2014: Influence of the anthropogenic interference, *Continental Shelf Research*, 124, 83–94, doi:10.1016/j.csr.2016.05.011, 2016.
- Wei, W., Dai, Z., Mei, X., Liu, J. P., Gao, S., and Li, S.: Shoal morphodynamics of the Changjiang (Yangtze) estuary: Influences from river damming, estuarine hydraulic engineering and reclamation projects, *Marine Geology*, 386, 32–43, doi:10.1016/j.margeo.2017.02.013, 2017.
- Wernberg, T., Bennett, S., Babcock, R. C., De Bettignies, T., Cure, K., Depczynski, M., Dufois, F., Fromont, J., Fulton, C. J., Hovey, R. K., et al.: Climate-driven regime shift of a temperate marine ecosystem, *Science*, 353, 169–172, 2016.
- Winterwerp, J.: On the dynamics of high-concentrated mud suspensions, Thesis, doi: <http://resolver.tudelft.nl/uuid:0b503064-91ad-48de-8174-761c315f8132>, 1999.
- Winterwerp, J.: On the deposition flux of cohesive sediment, proceedings in marine science, 8, 209–226, 2007.
- Winterwerp, J. C.: Stratification effects by cohesive and noncohesive sediment, *Journal of Geophysical Research: Oceans*, 106, 22 559–22 574, doi:10.1029/2000jc000435, 2001.
- Winterwerp, J. C.: Fine sediment transport by tidal asymmetry in the high-concentrated Ems River: indications for a regime shift in response to channel deepening, *Ocean Dynamics*, 61, 203–215, doi:10.1007/s10236-010-0332-0, 2011.
- Winterwerp, J. C. and van Kessel, T.: Siltation by sediment-induced density currents, *Ocean Dynamics*, 53, 186–196, doi:10.1007/s10236-003-0038-7, 2003.

- Winterwerp, J. C. and Van Kesteren, W. G.: Introduction to the physics of cohesive sediment dynamics in the marine environment, Elsevier, 2004.
- Winterwerp, J. C. and Wang, Z. B.: Man-induced regime shifts in small estuaries—I: theory, *Ocean Dynamics*, 63, 1279–1292, doi:10.1007/s10236-013-0662-9, 2013.
- Winterwerp, J. C., Lely, M., and He, Q.: Sediment-induced buoyancy destruction and drag reduction in estuaries, *Ocean Dynamics*, 59, 781–791, doi:10.1007/s10236-009-0237-y, 2009.
- Winterwerp, J. C., Wang, Z. B., van Braeckel, A., van Holland, G., and Kösters, F.: Man-induced regime shifts in small estuaries—II: a comparison of rivers, *Ocean Dynamics*, 63, 1293–1306, doi:10.1007/s10236-013-0663-8, 2013.
- Wolanski, E. and McLusky, D. S.: Treatise on estuarine and coastal science, Elsevier Amsterdam, 2011.
- Wolanski, E., Ngoc Huan, N., Trong Dao, L., Huu Nhan, N., and Ngoc Thuy, N.: Fine-sediment Dynamics in the Mekong River Estuary, Vietnam, *Estuarine, Coastal and Shelf Science*, 43, 565–582, doi:10.1006/ecss.1996.0088, 1996.
- Wolanski, E., Nhan, N. H., and Spagnol, S.: Sediment dynamics during low flow conditions in the Mekong River estuary, Vietnam, *Journal of Coastal Research*, pp. 472–482, 1998.
- Woodworth, P.: A survey of recent changes in the main components of the ocean tide, *Continental shelf research*, 30, 1680–1691, 2010.
- Wu, H., Zhu, J., and Ho Choi, B.: Links between saltwater intrusion and subtidal circulation in the Changjiang Estuary: A model-guided study, *Continental Shelf Research*, 30, 1891–1905, doi:10.1016/j.csr.2010.09.001, 2010.
- Wu, J., Liu, J. T., and Wang, X.: Sediment trapping of turbidity maxima in the Changjiang Estuary, *Marine Geology*, 303–306, 14–25, doi:10.1016/j.margeo.2012.02.011, 2012.
- Wu, S., Cheng, H., Xu, Y. J., Li, J., and Zheng, S.: Decadal changes in bathymetry of the Yangtze River Estuary: Human impacts and potential saltwater intrusion, *Estuarine, Coastal and Shelf Science*, 182, 158–169, doi:https://doi.org/10.1016/j.ecss.2016.10.002, URL <http://www.sciencedirect.com/science/article/pii/S0272771416304309>, 2016.
- Xue, P., Chen, C., Ding, P., Beardsley, R. C., Lin, H., Ge, J., and Kong, Y.: Saltwater intrusion into the Changjiang River: A model-guided mechanism study, *Journal of Geophysical Research*, 114, doi:10.1029/2008jc004831, 2009.
- Yang, H. F., Yang, S. L., Meng, Y., Xu, K. H., Luo, X. X., Wu, C. S., and Shi, B. W.: Recent coarsening of sediments on the southern Yangtze subaqueous delta front: A response to river damming, *Continental Shelf Research*, 155, 45–51, doi:10.1016/j.csr.2018.01.012, 2018.

- Yang, S., Belkin, I., Belkina, A., Zhao, Q., Zhu, J., and Ding, P.: Delta response to decline in sediment supply from the Yangtze River: evidence of the recent four decades and expectations for the next half-century, *Estuarine, Coastal and Shelf Science*, 57, 689–699, 2003.
- Yang, S., Li, H., Ysebaert, T., Bouma, T., Zhang, W., Wang, Y., Li, P., Li, M., and Ding, P.: Spatial and temporal variations in sediment grain size in tidal wetlands, Yangtze Delta: on the role of physical and biotic controls, *Estuarine, Coastal and Shelf Science*, 77, 657–671, 2008.
- Yang, S., Xu, K., Milliman, J., Yang, H., and Wu, C.: Decline of Yangtze River water and sediment discharge: Impact from natural and anthropogenic changes, *Scientific reports*, 5, 1–14, 2015.
- Yang, S. L., Ding, P. X., and Chen, S. L.: Changes in progradation rate of the tidal flats at the mouth of the Changjiang (Yangtze) River, China, *Geomorphology*, 38, 167–180, doi:10.1016/S0169-555x(00)00079-9, 2001.
- Yang, S. L., Milliman, J. D., Li, P., and Xu, K.: 50,000 dams later: Erosion of the Yangtze River and its delta, *Global and Planetary Change*, 75, 14–20, doi:10.1016/j.gloplacha.2010.09.006, 2011.
- Yang, S. L., Milliman, J. D., Xu, K. H., Deng, B., Zhang, X. Y., and Luo, X. X.: Downstream sedimentary and geomorphic impacts of the Three Gorges Dam on the Yangtze River, *Earth-Science Reviews*, 138, 469–486, doi:https://doi.org/10.1016/j.earscirev.2014.07.006, URL <https://www.sciencedirect.com/science/article/pii/S0012825214001317>, 2014.
- Yang, S. L., Luo, X., Temmerman, S., Kirwan, M., Bouma, T., Xu, K., Zhang, S., Fan, J., Shi, B., and Yang, H.: Role of delta-front erosion in sustaining salt marshes under sea-level rise and fluvial sediment decline, *Limnology Oceanography*, 2020.
- Yang, Y., Zhang, M., Fan, Y., Li, Y., and Liu, W.: Variation trend and causes of suspended sediment characteristic in Yangtze Estuary, *Journal of Basic Science and Engineering*, 6, 48–55 (in Chinese with Abstract in English), 2016.
- Yu, Q., Wang, Y. W., Gao, J. H., Gao, S., and Flemming, B.: Turbidity maximum formation in a well-mixed macrotidal estuary: The role of tidal pumping, *Journal of Geophysical Research-Oceans*, 119, 7705–7724, doi:10.1002/2014jc010228, 2014.
- Yun, C.: Recent development of the Changjiang estuary, China Oceanpress, 2004.
- Zhan, Q., Li, M., Liu, X., Chen, J., and Chen, Z.: Sedimentary transition of the Yangtze subaqueous delta during the past century: Inspiration for delta response to future decline of sediment supply, *Marine Geology*, 428, 106 279, 2020.
- Zhang, E., Savenije, H. H., Wu, H., Kong, Y., and Zhu, J.: Analytical solution for salt intrusion in the Yangtze Estuary, China, *Estuarine, Coastal and Shelf Science*, 91, 492–501, 2011.

- Zhang, E., Gao, S., Savenije, H. H., Si, C., and Cao, S.: Saline water intrusion in relation to strong winds during winter cold outbreaks: North Branch of the Yangtze Estuary, *Journal of Hydrology*, 574, 1099–1109, 2019.
- Zhang, P., Yang, Q., Wang, H., Cai, H., Liu, F., Zhao, T., and Jia, L.: Stepwise alterations in tidal hydrodynamics in a highly human-modified estuary: The roles of channel deepening and narrowing, *Journal of Hydrology*, p. 126153, 2021.
- Zhao, J., Guo, L., He, Q., Wang, Z. B., van Maren, D., and Wang, X.: An analysis on half century morphological changes in the Changjiang Estuary: Spatial variability under natural processes and human intervention, *Journal of Marine Systems*, 181, 25–36, 2018.
- Zhou, Z., Coco, G., van der Wegen, M., Gong, Z., Zhang, C., and Townend, I.: Modeling sorting dynamics of cohesive and non-cohesive sediments on intertidal flats under the effect of tides and wind waves, *Continental Shelf Research*, 104, 76–91, doi:10.1016/j.csr.2015.05.010, 2015.
- Zhou, Z., Coco, G., Townend, I., Olabarrieta, M., Van Der Wegen, M., Gong, Z., D'Alpaos, A., Gao, S., Jaffe, B. E., Gelfenbaum, G., et al.: Is “morphodynamic equilibrium” an oxymoron?, *Earth-Science Reviews*, 165, 257–267, 2017.
- Zhou, Z., Ge, J., Wang, Z. B., van Maren, D., Ma, J., and Ding, P.: Study of lateral flow in a stratified tidal channel-shoal system: The importance of intratidal salinity variation, *Journal of Geophysical Research: Oceans*, 124, 6702–6719, 2019.
- Zhou, Z., Ge, J., van Maren, D., Wang, Z. B., Kuai, Y., and Ding, P.: Study of Sediment Transport in a Tidal Channel-Shoal System: Lateral Effects and Slack-Water Dynamics, *Journal of Geophysical Research: Oceans*, 126, e2020JC016334, 2021.
- Zhu, C., Guo, L., van Maren, D. S., Tian, B., Wang, X., He, Q., and Wang, Z. B.: Decadal morphological evolution of the mouth zone of the Yangtze Estuary in response to human interventions, *Earth Surface Processes and Landforms*, 44, 2319–2332, doi: 10.1002/esp.4647, 2019.
- Zhu, C., van Maren, D. S., Guo, L., Lin, J., He, Q., and Wang, Z. B.: Effects of sediment-induced density gradients on the estuarine turbidity maximum in the Yangtze Estuary, *Journal of Geophysical Research: Oceans* (underreview), 2021.
- Zhu, J., Ding, P., Zhang, L., Wu, H., and Cao, H.: Influence of the deep waterway project on the Changjiang Estuary, pp. 79–92, Springer, 2006.
- Zhu, J., Gu, Y., and Wu, H.: Determination of the period not suitable for taking domestic water supply to the Qingcaosha Reservoir near Changjiang River estuary, *Oceanologia et Limnologia Sinica/Hai Yang Yu Hu Chao*, 44, 1138–1145 (in Chinese), 2013.
- Zhu, J., Weisberg, R. H., Zheng, L., and Han, S.: Influences of Channel Deepening and Widening on the Tidal and Nontidal Circulations of Tampa Bay, *Estuaries and Coasts*, 38, 132–150, doi:10.1007/s12237-014-9815-4, 2014.

- Zhu, J., Wu, H., Li, L., and Qiu, C.: Saltwater intrusion in the Changjiang Estuary, *IntechOpen*, 2018.
- Zhu, L., He, Q., Shen, J., and Wang, Y.: The influence of human activities on morphodynamics and alteration of sediment source and sink in the Changjiang Estuary, *Geomorphology*, 273, 52–62, doi:10.1016/j.geomorph.2016.07.025, 2016.
- Zhu, L., He, Q., and Shen, J.: Modeling lateral circulation and its influence on the along-channel flow in a branched estuary, *Ocean Dynamics*, 68, 177–191, 2017.
- Zhu, W., Li, J., and Sanford, L. P.: Behavior of Suspended Sediment in the Changjiang Estuary in Response to Reduction in River Sediment Supply, *Estuaries and Coasts*, 38, 2185–2197, doi:10.1007/s12237-014-9929-8, 2015.

ACKNOWLEDGEMENTS

The 'acknowledgement' came to my mind many times when I read/heard others' acknowledgement, encountered difficulties, achieved successes and looked forward to finishing my PhD... At the time when the long PhD journey is finally going to be finished, it is not all about relief and excitement but also nostalgia. Looking back to the journey, the experience is valuable and memorable: happy and sad scenes leap before my eyes, pains and gains go together. I felt lucky to have so many people around to help me accomplish this dissertation. I would like to express my heartfelt thanks to all of these people.

The first acknowledgement belongs to my promoter *Prof. Qing He* who provided me with the great opportunity to come to ECNU-SKLEC and go abroad for a full doctoral study at TU Delft. *Prof. He*, I appreciate your kind support during my stay at SKLEC and TU Delft. You are wise and visionary. Many of your thoughts are advanced and valuable, leading the direction of my research. I am also very impressed by your clear and logical speech and presentations, which are great examples for me all the time. You not only teach me how to do research but also how to behave in society. Thank you so much and you are one of the most important mentors in my life.

My promoter, *Prof. Zheng Bing Wang*, is also a scientific model for me. Thank you for the expert guidance, constructive comments, and valuable suggestions to help me gain insights into the field. Your critical and rigorous attitudes towards scientific research have profoundly influenced me. Thanks for the kindness and patience to teach me how to write scientific papers. Your curiosity about the answers to research questions also shows me the meaning of research and what good researchers look like: we are trying to understand more unknowns.

My promoter, *Prof. Bas van Maren*, I was so grateful to have you as my supervisor. Without your help, I would struggle for a long time and may not come to an end. You are patient to answer all my questions and I feel encouraged to tell you the success I achieved and the problems I met. Thanks for your generous praise and constructive ideas to let me have a sense of accomplishment and become more confident and less anxious. I've learned so much from you. I appreciate your countless revisions and comments behind each paper and this dissertation.

Leicheng Guo, you are one of the best role models around me. You push me when the progress is slow and also encourage me when I meet difficulties. Thanks for editing my papers with a lot of useful suggestions. Thank you for sharing your ideas and experiences all the time when I need you.

Marcel Stive, Han Winterwerp, Bram van Prooijen, Qinghua Ye, although we only discussed a few times face to face, *Marcel*, your kindness; *Han*, your critical thoughts; *Bram*, your passion and smile, and *Qinghua*, your insights into Delft3D models leave a deep impression on me. *Marcel Zilijma*, thanks for providing me high-performance computers (HPC) to run Delft3D model scenarios. *Stef Hummel*, thanks for introducing me OpenDA and coming to TUD several times to help me solve technique problems. *Mariette van Tilburg*, thanks for polishing my first manuscript. *Liu Jin, Zhiying Yu, Pingxing Ding*, the few times discussed with you are valuable. *Zhong Peng, Xianye Wang, Bo Tian, Fan Xu*, you are both my friends and teachers. *Can Jin, Xiaoli Huo*, thanks for taking care of my student affairs apart from the research.

Jie Zhao, Weiming Xie, Lei Zhu, Chao Guo, Chaofeng Xing, Yu Chen, Dai Zhang, Zhirui Deng, Jianliang Lin, the 424 group, thanks a million to my colleges of the sediment group in my first year of PhD at SKLEC. We are like a family and I felt that I was cared for by all of you. I learned a lot from everything you shared, the data, skills, experiences and acknowledge etc. I regret to miss some of your graduation ceremonies but you will all be my best peers and friends. Special thanks to *Zhirui* and *Jianliang*, we spent so much time together both at SKLEC and TU Delft and the help from you is uncountable. The other new members of 424 and sediment group: *Jie Jiang, Yu Qiao, Yuning Zhang, Zhongquan Hou, Qingze Chen, Simin Zhou, Xuefeng Wu, Jiamin Chen, Shang Yu, Zhonghao Zhao, Zengbin Wu, Yuze Feng, Jian Dong, Haisheng Yu, Huichen Ma, Yating Hou, Yufan Chen etc*, are acknowledged to let the family larger and larger and also help me many times in this new group. I wish those not graduated all have plentiful outputs.

My seniors: *Xin Tian, Qin Zhu, Hualong Luan, Xiaoteng Shen*, thanks for sharing your experiences in research and careers with me. *Miao Zhang*, my first-year roommate and majoring in chemistry, you are caring and like my sister. I appreciate your help moving my staff from the campus in Putuo to the main campus in Minhang. *Xuerong Sun*, my last-year roommate and majoring in remote sensing. Thanks for sharing your ideas in remote sensing, which has broadened my views on scientific research. Many other friends are appreciated for the time being together at SKLEC: *Shuo Jiang, Liping Ye, Jiana Li, Lin Cheng, Qing Chen, Zhang Luo, Xiaodao Wei etc*.

My colleagues in TU Delft: *Lodewijk*, I appreciate that you installed Delft3D in the cluster and shared your Linux scripts and research with me. *Jill, Ana*, you are enthusiastic and prepared everything well for the project. Thanks for holding the meetings for us. *Stuart*, thanks for organizing us to go curling and ‘rubbing the floor’ is a lot of fun. *Bob*, thanks for sharing your useful small tools with me. *Thuong, May Ei, Anastasia*, being with you are happy, I was inspired by your research and also learned the culture in your home country. You are all beautiful dressing in your traditional clothes. *Chit, Dung*, chatting with you is fun too.

Living and studying in Delft was not lonely anymore because of all these friends: *Peng Yao, Min Su, Yang Zhou (also Wen Zhang), Sien Liu, Rong Zhang, Runxiang Li, Zhirui Deng, Jianliang Lin, Yu Kuai, Zaiyang Zhou, Yuning Zhang, Yujian Zhan, Lian Liu, Di-*

neng Zhao, the Chinese lunch team at TU Delft, I experienced a marvelous amount of enjoyment chatting with you at lunchtime. *Lixia Niu*, *Peng Yao*, *Min Su*, I inherited lots of things that were a basis for continuous party time. *Yang Zhou*, you are the 'life encyclopedia'. You are like my elder sister and always warm me when I have trouble. *Sien*, you are the 'Delft encyclopedia', with you everything became easier in Delft. *Rong*, talking to you is relaxed and you always give me valuable suggestions. *Runxiang*, 'master of hands-on ability', I could not remember how many times you have fixed our bicycles. *Jianliang*, 'master of chef', I am inspired by discussing with you. I also appreciate the moments you cooked delicious meals. *Yu (also Weiqiu)*, 'master of fitness', I respect your self-control on losing weight and I miss your delicious stewed pork leg. *Zaiyang*, you are talented and 'master of badminton' should not be your only tag. Thanks for being there whenever I ask for your help. *Yuning*, 'master of ppt', your brilliant ideas bring lots of fun to the group and thanks for the lovely time spent with you. *Lian Liu*, *Yujian Zhan*, *Dineng Zhao*, I am happy to meet you all. Special thanks to *Jianwei Sun* for my stay during the Covid-19 periods.

Zhilin Zhang, we spent so many lovely times together and I will always keep the photos and memories. *Cheng Dan*, you work hard, which inspired me a lot. I enjoyed the days we learned to swim together and had fun playing with water. *Mengshi Yang*, *Peiwen Meng*, *Jing Guo*, *Jun Nie*, *Guolei Tang*, thanks for the happy times in Delft. The first Chinese New Year celebrated together seems not far away. *Sixue Wu*, *Yaya Liu*, my Michiel 'housemates', I am happy to have you shared delicious food. There are many other people I would like to appreciate for having unforgettable times in Delft: *Ding Ding*, *Jiani Liu*, *Mei Liu*, *Lengxuan Zeng (Kelly)*, *Lei Zhong*, *Ye Tian*, *Xun Sun*, *Hao Yu*, *Yueqian Shen*, *Shengyue Yao*, *Riming Wang*, *Meng Meng*, *Mingzhao Zhuo*, *Zhanxiong Liu*, *Lizuo Xin*, *Yuan Li*, *Han Dun*, *Yunlong Li*, *Qian Ke*, *Jing Zhao*, *Jia Liu*, *Pengling Wang* etc. Forgive me if I forgot to mention you.

.....

Last but not least to my family, especially to my aunt. I left home for a long time since I went to middle school. Your unconditional support gives me much freedom. I feel so lucky to have you around.

Chunyan Zhu
Shanghai, November 2021

CURRICULUM VITÆ

Chunyan ZHU

Chunyan Zhu was born on 17 September, 1992 (Chinese lunar calendar) in a village in Jintan, Changzhou, Jiangsu Province, China. She spent 18 years in the lovely hometown and acknowledged to study at Shetou primary school, the second middle school and Hua Luogeng high school. Afterwards, she left Jiangsu to join the School of Water Resources and Hydropower Engineering at Wuhan University in Hubei Province, the central of China. Wuhan University is a beautiful university which is famous for the lovely sakura in spring and she enjoyed the college life there. The second year she chose her major in sediment dynamics. In 2014, she obtained Bachelor degree of Harbor, Waterway and Coastal Engineering. Her bachelor thesis was about analysis on variations of water and sediment flux in the Yangtze Estuary.

The further step into pursuing doctoral degree was decided in 2013 when she attended the summer school held by State Key Laboratory of Estuarine and Coastal Research (SKLEC) in East China Normal University (ECNU), Shanghai. In September 2014, she was recommended to directly continue her PhD study on estuarine sediment dynamics there, promoted by Prof. Qing HE. Prof. Qing HE recommended her to pursue the doctoral degree at Delft University of Technology (TU Delft) in the Netherlands, which was later signed as a dual-degree between ECNU and TU Delft. At that time, she spent the first year at SLKEC to complete courses and passed ielts to apply for the funding from Chinese Scholarship Council (CSC). Since September 2015, she arrived at TU Delft and worked on estuarine morphodynamics in Department of Hydraulic Engineering, under the supervision of prof. dr. Q. He, prof. dr. ir. Z.B. Wang, and prof. dr. D.S. van Maren.

LIST OF PUBLICATIONS

JOURNAL PAPERS

FIRST AUTHOR

5. **Zhu C.**, van Maren, D.S., Guo, L., He, Q. and Wang, Z.B., Future changes in saltwater intrusion in the Yangtze Estuary: the importance of sediment dynamics (draft).
4. **Zhu, C.**, van Maren, D.S., Guo, L., Lin, J., He, Q. and Wang, Z.B., Feedback effects of sediment suspension on transport mechanisms in estuarine turbidity maximum. *Journal of Geophysical Research-Oceans* (submitted).
3. **Zhu, C.**, Guo, L., van Maren, D.S., Wang, Z.B. and He, Q., 2021. Exploration of decadal tidal evolution in response to morphological and sedimentary changes in the Yangtze Estuary. *Journal of Geophysical Research-Oceans*, p.e2020JC017019.
2. **Zhu, C.**, van Maren, D.S., Guo, L., Lin, J., He, Q. and Wang, Z.B., 2021. Effects of sediment-induced density gradients on the estuarine turbidity maximum in the Yangtze Estuary. *Journal of Geophysical Research-Oceans*, doi: 10.1029/2020JC016927.
1. **Zhu, C.**, Guo, L., van Maren, D.S., Tian, B., Wang, X., He, Q. and Wang, Z.B., 2019. Decadal morphological evolution of the mouth zone of the Yangtze Estuary in response to human interventions. *Earth Surface Processes and Landforms*. 44(12), pp.2319-2332.

CO-AUTHOR

6. Guo, L., **Zhu, C.**, Cai, H., Wang, Z.B., Townend, I. and He, Q., 2021. River-enhanced non-linear overtide variations in river estuaries. *Hydrology and Earth System Sciences Discussions*, pp.1-31.
5. Lin, J., van Prooijen, B.C., Guo, L., **Zhu, C.**, He, Q. and Wang, Z.B., 2021. Regime shifts in the Changjiang (Yangtze River) Estuary: The role of concentrated benthic suspensions. *Marine Geology*, 433, p.106403.
4. Guo, L., **Zhu, C.**, Wu, X., Wan, Y., Jay, D.A., Townend, I., Wang, Z.B. and He, Q., 2020. Strong inland propagation of low-frequency long waves in river estuaries. *Geophysical Research Letters*, 47(19), p.e2020GL089112.

3. Guo, L., Xie, W., Xu, F., Wang, X., **Zhu, C.**, Meng, Y., Zhang, W. and He, Q., 2021. A historical review of sediment export–import shift in the North Branch of Changjiang Estuary. *Earth Surface Processes and Landforms*.
2. Guo, L., Su, N., Townend, I., Wang, Z.B., **Zhu, C.**, Wang, X., Zhang, Y. and He, Q., 2019. From the headwater to the delta: A synthesis of the basin-scale sediment load regime in the Changjiang River. *Earth-Science Reviews*, p.102900.
1. Guo, L., Su, N., **Zhu, C.** and He, Q., 2018. How have the river discharges and sediment loads changed in the Changjiang River basin downstream of the Three Gorges Dam?. *Journal of Hydrology*, 560, pp.259-274.

CONFERENCE ABSTRACTS

4. **Zhu, C.**, van Maren, D.S., Guo, L., Lin, J., He, Q. and Wang, Z.B., 2021. Feedback effects of sediment suspension on estuarine turbidity maximum. *INTERCOH 2021: 16th International Conference on Cohesive Sediment Transport Processes*, Delft, the Netherlands, 13-17 September.
3. Guo, L., He, Q., **Zhu, C.** and Wang, Z.B., 2017. Impacts of bed slope factor on large scale fluvio-deltaic morphodynamic development. *10th Symposium on River coastal and estuarine morphodynamics: Back to Italy*, Trento - Padova, Italy, 15-22 September.
2. Guo, L., **Zhu, C.**, He, Q., 2017. How important is mud transport on large scale estuarine and deltaic morphodynamics? *INTERCOH 2017: 14th International Conference on Cohesive Sediment Transport Processes*, Montevideo, Uruguay, 13-17 November.
1. **Zhu, C.**, Guo, L., van Maren, D.S., Tian, B., Wang, X., He, Q. and Wang, Z.B., 2017. Estuarine morphodynamic adaptation to sediment supply and human activities: A case study of turbidity maximum. *INTERCOH 2017: 14th International Conference on Cohesive Sediment Transport Processes*, Montevideo, Uruguay, 13-17 November.

